POLYMER SIDE-CHAINS AS ARMS FOR MOLECULAR RECOGNITION

A Dissertation
Presented to
The Academic Faculty

By

Clinton Ray South

In Partial Fulfillment
Of the Requirements for the Degree
Doctor of Philosophy in Chemistry

Georgia Institute of Technology

April, 2008

POLYMER SIDE-CHAINS AS ARMS FOR MOLECULAR RECOGNITION

Dr. Marcus Weck
Chemistry and Biochemistry
Georgia Institute of Technology

Dr. Christopher W. Jones
Chemical and Biomolecular Engineering
Georgia Institute of Technology

Dr. Seth Marder
Chemistry and Biochemistry
Georgia Institute of Technology

Dr. Haskell Beckham
Polymer, Textile, and Fiber Engineering
Georgia Institute of Technology

Dr. Uwe H. F. Bunz
Chemistry and Biochemistry
Georgia Institute of Technology

Date Approved: February 1, 2008

To my family and to my fiancé Toni

ACKOWLEDGEMENTS

A number of colleagues, friends, and family members were instrumental in helping me complete my Ph.D. research and deserve a proper thanks. First and foremost, I would like to thank my family for instilling in me a drive to succeed at a very young age. Without their loving guidance, encouragement, and support, I would certainly not have been capable of enduring a Ph.D. degree program.

I would like to thank my family for teaching me the value of hard work, a value that I intend to pass down to my own family one day. The countless days I've spent with my dad working on our farm and doing carpentry work during hot Alabama summers not only engrained within me a hard working stamina but also made the days in an air-conditioning laboratory seem relatively easy. Ironically, too much of an air-conditioned laboratory can make one miss a hot Alabama summer. Likewise, I thank both of my grandfathers, Gene McDaniel and Willard South, for further instilling in me the value of hard work. I would also like to thank my mom, Desiree South, for giving me all the encouragement that made getting through a PhD program much easier. My tenure at Georgia Tech would have been much more difficult without her constant loving support. Similarly, I thank my sister, Chrissy South, for providing encouragement and oftentimes understanding in my times of absence. Finally, I thank my grandmothers, Dean McDaniel and Dora South, for providing the type of unconditional encouragement only a grandmother can.

I am thankful to all the members of my family for their patience and constant understanding during my graduate school years, and I regret not being able to devote more of my time to them during this period of my life.

Last but not least, I thank the latest addition to my family, my loving fiancé, Toni Bonhivert. Her daily support, love, and encouragement not only made the last couple of graduate school years pass quickly but also much more bearably. I intend to provide to her the same level of support as she did for me during the remaining years of her Ph.D. studies. I look forward to our life together and to the beginning of our own family.

I am also indebted to the many colleagues that provided training, education and friendship during my graduate school career. First, I thank the person that taught me how to do synthetic chemistry, Dr. J. D. Cho, formerly of the Marder group at Georgia Tech. J. D. is a hard working individual and deserving of the many successes that he has achieved. Similarly, I thank Dr. Amy Meyers, my NSF-REU mentor, for teaching me the basics of practical organic chemistry in only ten weeks. I also thank A. J. Zucchero, a good friend of mine, for the countless poker nights and the hard work on several collaborative projects. Likewise, I thank Dr. Warren Gerhardt, for making lab seem more like a competitive sporting event than an academic setting and also for providing me with knowledge and advice during my first years as a graduate student. Additionally, I thank Trey Piñón for his support with projects discussed in Chapter 7.

I also thank the many other friends in the chemistry department at Georgia Tech for making my graduate school years enjoyable and for providing a much needed outlet during times of stress.

Finally, I thank my senior collaborators and colleagues, including Dr. Al Nelson and Dr. Connie Hou of the Grubbs group, and Drs. Ken Leung and Daniella Lanara of the Stoddart group, for their hard work on projects discussed in Chapters 3, 4, and 5. I also thank my committee members for assisting in my training and providing me with suggestions throughout my graduate career. I would like to specifically thank Dr. Christopher Jones for his suggestions and guidance during joint group meetings. Last but not least, I thank my advisor, Dr. Marcus Weck, who was instrumental in my training and mentorship throughout my graduate career.

TABLE OF CONTENTS

LIST OF TABLES

LIST OF FIGURES

LIST OF SCHEMES

LIST OF ABBREVIATIONS

Å	angstrom
AC	alternating current
ADA	acceptor-donor-acceptor
ADMET	acyclic diene metathesis
AFM	atomic force microscopy
BDE	bond dissociation energy
bipy	bipyridine
CA	cyanuric acid
cal	calorie
CM	cross-metathesis
cm^{-1}	wavenumber
CoPM	coordination polymer multilayer
DAD	donor-acceptor-donor
DAP	diamidopyridine
DB24C8	dibenzo-[24]-crown(8)
DBA	dibenzylammonium
DCC	dicyclohexylcarbodiimide
DCM	dichloromethane
DIEA	diisopropylethylamine
DMAP	dimethylaminopyridine
DMF	dimethylformamide

DNA	deoxyribonucleic acid
DP	degree of polymerization
DTS	DNA templated synthesis
ESI	electrospray ionization
FAB	fast atom bombardment
FT	fourier transform
g	gram
GPC	gel-permeation chromotography
HATU	O-(7-Azabenzotriazol-1-yl)-N,N,N',N'-tetramethyluronium-hexafluorophosphate
HCl	hydrochloric acid
HPLC	high performance liquid chromatography
Hz	Hertz
IR	infrared
ITC	isothermal titration calorimetry
J	coupling constant
KCl	potassium chloride
LAH	lithium aluminum hydride
M	molar
mL	milliliter
mmol	millimole
M_n	number average molecular weight
MPTMS	mercaptopropyltrimethylsilane
MS	mass spectrometry

M_w	weight average molecular weight
NaCl	sodium chloride
NBE	norbornene
NBT	*N*-butyl thymine
NCN	nitrogen-carbon-nitrogen
NMR	nuclear magnetic resonance
OLED	organic light emitting diode
OM	optical microscopy
PAA	poly(acrylic acid)
PAH	poly(allylamine hydrochloride)
PDC	pyridinium dichromate
PDI	polydispersity index
PNBE	poly(norbornene)
ppm	parts per million
PSOH	poly(4-vinyl phenol)
PSS	poly(styrene sulfonate)
PVP	poly(vinyl pyridine)
PYR	pyridine
RAS	reflective absorbance spectroscopy
RCM	ring-closing metathesis
RMS	root-mean square
RNA	ribonucleic acid
ROMP	ring-opening metathesis polymerization

rt	room temperature
SCS	sulfur-carbon-sulfur
SDP	sodium dodecyloxyphenate
TBAF	tetrabutylammonium fluoride
TBDMS	*tert*-butyldimethylsilyl chloride
TFA	trifluoroacetic acid
THF	tetrahydrofuran
THY	thymine
TLC	thin-layer chromatography
trpy	terpyridine
UPB	universal polymer backbone
UV/vis	ultraviolet / visible
XPS	x-ray photoelectron spectroscopy

SUMMARY

This thesis describes research based on synthetic protocols, methodologies, and applications of polymers containing side-chain molecular recognition elements. The motivation for the thesis lies in the belief among many in the field that a strict covalent paradigm for polymer chemistry is reaching its limit. The use of molecular recognition, in lieu of covalent chemistry, potentially presents a path through the current limits of polymer science. The work described in the following chapters of this thesis is, at least in part, a testament to this proposal.

The first two chapters presen a basic introduction and survey of the fundamental noncovalent interactions that are ubiquitous in the research of supramolecular polymers and molecular recognition. A hierarchy of noncovalent interactions, molecular recognition, and self-assembly is outlined and discussed. Chapter 2 lays the foundation for the remaining chapters of this thesis by presenting several examples of prior work related specifically to the use of molecular recognition on the side-chains of polymers.

The next two chapters present research focused on advancing the functionalization of polymers through molecular recognition. The goal of this research is primarily to develop a general polymer backbone that both site-specifically and strongly associates noncovalently with small molecular substrates. These chapters demonstrate that both architecturally controlled block copolymers and random terpolymers can accept a full load of different substrates without interference among distinct molecular recognition elements along the polymer backbone.

Chapters 5 and 6 present a unique application of polymers containing molecular recognition elements, templated synthesis. Chapter 5 first discusses lessons learned from small molecule based templated synthesis in which a template and a substrate are held together by metal coordination and a subsequent bond forming reaction occurs. Ultimately, the results of this chapter directed our work towards a hydrogen bonding based system in lieu of metal coordination. In this case, a polymeric template was used, and a daughter monomer was polymerized while attached to the template.

Another application of polymers containing molecular recognition elements is presented in Chapters 7 and 8. In these chapters, metal coordination is used to assemble polymer multilayer thin films that are both responsive to external stimuli, stable, and erasable.

Finally, Chapter 9 summarizes the main conclusions of each chapter and presents a potential view of new projects that might result from the research presented in this thesis.

CHAPTER 1

Noncovalent Bonding, Molecular Recognition, and Self-Assembly

1.1 Abstract

This Chapter introduces concepts in noncovalent bonding, molecular recognition, and self-assembly starting with an initial fundamental review of noncovalent binding interactions. Ionic and electrostatic interactions, hydrogen bonding, metal coordination, π system interactions, and weaker forces such as Van Der Waals interactions and hydrophobic interactions are surveyed. An emphasis is placed both on the fundamental physical phenomena that gives rise to these forces and aspects of these forces that can further lead to molecular recognition and self-assembly. A consequence of noncovalent bonding is often molecular recognition, and fundamentals of this concept are reviewed. Likewise, molecular recognition can often result in self-assembly, and this process is highlighted and reviewed.

1.2 Introduction

Molecular recognition and self-assembly together define a burgeoning field known as supramolecular chemistry. While supramolecular chemistry is a relatively young field, with its origin dated to at least thirty years ago,[1] the principles governing this field are largely based on a Natural approach to molecular systems. That is, supramolecular chemistry, like Nature, directs features of chemical species to organize, attract, or otherwise assemble to one another through intermolecular noncovalent binding interactions.[2] Supramolecular chemistry not only fascinates researchers because we are

naturally attracted to order or the appearance of order rather than disorder, but also because numerous research groups in the field have recognized the inherent limitations of the covalent bond for the goal of assembling or otherwise functionalizing nanostructures.[3-5] Indeed, the evidence for this fascination lies in the coming of age of this relatively young field as witnessed by numerous meetings, workshops, extensive publications, a Nobel Prize, and recently a journal, *Supramolecular Chemistry*, devoted entirely to this field.

Supramolecular chemistry has roots in chemistry dating back to the late 1800s. One obvious heritage relates back to Alfred Werner's idea of coordination chemistry reported in 1893.[6] Likewise, the renown "lock and key" concept developed by Emil Fischer in 1894[7, 8] was probably the first pure example of molecular recognition, although little was known about the importance of the individual noncovalent forces giving rise to such a phenomenon. Daniel Koshland later refined the "lock and key" principle to accommodate a more static interpretation of biological binding events, in what he deemed the induced fit model,[9] which took into account biological equilibrium concepts widely accepted today, such as binding cooperativity. Another catalyst giving rise to supramolecular chemistry comes from medical studies during the late 19th and early 20th centuries. One example, reported by Paul Ehrlich, is summarized in the Latin phrase, *Corpora non agunt nisi fixata*, meaning that a molecule can only have an effect on the body when it is bound.[10] Supramolecular chemistry could have arguably began in 1937, when Wolf and his coworkers used the term "Übermolekül" (supermolecule) to characterize carboxylic acid dimers.[11] However, while supramolecular chemistry dates back to the late 19th century, and could have begun as early as 1937, most in the field

deem Lehn the father of supramolecular chemistry[12-16] as he set forth the first clear definition of the molecular recognition concept as the "chemistry of molecular assemblies and of the intermolecular bond."[1] Moreover, Donald Cram was also instrumental in the development of many of the basic concepts upon which supramolecular chemistry is based.[1]

This thesis is primarily concerned with molecular recognition of polymers, with applications of such polymers ranging from templated olefin metathesis to complex materials and surface science. Inherent in all of the research in this thesis is a strategy that relies on noncovalent rather than covalent interactions to address several important problems associated with: (i) efficient and high-yielding polymer multifunctionalization (Chapters 2-4), (ii) template assisted oligimer and polymer synthesis (Chapters 5-6), and (iii) materials and surface applications of supramolecular polymers (Chapters 7-8). This Chapter sets forth basic and fundamental concepts of molecular recognition and self-assembly and highlights noncovalent binding principles giving rise to such phenomena, while Chapter 2 introduces molecular recognition in the context of side-chain supramolecular polymers.

1.3 Noncovalent Interactions

While molecular recognition can be thought of as an intermediate to a supramolecular self-assembled species, single noncovalent interactions can be thought of as an even more elementary component of self-assembly, and thus it is fitting to examine the forces driving noncovalent interactions at the outset of this thesis. As an example, in the case of a diamidopyridine-thymine complex (*vide infra*), each individual hydrogen

bond constitutes a distinct noncovalent interaction, while the combination of all three in unison create the full molecular recognition complex. Likewise, if multiple diamidopyridine-thymine components were present in a supramolecule, a self-assembled species could conceivably arise. Such a hierarchy is outlined in Figure 1.1. There are numerous single noncovalent bonds that can lead to molecular recognition and self-assembly, and each will be examined in the following sections.

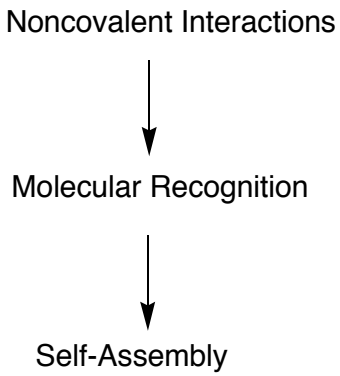

Figure 1.1. Diagram illustrating hierarchy of events leading to self-assembly. Arrows are meant to indicate that the proceeding event can occur but does not have to occur.

1.3.1 Ionic Bonding

Ion-ion interactions, when present in a non-competing solvent, are among the strongest type of noncovalent bonding, and as such they can be pivotal in enabling molecular recognition and in forming supramolecular structures. Ionic bonds, by themselves, may not be capable of forming molecular recognition partners in the true sense of the concept because they are generally not specific. A classic example of an ionic-ionic interaction is table salt, or NaCl, which forms due to the attractive charges on a Na cation and Cl anion, shown in Scheme 1.1.

a) $Na^+ + Cl^- \longrightarrow NaCl$

b) $K^+ + Cl^- \longrightarrow KCl$

Scheme 1.1. Formation of Cl salts from corresponding cation.

The lack of specificity among ionic atoms or molecules is also evident from Scheme 1.1. While a NaCl complex and a KCl complex are not the same in terms of electronic distributions, a Cl anion generally has very little specificity for a Na cation over, for example, a K cation. In short, the driving force for this type of interaction is purely charge stabilization. Given this fact, there are plenty examples in the literature of molecular recognition partners that are at least partially stabilized by ionic bonds, but other more specific interactions, such as a hydrogen bond array, are usually present to add specificity to the combination.[1] Despite this fact, some may argue that pure simple ionic interactions can lead to the supramolecular formation of crystal structures, which are, by definition, a precise repeating arrangement of atoms that form without outside intervention. For example, the NaCl crystal lattice is of the most basic crystal structures, a simple cubic, shown in Figure 1.2.

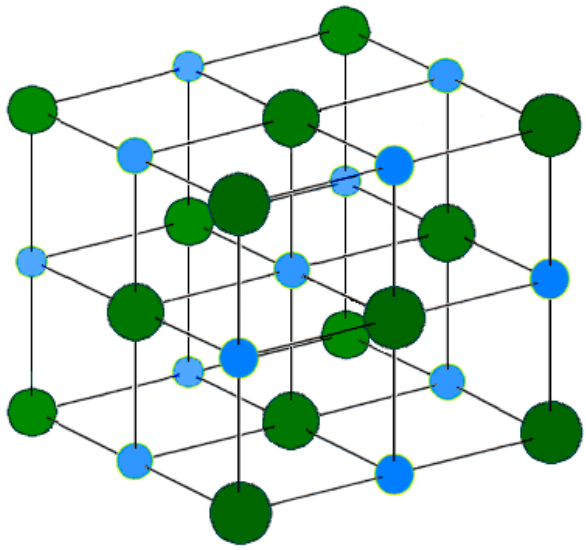

Figure 1.2. A NaCl simple cubic crystal lattice. Na shown in blue; Cl shown in green.

The discovery of ionic interactions can be traced back to the late 1800s. J.J. Thompson speculated about the bonding nature of HCl when he wrote, "*There seems to me to be some evidence that the charges carried by the corpuscles in the atom are large compared with those carried by the ions of an electrolyte. In the molecule of HCl, for example, I picture the components of the hydrogen atoms as held together by a great number of tubes of electrostatic force; the components of the chlorine atom are similarly held together, while only one stray tube binds the hydrogen atom to the chlorine atom,*"[17] in a treatise in 1897. In fact, around 1904, J.J. Thompson attempted to explain all chemical bonding in terms of Faraday units, speculating that chemical interactions can be fully explained with known electrical theory.[17] While this theory was revolutionary in defining what is now widely understood as an ionic bond, it failed to address bonding in non-ionizing substances, or put simply, covalence.

Given that ionic-ionic interactions arise from a charge on an atom or molecule, these interactions can be either attractive or repulsive or both if multiple charges are

simultaneously present on a single species or conglomerate of species acting in unison. This can be an important feature of this type of interaction. For example, DNA is negatively charged on both strands, and the repulsive forces between strands minimize the intermolecular aggregation of neighboring strands in solution. In supramolecular terms, either attractive forces, repulsive forces, or both can contribute to the overall architecture of the structure.

Since ionic-ionic bonds are stabilized primarily through charge-charge interactions of full positive or negative charges, they are among the strongest type of interaction. The strengths of ion-ion interactions generally fall within the range of 100-350 kJ mol^{-1}, depending on the solvent.[18] In contrast, van der Waals interactions are generally only a few kJ mol^{-1}.[18] The strength of any given ionic bond is dependant on a number of factors. (i) The distance between the two charges in the bonded state: as the distance between the charge center of a bonding cation and corresponding anion increases, the bond strength decreases, and *vice versa*. This consequence, in terms of supramolecular chemistry, will usually be determined by the supramolecular aggregate geometry that will either serve to increase or decrease the distance between two bonded charges. (ii) The localization of charge on either the cation or anion: as charge localization increases, or as charge density increases, the corresponding strength of the stabilized, bonded ionic complex will increase. The charge density is usually a function of the size of the charged species. This is an important quality of an ionic bond, and an exploitation of this quality is highlighted in later Chapters. Briefly, in the context of pseudorotaxanes, however, decreasing the charge density present on a stabilizing anion can increase the binding stability of a pseudorotaxane complex. As illustrated in Figure

1.3, as the size of the negatively charged species stabilizing a dibenzylammonium cation, **DBA**$^+$, decreases, the binding affinity between **DBA**$^+$ and a dibenzo-24-crown[8] macrocycle, **DB24C8**, decreases accordingly. A larger anion allows more charge to be localized on **DBA**$^+$, thus increasing its affinity for **DB24C8** (*infra*).

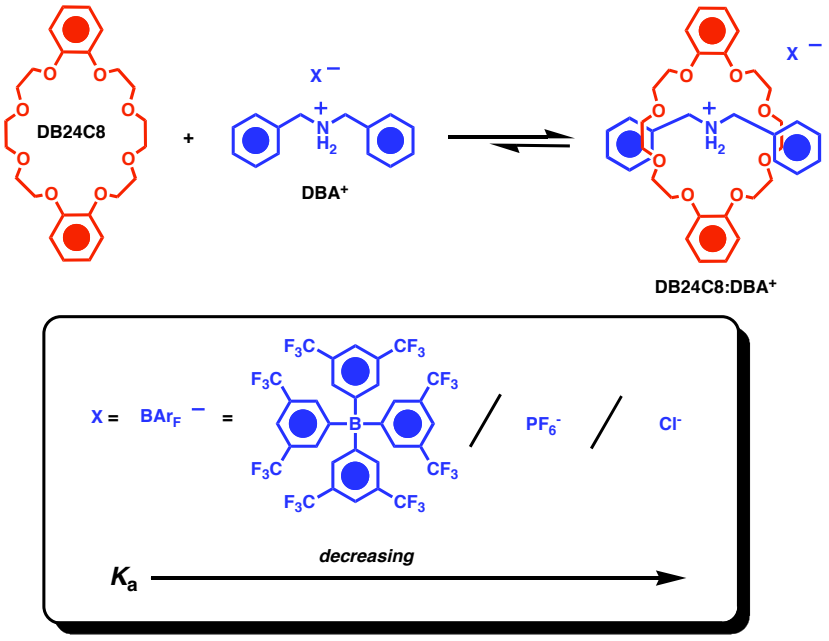

Figure 1.3. Effect of counterion size on binding strength of DB24C8 with DBA$^+$

(iii) The external environment of the ionic complex strongly influences the binding energy of the species. For example, a polar protic solvent, such as water, can strongly stabilize charge, and thus shield the charge from binding strongly to another oppositely charged species. Again referring to the pseudorotaxane example, if we examine this interaction in water, almost no binding affinity between **DBA**$^+$, and **DB24C8** is observed.

Ion-dipole interactions, a sub-class of ionic bonds, are also commonly found among supramolecular species. Ion-dipole interactions are generally weaker in strength when compared to fully ionic bonds, with bond energies ranging from 50 to 200 kJ mol$^-$

[1].[18] Supramolecular chemistry has its beginning in the study of these interactions with the discovery of the first crown ether host-guest complex (shown in Figure 1.4) by Pederson in 1967, and the later discovery of the similar cryptand by Lehn in 1969.[15]

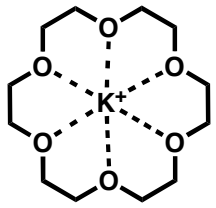

Figure 1.4. 18-crown[6]:K^+ host-guest complex.

In the context of later Chapters in this thesis, ion-dipole interactions play an important role in the pseudorotaxane depicted in Figure 1.3, similar to the host-guest complex shown in Figure 1.4. Likewise, coordination complexes similar to the ones discussed in this thesis often have a strong ion-dipole character, particularly if a metal ion serves as the core of the complex with the metal ion surrounded by ligands. In this case, however, the dative bond generally has more covalent character, and thus it becomes difficult to draw the line between supramolecular and molecular chemistry.[18]

1.3.2 Hydrogen Bonding

Similar to the ionic bond is the hydrogen bond, in the sense that both rely on an attraction or repulsion of charge; albeit in the case of the hydrogen bond, the charge is only partial. Hydrogen bond strengths range from 5-50 kJ mol^{-1};[18] and the properties governing hydrogen bonding interactions are very similar to the ones governing ion-dipole or ion-ion interactions. Hydrogen bonds generally exist between an electronegative atom and a hydrogen atom bonded to another electronegative atom.

Hydrogen bonds are pivotal in supramolecular chemistry since they can contribute to the architecture of a structure by both inter- and intra- molecular bonding. For example, a carboxylic acid can engage in intermolecular hydrogen bonding whereas the enol tautomer of acetylacetone can engage in intramolecular hydrogen bonding (depicted in Figure 1.5).

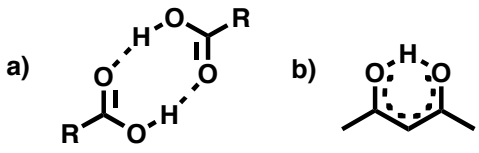

Figure 1.5. Examples of intermolecular (a) and intramolecular (b) hydrogen bonding.

Equally important to the hydrogen bonds' inter and intra molecular capabilities is the ability to control supramolecular architecture or geometry with hydrogen bonds.[19] Excellent examples of this level of architectural control in biochemistry include the double-stranded DNA helix and folded proteins, both of which are assisted by both inter- and intramolecular hydrogen bonds and by the directionality of those hydrogen bonds.[18] There are numerous examples in supramolecular chemistry where these aspects of the hydrogen bond can be useful in defining supramolecular architectures.

It is important to distinguish hydrogen bonds based on their binding energies in addition to their internuclear distances, since these parameters can define whether a hydrogen bond is purely supramolecular or simply molecular with a covalent bond character. Strong hydrogen bonds generally have binding energies in the range of 60-120 kJ mol^{-1} and heteroatom-heteroatom distances between 2.2 and 2.5 Å; moderate hydrogen bonds generally have binding energies in the range of 15-60 kJ mol^{-1} with heteroatom-

heteroatom distances between 2.5 and 3.2 Å, while weak hydrogen bonds have binding energies below 15 kJ mol^{-1} and longer acceptor distances of up to 4Å.[18] The former ranges are evident particularly from quantum mechanical calculations suggesting that a substantial covalent character exists in strong hydrogen bonds. Additionally, the geometrical range in strong hydrogen bonds is much more constrained (175-180º) when compared to moderate (130-180º) and weak (90-150º) hydrogen bonds.[18] Geometry, strength, and heteroatom-heteroatom distance (which are all interrelated) play important roles in the binding affinity and binding architecture of supramolecular species. Another important distinguishing factor among hydrogen bonds is whether the bond is between a neutral or charged species. In general, hydrogen bonds between charged species tend to be much stronger.[18] For example, the F-H•••F^- hydrogen bond has a binding energy of 155 kJ mol^{-1}, making it the strongest hydrogen bond known.[18] Other binding energies of various selected hydrogen bonds are summarized in Table 1.1.

Table 1.1 List of common hydrogen bonds and their corresponding bond disassociation energies (gas-phase).[19]

Hydrogen Bond	BDE / kJ mol^{-1}
F-H•••F	155
O-H•••N	29
O-H•••O	21
HO-H•••OH_3^+	18
N-H•••N	13
N-H•••O	8

Many supramolecular complexes rely exclusively on hydrogen bonding or arrays of hydrogen bonds for their formation. Typical examples include purely supramolecular polymers, in which the monomeric components hydrogen bond to each other to "propagate" the formation of a growing polymer chain, with a degree of polymerization (DP) generally proportional to the square root of the binding constant.[20] In general, a supramolecular species gains more stability as the number of hydrogen bonds increase. In fact, some reports indicate that the binding strength of hydrogen bonded complexes varies linearly with the number of hydrogen bonds present in the overall species.[21] An example of a hydrogen bond array complex commonly discussed in this thesis is the diamidopyridine-thymine complex diagrammed in Figure 1.6. In this case, three hydrogen bonds are formed, which give this complex an association constant of around 1000 M^{-1} in nonpolar solvents, such as methylene chloride. Details about this particular interaction, specifically as it relates to supramolecular polymers, will be discussed in later Chapters.

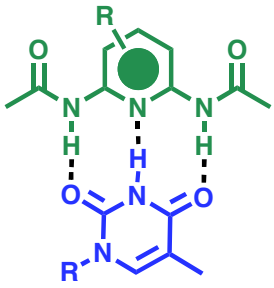

DAP:THY

Figure 1.6. 1:1 DAD-ADA complex formed between diamidopyridine and thymine derivatives.

1.3.3 Metal Coordination

While most metal complexes are simply classified as coordination complexes, with strong covalent character traits (much like the strongest hydrogen bonds), such as directionality, constrained geometry, and electronic orbital overlaps, the metal complexes typically exploited in supramolecular chemistry are at least reversible and usually have at least a partial noncovalent attribute.[18] This is not to imply that the metal complexes discussed in this thesis are noncovalent complexes, but rather that such metal complexes have noncovalent character or at least conduct themselves as a noncovalent complex. As such, metal complexation will be briefly discussed in this introductory portion of the thesis, and a general focus will be kept on metal complexes discussed in the latter part of this thesis.

Metal complexes were previewed in the context of ionic bonding, since many metal complexes arise from interactions between ligands with partial or full negative charges and metals with positive charges. In this manner, many metal complexes function as ionic complexes, in many cases with much stronger bond energies. Numerous examples of metal complexes have been used in supramolecular chemistry. For example, classic "Werner" complexes have been utilized, such as Co and Fe based complexes with ligands being both partially polarized, such as nitrogen based ligands, and fully charged, such as the harder, halide based ligands.[13] In this thesis, metal pincer-type complexes are commonly used in research examples, given their compatibility with a variety of other noncovalent interactions. These metal complexes will be discussed further as the context in which they are presented arises. However, a brief description of the pincer-type complexes utilized in this thesis is presented in Figure 1.7.

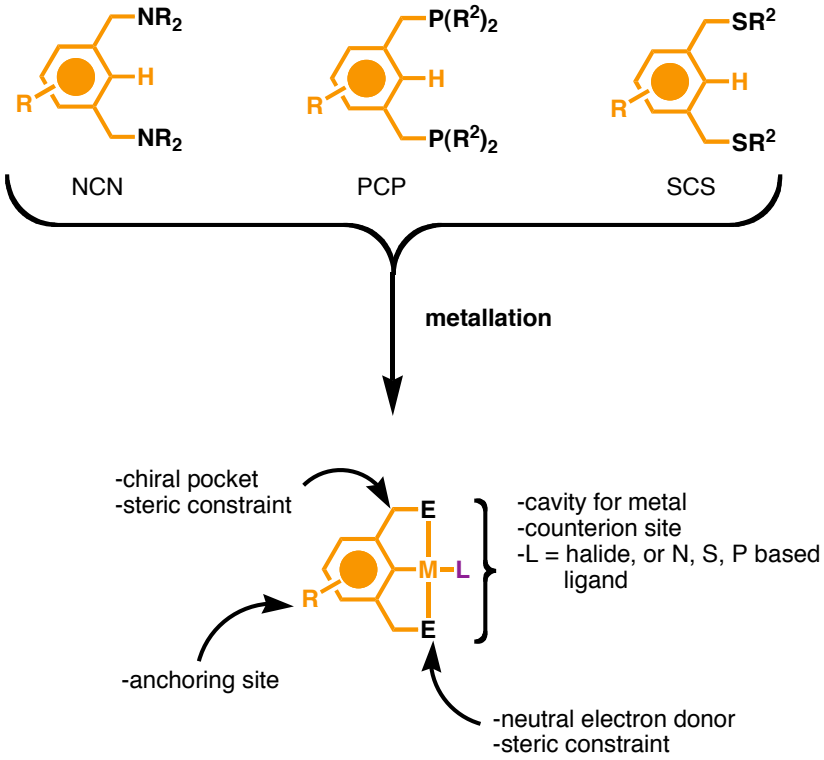

Figure 1.7. Formation and highlighted aspects of Pincer-type complexes.

Pincer-type complexes that have been used in supramolecular chemistry can accommodate nitrogen-carbon-nitrogen (NCN), phosphorus-carbon-phosphorus (PCP), or sulfur-carbon-sulfur (SCS) based ligands, which after metallation produce a pincer type complex in which the metal core is flanked by two neutral (E) electron donors, and coordinated to an anionic aromatic core.[22] The research in this thesis utilizes such complexes on polymer backbones for functionalization and on small molecules for molecular recognition based templated synthesis.

1.3.4 π–system Interactions

Many examples of noncovalent supramolecular chemistry also involve π systems. Interactions in such systems can range from fundamental π–π interactions to more complicated π–anion or cation interactions.[1] The cation π interaction, for example, plays an important role in biology and typically has a bond strength of 5-80 kJ mol^{-1}.[18] A relatively straightforward explanation for the existence of π–interactions exists. Aromatic rings possess a quadrupole moment with at least a partially positive σ-scaffold and a partially negative π cloud above and below the ring plane (this is the reason why the ^{1}H NMR chemical shifts of an aromatic compound resonate so far downfield). As a result, a cation, metal, or oppositely polarized neighboring aromatic compound can be attracted to the aromatic ring when positioned above the center of the π cloud. These interactions can be quite strong as evident from gas-phase binding studies. The gas-phase binding energy of a potassium cation to benzene (80 kJ mol^{-1}) is higher than the binding energy (75 kJ mol^{-1}) of a single water molecule to the same potassium cation![18]

Likewise, aromatic rings can interact with other neighboring aromatic rings through π–π stacking interactions. Two negatively charged π clouds ordinarily repel one another.[23] However, this repulsive force can be overcome in one of two ways. (i) Two or more aromatic components may adopt an edge-to-face orientation, which allows an attraction between the negatively charged face of one aromatic component with the partially positive σ edge of another. (ii) Two or more aromatic components may align themselves with an even more favorable face-to-face orientation, and often one of the aromatic components shifts sideways to further reduce the negative repulsion and align oppositely charged poles. Even stronger π–π stacking interactions are observed when one

aromatic component is electron rich and one is electron poor, in which case significant charge-transfer reactions can take place and can often be identified by UV/vis spectroscopy.[23]

π–π stacking interactions have led to the successful construction of numerous supramolecular species. For example, in the context of this thesis, π–π stacking contributes to the stability of the pseudorotaxane complex shown in Figure 1.3. This is evident not only from the crystal structure, which identifies that the phenyl rings of the **DB24C8** macroring and the corresponding aromatic groups on **DBA$^+$** are in close enough proximity to one another to engage in π–π stacking but also from an examination of the association constants of similar pseudorotaxanes (Figure 1.8). The complex **DB24C8:DBA$^+$** associates the strongest, while similar pseudorotaxanes, such as 24-crown[8]:dibenzylammonium (**24C8:DBA$^+$**) have weaker association strengths due to the absence of the π system on the crown ether macroring.[24]

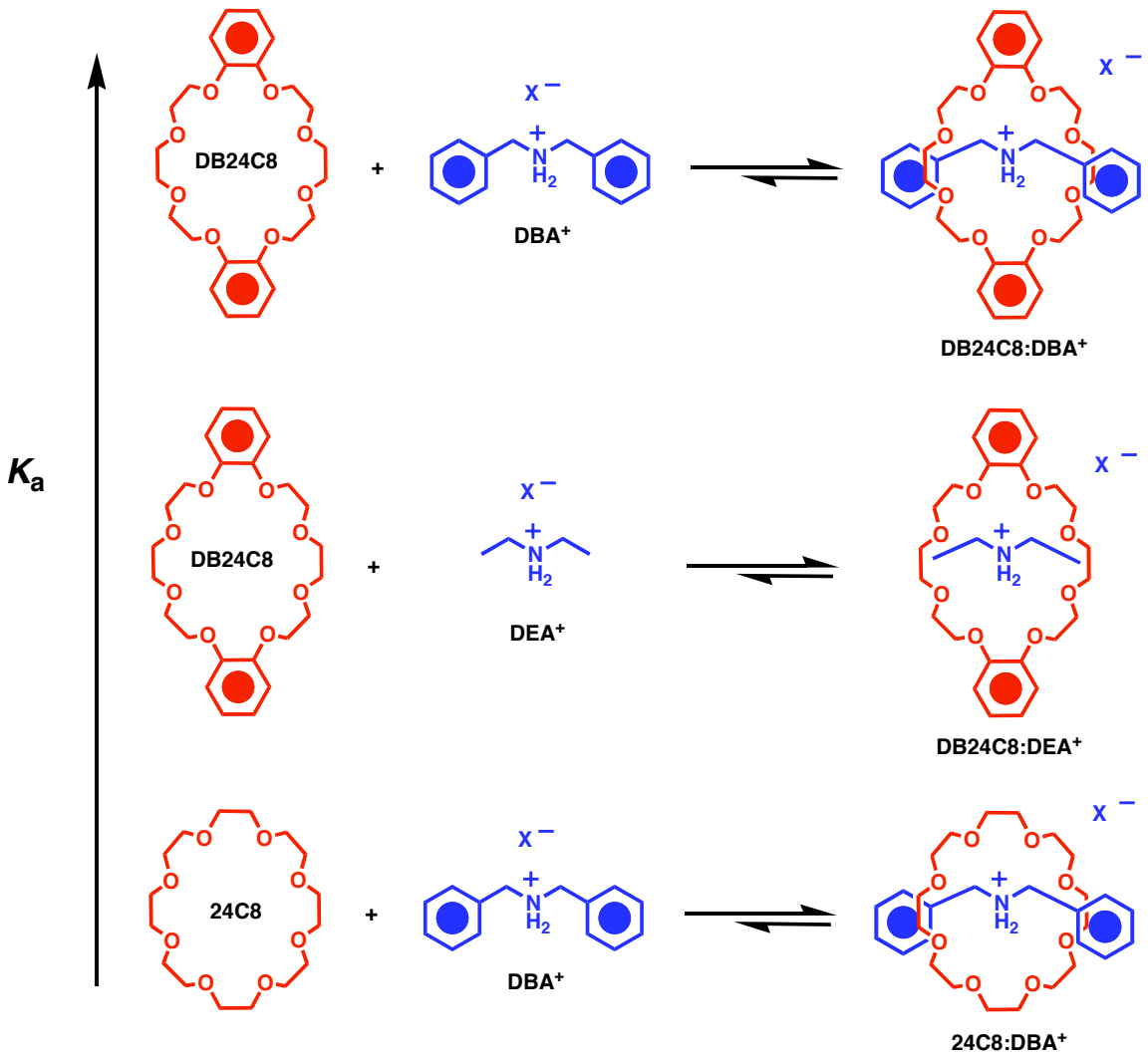

Figure 1.8. Association complexes formed between ammonium cations and 24-C8 macrorings (in $CHCl_3$ or DCM). Specific K_a values have not been reported, only relative scales.

1.3.5 Hydrophobic Interactions

Hydrophobic interactions are generally not exploited in the research presented in this thesis, but a brief discussion of these forces is warranted to demonstrate the environmental susceptibility of supramolecular forces. Hydrophobic forces give rise to the Hydrophobic Effect, which is dependent on the minimization of energy on unfavorable interfaces between polar/protic and unpolar/aprotic molecules.[18] The classic

example stemming from biology is the cell membrane, which is formed with polar head groups pointing outward toward the extracellular matrix and the nonpolar hydrophobic tail groups oriented together forming a membrane.[25]

Hydrophobic forces, unlike forces based generally on electrostatics and charge, are more difficult to characterize thermodynamically. The hydrophobic effect is often explained on the basis of Gibbs Free Energy. If free energy is transferred from a hydrophobic molecule, ΔG is positive, and, at room temperature, ΔH is around zero, and ΔS is of course, negative. In this interpretation, the hydrophobic effect is entropy driven due to the release of free energy from a nonpolar molecule to a more polar solvent. On the other hand, the hydrophobic effect can be viewed from a different thermodynamic perspective. Polar molecules, such as water, generally adopt a configuration that seeks to maximize entropy. The presence of a hydrophobic molecule in such a solution of polar molecules will serve to disrupt at least some of this entropy. This creates a pocket or void in which little to no electrostatic interaction can exist between the nonpolar molecules and their polar counterparts. To counter this effect, polar molecules can push the hydrophobic molecules together forming a tight structure around them and thus leaving a smaller surface area in relation to the total surface area of the nonpolar void regions. This serves to maximize the amount of free polar molecules and thus the entropy. This phenomenon is known as the lipophobicity of polar molecules, which is generally described in terms of water.[26]

Numerous examples of supramolecular chemistry exist in the literature in which the hydrophobic effect has a noncovalent contribution. For example, the hydrophobic effect contributes strongly to the formation of cyclodextrin inclusion complexes.[1] Water

molecules that reside in the interior of an unpolar cavity, such as present in a cyclodextrin, cannot interact with the cavity wall very strongly, because of an essential absence of electrostatic forces in the hydrophobic cavity. If the water molecules are replaced, however, with a guest with less polarity, the water molecules are then free to interact with other water molecules outside the cavity, resulting in a net gain in enthalpy for the whole system. Moreover, as in the previous discussion, entropy changes can also contribute; when water molecules are replaced by one or more guest molecules, the total number of translationally free molecules increases, provided that the size of the guest molecule(s) is at least greater than the size of a water molecule.[27]

1.3.6 Other Weak Interactions

Other noncovalent forces, particularly weaker noncovalent forces, exist and contribute to supramolecular chemistry. Such interactions include van der Waals forces with binding strengths generally less than 5 kJ mol^{-1} that arise when electron clouds are polarized by adjacent nuclei. Van der Waals forces can be thought of as a registration of attractive dispersion interactions, which decrease proportionally to the internuclear distance r, with an r^{-6} dependence and with an exchange repulsion decreasing with an r^{-12} dependence.[18] Similary, forces between multipoles,[28] interactions between nitrogen and halogen atoms,[29] and dihydrogen interactions[30] are weak noncovalent forces than can contribute to supramolecular chemistry.

1.4 Molecular Recognition

A detailed examination of many of the noncovalent forces previously outlined has led to the development of molecular recognition. Singular noncovalent interactions, when placed at appropriate places on a given molecule, can act in unison or in cooperation to form a molecular recognition pair. Most molecular recognition pairs, according to Lehn, involve *molecular information* stored within molecules.[21] Molecular recognition can be divided into two separate subclasses commonly known as dynamic and static molecular recognition.[5] These terms apply generally to abiotic systems, but in biological terms, these terms are generally equivalent to binding cooperativity or the lack thereof. These subclasses are best illustrated in Figure 1.9. In static molecular recognition, one or more components bind together, with each binding event essentially unrelated to the next (this is also referred to in this thesis as "orthogonality"). In simplest terms, this can involve a 1:1 complex formed as depicted in Figure 1.9A. In contrast, dynamic molecular recognition (Figure 1.9B) usually involves a sequence of binding events, with at least one binding mode affecting the other(s). The dynamic nature of these events can result either from binding cooperativity or binding decooperativity. Cooperativity, the lack thereof, or decooperativity can result from a number of structural, physical, or chemical responses from a previous binding event.

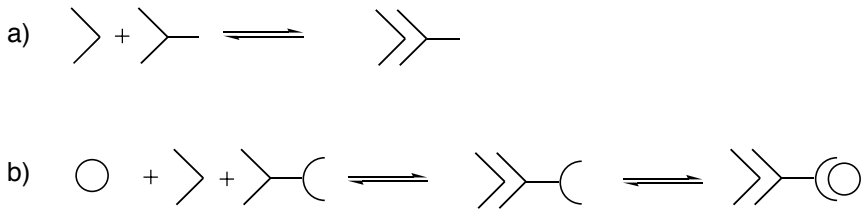

Figure 1.9. Schematic diagram illustration static (a) and dynamic (b) molecular recognition.

For example, in the case of antigen-antibody interactions, binding can be strongly influenced by allosteric effects.[31] In other abiotic examples, cooperativity can arise from a confinement effect.[24] For example, a **DBA$^+$** dimer binds two molecules of **DB24C8**. The first binding event is the weaker of the two, because the crown ether macroring can situate itself on either cationic side of the dimer. In other words, it can float back and forth. In contrast, the second binding event is at least 25 times stronger than the first since the second crown ether can only orient on one cationic site, effectively filling the binding site. In a sense, the second binding event does a better job of confining both equivalents of the crown ether to the ammonium cation, and thus the overall association is greater for the second binding event.

1.4.1 Molecular Complementarity

An important facet of molecular recognition is specificity between interacting molecules, which gives rise to the design of orthogonal supramolecular systems, i.e. a system comprising multiple noncovalent binding components that interact in or on the appropriate molecular partners. Much like Emil Fischer's original analysis,[7,8] supramolecular chemists generally accept the idea that the more specific the molecular recognition pair, the stronger the association strength of that pair.[18] The specificity of a given molecular recognition pair relates not only to the strength of the individual noncovalent bonds involved, but also to the entire electrostratic surface of both engaged molecules. Thus, specificity is a result of both steric fit (based on the individual noncovalent bonding) and a proper match of charge distributions that give rise to a

thermodynamically stable spatial arrangement in which the attractive forces between the two (or more) molecules are maximized and the repulsive forces are minimized. This important point is precisely the reason why supramolecular chemists often encounter challenging obstacles in trying to develop molecular recognition systems with tight binding between neutral components,[32-37] although in recent years, systems developed by Meijer and Zimmerman[15] seem to have at least partially overcome many of these challenges with the use of strongly associated and often self-complementary hydrogen bond arrays. One could argue, however, that these systems are so individually polarized that they should not be classified as "neutral."

1.4.2 Molecular Preorganization and Entropy

An important question to ask in the context of supramolecular chemistry is "how do two or more molecular recognition components bind so strongly to one another while paying the required entropic penalties?" In general, when a molecule binds spontaneously to another, entropic costs must be paid due to the reaction enthalpy released upon binding. In the context of metal coordination, one way to overcome a large entropic barrier is through the chelate effect in which more than one binding site exists on a particular molecule. As such, when a first metal coordination bond is formed, entropic penalties for binding the rest of the molecule are already minimized. Subsequent noncovalent binding events of the two partners then should not suffer the same entropic penalty accrued during the first event. Similar effects in the context of supramolecular chemistry as a whole have been termed macrocyclic and macrobicyclic effects which have been succinctly described by Cram as the "preorganization principle."[38]

1.4.3 Molecular Recognition Examples

Several examples of molecular recognition partners have been developed over the years,[15] and far too many exist to adequately review in this thesis. In each case of molecular recognition, however, there exists a partnership formed between two or more molecular components ultimately relying on an orchestration of individual noncovalent interactions. Among these interactions, which were previously discussed, are relatively weak noncovalent interactions including single hydrogen bonds and van der Waals interactions, among others. Stronger interactions include arrays of hydrogen bonds and weak metal coordination interactions, while the strongest of noncovalent interactions generally include ionic interactions and metal coordination interactions (albeit with strong covalent character traits).

Early examples of noncovalent partners later classified as molecular recognition partners include crown ether-cation interactions.[1] For example, organic chemists had observed early in the development of the Williamson ether synthesis that the addition of a crown ether of an appropriate size to accept a corresponding cation originating from the alkoxide species could increase the nucleophilicity of the alkoxide.[21] Other early examples include cryptands, cavitands, calixarenes,[39] and various other macrocyclic host-guest complexes involving metal coordination, hydrogen bonding, ionic interactions, or various combinations thereof.[40]

This thesis is primarily concerned with three unique types of molecular recognition partners (shown in Figure 1.10 in order of association strength). The synthesis and applications of these molecular recognition partners in or on polymer

systems or oligomeric systems is the central theme of this thesis. These molecular recognition components have been briefly discussed, and will be discussed later in the context in which they are presented.

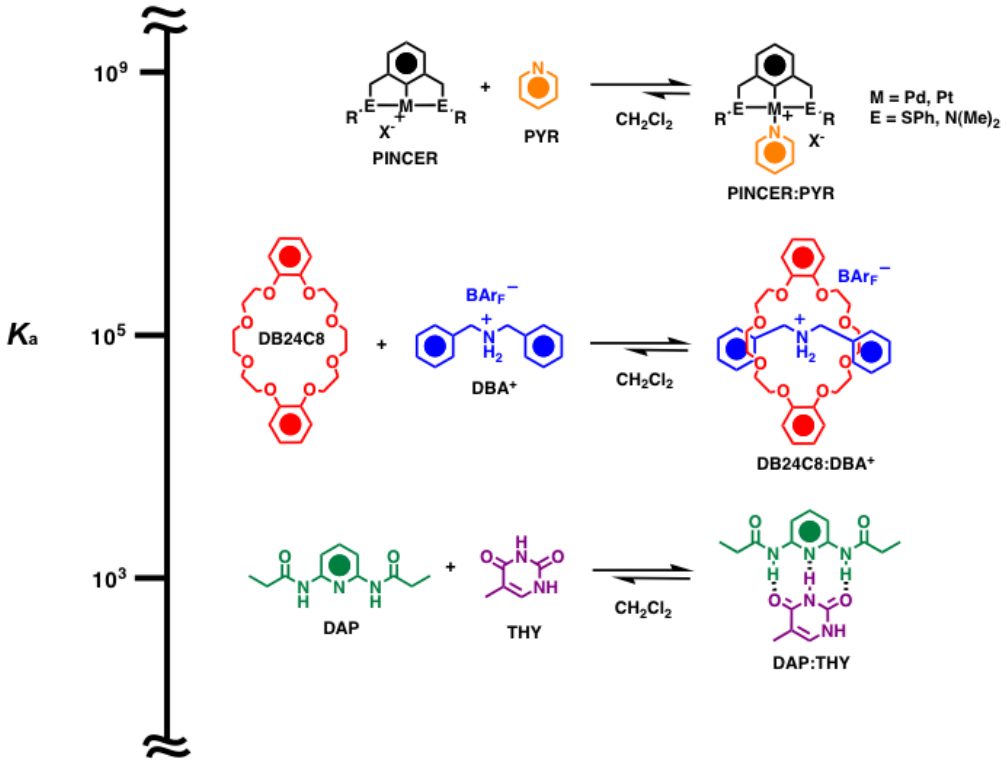

Figure 1.10. Three types of molecular recognition partners explored in this thesis.

1.5 Self-Assembly

"Supramolecular interactions," "self-assembly," "molecular recognition," and "noncovalent interactions" are general terms prominently used in the field of supramolecular chemistry. While these terms are often used interchangeably in the literature, several distinctions should be made to delineate between these terms.

Particularly since the liberal use or misapplication of one or more of these terms has resulted in extensive debates at conferences and in the literature.[5] This distinction is probably best described by the hierarchy diagrammed in Figure 1.1.

The term "self-assembly," is perhaps becoming the most limited phenomena in the field of supramolecular chemistry. George Whitesides defines "self-assembly" succinctly as "the autonomous organization of components into patterns or structures without human intervention."[5] This is not to say that mixing components in solution would be construed as "human intervention," but rather that the assembly process itself occurs without outside intervention. Obviously, one can see that this definition, even in its strictest sense could be applied broadly. However, many in the field believe that self-assembly does *not* include processes such as the association of organic molecules in solution or the growth of quantum dots on solid substrates.[5] Rather, "self-assembly" should be limited to processes that involve coded information embedded within or on individual molecular components. In general, coded information can range from noncovalent forces such as electrostatic interactions to van der Waals forces. However, all of these forces must cooperate in some fashion such that a super organized or patterned structure can form. Six examples of self-assembly that fall under this interpretation are shown in Figure 1.11. Additionally, further examples of self-assembly and applications thereof are summarized in Table 1.2.

Table 1.2 Examples of self-assembly and applications (adapted from ref. 5)

Entry	Application
Molecular crystals	Materials, optoelectronics[3, 4, 41]
Self-assembled monolayers	Nanoelectronics[42]
Lipid bilayers	Biomembranes[25]
Liquid crystals	Displays[43]
Ant Swarms, Fish schools	Computation models[44, 45]

While self-assembly in its pure sense is not exploited in this thesis, the use of the term self-assembly is often applied to molecular recognition partners in which data suggest that an actual assembly forms, and the interaction is more than simply an orchestra of single noncovalent interactions, such as, for example, the interaction leading to the pseudorotaxane shown in Figure 1.10.

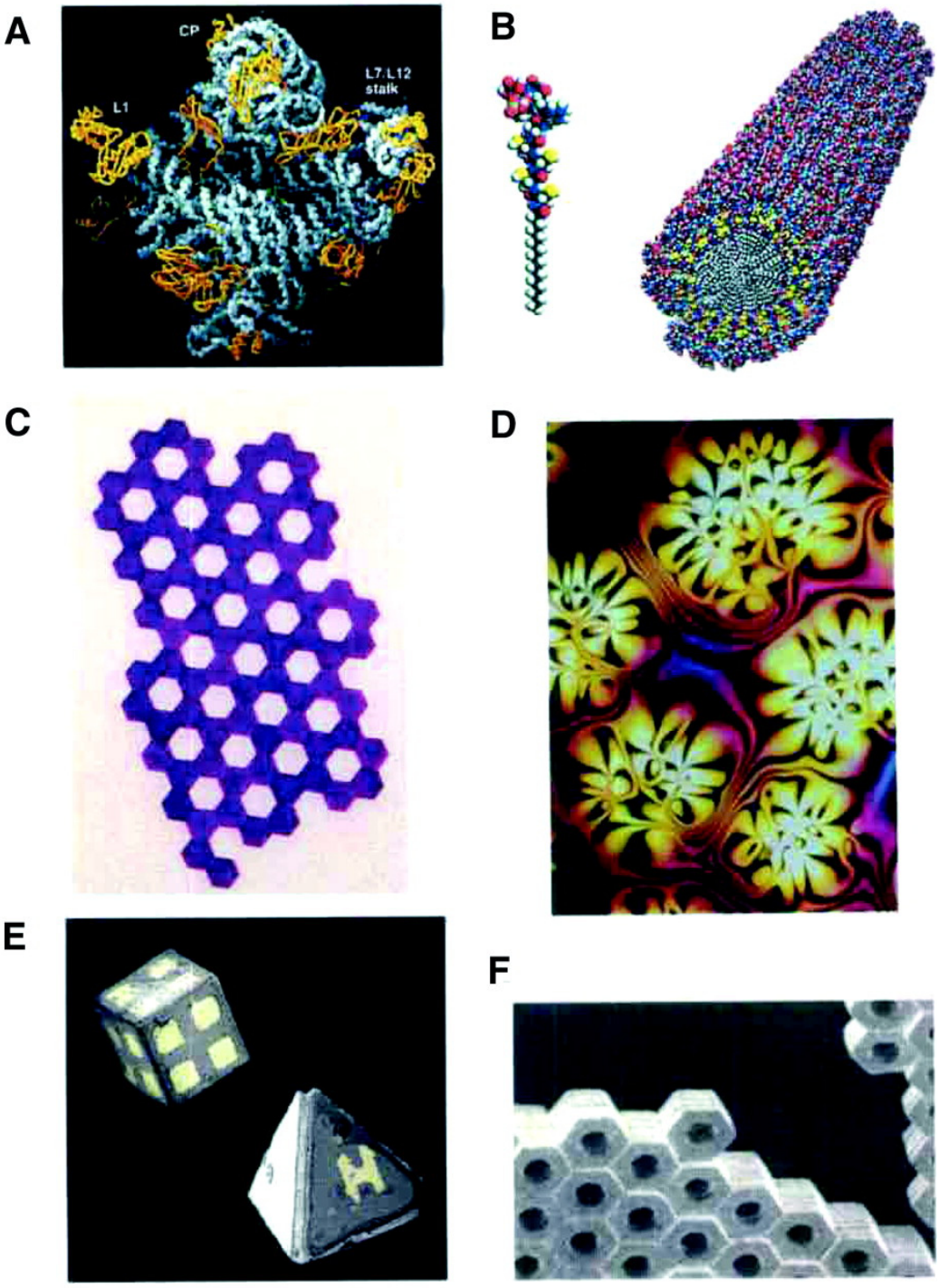

Figure 1.11. (A) Ribosome crystal structure; (B) Peptide amphiphiles; (C) Polymeric plates; (D) Liquid crystal thin film; (E) Micrometer polyhedra; (F) Micrometer plates. [Figure adapted from ref. 5]

1.6 Conclusion

Supramolecular systems are defined by individual molecular properties that give rise first to one or more single, discreet noncovalent interactions, followed optionally by an array or cooperation among each individual interaction to produce molecular recognition. Molecular recognition, then, can lead to a fully organized, patterned, or otherwise self-assembled structure. Noncovalent interactions leading to molecular recognition include ionic and electrostatic interactions, hydrogen bonding, metal coordination interactions (although these may be more appropriately characterized as dative or coordinative), π–π stacking interactions, hydrophobic interactions, and weaker forces such as van Der Waals interactions. In many molecular recognition systems, combinations of the aforementioned forces contribute to the overall thermodynamically stabilized and/or preorganized structure. In the chapters that follow, an emphasis on molecular recognition in polymer and oligomeric systems is discussed first with an overview of molecular recognition on the side-chains of polymers followed by several research applications of these polymers and oligimers.

1.7 References

1. Lehn, J.-M., Cryptates: inclusion complexes of macropolycyclic receptor molecules. *Pure Appl. Chem.* **1979,** *50*, 871.

2. Lehn, J.-M., Supramolecular Chemistry: Receptors, Catalysts, and Carriers. *Science* **1985,** *227*, 849.

3. Isaacs, L.; Chin, D. N.; Bowden, N.; Xia, Y.; Whitesides, G. M., in *Supramolecular Technology*. Wiley: New York, 1999.

4. Philp, D.; Stoddart, J. F., Self-Assembly in Natural and Unnatural Systems. *Angew. Chem. Int. Ed.* **1996,** *35*, 1154.

5. Whitesides, G. M.; Grybowski, B., Self-Assembly at All Scales. *Science* **2002,** *295*, 2418.

6. Werner, A., *Zeitschr. Anorg. Chem.* **1893,** *3*, 267.

7. Fischer, E., *Ber. Deutsch. Chem. Ges.* **1894,** *27*, 2985.

8. Behr, J.-P., *The Lock and Key Principle. The State of the Art - 100 Years On*. Wiley: Chichester, 1994.

9. Koshland Jr., D.E., Application of a Theory of Enzyme Specificity to Protein Synthesis. *Proc. Natl. Acad. Sci. USA* **1958,** *44*, 98.

10. Ehrlich, P., *Studies on Immunity*. Wiley: New York, 1906.

11. Wolf, K. L.; Frahm, H.; Harms, H., *Z. Phys. Chem. (B)* **1937,** *36*, 237.

12. Lehn, J.-M., *Supramolecular Chemistry*. Verlag Chemie: Weinheim, 1995.

13. Lehn, J.-M., *Supramolecular Chemistry: Concepts and Perspectives*. Wiley-VCH: Weinhein, 1995.

14. Schneider, H.-J., *Principles and Methods in Supramolecular Chemistry*. Wiley: New York, 2000.

15. Steed, J. W.; Atwood, J. L., *Supramolecular Chemistry*. Wiley: New York, 2000.

16. Vögtle, F., *Supramolekulare Chemie*. Stuttgart: Teubner, 1992.

17. Hopwood, S. J., *The Growth of Physical Science*. Cambridge University Press: Cambridge, 1948.

18. Schalley, C., *Analytical Methods in Supramolecular Chemistry*. Wiley-VCH: Weinheim, 2007.

19. Jeffrey, G. A., *An Introduction to Hydrogen Bonding*. Oxford University Press: Oxford, 1997.

20. Ciferri, A., *Supramolecular Polymers*. 2 ed.; CRC Press: Boca Raton, 2005.

21. Schneider, H.-J.; Durr, H., *Frontiers in Supramolecular Organic Chemistry and Photochemistry*. 1991.

22. Albrecht, M.; Koten, G. v., Platinum Group Organometallics Based on Pincer Complexes: Sensors, Switches, and Catalysts. *Angew. Chem. Int. Ed.* **2001,** *40*, 3750.

23. Hunter, C. A.; Sanders, J. K. M., The nature of π–π interactions. *J. Am. Chem. Soc.* **1990,** *112*, 5525.

24. Aricó, F.; Badjic, J. D.; Cantrill, S. J.; Flood, A. H.; Leung, K. C.-F.; Liu, Y.; Stoddart, J. F., Templated Synthesis of Interlocked Molecules. *Topics in Current Chemistry* **2005,** *249*, 203.

25. Jones, M. N.; Chapman, D., *Micelles, Monolayers, and Biomembranes*. Wiley-Liss: New York, 1995.

26. I.U.P.A.C., Hydrophobic Interaction. In *Compendium of Chemical Terminology*, Vol. Internet Ed. .

27. Szejtli, J., *Cyclodextrin Technology*. Springer: New York, 1988; Vol. 1.

28. Paulini, R.; Müller, K.; Diederich, F., Orthogonal Multipolar Interactions in Structural Chemistry and Biology. *Angew. Chem. Int. Ed.* **2005,** *44*, 1788.

29. Auffinger, P.; Hays, F. A.; Westhof, E.; Ho, P. S., Halogen bonds in biological molecules. *Proc. Natl. Acad. Sci. USA* **2004,** *101*, 16789.

30. Crabtree, R. H.; Siegbahn, P. E. M.; Eisenstein, O.; Rheingold, A. L.; Koetzle, T. F., A New Intermolecular Interaction: Unconventional Hydrogen Bonds with Element-Hydride Bonds as Proton Acceptor. *Acc. Chem. Res.* **1996,** *29*, 348.

31. Shinkai, S.; Ikeda, M.; Sugasaki, A.; Takeuchi, M., Positive Allosteric Systems Designed on Dynamic Supramolecular Scaffolds: Toward Switching and Amplification of Guest Affinity and Selectivity. *Acc. Chem. Res.* **2001,** *34*, 494.

32. Beer, P. D.; Gale, P. A., Anion Recognition and Sensing: The State of the Art and Future Perspectives. *Angew. Chem. Int. Ed.* **2001,** *40*, 487.

33. Bowman-James, K., Alfred Werner Revisited: The Coordination Chemistry of Anions. *Acc. Chem. Res.* **2005,** *38*, 671.

34. Lavigne, J. J.; Anslyn, E. V., Sensing A Paradigm Shift in the Field of Molecular Recognition: From Selective to Differential Receptors. *Angew. Chem. Int. Ed.* **2001,** *40*, 3119.

35. Schmidtchen, F. P.; Berger, M., Artificial Organic Host Molecules for Anions. *Chem. Rev.* **1997,** *97*, 1609.

36. Seel, C.; Galán, A.; Mendoza, J. d., Supramolecular Chemistry II — Host Design and Molecular Recognition. *Top. Curr. Chem.* **1995,** *175*, 101.

37. Sessler, J. L.; Davis, J. M., Sapphyrins: Versatile Anion Binding Agents. *Acc. Chem. Res.* **2001,** *34*, 989.

38. Cram, D., Preorganization - From Solvents to Spherands. *Angew. Chem. Int. Ed.* **1986,** *25*, 1039.

39. Lehn, J.-M., **1973,** *16*, 1.

40. Izatt, R. M.; Christensen, J. J., *Progress in Macrocyclic Chemistry*. Wiley: New York, 1979.

41. Desiraju, G. R., *Crystal Engineering: The Design of Organic Solids*. Elsevier: New York, 1989.

42. Aizenberg, J.; Black, A. J.; Whitesides, G. M., Control of crystal nucleation by patterned self-assembled monolayers. *Nature* **1999**, *398*, 495.

43. Loudet, J.-C.; Barois, P.; Poulin, P., Colloidal ordering from phase separation in a liquid- crystalline continuous phase. *Nature* **2000**, *407*, 611.

44. Bonabeau, E.; Dorigo, M.; Theraulaz, G., Inspiration for optimization from social insect behaviour. *Nature* **2000,** *406*, 39.

45. Shimonoyama, N.; Sugawara, K.; Mizuguchi, T.; Hayakawa, Y.; Sano, M., Collective Motion in a System of Motile Elements. *Phy. Rev. Lett* **1996,** *76*, 3870.

CHAPTER 2

Molecular Recognition on the Side-Chains of Polymers

2.1 Abstract

The design and synthesis of multifunctionalized, architecturally controlled polymers is a prerequisite for a variety of future applications of polymeric materials. Based on Nature's use of self-assembly in the creation of biomaterials, this Chapter describes concepts that were developed over the past five years and that utilize noncovalent interactions such as hydrogen bonding, ionic interactions, electrostatic interactions, metal coordination, and π–π stacking in the modification of side-chain copolymers to obtain multi-functional polymeric materials, induce polymer morphology changes, and influence bulk-polymer properties.

2.2 Introduction

An important aspect of this thesis is the utilization of polymers bearing side chain molecular recognition components in applications ranging from improved synthetic methods to materials and surface chemistry. This Chapter relates the basic concepts discussed in Chapter 1 to polymeric systems developed in the Weck laboratories and provides a context for the rest of the thesis by examining several approaches to these polymers and applications thereof.

Current research in polymer chemistry has been recently described as highly interdisciplinary with a large number of new research foci ranging from nanoscience to bio-related materials.[1] Challenges in polymer science have been changing dramatically

over the past two decades, specifically in the ever-expanding field of polymer synthesis. In particular, three basic research efforts have fascinated the synthetic polymer chemist since the 80's: (i) the development of highly controlled and living polymerization methods, (ii) investigations into new catalysts that allow for full stereo-control during polymerizations, and (iii) the rapid synthesis of multifunctional copolymers.[2] The first two research foci are still areas of intense investigation but have resulted already in a number of impressive accomplishments. Consider, for example, the developments in controlled polymerization methods. Twenty years ago, the only widely useful living polymerization method was ionic polymerization.[2]

Today, polymerization methods such as ring-opening metathesis polymerization (ROMP)[3] and controlled radical polymerization[4] are standard methods in every polymer chemists' synthetic repertoire. Similar advances in the design and synthesis of stereospecific catalysts for a wide variety of polymerization methods have been accomplished.[2] Ziegler Natta polymerizations, for example, can be carried out in a highly stereoregular fashion using a wide variety of early, and more recently, late transition metals.[5] Another example is the stereoregular ring-opening polymerization of lactides resulting in the formation of poly(lactic acid), an important bio-renewal and biodegradable polymer for biomedical applications.[6] In contrast, the third research focus, the easy and rapid synthesis of multifunctional copolymers is lacking behind.

The syntheses of highly functional polymers and copolymers are key for a wide variety of materials applications ranging from organic light-emitting diodes and photovoltaic cells to drug delivery vehicles and tissue engineering. Over the past century, polymer scientists have used covalent approaches to synthesize multifunctional

polymers.[2] While highly successful, covalent chemistry is time consuming, often low yielding, and does not allow for the employment of rapid prototyping and optimization methods. If Nature would have used covalent chemistry for the development of biopolymers such as DNA, RNA, and proteins, we might not have the high degree of sophistication on earth today that we take for granted. Nature uses other concepts in addition to covalent chemistry to 'screen' biopolymers for activity and to optimize them. Nature's principles are based on a limited number of building blocks to achieve a high degree of complexity in materials and rely on *weak and reversible interactions* between building blocks to introduce function and diversity.[7] Nature utilizes these noncovalent interactions to create vast libraries of biological materials in a simultaneous multi-step self-assembly process that is reversible, selective, self-healing, and spontaneous. Over the past twenty years, polymer chemists have started to learn how to mimic Nature's use of noncovalent chemistry in polymer science resulting in the foundation of supramolecular polymer science.

Supramolecular polymer chemistry started as an independent field in the 1980's mainly based on the work of Jean-Marie Lehn,[8] and the history of this development is surveyed in Chapter 1. Since then, a number of research groups have developed impressive strategies towards the synthesis, characterization and use of supramolecular polymers. In general, the field can be divided into two categories: (i) main-chain supramolecular polymer science, *i.e.* the weak interaction(s) reside(s) in the polymer backbone thereby noncovalently connecting monomer units, oligomers and/or polymers and (ii) side-chain supramolecular polymers, *i.e.* the noncovalent interaction(s) is(are) used to either functionalize and/or cross-link the covalent polymer backbone thereby

creating highly functionalized polymers with tailorable properties. This Chapter will concentrate on the second strategy, side-chain functionalized supramolecular polymers, and describe current approaches to noncovalently side-chain functionalized polymers with an emphasis on multifunctionalization.

2.2 Monofunctionalization via Side-chain Molecular Recognition

A first approach in among side-chain supramolecular chemists was the attempt at polymer functionalization using a single molecular recognition component or receptor. The central goal was to monofunctionalize a polymeric receptor at each repeating unit with a small molecule substrate (Scheme 2.1). This strategy, in contrast to typical covalent approaches, allowed for the production of different types of functional homopolymers from the same, generic polymeric precursor (Scheme 2.1).

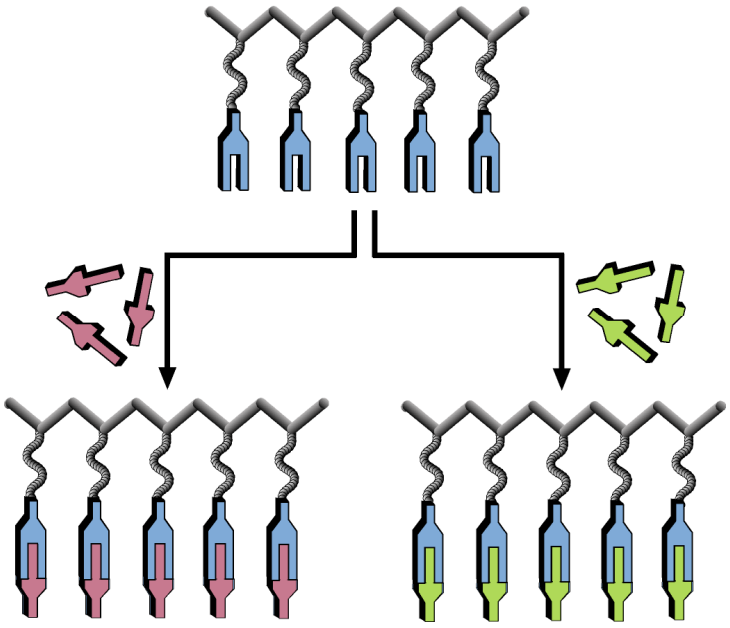

Scheme 2.1. Noncovalent synthesis of different polymers from a generic polymer backbone.

2.3 Monofunctionalization *via* Hydrogen Bonding

The majority of reports on the monofunctionalization of polymers rely on hydrogen bonding as the assembly mechanism.[9, 10] The versatility of hydrogen bonding in polymer functionalization is owed primarily to the responsiveness of these bonds. Hydrogen bonds can be manipulated with a variety of external stimuli, including temperature, solvent, and pH.[9] While single hydrogen bonds are fairly weak (2-5 kcal/mol), arrays of multiple hydrogen bonds can be significantly stronger, with association constants approaching 10^9 M^{-1} (in non-polar solvents) for some quadruple hydrogen bonded structures (Figure 2.2).[9]

Self-complementary systems, such as ureidopyrimidone (**UPy_2**) are undesirable for polymer functionalization since they result in the uncontrolled crosslinking of polymers and not in the controlled functionalization of the materials.[9] Therefore, researchers have focused their attention on non self-complementary recognition pairs such as the diaminopyridine:thymine (**DAP:THY**) interaction, *i.e*. they have focused on hydrogen bond arrays originating from functional groups that have a low tendency to self-dimerize in non-polar solvents ($K_d < 50$ M^{-1}).[9]

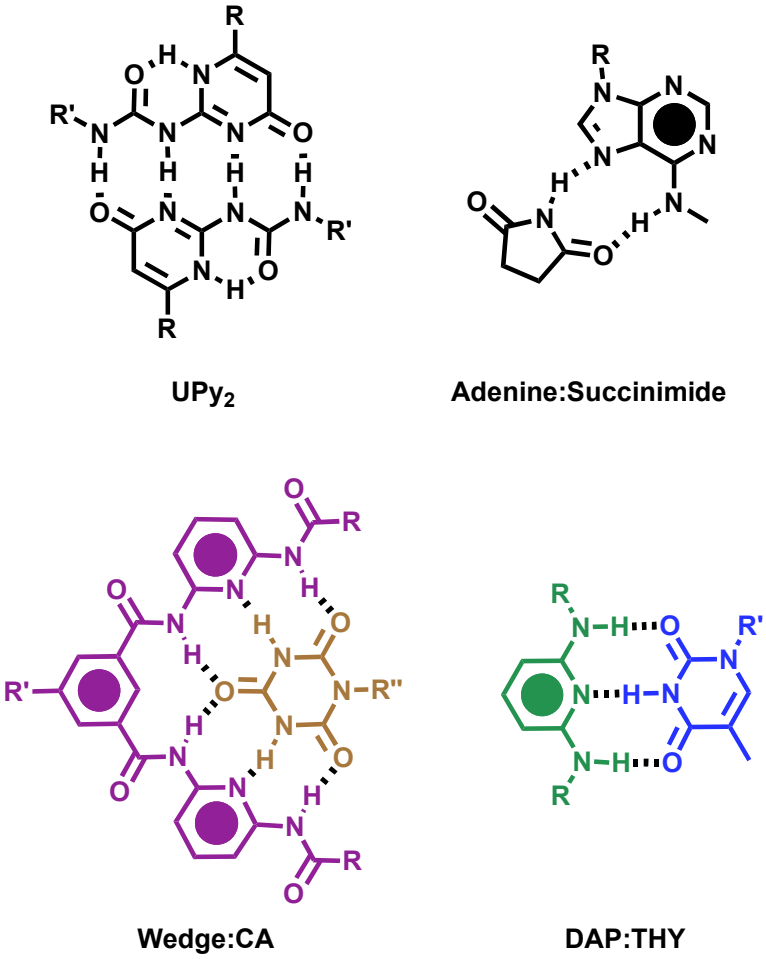

Figure 2.1. Complementary hydrogen bonding pairs frequently used in supramolecular assemblies.

Kato and Fréchet pioneered early work involving hydrogen bonding based functionalization of polymers to synthesize liquid crystalline materials.[11] While these studies are instrumental to the field, they have been reviewed extensively before[11] and the field has moved to more general functionalized systems ranging from nanomaterials to biomimetic materials.[12, 13]

Among the leading research groups working on side-chain supramolecular polymer functionalization is the group of Rotello. The majority of their contributions are based on the noncovalent functionalization of polymers with small molecules via

hydrogen bonding. The Rotello group coined the phrase "plug and play" to describe this modular hydrogen bonding functionalization strategy.[15] The 'plug and play' approach uses noncovalent synthesis to expand organic polymers into functional composite materials using a variety of small molecules for functionalization which can be used to influence bulk material properties.[16] Among the first examples was the functionalization of a diaminotriazine-bearing poly(styrene) (**1**) with flavin (**2**) through a triple, non self-complementary hydrogen bond array (Scheme 2.2).[14] In this case, the polymer morphology changed from a folded state (due to triazine dimerization) to a fully unfolded state (**1:(2)$_n$**) upon the introduction of flavin. In addition, by using spin casting to kinetically trap host-guest complexes in poly(styrene) films, the Rotello group was able to demonstrate the recognition of guests in various polymeric host systems.[15] This methodology was then expanded further by Rotello into nanoscience with the development of the "brick and mortar" strategy.[17] For example, poly(styrene)s (mortar) functionalized with terminal thymine groups were hydrogen bonded to gold nanoparticles (bricks) containing complementary diaminopyridine receptors. These polymer-gold nanoparticle assemblies served then as the basis for the exploration of multivalency in recognition induced polymersomes (RIPs).[17]

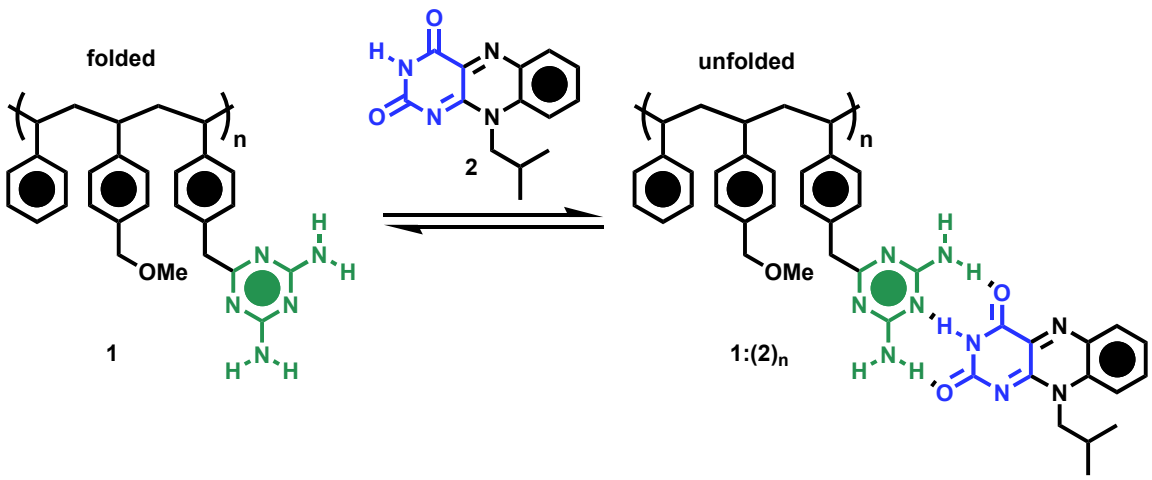

Scheme 2.2. Hydrogen bonding between diaminotriazine functionalized copolymer and flavin.

Similarly, the research efforts of the Weck laboratories have focused on rapidly optimizing materials via functional polymer libraries. The objectives were two-fold; (i) the employment of a fully functional group tolerant and living polymerization method that results in highly controllable and well-defined polymers and (ii) the use of a recognition unit that will allow for high yielding functional group attachment during the noncovalent functionalization steps. To achieve the first objective we employed ROMP, a living and fully functional group tolerant polymerization method.[3] Objective two was met with the introduction of *N*-butylthymine (**NBT**) onto both diaminopyridine (**3**) and diaminotriazine polymeric receptors (Scheme 2.3).[18] These diaminopyridine (**3:(NBT)$_n$**) and diaminotriazine functionalized polymers were then self-assembled with thymine-based molecules to create highly functionalized polymers (**3:(NBT)$_n$**). The presence of the polymer did not significantly impact the association constant between the recognition partners, and it was possible to tune the polymer properties by adding small molecule substrates to the polymeric receptors.

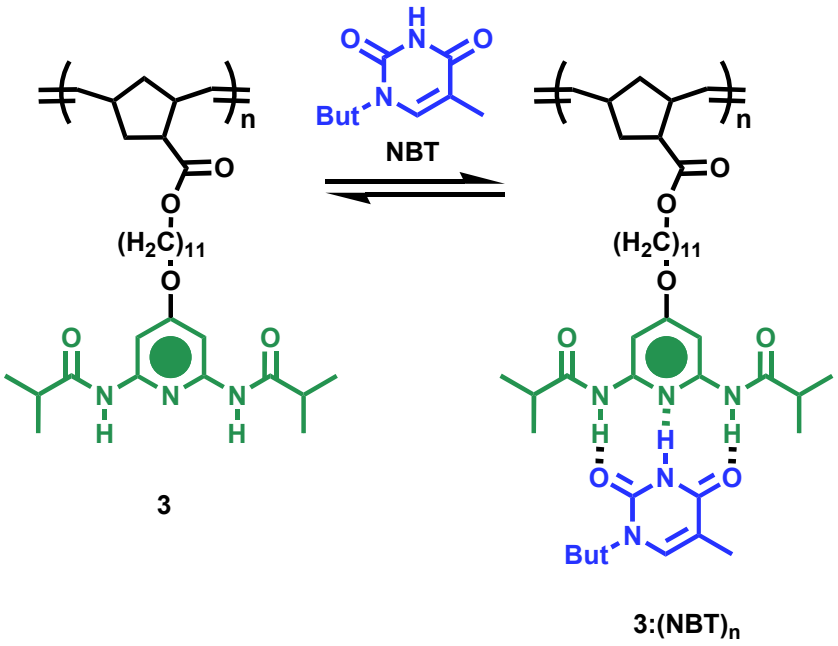

Scheme 2.3. Noncovalent functionaliziation of diaminopyridine-based polymers with complementary thymine substrates.

While self-complementary hydrogen bonding systems are undesirable for polymer functionalization, such systems can be used to influence polymer morphology. Using ROMP, the Sleiman group synthesized adenine functionalized copolymers that are able to fold into cylindrical morphologies arising from the self-complementary of the adenine units.[19] A similar self-complementary backbone was explored further with a series of triblock copolymers containing diacetoamidopyridine and its complementary dicarboximide.[20] Sleiman reported that varying the triblock sequence and ratio resulted in different self-assembled architectures. These differences in properties were only observed in the hydrodynamic radii without real control over the types of aggregations formed.[20]

2.4 Side-chain Functionalization via Metal Coordination

The second class of noncovalent (or partially noncovalent) interactions that have been employed in supramolecular polymer functionalization is metal coordination. Despite the extensive use of metal coordination in main-chain supramolecular polymers,[21] its use for the functionalization of side-chain supramolecular polymers has been explored extensively only in the past five years. While hydrogen bonding is a relatively weak interaction, metal coordination is a significantly stronger binding interaction and yet can still be manipulated by external media, such as solvent and competitive coordinating ligands. An obvious place to start investigating the viability of polymerizable metal complexes, and polymers functionalized through metal coordination are pyridyl-based systems, since a number of pyridine-based ligands are commercially available and many pyridine-based ligands can be structurally modified. Moreover, pyridyl based complexes are prominent as actors in various materials including light-emitting materials and solar cells.[22] Specifically, bipyridines (bpy) and terpyridines (trpy) are desirable since they can act as π acceptors to stabilize various metal oxidation states and are known to coordinate a variety of metals. We and others have explored the polymerization behavior of various norbornene-based transition metal complexes containing bpy monomers that can be polymerized via ROMP.[22, 23] Norbornene based monomers containing (tris-bpy) ruthenium (II) (**5**), (bis-bpy) palladium (II) (**6**), and heterolyptic ruthenium complexes (**4**) (Figure 2.2) were synthesized and polymerized. Similarly, Ru(II) tris bpy block copolymers synthesized by Sleiman were found to self-assemble in acetonitrile/toluene solutions into micellar aggregates with luminescent properties similar to the monomeric analogues.[22]

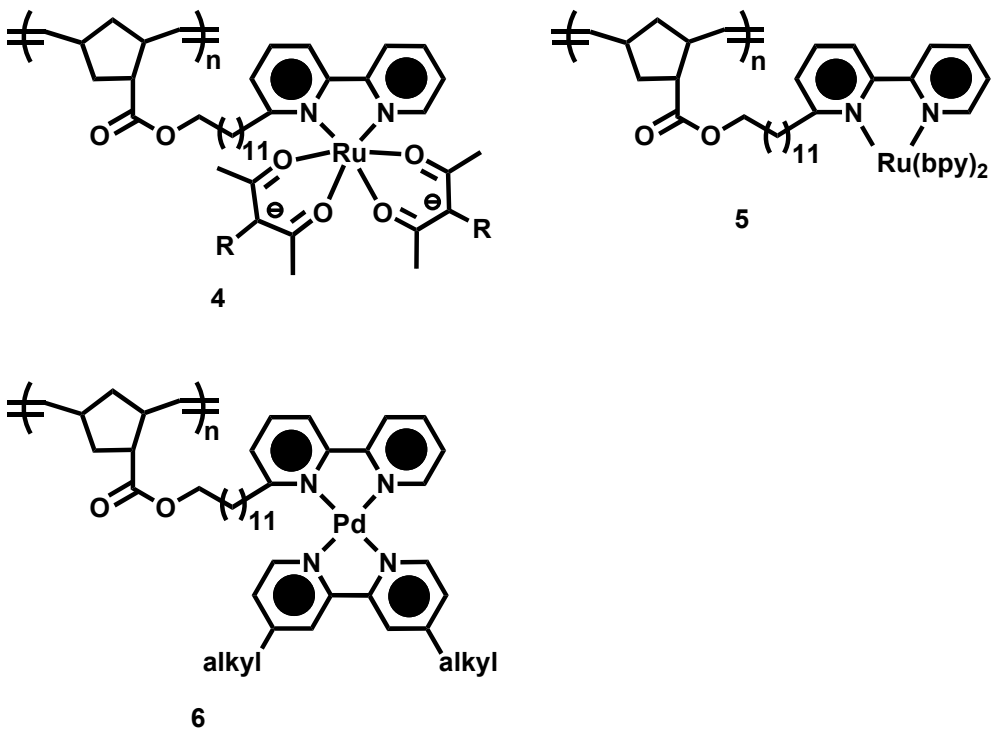

Figure 2.2. Bipyridine containing polymers reported in the literature.

While ROMP has been highly successful in producing well-defined polymers containing pyridyl based metal complexes, other polymerization methods have also been investigated. Tew and Schubert have demonstrated the controlled radical polymerization of trpy containing monomers to yield trpy functionalized poly(styrene) and poly(acrylate) copolymers. Postpolymerization modification via metal coordination of the copolymers proved to be a versatile route to polymers functionalized with metal complexes.[24-27]

Pincer type complexes containing platinum group metals have also become versatile tools in supramolecular science.[28] Van Koten and others have used pincer complexes as supramolecular synthons for a variety of applications in supramolecular chemistry and catalysis.[28] Covalent tethering of pincer complexes to polymers can give

rise to versatile and responsive materials via simple noncovalent functionalization. In 2002, we reported the first side-chain pincer functionalized polymer (**7**) that could be functionalized easily and quantitatively with pyridines (**9**) and nitriles (**10**) resulting in the formation of fully soluble and highly functionalized metal-coordination polymers (**8:(9)$_n$, 8:(10)$_n$**) (Scheme 2.4).[29]

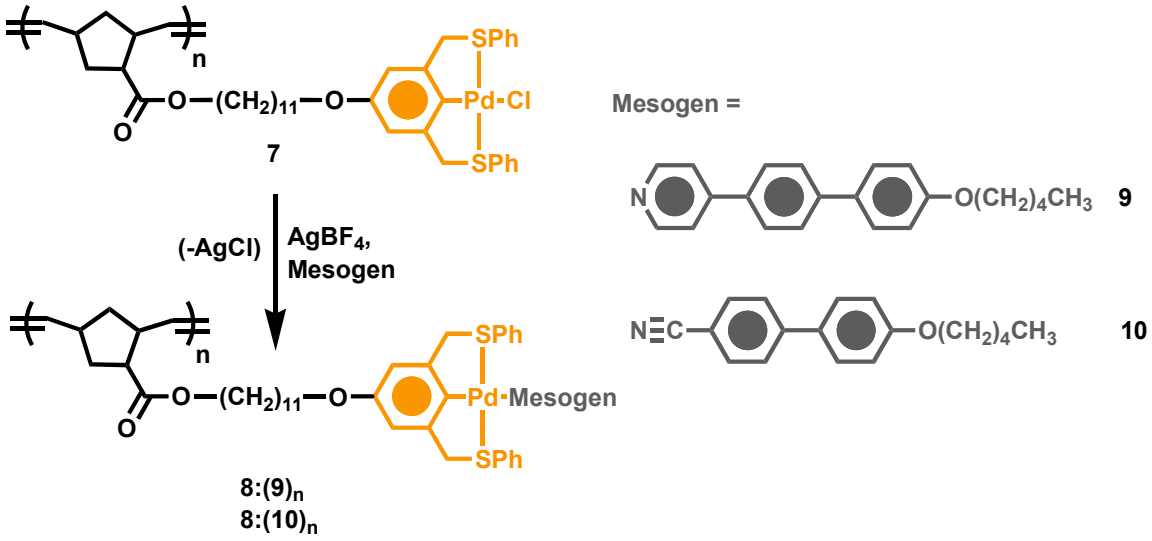

Scheme 2.4. Formation of polymeric liquid crystals through the noncovalent functionalization of pincer containing homopolymers.

While we and others have shown that rapid functionalization of polymers can be accomplished via side-chain self-assembly by either hydrogen bonding or metal coordination, our ultimate goal lies in extending these techniques to incorporate multiple functionalities for highly complex materials. However, a reoccurring problem we encountered in using poly(norbornene)s as scaffolds for noncovalent polymer functionalization was an inability to control the polymerization rate of *endo*/*exo* norbornene mixtures. To overcome this problem, we employed isomerically pure *exo*-

norbornene esters as monomers. We not only obtained efficient and controlled polymerizations of all functionalized monomers but were also able to polymerize norbornenes containing Pd(II) pincer complexes and/or diaminopyridine groups in a living fashion.[30] This was an important step in advancing our methodology into more complicated systems and enabled full architectural control in the next generation of noncovalently functionalized polymers.

2.5 Multifunctionalization via Side-chain Molecular Recognition

In the previous section we have outlined some examples where scientists have used noncovalent interactions to produce monofunctional polymers. One remaining challenge is the development of *abiotic* systems with non-biological functions that rival Nature's complexity.[8] An important problem in polymer chemistry is one that Nature probably encountered a long time ago: the production of multifunctional polymeric architectures with narrow polydispersities. Years of research have been devoted to create functional group tolerant catalysts and living polymerization techniques. However, such covalent approaches often fall short of natural analogues that utilize noncovalent interactions. Therefore, we and others began to envision noncovalent multifunctionalization strategies as simple alternatives to covalent approaches towards multifunctional polymers.

A number of groups have taken advantage of multiple types of noncovalent interactions to produce supramolecular structures based on both natural and non-natural recognition motifs. Metal coordination in concert with hydrogen bonding has been used to synthesize dendrimers[31] and supramolecular polymers.[32] Both hydrogen bonding and

ionic interactions have been used in the synthesis of thermotropic liquid-crystals,[33] self-organizing polymeric materials,[34] interwoven supramolecular arrays,[35] electrochemical switchable dyes,[36] molecular elevators,[37] and functionalized surfaces.[38]

While these are examples of supramolecular structures formed through multiple types of noncovalent interactions, the use of different types of interactions on the side-chains and in the main-chains of polymers was not demonstrated when we started investigating this strategy six years ago in the Weck group.[13] This was surprising given that noncovalently functionalized copolymers can potentially minimize many of the problems associated with traditional covalent copolymer synthesis.[39] For instance, multiple functionalities can be introduced noncovalently onto a copolymer with few side-reactions. Side-reactions that might occur can be corrected, since the multi-functionalized polymer has the ability to "self-heal". We envisaged a strategy that would allow for the functionalization of a single polymer backbone bearing noncovalent receptors with different types of substrate motifs (Scheme 2.5) thereby creating fully functionalized copolymers fast and efficiently.

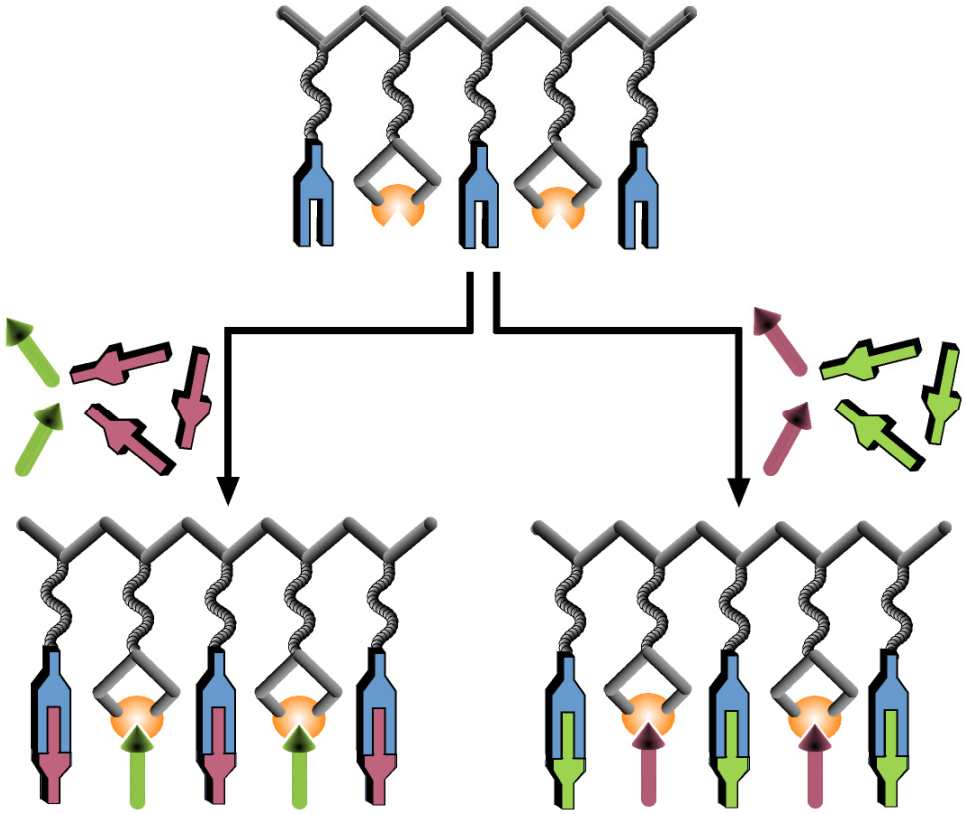

Scheme 2.5. Noncovalent approach to different copolymers from a generic polymer backbone.

In our laboratories, the use of multiple noncovalent interactions to functionalize a single polymer backbone has proven to be an exciting new route to densely functionalized random and block copolymers as well as terpolymers. In a series of reports,[13, 40-47] we were able to functionalize polymers bearing two or three complementary noncovalent receptors and/or hosts with their corresponding substrates and/or guests. We examined in detail different strategies for obtaining densely functionalized polymers, including the use of (i) two different hydrogen bonding motifs, (ii) both weak and strong hydrogen bonding motifs in concert with metal coordination, and (iii) ionic interactions combined with metal coordination and/or hydrogen bonding.

Our goal in all of these endeavors was to develop a generalized route to highly functional polymers. Of foremost concern was the orthogonality of the functionalization sequence. Keeping this in mind, we designed and synthesized several polymeric scaffolds that can accommodate a variety of noncovalent functionalities that interact very little, if any, with neighboring groups. This allowed us to modify the order of the post-polymerization functionalization steps as well as achieve a rapid, one-pot functionalization in many cases (Scheme 2.6).

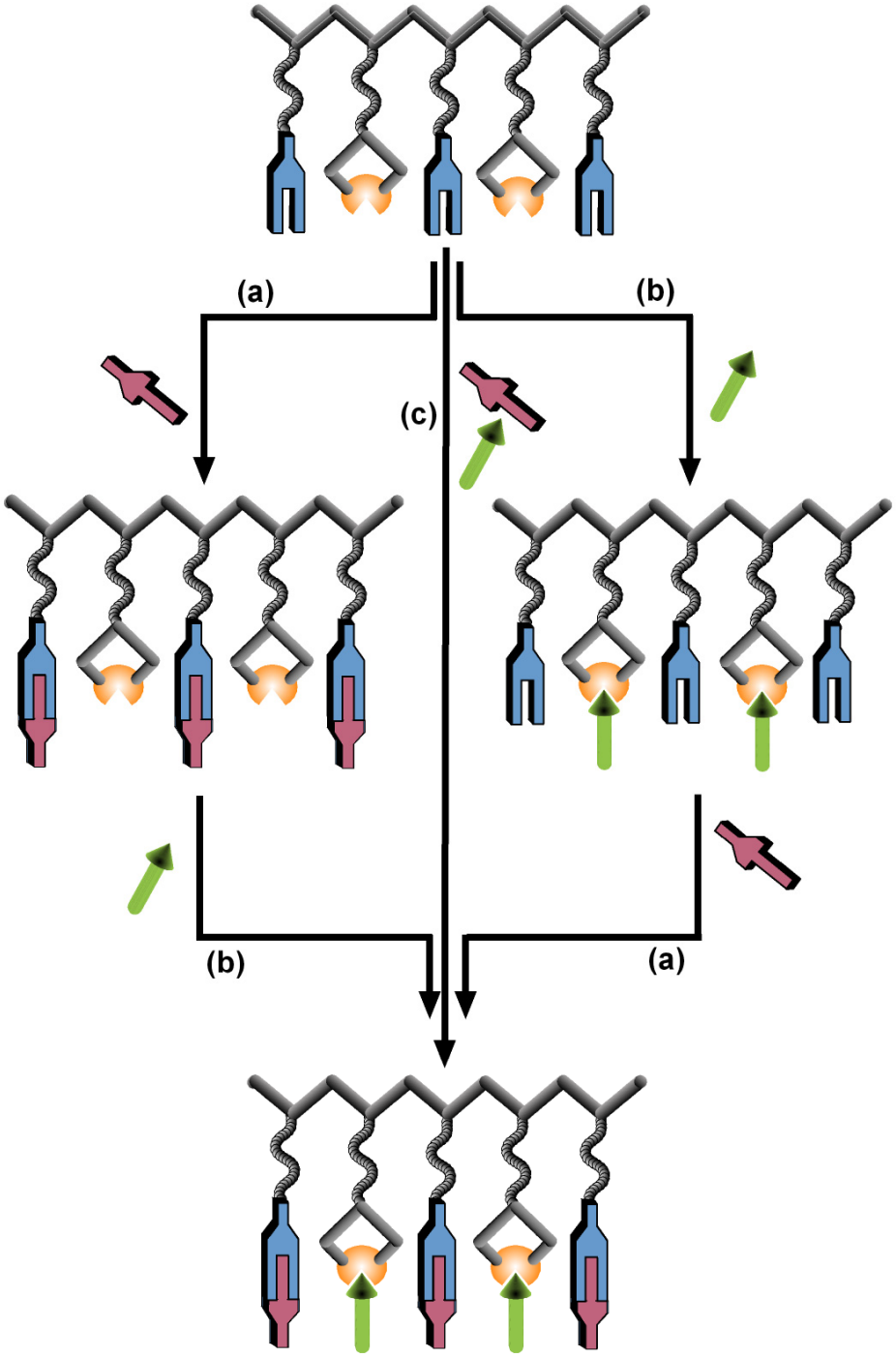

Scheme 2.6.[a] Generalized, orthogonal route to multifunctional polymers.[a] Addition of substrate with (a) recognition type I; (b) recognition type II; (c) one-pot addition of both substrates.

2.6 Polymer Multifunctionalization via Self-Sorting

First, we examined the possibility of using different hydrogen bonding recognition processes to functionalize copolymers using the same *type* of interaction through a process known as "self-sorting" (molecules that specifically associate with themselves: *narcissistic molecules*[48] or other molecules: *social molecules*[49] through noncovalent interactions in the presence of other competitive noncovalent forces are referred to as "self-sorting" molecules). Hallmark examples of a hydrogen bonding "self-sorters" are the biopolymers DNA and RNA that are able to match base pairs with very few mistakes along a polymeric backbone, despite the presence of competing non-specific hydrogen bonding interactions.[50] Isaacs and coworkers have found that many molecular systems are capable of "self-sorting."[50] Based on the incredible fidelity of small molecule "self-sorters," and biomacromolecular "self-sorters" like DNA and RNA, we decided to investigate unnatural, polymeric "self-sorters". The "self-sorting" processes we chose to study along polymer backbones were the association between thymine (**THY**) and diaminopyridine (**DAP**) through DAD-ADA triple hydrogen bond arrays and the association between cyanuric acid (**CA**) and isophthalic wedge type receptors (**Wedge**) through DAD-ADA sextuple hydrogen bond arrays (Scheme 2.7).

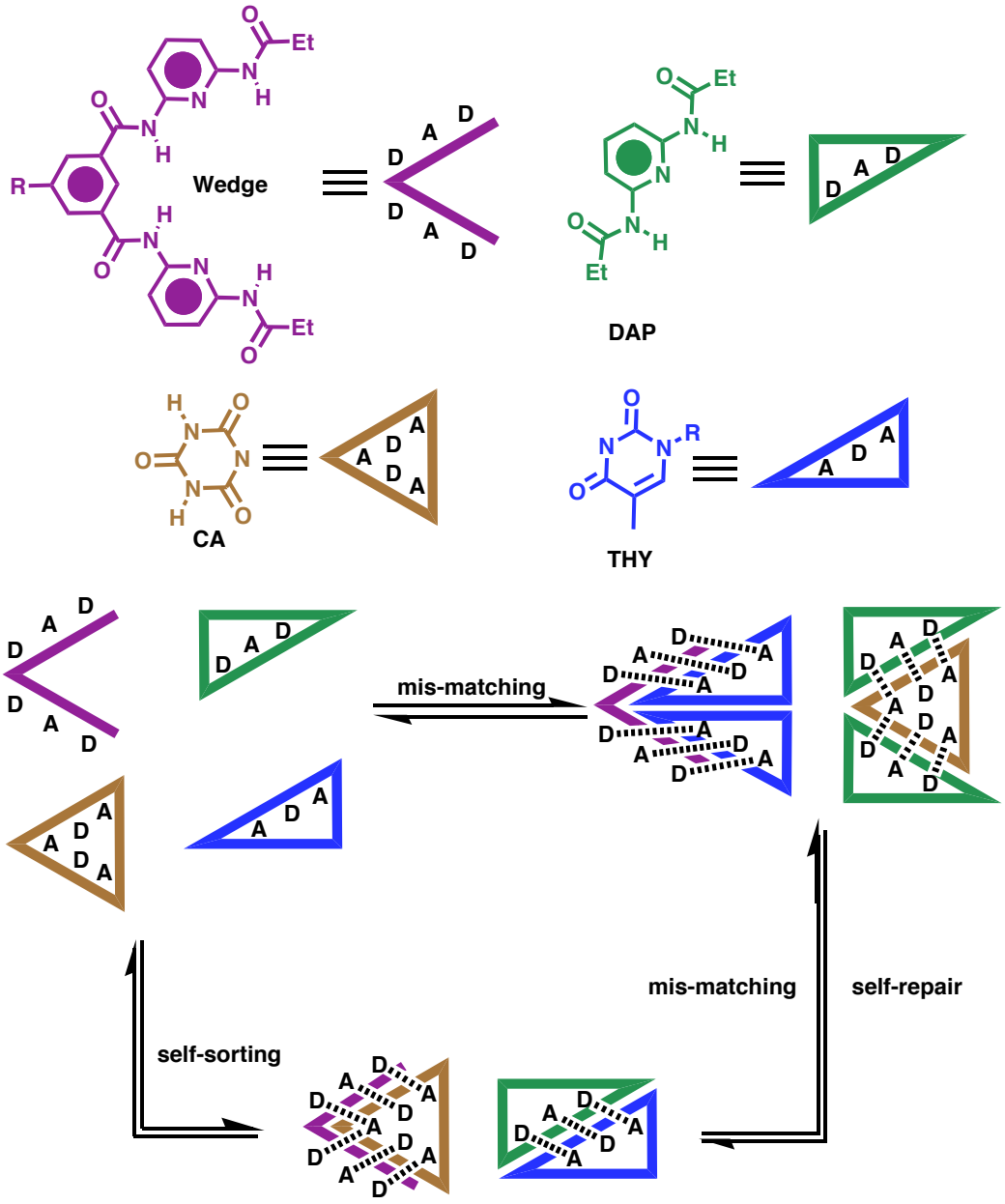

Scheme 2.7. Self-sorting, mis-matching and self-repair in triple DAD-ADA and sextuple DAD-ADA hydrogen bond arrays.

A potential challenge for achieving "self-sorting" in polymer solutions is overcoming competitive interactions beyond those that exist in dilute small molecule solutions because of a high *local* concentration of competitive noncovalent interactions along a polymer chain. Despite this obstacle, we found that in both block and random copolymers (**11**) bearing competitive hydrogen bonding receptors, "self-sorting" can be achieved, *i.e.* two competitive recognition pairs along a polymer backbone are able to recognize each other with high fidelity (Scheme 2.8).[43]

In addition to the observation of "self-sorting" in supramolecular polymers, we also investigated the possibility of using two competitive hydrogen bonding interactions to achieve step-wise site-specific polymer multifunctionalization. We studied the addition of diaminopyridine (**DAP**) to a random copolymer (**11**) containing both cyanuric acid and thymine receptors. While the thymine is the target receptor for **DAP**, cyanuric acid is also able to hydrogen bond with **DAP** via a triple hydrogen bond-based interaction thereby competing with the thymine receptors. Using ^{1}H NMR spectroscopic titration experiments, we established that **DAP** and the cyanuric acid recpeptors are indeed interacting with each other through a mis-match that could be relieved upon the addition of **Wedge** to the mixture, resulting in the fully functional copolymer (**11:(DAP)$_n$(Wedge)$_m$**).

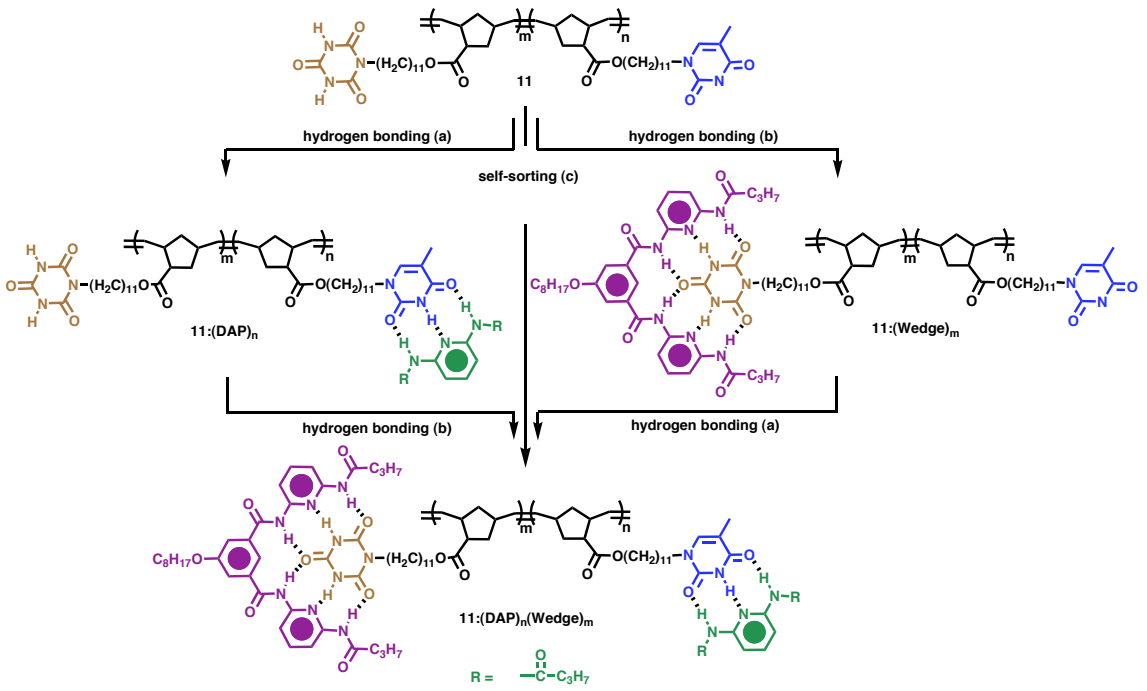

Scheme 2.8.[a] Stepwise and one-pot ("self-sorting") functionalization of copolymers. [a]Reagents: (a) diaminopyridine (DAP); (b) isopthalic wedge (Wedge); (c) (DAP) and (Wedge), one-pot.

Our unnatural polymeric "self-sorters" behave similarly to biomacromolecular analogues such as DNA or RNA. Despite the presence of very high local concentrations of competitive hydrogen bonding actors along the polymer backbones, we observed that highly specific hydrogen bonding interactions prevail over non-specific mis-matches. Clearly, polymeric "self-sorting" functions as an efficient means for obtaining multifunctional polymers at the very least and serves as an interesting example of how tools used by Nature can potentially be translated to synthetic systems.

2.7 Polymer Multifunctionalization *via* Metal Coordination and Hydrogen Bonding

We hypothesized that a more modular polymer functionalization strategy could be realized through the use of two unique types of molecular recognition that would not interfere with each other, such as metal coordination and hydrogen bonding. We demonstrated that random copolymers (**12**) bearing side-chains with Pd(II) pincer complexes and diaminopyridine receptors could be functionalized with pyridines (**Pyr**) (through metal coordination) and thymines (**NBT**) (through DAD-ADA hydrogen bond arrays) by both step-wise and one-step, orthogonal synthetic strategies (Scheme 2.9).[41]

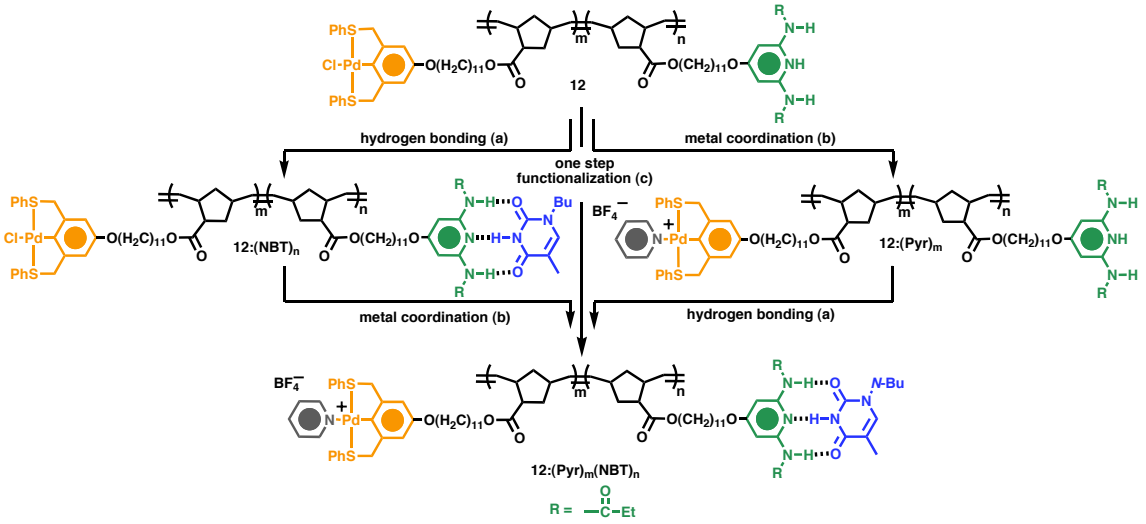

Scheme 2.9. Step-wise and one-step orthogonal functionalization of copolymers through metal coordination and hydrogen bonding [a]Reagents: (a) *N*-butylthymine (NBT); (b) pyridine (Pyr), $AgBF_4$, and (c) *N*-butylthymine (NBT), pyridine (Pyr), $AgBF_4$, one-step.

This multicomponent functionalization strategy was found to be efficient and fully functionalized random copolymers could be obtained easily. Most importantly, characterization of the functionalized polymers proved facile. The lack of interference between the two functionalized side-chains could be established by ^{1}H and ^{13}C NMR

spectroscopy experiments. Figure 2.3 shows an example of a ^{1}H NMR spectroscopic characterization of the one-pot functionalization strategy. The α-pyridyl signals display a marked upfield shift upon coordination and the imide proton signal originating from the thymine substrate displays a characteristic downfield shift upon hydrogen bonding to the diaminopyridine receptor.

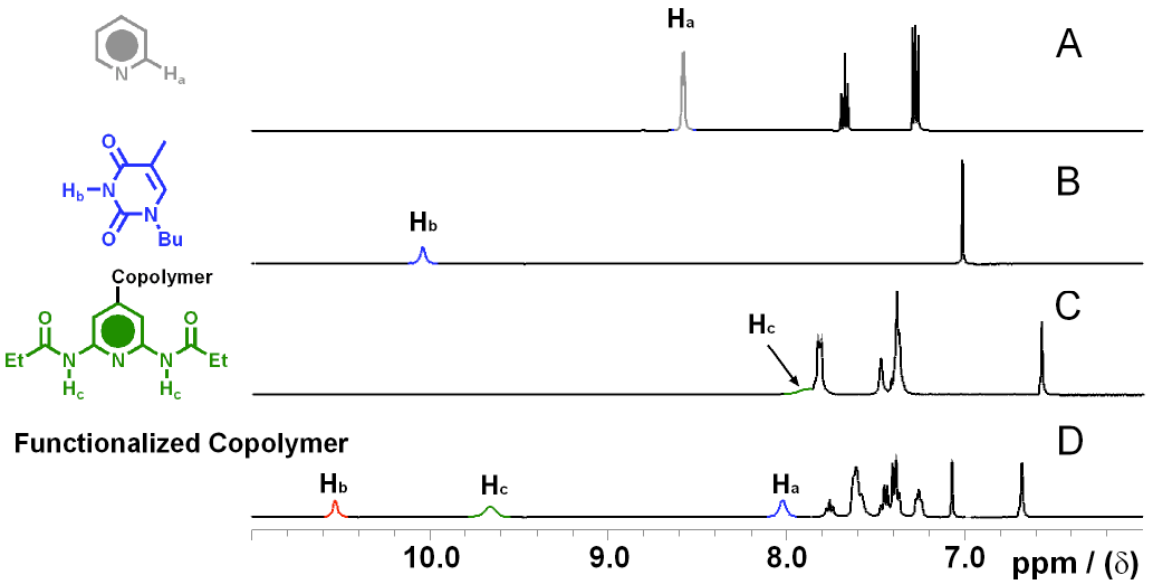

Figure 2.3. Stacked Plot of partial ^{1}H NMR spectra (400 MHz, 298 K, CD_2Cl_2) used to characterize copolymer functionalization: (A) (Pyr); (B) (NBT); (C) 12; (D) fully functionalized 12:$(Pyr)_m(NBT)_n$.

The orthogonality of combining pincer-type metal coordination and hydrogen bonding was tested through an examination of the association constants between receptors and substrates. We found that association constants (K_as) for the hydrogen bonding event between diaminopyridine receptors (**12**, **12:(Pyr)$_m$**) and thymine substrates

(**NBT**) to be approximately 500 M^{-1} (in CH_2Cl_2) regardless of whether or not pyridines (**Pyr**) were assembled onto pincer complexes. Likewise, the assembly of the hydrogen bonding units did not affect subsequent metal coordination steps. In contrast to our previous "self-sorting" experiments, the use of metal coordination and hydrogen bonding provides an efficient platform for obtaining polymers with functional groups that can be manipulated independently by external stimuli.

Afterwards, we extended the orthogonal multifunctionalization strategy from random to block copolymers.[46] We found that in the case of a thymine functionalized block copolymer receptor (**13**), association constants for the formation of ADA-DAD hydrogen bond arrays between the thymine receptor and **DAP** substrate were slightly lower than those observed for polymeric diaminopyridine receptors (**12**) functionalized with **THY** substrates which can be attributed to the greater degree of self-association of the thymine receptor verses the diaminopyridine receptor. However, the independence of the two recognition events remained intact and an orthogonal functionalization (Scheme 2.10) could be achieved just as in the previous study. Therefore, we concluded that both block and random copolymers are excellent candidates for obtaining multifunctional polymers through a combination of metal coordination and hydrogen bonding.

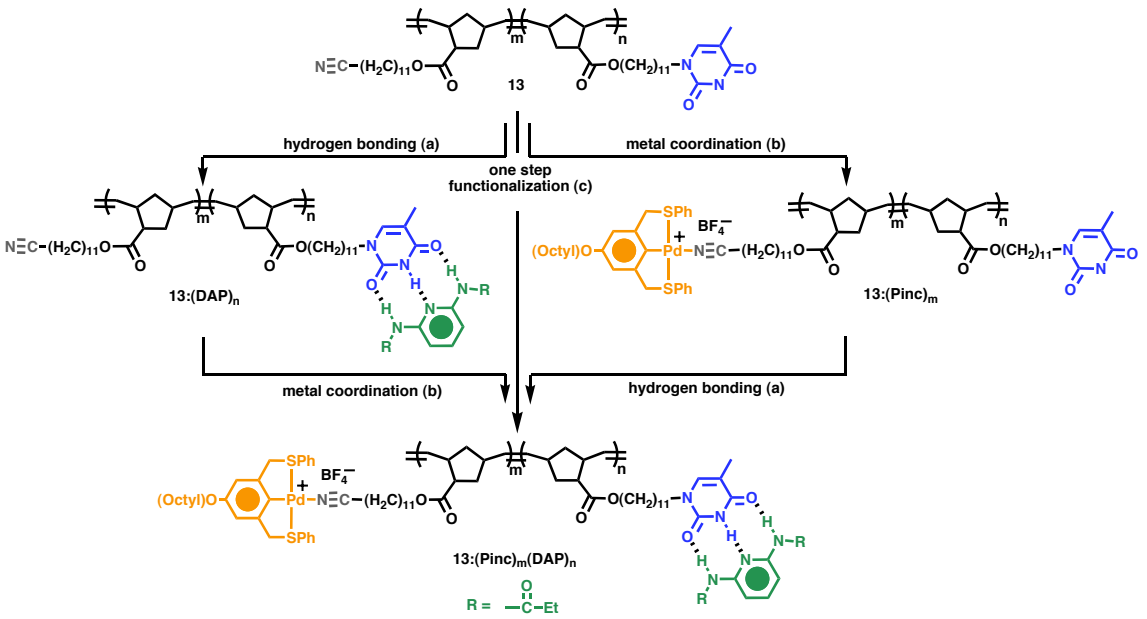

Scheme 2.10. Block copolymer functionalization through metal coordination and hydrogen bonding. Reagents: (a) DAP; (b) Pincer complex (Pinc); (c) DAP, Pinc, one-pot.

2.8 Polymer Multifunctionalization *via* Hydrogen Bonding and Ionic Interactions

We reasoned that other types of interactions such as coulombic forces could also be used in our orthogonal multifunctionalization strategy. Our hypothesis was that the combination of hydrogen bonding and ionic interactions would be an interesting new route to bifunctional ionomers. We found that bifunctional ionomers based on diaminopyridine and thymine recognition partners and ammonium salts could be synthesized through stepwise, or one-step orthogonal strategies (Scheme 2.11).[47] Most importantly, the presence of the ionic complex does not interfere with the hydrogen bonding strength of the **DAP**:**THY** pair and the hydrogen bonding interactions do not impede ion exchange. These results demonstrate that noncovalent synthetic strategies based on two recognition events are not limited to metal coordination and hydrogen bonding.

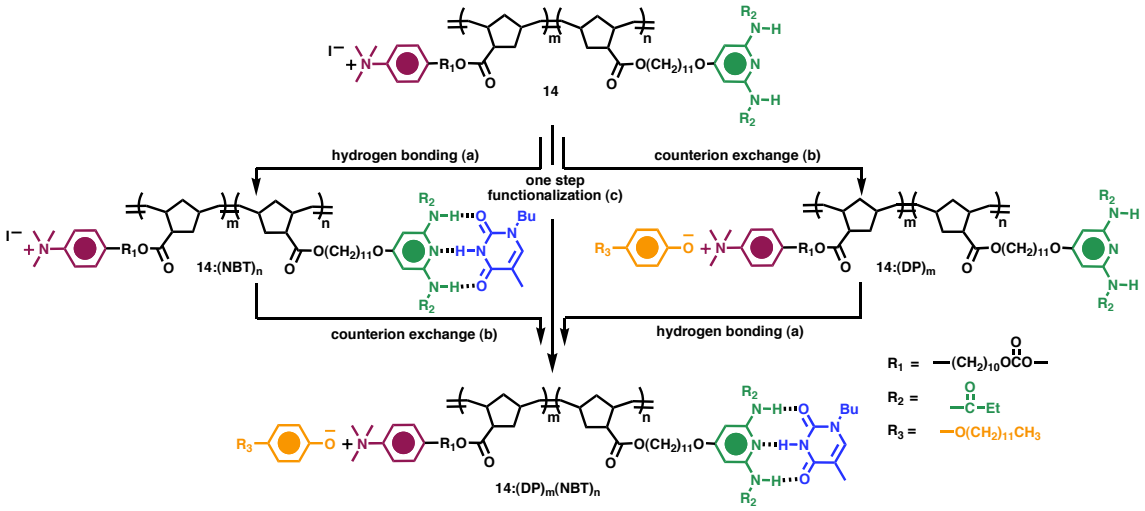

Scheme 2.11. Copolymer functionalization through ion exchange and hydrogen bonding. Reagents: (a) NBT; (b) sodium dodecyloxyphenate (SDP); (c) NBT and SDP.

2.9 Cross-linking

The possibility of obtaining functional materials using our noncovalent functionalization strategies is key for the success of this methodology.[42] Our first goal was to produce both densely cross-linked and densely functionalized polymers using exclusively noncovalent side-chain interactions (Scheme 2.13). One advantage of combining both metal coordination and hydrogen bonding containing materials is that the dynamics of each interaction can be co-opted individually or in concert with the other to obtain a variety of polymers responsive to a catalogue of external stimuli, including temperature, pH, solvent, polymer concentration, and competitive metal coordinating ligands. For example, when hydrogen bonding is used to cross-link polymers and pincer type metal coordination to functionalize the side-chains of the resulting cross-linked arrays, it is possible to break up the cross-links thermally and yet maintain the integrity of the metal complex. On the other hand, when metal coordination is used to crosslink

polymers and hydrogen bonding for the functionalization, the cross-links can be reversed by the addition of PPh_3 which coordinates stronger to the Pd(II) pincer complex than pyridine.

Polymer multifunctionalization can often be difficult to achieve with traditional covalent synthetic strategies due to incompatibilities between functional groups and polymerization methods, interferences among functional groups, and differences in comonomer reactivity ratios. Over the past five years, we have shown that a viable solution to these three common problems is the employment of noncovalent synthetic strategies to produce multifunctional polymers. Using this approach, multifunctional polymers can be easily obtained with the use of hydrogen bonding self-sorters, copolymer receptors bearing hydrogen bonding and metal coordination recognition units or ionic complexes, and copolymer receptors bearing hydrogen bonding and pseudorotaxane recognition units. Moreover, these synthetic strategies are not only limited to two recognition types, but can be extended to higher orders of functionalization. Finally, we have proven that these approaches can be applied to materials chemistry by fabricating highly responsive and densely functionalized cross-linked polymers.

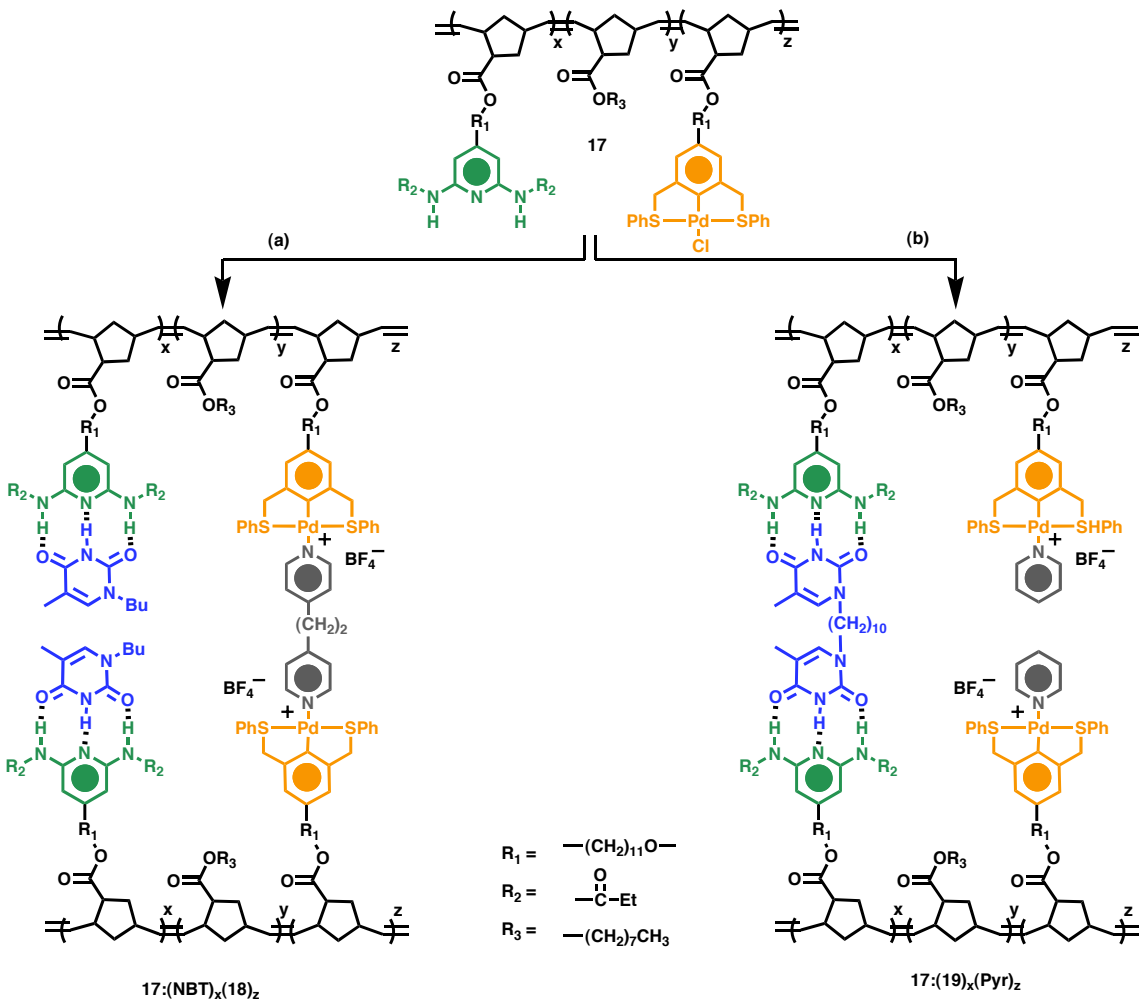

Scheme 2.12. Noncovalent synthetic approach to functionalized, cross-linked polymers. [a] Reagents: (a) NBT, $AgBF_4$, 18; (b) 19, $AgBF_4$, Pyr.

2.10 Conclusion and Outlook

In this Chapter, strategies for obtaining densely functionalized polymers through noncovalent synthetic strategies have been surveyed. Noncovalent interactions such as hydrogen bonding, ionic interactions, metal coordination, electrostatic interactions, and π–π stacking can be used individually or in concert with one another to obtain mono- or multiply-functionalized polymers. These noncovalent synthetic strategies can be advantageous over covalent analogues for several reasons: (i) noncovalently

functionalized polymers have the ability to self-heal due to the reversibility of noncovalent bonds, (ii) a generic polymer backbone can be used to obtain a library of fully functionalized polymers, (iii) several different types of noncovalent interactions are orthogonal to one another, while many covalent modifications are not, and (iv) such polymers are highly responsive to external stimuli. Aside from simply adding functionality to a polymer, this approach also allows for the tuning of bulk polymer properties such as morphology or the degree of crosslinking. The research efforts described in this Chapter clearly demonstrate the potential of noncovalently functionalized polymers and have certainly laid the ground work for future endeavors in this area.

2.11 Thesis Hypothesis

Based on many of the research examples presented in this chapter, further research as well as new research areas will be presented in the remainder of this thesis. The central hypothesis of the thesis is the following: *Noncovalently bonded polymers can present viable alternatives to covalent bonded analogues*. Within this hypothesis lies a prediction that many common problems associated with covalently based polymers can be overcome with the use of polymers comprising molecular recognition elements. As each research topic is presented, an eye toward the aforementioned hypothesis will be maintained.

Specifically, Chapters 3 and 4 present research focused on advancing the functionalization of polymers through molecular recognition. The goal of this research is primarily to develop a general polymer backbone that both site-specifically and strongly

associates noncovalently with small molecular substrates. These chapters demonstrate that both architecturally controlled block copolymers and random terpolymers can accept a full load of different substrates without interference among distinct molecular recognition elements along the polymer backbone.

Chapters 5 and 6 present a unique application of polymers containing molecular recognition elements, templated synthesis. Chapter 5 first discusses lessons learned from small molecule based templated synthesis in which a template and a substrate are held together by metal coordination and a subsequent bond forming reaction occurs. Ultimately, the results of this chapter directed our work towards a hydrogen bonding based system in lieu of metal coordination. In this case, a polymeric template was used, and a daughter monomer was polymerized while attached to the template.

Another application of polymers containing molecular recognition elements is presented in Chapters 7 and 8. In these chapters, metal coordination is used to assemble polymer multilayer thin films that are both responsive to external stimuli, stable, and erasable.

Finally, Chapter 9 summarizes the main conclusions of each chapter and presents a potential view of new projects that might result from the research presented in this thesis.

2.12 References

1. Lovinger, A.J., Nano-, Bio-, Multi-, Inter-, ...: Polymer Research in an Era of Prefixes. *J. Macromol. Sci. Part C: Polym. Rev.* **2005,** *45*, 195.

2. Odian, G., *Principles of Polymerization*. John Wiley & Sons: New York, 1991.

3. *Handbook of Metathesis*. Wiley-VCH: Weinheim, 2003.

4. Fischer, H., The Persistent Radical Effect: A Principle for Selective Radical Reactions and Living Radical Polymerizations. *Chem. Rev.* **2001,** *101*, 3581.

5. Coates, G.W., Precise Control of Polyolefin Stereochemistry Using Single-Site Metal Catalysts. *Chem. Rev.* **2000,** *100*, 1223.

6. Dechy-Cabaret, O.; Martin-Vaca, B.; Bourissou, D., Controlled Ring-Opening Polymerization of Lactide and Glycolide. *Chem. Rev.* **2004,** *104*, 6147.

7. Philp, D.; Stoddart, J.F., Self-Assembly in Natural and Unnatural Systems. *Angew. Chem. Int. Ed. Engl.* **1996,** *35*, 1154.

8. Lehn, J.-M., Toward Complex Matter: Supramolecular Chemistry and Self-Organization. *Proc. Natl. Acad. Sci. USA* **2002,** *99*, 4763.

9. Brunsveld, L.; Folmer, B.J.B.; Meijer, E.W.; Sijbesma, R.P., Supramolecular Polymers. *Chem. Rev.* **2001,** *101*, 4071.

10. Farnik, D.; Kluger, C.; Kunz, M. J.; Machl, D.; Petraru, L.; Binder, W.H., Synthesis and Self Assembly of Hydrogen-Bonded Supramolecular Polymers. *Macromol. Symp.* **2004,** *217*, 247.

11. Kato, T.; Mizoshita, N.; Kishimoto, K., Functional Liquid-Crystalline Assemblies: Self-Organized Soft Materials. *Angew. Chem. Int. Ed.* **2006,** *45*, 38.

12. Gohy, J.-F.; Lohmeijer, B.G.G.; Schubert, U.S., From Supramolecular Block Copolymers to Advanced Nano-Objects. *Chem. Eur. J.* **2003,** *9*, 3472.

13. Pollino, J.M.; Weck, M., Non-Covalent Side-Chain Polymers: Design Principles, Functionalization Strategies, and Perspectives. *Chem. Soc. Rev.* **2005,** *34*, 193.

14. Deans, R.; Ilhan, F.; Rotello, V.M., Recognition-Mediated Unfolding of a Self-Assembled Polymeric Globule. *Macromolecules* **1999,** *32*, 4956.

15. Ilhan, F.; Gray, M.; Rotello, V.M., Reversible Side Chain Modification Through Noncovalent Interaction. "Plug and Play" Polymers. *Macromolecules* **2001,** *34*, 2597.

16. Carroll, J.B.; Waddon, A.J.; Nakade, H.; Rotello, V.M., "Plug and Play" Polymers. Thermal and X-ray Characterizations on Noncovalently Grafted Polyhedral Oligomeric Silsesquioxane (POSS)-Polystyrene Nanocomposites. *Macromolecules* **2003,** *36*, 6289.

17. Shenhar, R.; Rotello, V.M., Nanoparticles: Scaffolds and Building Blocks. *Acc. Chem. Res.* **2003,** *36*, 549.

18. Stubbs, L.P.; Weck, M., A Polymeric Scaffold for the Self-Assembly of Receptors Through Hydrogen Bonding. *Chem. Eur. J.* **2003,** *9*, 992.

19. Bazzi, H.S.; Sleiman, H.F., Adenine-Containing Block Copolymers via Ring-Opening Metathesis Polymerization: Synthesis and Self-Assembly into Rod Morphologies. *Macromolecules* **2002,** *35*, 9617.

20. Bazzi, H.S.; Bouffard, J.; Sleiman, H.F., Self-Complementary ABC Triblock Copolymers via Ring-Opening Metathesis Polymerization. *Macromolecules* **2003,** *36*, 7899.

21. Lohmeijer, B.G.G.; Schubert, U.S., Playing LEGO with Macromolecules: Design, Synthesis, and Self-Organization with Metal Complexes. *J. Polym. Sci. Part A: Polym. Chem.* **2003,** *41*, 1413.

22. Chen, B.; Sleiman, H.F., Ruthenium Bipyridine-Containing Polymers and Block Copolymers via Ring-Opening Metathesis Polymerization. *Macromolecules* **2004,** *37*, 5866.

23. Carlise, J.R.; Weck, M., Side-Chain Functionalized Polymers Containing Bipyridine Coordination Sites: Polymerization and Metal Coordination Studies. *J. Polym. Sci. Part A: Polym. Chem.* **2004,** *42*, 2973.

24. Aamer, K.A.; Tew, G.N., Synthesis of Terpyridine-Containing Polymers with Blocky Architecture. *Macromolecules* **2004,** *37*, 1990.

25. Tew, G.N.; Aamer, K.A.; Shunmugam, R., Incorporation of Terpyridine into the Side Chain of Copolymers to Create Multi-Functional Materials. *Polymer* **2005,** *46*, 8440.

26. Shunmugam, R.; Tew, G.N., Efficient Route to Well-Characterized Homo, Block, and Statistical Polymers Containing Terpyridine in the Side Chain. *J. Polym. Sci. Part A: Polym. Chem.* **2005,** *43*, 5831.

27. Gohy, J.-F.; Hofmeier, H.; Alexeev, A.; Schubert, U.S., Aqueous Micelles from Supramolecular Graft Copolymers. *Macromol. Chem. Phys.* **2003,** *204*, 1524.

28. Albrecht, M.; van Koten, G., Platinum Group Organometallics Based on "Pincer" Complexes: Sensors, Switches, and Catalysts. *Angew. Chem. Int. Ed.* **2001,** *40*, 3750.

29. Pollino, J.M.; Weck, M., Supramolecular Side-Chain Functionalized Polymers: Synthesis and Self-Assembly Behavior of Polynorbornenes Bearing Pd^{II} SCS Pincer Complexes. *Synthesis* **2002**, 1277.

30. Pollino, J.M.; Stubbs, L.P.; Weck, M., Living ROMP of *Exo*-Norbornene Esters Possessing Pd(II) SCS Pincer Complexes or Diaminopyridines. *Macromolecules* **2003,** *36*, 2230.

31. Huck, W.T.S.; Hulst, R.; Timmerman, P.; van Veggel, F. C.J.M.; Reinhoudt, D. N., Noncovalent Synthesis of Nanostructures: Combining Coordination Chemistry and Hydrogen Bonding. *Angew. Chem. Int. Ed.* **1997,** *36*, 1006.

32. Hofmeier, H.; El-ghayoury, A.; Schenning, A.P.H.J.; Schubert, U.S., New Supramolecular Polymers Containing both Terpyridine Metal Complexes and Quadruple Hydrogen Bonding Units. *Chem. Commun.* **2004**, 318.

33. Bazuin, C.G.; Brodin, C., Thermotropic Liquid Crystalline Complexes of Hydrogen-Bonded Poly(pyridylpyridinium dodecyl methacrylate) Bromide and Octylphenol. *Macromolecules* **2004,** *37*, 9366.

34. Ruokolainen, J.; Mäkinen, R.; Torkkeli, M.; Mäkelä, T.; Serimaa, R.; TenBrinke, G.; Ikkala, O., Switching Supramolecular Polymeric Materials with Multiple Length Scales. *Science* **1998,** *280*, 557.

35. Fyfe, M. C.T.; Stoddart, J.F., Interwoven Supramolecular Arrays via the Noncovalent Polymerization of Pseudorotaxanes. *Coord. Chem. Rev.* **1999,** *183*, 139.

36. Deng, W.-Q.; Flood, A.H.; Stoddart, J.F.; Goddard III, W.A., An Electrochemical Color-Switchable RGB Dye: Tristable [2]Catenane. *J. Am. Chem. Soc.* **2005,** *127*, 15994.

37. Badjic, J.D. ; Ronconi, C.M.; Stoddart, J.F.; Balzani, V.; Silvi, S.; Credi, A., Operating Molecular Elevators. *J. Am. Chem. Soc.* **2006,** *128*, 1489.

38. Xu, H.; Hong, R.; Lu, T.; Uzun, O.; Rotello, V., Recognition-Directed Orthogonal Self-Assembly of Polymers and Nanoparticles on Patterned Surfaces. *J. Am. Chem. Soc.* **2006,** *128*, 3162.

39. Odian, G., *Principles of Polymerization*. 4 ed.; Wiley-Interscience: Hoboken, 2004.

40. Gerhardt, W.; Crne, M.; Weck, M., Multifunctionalization of Synthetic Polymer Systems via Self-Assembly. *Chem. Eur. J.* **2004,** *10*, 6212.

41. Pollino, J.M.; Stubbs, L.P.; Weck, M., One-Step Multi-Functionalization of Random Copolymers via Self-Assembly. *J. Am. Chem. Soc.* **2004,** *126*, 563.

42. Pollino, J.M.; Nair, K.P.; Stubbs, L.P.; Adams, J.; Weck, M., Cross-linked and Functionalized 'Universal Polymer Backbones' via Simple, Rapid, and Orthogonal Multi-site Self-assembly. *Tetrahedron* **2004,** *60*, 7205.

43. Burd, C.; Weck, M., Self-sorting in Polymers. *Macromolecules* **2005,** *38*, 7225.

44. South, C.R.; Higley, M.N.; Leung, K.C.-F.; Lanari, D.; Nelson, A.; Grubbs, R.H.; Stoddart, F.F.; Weck, M., Self-Assembly With Block Copolymers Using SCS Pd(II) Pincer Metal Coordination and Pseudorotaxane Formation. *Chem. Eur. J.* **2006**, *12*, 3789.

45. South, C.R.; Leung, K.C.-F.; Lanari, D.; Stoddart, J.F.; Weck, M., Noncovalent Side-Chain Functionalization of Terpolymers. *Macromolecules* **2006,** *39*, 3738.

46. Nair, K.P.; Pollino, J.M.; Weck, M., Non-Covalently Functionalized Block Copolymers Possessing Both, Hydrogen-Bonding and Metal-Coordination Centers. *Macromolecules* **2006,** *39*, 940.

47. Nair, K.P.; Weck, M., Noncovalently Functionalized Poly(norbornene)s Possessing both Hydrogen Bonding and Coulombic Interactions. *Macromolecules* **2006**, submitted.

48. Taylor, P.N.; Anderson, H.L., Cooperative Self-Assembly of Double-Strand Conjugated Porphyrin Ladders. *J. Am. Chem. Soc.* **1999,** *121*, 11538.

49. Shivanyuk, A.; Rebek Jr., J., Social Isomers in Encapsulation Complexes. *J. Am. Chem. Soc.* **2002,** *124*, 12074.

50. Wu, A.; Isaacs, L., Self-Sorting: The Exception or the Rule? *J. Am. Chem. Soc.* **2003,** *125*, 4831.

CHAPTER 3

Functionalization of Block Copolymers Through Molecular Recognition

3.1 Abstract

Poly(norbornene)-based block copolymers containing side-chains consisting of palladated-pincer complexes/dibenzo[24]crown-8 or palladated-pincer complexes/dibenzylammonium salts were synthesized. Noncovalent functionalization was accomplished with their corresponding recognition units through simple 1:1 addition with association constants (K_a) greater than 10^5 M^{-1}. The self-assembly processes were monitored using both ^{1}H NMR spectroscopy and isothermal titration calorimetry. In all cases, we found that the self-assembly of the recognition units along each polymer block do not preclude the self-assembly processes along the other block.

3.2 Introduction

In previous chapters, basic concepts in molecular recognition and self-assembly have been set forth. This chapter presents the results of a research endeavor aimed at applying some of the principles discussed in previous sections to block copolymers. It is noteworthy to point out that the functionalization of block copolymers through molecular recognition is a significant goal particularly from a materials science aspect, in which block copolymer are widely used. As such, a theme of this chapter is architectural control of the synthesis of block copolymers and their subsequent functionalization.

As the field of materials science advances, the demand for highly functional and versatile materials will likewise increase. Materials for applications such as organic-light

emitting diodes (OLEDs), photorefractives, solar cells, drug delivery vehicles, sensors, and molecular machines will require fast and cost effective synthesis and optimization.[1-5] To meet these demands, future synthetic strategies to produce polymeric materials should be generic, such that similar functionalization techniques could be applied to a variety of applications. Nevertheless, these functionalization strategies should be tailored to a specific application. For example, a drug delivery application may require functionalities with weak noncovalent attachments in order to facilitate effective drug release in response to a stimulus at a target site.[6] In contrast, materials for use in electro-optics require strong and dense functionalization capable of withstanding thousands of working hours.[7]

Nature has created a system with incredible fidelity in which a myriad of biomaterials can be produced from noncovalent mediated synthesis.[8] Borrowing from this approach, our system uses similar noncovalent forces to create functionalized copolymers. Various strategies to use this approach on polymeric systems are outlined in Chapter 2.[3, 8-10] Herein, we report the next generation of side-chain supramolecular polymers by functionalizing an architecturally controlled block copolymer with two strong noncovalent functionalities based on (i) pseudorotaxane hydrogen-bonding and (ii) metal coordination between palladated Sulfur-Carbon-Sulfur (SCS) pincer complexes and pyridines. This specific approach toward polymer synthesis possesses unique advantages. First, the copolymer architecture is defined prior to functionalization, allowing for the introduction of a variety of functional groups that might otherwise hinder architectural control if introduced prior to polymerization. Second, this generation of supramolecular polymers rivals covalently functionalized copolymers by utilizing two

recognition units with high binding affinities for their corresponding complementary recognition units (small molecules), which ensure the production of a densely functionalized and monodisperse material. Finally, our new system retains all the benefits of noncovalent modification, including reversibility, self-healing, and ease of functionalization, all of which are discussed in detail in Chapter 2.

In our search for the next generation of supramolecular polymers, depicted in Figure 3.1, we sought two important design requirements: (1) architectural control of the polymer scaffold, and (2) distinct recognition partners with sufficiently high noncovalent binding strengths.

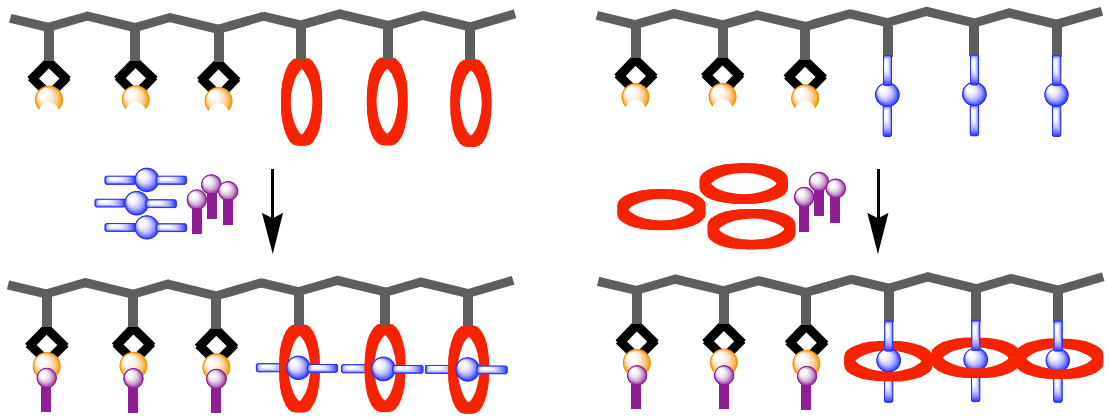

Figure 3.1. Schematic representation of the next generation of universal polymer backbones.

Block copolymers, which have been used widely in applications ranging from drug delivery to electro-optics, form our basis for the architectural control.[11] We achieve such architectural control by the use of ring-opening metathesis polymerization (ROMP)[10, 12-19] to produce block copolymers. ROMP via the ruthenium alkylidene

initiator **1** (Figure 3.2) not only provides the basis of our architectural control, but **1** is also highly functional group tolerant.[20-23]

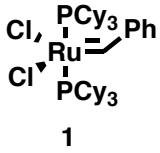

1

Figure 3.2. Ruthenium alkylidene initiator **1** employed in this work for ROMP.

Requirement (2) is met with the use of two strong noncovalent interactions involving both metal coordination and hydrogen-bonding as shown in Figure 3.3. The hydrogen-bonding system is based on the threading of a dialkylammonium cation **2** into a dibenzo[24]crown-8 (DB24C8) macrocyle **3** to form a [2]pseudorotaxane.[24-42] Since the discovery of rotaxane formation resulting from the threading of an ammonium cation into a crown ether macrocycle in 1995,[43] a number of interactions between ammonium cations and crown ether macrocycles have been studied, resulting in a myriad of supramolecular structures[44-50] and the evolution[51] of a "molecular meccano kit." The driving force for the formation of threadlike structures from dialkylammonium cations and crown ether macrocyles is the formation of strong hydrogen bonds between the acidic NH_2^+ protons and the oxygen atoms in the ring of the crown ether macrocyle. In addition to strong N-H•••O hydrogen-bonding, C-H•••O hydrogen-bonding, π-π stacking interactions, and electrostatic forces also contribute to the strong affinity between dialkylammonium cations and DB24C8 macrocycles. Further details about this molecular recognition pair are discussed in Chapter 1. Such interactions are highly

solvent dependent. In apolar solvents, high association constants (K_a) are attainable for the dialkylammonium and DB24C8 system (*vide supra)*.

The metal coordination system we employ is based on a Pd^{II} SCS pincer complex **4** which binds pyridines, nitriles, and phosphines with high efficiencies.[10, 52, 53] The palladium pincer complex was chosen because of its high stability and the ability of the palladium species to undergo substitution with a variety of ligands.[52] Pyridine **5** was chosen as the ligand for the pincer complex because it can be displaced easily by a stronger coordinating phosphorous ligand.[53] Moreover, a pincer-pyridine self-assembly process can be characterized easily using standard methods such as ^{1}H NMR spectroscopy.[9]

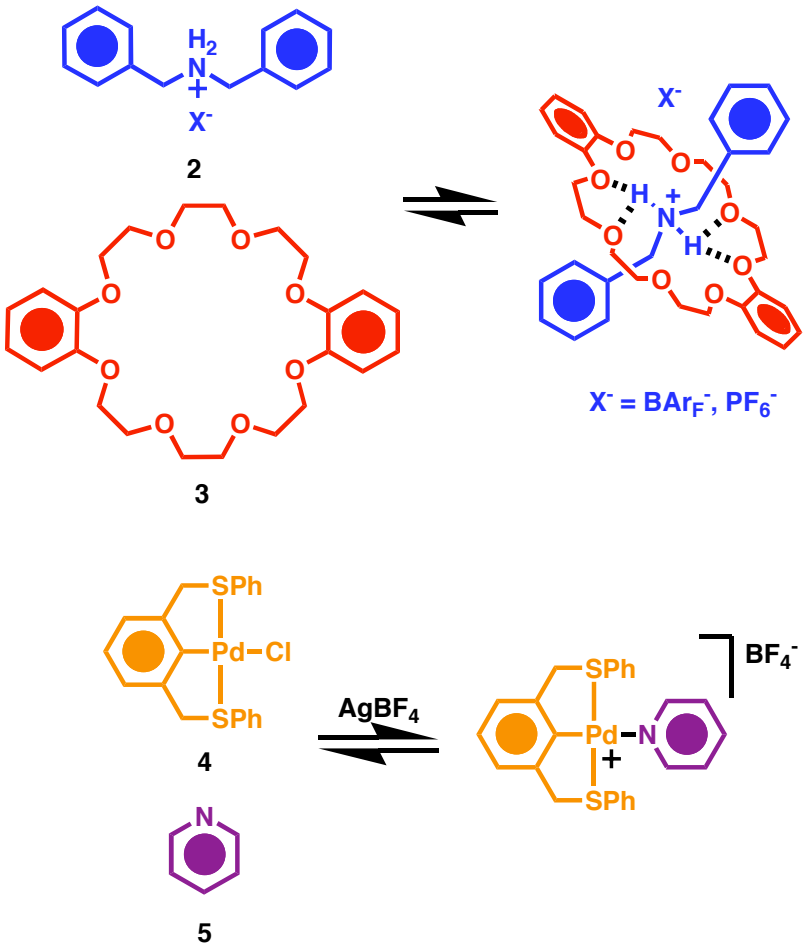

Figure 3.3. The two types of molecular recognition pairs employed in this study.

3.3 Results and Discussion

3.3.1 Monomer Synthesis and Homopolymerizations

Isomerically pure *exo*-norbornene esters often result in short polymerization times as well as living polymer growth.[10] Thus, *exo*-norbornene acid **6**[54-56] was chosen as the starting point in our synthetic pathway. The addition of an alkyl spacer onto **6** was accomplished by the DCC/DMAP esterification with 1,10-decanediol to yield **7**. The *exo*-decanol **7** was then oxidized to the corresponding carboxylic acid **8** using pyridinium

dichromate (DMAP) in DMF. Compound **8** was functionalized with the Boc protected dialkyl amine **9**[57] or the DB24C8 derivative **10**[49] using DCC/DMAP esterification to afford **11** and **12**, respectively. Monomer **12** was polymerized using initiator **1** to yield the resulting polymeric DB24C8 crown ether **14a-e**. Likewise, monomer **11** was polymerized to give the polymeric Boc protected amine **13a-e**. The synthetic pathway is outlined in Scheme 3.1.

Monomers **11** and **12** were found to polymerize in a living fashion. The absence of chain-transfer and chain-termination in addition to controlled molecular weights are criteria for living polymerizations.[58, 59] A linear relationship between M_n and [M]:[I] was established for **11** and **12** (Figure 3.4). Such a linear relationship indicates the living nature of the polymerization for monomers **11** and **12**. Additional analysis by GPC of block copolymer tests, in which monomers **11** and **12** were polymerized at a low DP and more monomer was subsequently added to the mixture, confirm the living nature of polymers (Appendix A). The corresponding gel-permeation chromatography (GPC) data are summarized in Table 3.1.

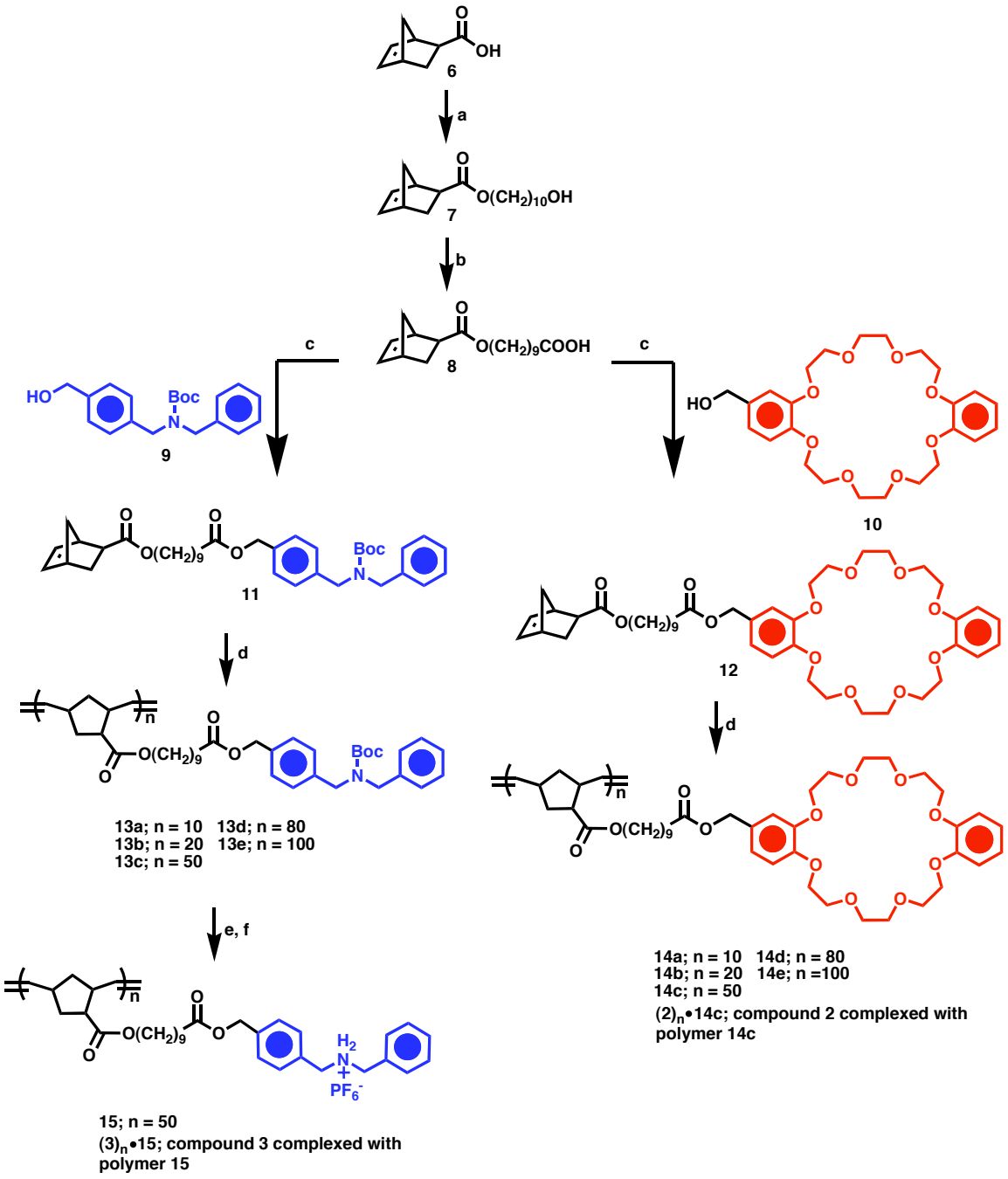

Scheme 3.1. Synthesis of Molecular Recognition Monomers and Subsequent ROMP. Reagents and conditions: a) Decane-1,10-diol, DCC/DMAP, CH_2Cl_2, reflux, **12** h, 60%; b) PDC, DMF, 48 h, 80%; c) DCC/DMAP, CH_2Cl_2, reflux, 12 h, 90%; d) **1**, CH_2Cl_2, 8 h, 100%; e) TFA, CH_2Cl_2, 3 h; f) NH_4PF_6, CH_2Cl_2, 3 h, 92% from **11**.

Table 3.1. Polymer characterization data (GPC) for **13**, **14**, **18**, and **19**.

polymer	[M]:[I]	M_n (10^{-3})	M_w(10^{-3})	PDI
13a	10	11.5	14.1	1.23
13b	20	16.0	18.6	1.16
13c	50	38.2	41.4	1.08
13d	80	59.2	68.6	1.16
13e	100	70.3	93.3	1.33
14a	10	9.3	13.1	1.41
14b	20	11.6	17.4	1.49
14c	50	30.0	61.7	2.05
14d	80	44.8	83.7	1.87
14e	100	57.4	138.0	2.41
18	50	29.5	35.6	1.21
19	50	66.0	75.1	1.14

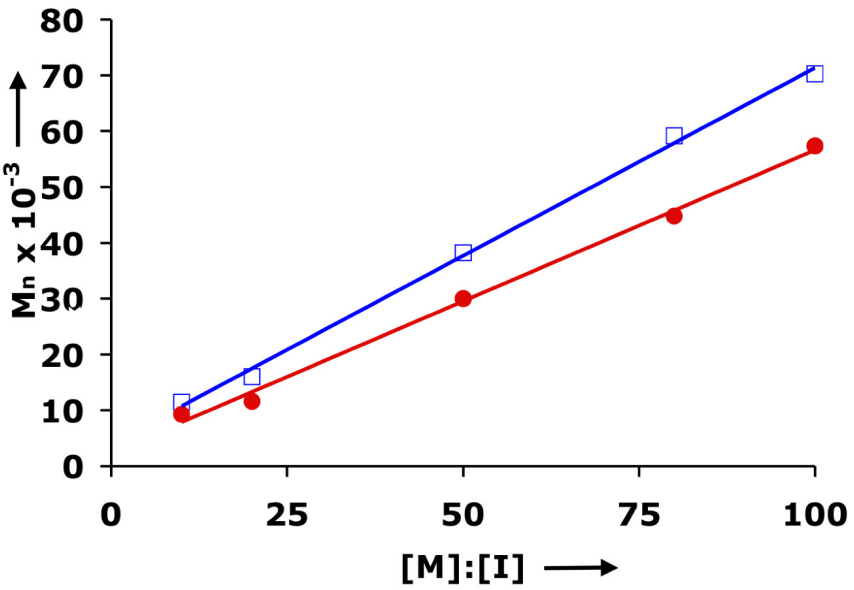

Figure 3.4. Plot of M_n vs monomer-to-initiator ratios for polymers **13** (□) and **14** (●).

We also investigated whether the unprotected amine **11** (**11a**), could be polymerized in a living fashion. For these experiments, **11** was deprotected using TFA, and the resulting **11a** was polymerized using **1**. Unfortunately, the polymerization behavior of **11a** was uncontrolled, and the formation of high molecular weight polymers was observed regardless of the [M]:[I] feed ratios. Additionally, salt exchange was achieved with the **11a** using ammonium hexafluorophosphate, but the monomeric PF_6^- salt would not polymerize using initiator **1**. Thus, monomer **11** was chosen for all polymerization experiments. The conversion of polymer **13c** to the dialkylammonium PF_6^- salt **15** was accomplished by deprotection with TFA followed by salt exchange using a 100-fold excess of ammonium hexafluorophosphate. Unfortunately, the resulting polyelectrolyte **15** could not be characterized by GPC; the charges either interacted with the column packing material or the polymer formed aggregates in an ionomeric fashion and did not elute.

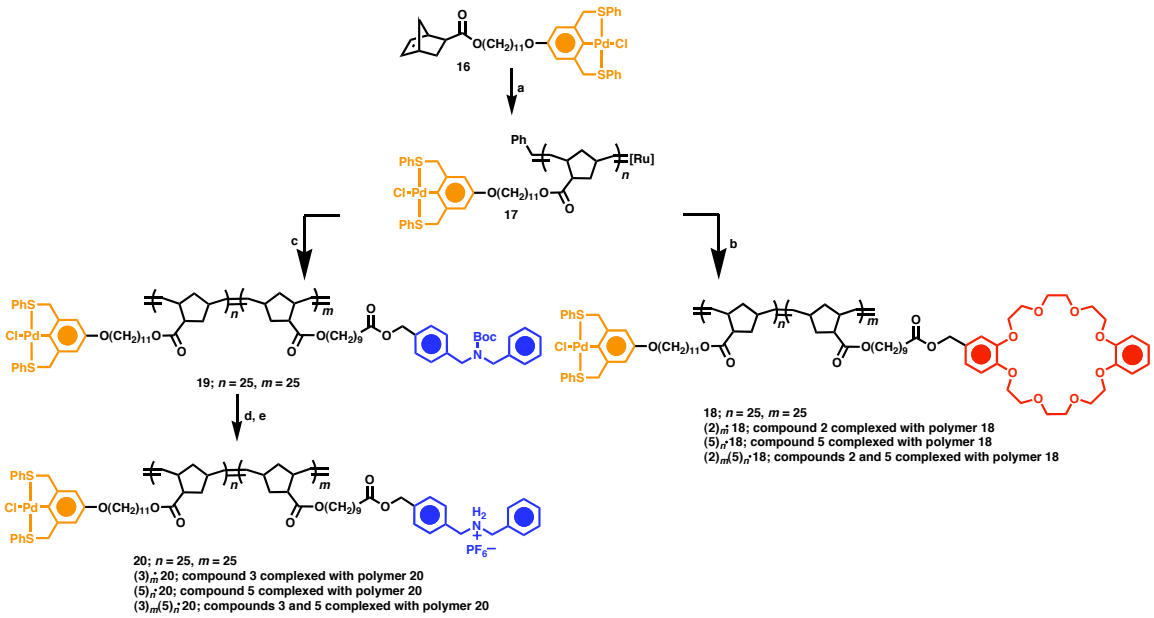

Scheme 3.2. Synthesis of AB Block Copolymers bearing DB24C8, $DBA^{+}PF_6^{-}$, and SCS-Pd-Pincer Recognition Units. Reagents and conditions: a) Initiator **1**, CH_2Cl_2, 120 min; b) 12, 8 h, 100%; c) **11**, CH_2Cl_2, 8 h, 100%; d) TFA, CH_2Cl_2, 3 h; e) NH_4PF_6, CH_2Cl_2, 3 h, 90% from **19**.

3.3.2 Copolymerizations

After establishing that **11** and **12** could be polymerized in a controlled manner, AB block copolymerizations were carried out with the SCS-Pd-Pincer monomer **16** (Scheme 3.2). The synthesis, polymerization, and living characterization of **16** have been reported previously.[3, 9, 10, 60] Following the polymerization of **16** using **1**, monomers **11** and **12** were added to **17** to form the bi-functional AB block copolymers **18** and **19**. Following the deprotection of **19** with TFA and subsequent salt exchange with ammonium hexafluorophosphate, copolymer **20** was obtained. GPC analysis of copolymers **18** and **19** were carried out. Both copolymers have low polydispersities demonstrating the living character of the polymerization. Table 1 summarizes the GPC results.

3.3.3 Self-Assembly

The aim of this study is to establish the complementarities of polymeric systems bearing the strong noncovalent recognition motifs **2**, **3**, and **4**. We initially established that a polyvalent scaffold does not interfere with the self-assembly of homopolymers **14c** and **15** with their corresponding small molecule receptors. Using ^{1}H NMR spectroscopic studies, we were able to prove that both polymers **14c** and **15** can be quantitatively functionalized. Figure 3.5 shows the ^{1}H NMR spectra for the self-assembly of polymer **14c** with the small molecule **2**. Upon the addition of the dibenzylammonium cation **2**•Bar_F^- to homopolymer **14c**, the fully complexed polymer **(2)$_n$•14c** forms. The ammonium benzylic signals move to 4.5 ppm from their original position at 4.2 ppm (spectra A and C). In addition, upon the threading of **2** into polymer **14c**, the crown ether signals move from 4.1 ppm, 3.9 ppm, and 3.8 ppm to 4.0 ppm, 3.6 ppm, and 3.2 ppm, respectively, indicating the quantitative complexation of the homopolymer (spectrum C). After the addition of excess **2**•Bar_F^- to polymer **(2)$_n$•14c**, a new signal at 4.2 ppm is observed that corresponds to the "free" dibenzylammonium salt. Moreover, after the deprotonation of the dialkylammonium cation **2**•Bar_F^- with triethylamine to form dibenzylamine, the benzylic ammonium signals disappear along with the complexed crown ether signals, and the original signals are evident (spectrum D). These results clearly demonstrate that self-assembly occurred and that the self-assembly step is reversible. Similar results were found for the self-assembly of **3** with polymer **15**.

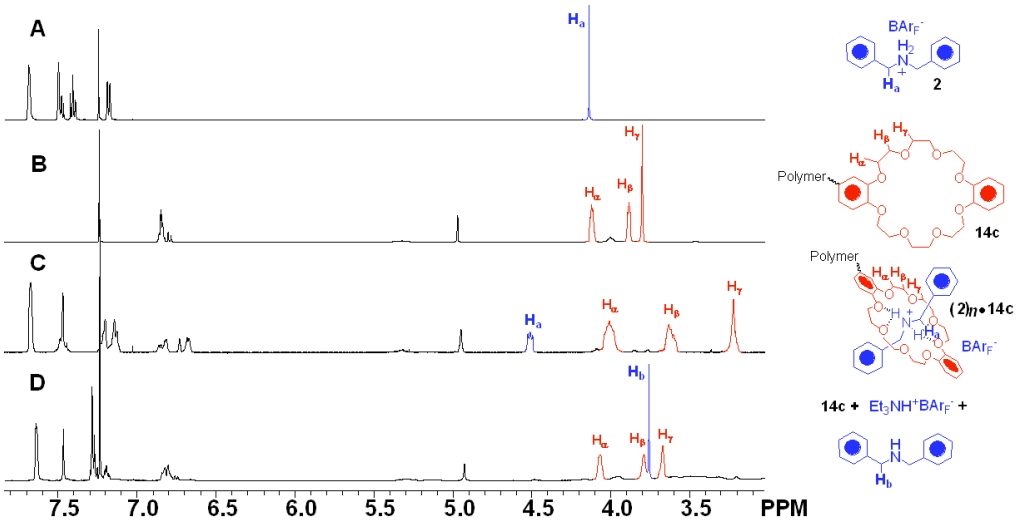

Figure 3.5. ^{1}H NMR spectra (500 MHz) representing the self-assembly of polymer **14c** with **2•Bar$_F$**$^-$ in $CDCl_3$. (A) **2•Bar$_F$**$^-$, H_a represents benzylic protons; (B) **14c** H_a, H_b, H_g represent un-equivalent sets of crown ether protons; (C) Formation of **(2)$_n$•14c** upon the addition of 1 eq. of **2** to polymer **14c** (based on integrations of crown ether / dibenzylammonium signals), H_a represents complexed benzylic proton , H_a, H_b, H_g represent un-equivalent sets of complexed crown ether protons; (D) Regeneration of **14c** after the addition of excess Et_3N to polymer **(2)$_n$•14c**, H_b represents benzylic protons on dibenzylamine, H_a, H_b, H_g represent un-equivalent sets of un-complexed crown ether protons.

Once the self-assembly of homopolymers **14c** and **15** with their small molecule receptors was found to be independent of the polymer backbone, the self-assembly behavior of block copolymers **18** and **20** were examined. Two distinct routes for the functionalization of copolymers **18** and **20** were investigated, one in which the hydrogen-bonding step precedes the metal coordination and *vice versa*. In the case of both copolymers **18** and **20**, the self-assembly was independent of the order of functionalization.

The DB24C8 recognition moiety **4** assembles spontaneously with the dibenzylammonium cation **2** in aprotic solvents. The palladated pincer, however, requires activation via the addition of silver tetrafluoroborate. Upon activation, the Pd^{II} pincer immediately assembles with pyridines such as **5**. The same behavior was observed

for both copolymers. Figure 3.6 shows the ^{1}H NMR spectra of the stepwise self-assembly of copolymer **18** with **5** and **2**•Bar_F^- and the subsequent stepwise de-functionalization of copolymer $\mathbf{(2)}_m\mathbf{(5)}_n\bullet\mathbf{18}$. Spectrum B shows the copolymer **18** (shown by itself in spectrum A) with pyridine **5** added. Upon the addition of silver tetrafluoroborate, the pincer is activated upon removal of the chloride ligand and pyridine **5** rapidly coordinates to the pincer receptor to form copolymer $\mathbf{(5)}_n\bullet\mathbf{18}$ (spectrum C). The diagnostic a-pyridyl proton moves upfield to 8.1 ppm, while the Pincer methylene arms become sharper and move slightly downfield from about 4.6 ppm to 4.8 ppm. The dibenzylammonium cation **2**•Bar_F^- is subsequently added, and the crown ether complexation occurs, resulting in the fully functionalized copolymer $\mathbf{(2)}_m\mathbf{(5)}_n\bullet\mathbf{18}$ (spectrum D). The same characteristic shifts for the complexations of **2**•Bar_F^- with the crown ether moiety of **18** as detailed above for the complexation of **2**•Bar_F^- with **14** are observed. The noncovalent assembly can then be reversed in a one-step or step-wise manner with the addition of triethylamine and triphenylphosphine. Triethylamine deprotonates the dibenzylammonium cation **2**•Bar_F^- resulting in the formation of dibenzylamine, effectively de-threading the crown complexation but leaving the pyridine fully assembled to the pincer recognition unit (Spectrum E). Finally, upon the addition of triphenylphospine, the pyridine ligand **5** is quantitatively displaced from the pincer complex (Spectrum F). The decomplexation of **5** and **2**•Bar_F^- from the copolymers is evident by the shifting of all signals of **18** in the ^{1}H NMR spectrum back to their original position that are detailed in spectrum A. It is important to note that spectrum F contains a variety of signals corresponding to non-coordinated pyridine, coordinated triphenylphosphine, dibenzylamine and triethylamine that are all absent in spectrum A.

However, all signals characteristic of the uncomplexed **18** are evident in spectrum F. These results clearly demonstrate that the functionalization of the recognition units are independent of each other and can be addressed in an orthogonal fashion.

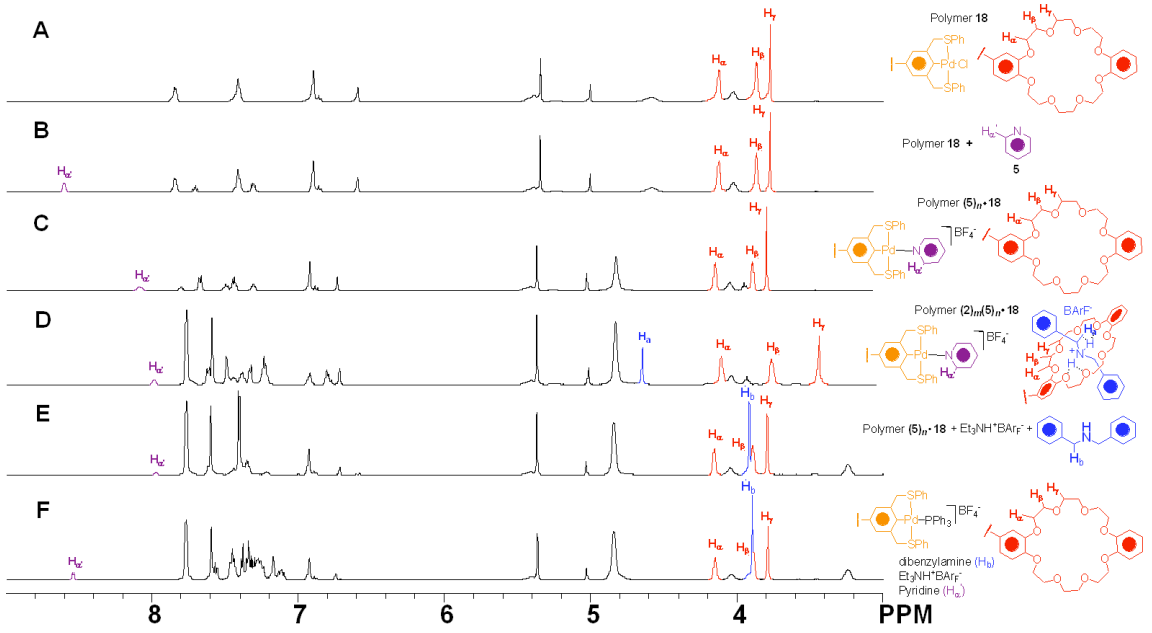

Figure 3.6. ^{1}H NMR spectra (500 MHz, 298K) in CD_2Cl_2[61] showing the stepwise functionalization of copolymer 18 with 2 and 5 and the subsequent receptor removal. (A) Copolymer **18**, H_a, H_b, H_g represent inequivalent sets of crown ether protons; (B) copolymer **18** and receptor **5**, (H_a = a-pyridyl protons); (C) activation of copolymer **18** with $AgBF_4$ to form copolymer $\mathbf{(5)_n \bullet 18}$ (H_a = a-pyridyl protons on pyridine-pincer complex); (D) fully functionalized copolymer $\mathbf{(2)_m(5)_n \bullet 18}$ after addition of $\mathbf{2 \bullet Bar_F^-}$ to $\mathbf{(5)_n \bullet 18}$, ($H_a$ = a-pyridyl protons on pyridine-pincer complex), (H_a, H_b, H_g = inequivalent sets of complexed crown ether protons), (H_a = complexed benzylic protons on $2 \bullet Bar_F^-$); (E) copolymer $\mathbf{(2)_m(5)_n \bullet 18}$ after addition of Et_3N, (H_a, H_b, H_g = inequivalent sets of un-complexed crown ether protons), (H_a = a-pyridyl protons complexed pyridine), (H_b = benzylic protons on dibenzylamine). (F) copolymer $\mathbf{(5)_n \bullet 18}$ after addition of PPh_3, (H_a, H_b, H_g = inequivalent sets of un-complexed crown ether protons), (H_a = a-pyridyl protons un-complexed pyridine).

To measure if the bond strengths of the recognition units are independent of each other, association constants for all polymers and hydrogen-bonding molecular receptors in $CHCl_3$ were obtained using isothermal titration calorimetry (ITC). The results of these experiments are summarized in Table 3.2. The measured K_a values were determined

using a single-site binding model; thus, the association constants are representative of the average binding strength of a single side-chain on the polymer, *i.e.* the binding of each receptor unit is treated as an independent recognition event. In general, our ITC results show that our polymeric hydrogen-bonding system results in very high association strengths. The highest association constant (K_a = 2 x 10^6 M^{-1}) was measured for homopolymer **14c** upon binding with the dialkylammonium cation **2**. Binding of the complementary homopolymer **15** with the small molecule **3** resulted in a slightly lower association constant (K_a = 1 x 10^5 M^{-1}). Potential reasons for the lowered association strength are steric hinderence created by the bound DB24C8 **3** along the sites of the polymer backbone as well as different solubility behavior of the two homopolymers. In general, hydrogen-bonding association constants for all copolymers were less than the association constants of their homopolymer analogs, in part due to differences in solubility of the individual blocks of the copolymers in comparison to their homopolymer analogs. However, the hydrogen-bonding binding strengths of both copolymers **18** and **20** were independent of the metal coordination step. The association constants measured before and after metal-coordination for both polymers were identical within experimental error. These results clearly demonstrate that the two employed recognition units do not interfere with each other and that the self-assembly of our copolymers can be executed orthogonally.

Table 3.2. Association constants for the hydrogen-bonding interactions in all polymers.

Polymer	Ligand	K_a (10^4 M^{-1})	Error (10^4 M^{-1})
14c	**2**•Bar_F^-	290	± 54
15	**3**	10	± 4
18	**2**•Bar_F^-	40	± 15
(5)$_n$•18	**2**•Bar_F^-	50	± 17
20	**3**	9	± 4
(5)$_n$•20	**3**	5	± 2

3.4 Conclusion

In this chapter, a next generation supramolecular polymer has been reported that possess recognition moieties that assemble with their complementary receptor molecules with very high association strengths. We have established that through the employment of living polymerization techniques, we can control the architecture of such polymeric systems. In this contribution, we have demonstrated this control by synthesizing block copolymers. Using ^{1}H NMR spectroscopic and ITC studies, we have proven that the self-assembly of our polymers is quantitative, reversible, and can be achieved in an orthogonal fashion. Our study demonstrates the potential for the employment of such a functionalization strategy in polymeric materials. Generic polymer backbones based on such high association constant-based recognition units are a prerequisite for the employment of the UPB in materials science and the results presented in this Chapter further this goal.

3.5 Experimental Section

3.5.1 General Methods

Reagents were purchased either from Acros Organics, Aldrich Company, or Strem Chemicals and used without further purification unless otherwise noted. CH_2Cl_2 was dried via passage through copper oxide and alumina columns. Routine NMR spectra were recorded using a 300 MHz (^{1}H, 300 MHz; ^{13}C, 75 MHz) or 500 MHz (^{1}H, 500 MHz; ^{13}C, 125 MHz) Varian Mercury spectrometer; spectra were referenced to residual proton solvent. The Georgia Tech Mass Spectrometry Facility provided mass spectral analysis using a VG-70se spectrometer. Atlanta Microlabs, Norcross, GA, performed all elemental analysis. Gel-permeation chromatography (GPC) analyses for all polymers were carried out using a Waters 1525 binary pump linked to a Waters 2414 refractive index detector using HPLC grade CH_2Cl_2 as the eluting solvent on an American Polymer Standards 10 μm particle size, linear mixed bed packing columns (2x). Poly(styrene) standards were used to calibrate all GPCs. Isothermal titration calorimetry (ITC) was performed on a Microcal VP-ITC Isothermal Calorimeter. Degassed, HPLC grade solvents were used for all ITC experiments.

3.5.2 Synthesis

Dibenzylammonium BAr_F (2).

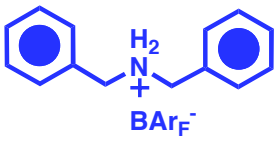

In a degassed flask, $NaBAr_F$[62] (380 mg, 0.43 mmol) was added to a solution of dibenzylammonium chloride (100 mg, 0.43 mmol) in anhydrous Et_2O (10 mL). The mixture was stirred vigorously for four hours and then filtered. Subsequently, the filtrate was evaporated to dryness under reduced pressure to afford the product (450 mg, 99%) as a white solid. ^{1}H NMR (CD_2Cl_2): δ = 4.29 (br s, 4H), 7.18 (d, 4H, *J* = 8.7 Hz), 7.45 (t, 4H, *J* = 8.7 Hz), 7.50 (t, 2H, *J* = 8.7 Hz), 7.52 (br s, 4H), 7.68 (br s, 8H). ^{13}C NMR (CD_2Cl_2): δ = 51.4, 117.3, 123.4, 125.5, 128.1, 129.1, 130.2, 131.0, 131.5, 134.6. MS (ESI) for $C_{14}H_{16}N$: m/z 198.1277, found m/z 198.1386 ($[M–BAr_F]^+$, 100%). Anal. Calcd for $C_{48}H_{28}BF_{24}N$: C, 52.05; H, 2.66; N, 1.32. Found: C, 52.16; H, 2.69; N, 1.44.

***exo*-Bicyclo[2.2.1] hept-5-ene-2-carboxylic acid 10-hydroxy-decyl ester (7).**

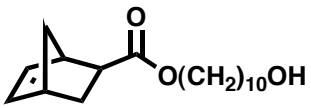

exo-Bicyclo[2.2.1] hept-5-ene-2-carboxylic acid (2.6 g, 19 mmol) and decane-1,10 diol (9.9 g, 57 mmol) were dissolved in anhydrous CH_2Cl_2 (25 mL) under an argon atmosphere. To the stirred solution, DCC (3.92 g, 19 mmol) in CH_2Cl_2 (5 mL) and DMAP (catalytic amount) were added at 25 °C. Following stirring at reflux for twelve hours, the mixture was cooled to room temperature, and the precipitate was filtered off. The filtrate was dried ($MgSO_4$) and the solvent removed under reduced pressure to give a yellow oil that was further purified by column chromatography (SiO_2, eluant: 3:1 hexanes/EtOAc) to yield a clear oil (3.35 g, 60%). ^{1}H NMR ($CDCl_3$): δ = 6.12 (m, 2H), 4.07 (t, 2H, *J* = 6.6 Hz), 3.63 (t, 2H, *J* = 6.6 Hz), 3.03 (m, 1H), 2.92 (m, 1H), 2.21 (m, 1H), 1.91 (m, 1H) 1.67-1.50 (m, 5H) 1.43-1.24 (m, 15H). ^{13}C NMR ($CDCl_3$): δ = 176.6, 138.3, 136.0, 64.8, 63.2, 46.8, 46.6, 43.4, 41.9, 33.0, 30.5, 29.7, 29.7, 29.6, 29.4, 28.9,

26.1, 25.9. MS (ESI+): *m/z* = 295.2 (M+1). Anal. Calcd for $C_{18}H_{30}O_3$: C, 73.43; H, 10.27. Found: C, 72.99; H, 10.29.

***exo*-Bicyclo[2.2.1] hept-5-ene-2-carboxylic Acid 9-carboxy-nonyl Ester (8).**

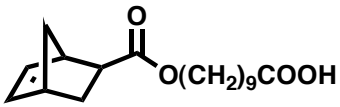

Compound **7** (2.27 g, 7.77 mmol) and PDC (17.13 g, 46.64 mmol) were dissolved in DMF (50 mL) and stirred at room temperature for 48 hours. Water (20 mL) was added and the mixture was extracted with Et_2O (3 x 15 mL). The combined organic layers were washed with H_2O (2 x 20 mL) and dried ($MgSO_4$). The solvent was removed under reduced pressure to give a brown oil that was further purified by column chromatography (SiO_2, eluant: 2:1 hexanes/EtOAc) to yield a clear oil (1.89 g, 80%). ^{1}H NMR ($CDCl_3$): δ = 6.12 (m, 2H), 4.07 (t, 2H, *J* = 6.6 Hz), 3.03 (m, 1H), 2.92 (m, 1H), 2.35 (t, 2H, *J* = 7.7 Hz), 2.20 (m, 1H), 1.90 (m, 1H), 1.63 (m, 4H), 1.53 (d, 1H, *J* = 8.3 Hz), 1.39-1.26 (m, 13H). ^{13}C NMR ($CDCl_3$): δ = 180.3, 176.7, 138.3, 136.0, 64.8, 46.8, 46.6, 43.4, 41.9, 34.3, 30.5, 29.5, 29.4, 29.2. 28.9, 26.1, 24.9. MS (ESI+): *m/z* = 309.2 (100), 617.5 (25, dimer). Anal. Calcd for $C_{18}H_{28}O_4$: C, 70.10; H, 9.15. Found: C, 69.87; H, 9.06.

***exo*-Bicyclo[2.2.1] hept-5-ene-2-carboxylic acid 9- (2,5,8,11,18,21,24,27-octaoxa-tricyclo[26.4.0.0^{12,17}]-dotriaconta-1(32), 12(17), 13, 15, 28, 30-hexaen-14-yl-methoxycarbonyl)-nonyl ester (12).**

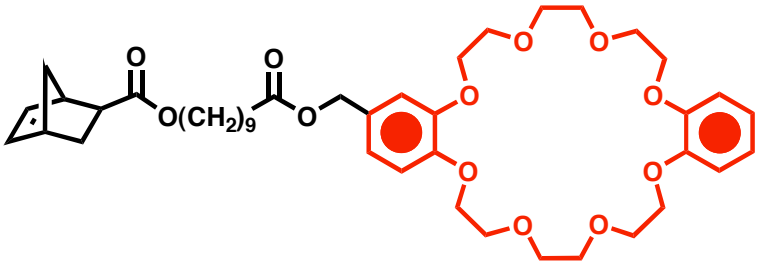

Compound **8** (0.38 g, 1.23 mmol) and compound **10** (0.59 g, 1.23 mmol) were dissolved in anhydrous CH_2Cl_2 (25 mL) under an argon atmosphere. To the stirred solution, DCC (0.3 g, 1.45 mmol) in CH_2Cl_2 (5 mL) and DMAP (catalytic amount) were added at 25 °C. Following stirring at reflux for twelve hours, the mixture was cooled to room temperature, and the precipitate was filtered off. The filtrate was dried ($MgSO_4$) and the solvent removed under reduced pressure to give a yellow oil that was further purified by column chromatography (SiO_2, eluant: EtOAc) to yield a white solid (0.86 g, 90%). ^{1}H NMR ($CDCl_3$): δ = 6.90 – 6.81 (m, 7H), 6.12 (m, 2H), 5.00 (s, 2H), 4.15 (t, 7H, *J* = 4.4 Hz), 4.07 (t, 2H, *J* = 7.2 Hz), 3.92 (t, 7H, *J* = 4.4 Hz), 3.83 (m, 7H), 3.03 (m, 1H), 2.92 (m, 1H), 2.32 (t, 2H, *J* = 7.2 Hz), 2.20 (m, 1H), 1.91 (m, 1H), 1.71-1.51 (m, 8H), 1.40-1.25 (m, 12 H). ^{13}C NMR ($CDCl_3$): δ = 176.0, 174.0, 149.1, 149.0, 138.3, 136.0, 129.3, 121.9, 121.6, 114.5, 114.2, 113.8, 71.6, 71.5, 70.2, 70.1, 69.7, 69.6, 66.3, 64.8, 46.8, 46.6, 43.4, 41.9, 34.6, 34.2, 30.5, 29.5, 29.4, 29.3, 28.9, 26.1, 25.9, 25.2, 25.1. MS (FAB+): *m*/*z* = 768.5 (30), 154.2 (100). Anal. Calcd for $C_{43}H_{60}O_{12}$: C, 67.17; H, 7.87. Found: C, 66.93; H, 7.90.

***exo*-Bicyclo[2.2.1]hept-5-ene-2-carboxylic acid 9-{3-[(benzyl-tert-butoxycarbonyl-amino)-methyl]-benzyl oxycarbonyl}-nonyl ester (11).**

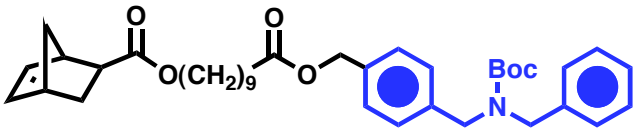

Compound **8** (0.76 g, 2.5 mmol) and compound **9** (0.95 g, 2.90 mmol) were dissolved in anhydrous CH_2Cl_2 (25 mL) under an argon atmosphere. To the stirred solution, DCC (0.60 g, 2.75 mmol) and DMAP (catalytic amount) were added at 25 °C. Following stirring at reflux for twelve hours, the mixture was cooled to room temperature, and the precipitate was filtered off. The filtrate was dried ($MgSO_4$) and the solvent removed under reduced pressure to give a yellow oil that was further purified by column chromatography (SiO_2, eluant: 3:1 Hexanes: EtOAc) to yield a clear oil (1.38 g, 90%). ^{1}H NMR ($CDCl_3$): δ = 7.33-7.21 (m, 9H), 6.12 (m, 2H), 5.1 (s, 2H), 4.41 (s, 2H), 4.33 (s, 2H), 4.07 (t, 2H, *J* = 6.6 Hz), 3.03 (m, 1H), 2.91 (m, 1H), 2.35 (t, 2H, *J* = 7.15 Hz), 2.20 (m, 1H), 1.91 (m, 1H), 1.71-1.58 (m, 4H), 1.49 (s, 9H), 1.40-1.23 (m, 13H). ^{13}C NMR ($CDCl_3$): δ = 176.7, 174.0, 156.4, 138.4, 136.2, 135.6, 128.9, 128.8, 128.4, 128.0, 127.7, 80.54, 66.21, 64.9, 49.2, 47.0, 46.8, 43.6, 42.0, 34.7, 30.7, 29.7, 29.56, 29.55, 29.5, 29.4, 29.1, 28.9, 26.3, 25.3. MS (ESI+): *m/z* = 618.5 (50). Anal. Calcd for $C_{38}H_{51}NO_6$: C, 73.87; H, 8.32; N, 2.27. Found: C, 73.87; H, 8.34; N, 2.36.

General Polymerization Procedure. An amount of monomer was weighed into a glass vial with a rubber septum cap, placed under an Argon atmosphere and dissolved in anhydrous, degassed CD_2Cl_2 or $CDCl_3$ (1 mL per 100 mg of monomer). A stock solution of the catalyst (in the corresponding solvent) was prepared, and the desired volume of solution was added to the polymerization vessel. Upon complete polymerization, ethyl vinyl ether was added to quench the polymerization. The polymer was isolated and purified by repeated precipitations into cold hexanes or MeOH.

Polymer 14.

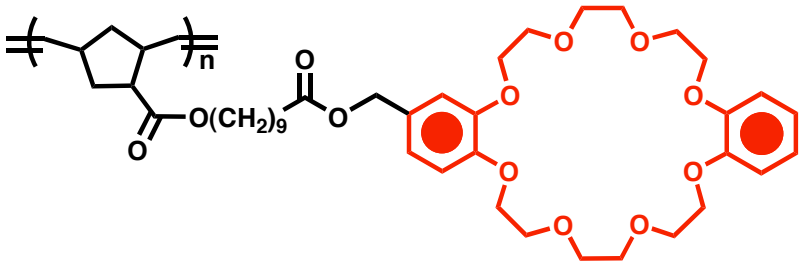

^{1}H NMR ($CDCl_3$): δ = 6.90-6.78 (m, 7H), 5.42-5.10 (br m, 2H), 5.00 (s, 2H), 4.17 (m, 7H), 4.05 (br m, 2H), 3.90 (m, 7H), 3.80 (m, 7H), 2.8-2.4 (br m, 4H), 2.25 (br t, 2H, *J* = 7.4 Hz), 2.2-1.45 (m, 8H), 1.40-1.00 (m, 12H). ^{13}C NMR ($CDCl_3$): δ = 176.2, 173.9, 149.1, 149.0, 129.4, 121.9, 121.7, 115-113, 72.9, 71.5, 71.4, 70.2, 70.1, 69.7, 69.6, 66.3, 64.7, 49.4, 34.5, 34.2, 29.6, 29-28, 26.1, 25.8, 25.1. Anal. Calcd for **14c**: C, 76.17; H, 7.87. Found: C, 66.45; H, 8.14.

Polymer 13.

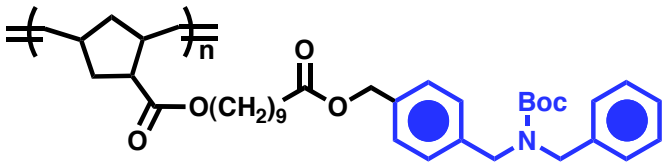

^{1}H NMR ($CDCl_3$): δ = 7.41-7.03 (m, 9H), 5.36-5.25 (m, 2H), 5.12 (s, 2H), 4.43 (s, 2H), 4.33 (s, 2H), 4.00 (br t, 2H, *J* = 6.5 Hz), 2.72-2.51 (m, 2H), 2.35 (t, 2H, *J* = 7.5 Hz), 2.10-1.86 (br m, 2H) 1.60 (m, 4H), 1.50 (s, 9H), 1.47-1.27 (m, 13). ^{13}C NMR ($CDCl_3$): δ = 173.9, 168.1, 156.3, 152.2, 138.5, 135-127, 99.8, 86.8, 80.5, 68.6, 66.2, 64.8, 64.0, 61.0, 39.2, 34.7, 31.31, 31.26, 30.8, 29.7, 29.6, 29.3, 29.11, 28.8, 26.3, 25.3, 24.2, 23.4, 20.4. Anal. Calcd for **13c**: C, 73.87; H, 8.40; N, 2.27. Found: C, 73.79; H, 8.40, N, 2.31.

Polymer 15.

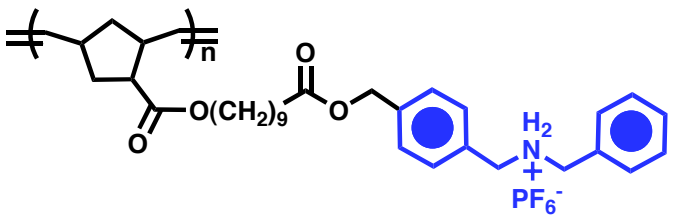

Polymer **13** (0.53 g, 0.85 mmol) was dissolved in anhydrous CH_2Cl_2 (4 mL) under an Argon atmosphere and TFA (1.0 mL, 13.51 mmol) was added. The mixture was stirred for three hours at room temperature. The solvent was removed under reduced pressure to yield the poly(DBA-TFA salt) (0.52 g, 96% yield). The resulting TFA salt (88 mg, 0.14 mmol) was dissolved in CH_2Cl_2 (10 mL) and NH_4PF_6 (2.3 g, 14 mmol) was added. The solution was stirred for three hours at room temperature to complete the ion exchange. An excess of CH_2Cl_2 was added and the mixture was washed with H_2O (2 x 20 mL). The organic layer was dried ($MgSO_4$) and the solvent was removed under reduced pressure to yield the title compound as a brown oil (85 mg, 93%). ^{1}H NMR ($CDCl_3$): δ = 9.10 (br s, 2H), 7.43-6.85 (m, 9H), 5.45-5.10 (m, 2H), 5.00 (s, 2H), 4.15-3.80 (m, 6H), 3.20-2.20 (m, 5H), 2.19-1.40 (4H), 1.40-1.10 (m, 14H). ^{13}C NMR ($CDCl_3$): δ = 174.0, 168.2, 156.4, 152.0, 138.5, 134-131, 99.8, 87.0, 80.6, 68.6, 66.2, 64.8, 64.0, 65.0, 61.1, 39.1, 34.7, 31.31, 31.25, 30.8, 29.6, 29.3, 28.8, 26.2, 25.3, 24.2, 23.4, 20.4.

Copolymer 18.

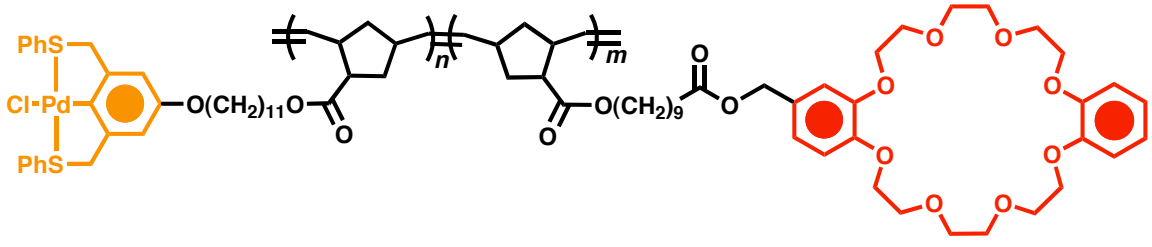

^{1}H NMR ($CDCl_3$): δ = 7.80 (m, 4H, SPh), 7.38 (m, 6H, SPh), 6.85 (m, 7H), 6.49 (s, 2H), 5.50-5.18 (m, 4H), 5.00, (s, 2H), 4.50 (br s, 4H), 4.17 (m, 7H), 4.05 (br m, 4H),

3.90 (m, 7H), 3.80 (m, 9H), 2.80-2.40 (br m, 4H), 2.25 (t, 2H, J = 7.0 Hz), 2.15-1.90 (br m, 4H), 1.80-1.40 (br m, 7H), 1.40-1.00 (br m, 34H). ^{13}C NMR ($CDCl_3$): δ = 176.2, 176.1, 173.9, 157.2, 151.7, 150.3, 149.1, 149.0, 140.0, 134-131, 130.0, 129.4, 121.9, 121.6, 114.5, 114.3, 113.8, 110.4, 109.0, 90.5, 86.6, 71.5, 70.2, 70.1, 69.7, 69.6, 68.3, 66.3, 64.7, 57.8, 51.9, 49.8, 49.4, 47.9, 42.2, 36.6, 34.5, 34.2, 29.8, 29.5, 28.9, 26.3, 26.1, 25.9, 25.2, 24.9. Anal. Calcd for **18**: C, 63.81; H, 6.94. Found: C, 64.19; H, 7.27.

Copolymer 19.

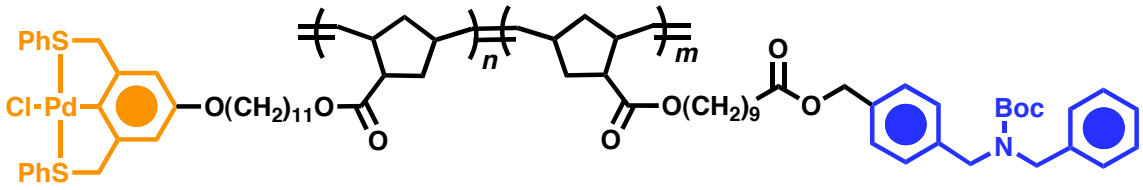

^{1}H NMR ($CDCl_3$): δ = 7.85 (m, 4H), 7.40-7.10 (m, 13H), 6.55 (s, 2H), 5.45-5.13 (m, 4H), 5.10 (s, 2H), 4.53 (br s, 4H), 4.40 (m, 4H), 4.05 (m, 4H), 3.85 (br t, 2H, J = 6.6 Hz), 2.80-2.45 (m, 6H), 2.35 (t, 2H, J = 7.6 Hz), 2.10-1.85 (m, 6H), 1.80-1.55 (m, 18H), 1.50 (s, 9H), 1.49-1.10 (m, 22H). ^{13}C NMR ($CDCl_3$): δ = 173.9, 168.1, 157.4, 156.4, 152.2, 151.9, 150.5, 135-127, 109.2, 99.8, 86.8, 80.5, 68.6, 66.2, 64.9, 64.0, 61.0, 58.8, 52.1, 39.2, 34.7, 31.3, 31.2, 30.8, 29.9, 29.7, 29.6, 29.3, 29.1, 28.8, 26.5, 26.3, 25.3, 24.2, 23.4, 20.4. Anal. Calcd for **19**: C, 66.65; H, 7.12; N, 1.01. Found: C, 64.96; H, 7.12; N, 0.83.

Copolymer 20.

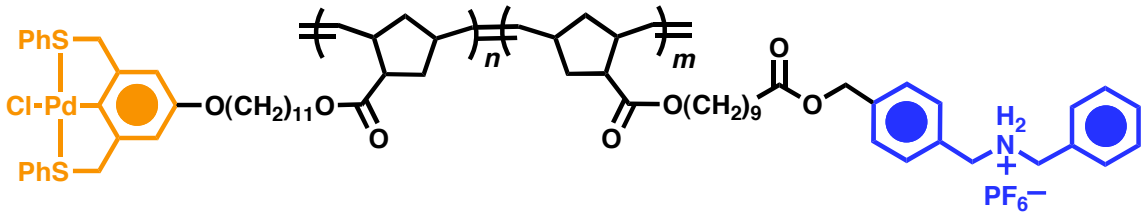

The block copolymer **20** was prepared analogously to **Polymer 15**. ^{1}H NMR ($CDCl_3$): δ = 9.00 (s, 2H), 7.85 (m, 4H), 7.40 (m, 13H), 6.60 (s, 2H), 5.40-5.10 (m, 4H), 5.00 (s, 2H), 4.60 (m, 4H), 4.30 (m, 4H), 4.10 (m, 4H), 3.90 (br t, 2H, *J* = 6.6 Hz), 2.80-2.40 (m, 6H), 2.30 (t, 2H, *J* = 7.5 Hz), 2.10-1.80 (m, 6H), 1.75-1.51 (m, 18H), 1.40-1.10 (m, 22H). ^{13}C NMR ($CDCl_3$): δ = 174.5, 173.8, 168.2, 156.8, 156.2, 152.2, 151.3, 150.0, 138.4, 134-127, 108.7, 99.8, 86.8, 80.5, 68.7, 67.9 66.2, 65.0, 64.2, 64.0, 61.0, 68.6, 51.3, 47.5, 45.3, 40.0, 39.1, 37.3, 36.0, 30.8, 30.1, 29.3, 24.2, 23.4.

3.6 References

1. J. D. Badjic´, V. Balzani, A. Credi, J. F. Stoddart, A Molecular Elevator. *Science* **2004**, *303*, 1845.

2. A. H. Flood, J. F. Stoddart, D. W. Steuerman, J. R. Heath, Enhanced: Whence Molecular Electronics? *Science* **2004**, *306*, 2055.

3. J. M. Pollino, M. Weck, Non-covalent side-chain polymers: design principles, functionalization strategies, and perspectives. *Chem. Soc. Rev.* **2005**, *34*, 193.

4. O. Ikkala, G. T. Brinke, Functional Materials Based on Self-Assembly of Polymeric Supramolecules. *Science* **2002**, *295*, 2407.

5. V. Balzani, A. Credi, F. M. Raymo, J. F. Stoddart, Artificial Molecular Machines. *Angew. Chem.* **2000**, *112*, 3484; *Angew. Chem., Int. Ed.* **2000**, *39*, 3348.

6. K. E. Uhrich, S. M. Cannizzaro, R. S. Langer, K. M. Shakesheff, Polymeric Systems for Controlled Drug Release. *Chem. Rev.* **1999**, *99*, 3181.

7. S. Arman, *J. New. Mat. Electrochem. Systems* **2001**, *4*, 173.

8. D. Philp, J. F. Stoddart, Self-Assembly in Natural and Unnatural Systems. *Angew. Chem.* **1996**, *108*, 1242; *Angew. Chem., Int. Ed. Engl.* **1996**, *35*, 1154.

9. J. M. Pollino, L. P. Stubbs, M. Weck, One-Step Multifunctionalization of Random Copolymers via Self-Assembly. *J. Am. Chem. Soc.* **2004**, *126*, 563.

10. J. M. Pollino, L. P. Stubbs, M. Weck, Living ROMP of exo-Norbornene Esters Possessing Pd^{II} SCS Pincer Complexes or Diaminopyridines. *Macromolecules* **2003**, *36*, 2230.

11. N. Yoda, Recent Development of Advanced Functional Polymers for Semiconductor Encapsulants of Integrated Circuit Chips and High-temperature Photoresist for Electronic Applications. *Polym. Adv. Technol.* **1997**, *8*, 215.

12. A. S. Abd-El-Aziz, L. J. May, J. A. Hurd, R. M. Okasha, First ring-opening metathesis polymerization of norbornenes containing cationic iron moieties. *J. Polym. Sci., Part A: Polym. Chem.* **2001**, *39*, 2716.

13. H. S. Bazzi, J. Bouffard, H. F. Sleiman, Self-Complementary ABC Triblock Copolymers via Ring-Opening Metathesis Polymerization. *Macromolecules* **2003**, *36*, 7899.

14. S. E. Bullock, P. Kofinas, Synthesis of an A/B/C Triblock Copolymer for Battery Materials Applications. *Macromolecules* **2004**, *37*, 1783.

15. J. Carlise, M. Weck, *J.* Side-chain functionalized polymers containing bipyridine coordination sites: Polymerization and metal-coordination studies. *J. Polym. Sci., Part A: Polym. Chem.* **2004**, *42*, 2973.

16. S. Kanaoka, R. H. Grubbs, Synthesis of Block Copolymers of Silicon-Containing Norbornene Derivatives via Living Ring-Opening Metathesis Polymerization Catalyzed by a Ruthenium Carbene Complex. *Macromolecules* **1995**, *28*, 4707.

17. S. Riegler, C. Slugovc, G. Trimmel, F. Stelzer, Block Copolymers via ROMP - Awakening the Sleeping Beauty. *Macromol. Symp.* **2004**, *217*, 231.

18. S. I. Stupp, M. Keser, G. N. Tew, Functionalized supramolecular materials. *Polymer* **1998**, *39*, 4505.

19. M. Weck, P. Schwab, R. H. Grubbs, Synthesis of ABA Triblock Copolymers of Norbornenes and 7-Oxanorbornenes via Living Ring-Opening Metathesis Polymerization Using Well-Defined, Bimetallic Ruthenium Catalysts. *Macromolecules* **1996**, *29*, 1789.

20. K. J. Ivin, *Olefin Metathesis*, Academic Press, London, **1996**.

21. C. W. Bielawski, R. H. Grubbs, Highly Efficient Ring-Opening Metathesis Polymerization (ROMP) Using New Ruthenium Catalysts Containing N-Heterocyclic Carbene Ligands. *Angew. Chem.* **2000**, *112*, 3025; *Angew. Chem., Int. Ed.* **2000**, *39*, 2903.

22. A. Fürstner, Olefin Metathesis and Beyond. *Angew. Chem.* **2000**, *112*, 1292 *Angew. Chem., Int. Ed.* **2000**, *39*, 3012.

23. M. S. Sanford, M. Ulman, R. H. Grubbs, New Insights into the Mechanism of Ruthenium-Catalyzed Olefin Metathesis Reactions. *J. Am. Chem. Soc.* **2001**, *123*, 749.

24. M. C. T. Fyfe, J. F. Stoddart, Interwoven supramolecular arrays via the noncovalent polymerization of pseudorotaxanes. *Coord. Chem. Rev.* **1999**, *183*, 139.

25. M. C. T. Fyfe, J. F. Stoddart, D. J. Williams, X-ray Crystallographic Studies on the Noncovalent Syntheses of Supermolecules. *Struct. Chem.* **1999**, *10*, 243.

26. M. Asakawa, T. Ikeda, N. Yui, T. Shimizu, Preparation of Porphyrin-stoppered Rotaxane Aiming at Immobilization on Substrate. *Chem. Lett.* **2002**, 174.

27. P. R. Ashton, P. J. Campbell, E. J. T. Chrystal, P. T. Glink, S. Menzer, D. Philp, N. Spencer, J. F. Stoddart, P. A. Tasker, D. J. Williams, Dialkylammonium

Ion/Crown Ether Complexes: The Forerunners of a New Family of Interlocked Molecules. *Angew. Chem.* **1995**, *107*, 1997; *Angew. Chem., Int. Ed. Engl.* **1995**, *34*, 1865.

28. T. Clifford, A. Abushamleh, D. H. Busch, Supramolecular Chemistry And Self-assembly Special Feature: Factors affecting the threading of axle molecules through macrocycles: Binding constants for semirotaxane formation. *Proc. Natl. Acad. Sci. USA* **2002**, *99*, 4830.

29. S. A. Duggan, G. Fallon, S. J. Langford, V. L. Lau, J. F. Satchell, M. N. Paddon-Row, Crown-Linked Porphyrin Systems. *J. Org. Chem.* **2001**, *66*, 4419.

30. V. Dvornikovs, B. E. House, M. Kaetzel, J. R. Dedman, D. B. Smithrud, Host-[2]Rotaxanes as Cellular Transport Agents. *J. Am. Chem. Soc.* **2003**, *125*, 8290.

31. Y. Furosho, T. Oku, T. Hasegawa, A. Tsuboi, N. Kihara, T. Takata, Dynamic Covalent Approach to [2]- and [3]Rotaxanes by Utilizing a Reversible Thiol-Disulfide Interchange Reaction. *Chem. Eur. J.* **2003**, *9*, 2895.

32. M. C. T. Fyfe, J. F. Stoddart, *Adv. Supramol. Chem.* **1999**, *183*, 139.

33. H. W. Gibson, N. Yamaguchi, J. W. Jones, Supramolecular Pseudorotaxane Polymers from Complementary Pairs of Homoditopic Molecules. *J. Am. Chem. Soc.* **2003**, *125*, 3522.

34. M. Horie, Y. Suzaki, O. Kohtaro, Formation of Pseudorotaxane Induced by Electrochemical Oxidation of Ferrocene-Containing Axis Molecule in the Presence of Crown Ether. *J. Am. Chem. Soc.* **2004**, *126*, 3684.

35. W.-C. Hung, K.-S. Liao, Y.-H. Liu, S.-M. Peng, S.-H. Chiu, Mild and High-Yielding Syntheses of Diethyl Phosphoramidate-Stoppered [2]Rotaxanes. *Org. Lett.* **2004**, *6*, 4183.

36. H. Iwamoto, K. Itoh, H. Nagamiya, Y. Fukazawa, Convenient synthesis of [3]catenane by olefin metathesis dimerizations. *Tetrahedron Lett.* **2003**, *44*, 5773.

37. S. I. Kawano, N. Fujita, S. Shinkai, Novel host–guest organogels as stabilized by the formation of crown–ammonium pseudo-rotaxane complexes. *Chem. Commun.* **2003**, 1352.

38. B. F. G. Johnson, C. M. G. Judkins, J. M. Matters, D. S. Shephard, S. Parsons, New linked and threaded cluster compounds. *Chem. Commun.* **2000**, 1549.

39. A. G. Kolchinski, N. W. Alcock, R. A. Roesner, D. H. Busch, Molecular riveting: high yield preparation of a [3]-rotaxane. *Chem. Commun.* **1998**, 1437.

40. C. P. Mandl, B. König, Luminescent Crown Ether Amino Acids: Selective Binding to N-terminal Lysine in Peptides. *J. Org. Chem.* **2005**, *70*, 670.

41. T. Oku, Y. Furusho, T. Takata, First poly[3]rotaxane synthesized through the noncovalent step-growth polymerization of a homoditopic dumbbell compound and a macrocycle with a reversible thiol-disulfide interchange reaction. *J. Polym. Sci., Part A: Polym. Chem.* **2003**, *41*, 119.

42. Y. Tokunaga, T. Seo, The contribution of complementary hydrogen bonding to supramolecular structure. *Chem. Commun.* **2002**, 970.

43. A. G. Kolchinski, D. H. Busch, N. W. Alcock, Gaining control over molecular threading: benefits of second coordination sites and aqueous–organic interfaces in rotaxane synthesis. *J. Chem. Soc., Chem. Commun.* **1995**, 1289.

44. A. M. Elizarov, S.-H. Chiu, J. F. Stoddart, An Acid-Base Switchable [2]Rotaxane. *J. Org. Chem.* **2002**, *67*, 9175.

45. T. Chang, A. M. Heiss, S. J. Cantrill, M. C. T. Fyfe, A. R. Pease, S. J. Rowan, J. F. Stoddart, A. J. P. White, D. J. Williams, Ammonium Ion Binding with Pyridine-Containing Crown Ethers. *Org. Lett.* **2000**, *2*, 2947.

46. H. W. Gibson, N. Yamaguchi, L. Hamilton, J. W. Jones, Cooperative Self-Assembly of Dendrimers via Pseudorotaxane Formation from a Homotritopic Guest Molecule and Complementary Monotopic Host Dendrons. *J. Am. Chem. Soc.* **2002**, *124*, 4653.

47. N. Yamaguchi, L. M. Hamilton, H. W. Gibson, Dendritic Pseudorotaxanes. *Angew. Chem.* **1998**, *110*, 3463; *Angew. Chem., Int. Ed.* **1998**, *37*, 3275.

48. N. Yamaguchi, H. W. Gibson, Non-covalent chemical modification of crown ether side-chain polymethacrylates with a secondary ammonium salt: a family of new polypseudorotaxanes. *Macromol. Chem. Phys.* **2000**, *201*, 815.

49. D. A. Fulton, S. J. Cantrill, J. F. Stoddart, Probing Polyvalency in Artificial Systems Exhibiting Molecular Recognition. *J. Org. Chem.* **2002**, *67*, 7968.

50. C. Gong, H. W. Gibson, Self-Assembly of Novel Polyrotaxanes: Main-Chain Pseudopolyrotaxanes with Poly(ester crown ether) Backbones. *Angew. Chem.* **1998**, *110*, 323; *Angew. Chem., Int. Ed.* **1998**, *37*, 310.

51. S. J. Cantrill, A. R. Pease, J. F. Stoddart, A molecular meccano kit. *J. Chem. Soc., Dalton Trans.* **2000**, 3715.

52. M. Albrecht, G. van Koten, Platinum Group Organometallics Based on ldquoPincerrdquo Complexes: Sensors, Switches, and Catalysts. *Angew. Chem.* **2001**, *113*, 3866; *Angew. Chem., Int. Ed.* **2001**, *40*, 3750.

53. M. Albrecht, M. Lutz, M. M. Antoine, E. T. H. Lutz, A. L. Spek, G. van Koten, *J. Chem. Soc., Dalton Trans.* **2000**, 3797.

54. D. D. Manning, L. E. Strong, X. Hu, P. J. Beck, L. L. Kiessling, Neoglycopolymer inhibitors of the selectins. *Tetrahedron* **1997**, *53*, 11937.

55. C. D. V. Nooy, C. S. l. Rondestvedt, Formation of Nortricyclene Derivatives by Bromination of exo-2,5-Methylene-1,2,5,6-tetrahydrobenzoic Acids. *J. Am. Chem. Soc.* **1955**, *77*, 3583.

56. J. D. Roberts, E. R. Trumbull, W. Bennett, R. Armstrong, The Reaction of Norbornylene with N-Bromosuccinimide. Nortricyclene and its Derivatives. *J. Am. Chem. Soc.* **1950**, *72*, 3116.

57. P. R. Ashton, M. C. T. Fyfe, P. T. Glink, S. Menzer, J. F. Stoddart, A. J. P. White, D. J. Williams, Multiply Stranded and Multiply Encircled Pseudorotaxanes. *J. Am. Chem. Soc.* **1997**, *119*, 12514.

58. R. P. Quirk, B. Lee, Experimental Criteria for Living Polymerizations. *Polym. Int.* **1992**, *27*, 359.

59. O. W. Webster, Living Polymerization Methods. *Science* **1991**, *251*, 887.

60. J. M. Pollino, M. Weck, *Synthesis* **2002**, 1277.

61. Spectra in CD_2Cl_2 are nearly identical to the spectra in $CDCl_3$ shown in Figure 5.

62. D. L. Reger, T. D. Wright, C. A. Little, J. J. S. Lamba, M. D. Smith, Control of the Stereochemical Impact of the Lone Pair in Lead(II) Tris(pyrazolyl)methane Complexes. Improved Preparation of $Na\{B[3,5\text{-}(CF_3)_2C_6H_3]_4\}$. *Inorg. Chem.* **2001**, *40*, 3810.

CHAPTER 4

Functionalization of Random Terpolymers through Molecular Recognition

4.1 Abstract

Random poly(norbornene)-based terpolymers containing Sulfur-Carbon-Sulfur (SCS) palladated pincer complexes, dibenzo[24]crown-8 (DB24C8) rings, and diaminopyridine moieties were synthesized by ring-opening metathesis polymerization. Examination of the kinetics of the polymerization led to the conclusion that the polymerization of a statistical mixture of the three monomers results in the formation of random terpolymers. The terpolymers have molecular weights between 30,000 to 50,000 Daltons, with polydispersity indices ranging form 1.3 - 1.5, as determined by gel-permeation chromatography. Side-chain functionalization of these terpolymers was achieved by self-assembling (i) pyridines to the palladated pincer complexes, (ii) dibenzylammonium ions to the DB24C8 rings, and (iii) thymines to the diaminopyridine receptors. ^{1}H NMR spectroscopy was used to monitor the self-assembly processes and revealed that all self-assembly steps were fast and near quantitative. Isothermal titration calorimetry was employed to determine the association constants for the individual noncovalent functionalization steps. For all the self-assembly steps, the association constants were unaffected by neighboring functionalities on the polymer backbone demonstrating orthogonality in the recognition expressed by the three pairs of recognition site.

4.2 Introduction

The previous chapter outlined strategies to functionalize architecturally controlled block copolymers through molecular recognition. While various materials and polymer applications require block or architecturally controlled copolymers, many of these applications also require the use of more than two functional groups along the side-chains of the polymer. Thus, a similar approach to the one outlined in Chapter 3 is applied here to terpolymers.

Highly functionalized random terpolymers are desirable synthetic targets for a large variety of biological and electronic applications. In the context of biomaterials, terpolymers have been studied as potential drug carriers.[1] Terpolymers have also been used as cross-linking materials,[2] in curing applications,[2] and as molecular switches.[3] Recently, Krzysztof *et al*. reported "smart" polymeric nanospheres produced from random terpolymers that change their conformation in response to light exposure in solution.[3] Moreover, terpolymers are candidates for solution processable materials, such as photorefractive devices that require three components in order to become operational.[4]

Despite the importance of terpolymers in materials science, synthetic strategies to produce such materials are cumbersome and time-consuming since they have relied exclusively to date on covalent approaches. A more modular approach would be to employ noncovalent synthesis which has been shown[5-7] to be an efficient tool in the formation of supramolecular materials.[9,10] In this chapter, the complexity of our approach is extended to produce an efficient strategy for the functionalization of random terpolymers using molecular recognition.

A requirement for the successful noncovalent functionalization of terpolymers is the selection of three molecular recognition motifs that can be assembled independently with their corresponding substrates. In two-component polymeric system[10] described in Chapter 3 that was based on metal coordination and hydrogen bonding, we have shown that the two self-assembly events occur in an orthogonal manner. However, in a two-component system in which both the noncovalent functionalizations are based on hydrogen bonding, we found that competition between the different recognition motifs exists.[9] Thus, in order to achieve site-specific, non-competitive, noncovalent functionalization of terpolymers, we designed a polymeric scaffold bearing three independent receptors that can be functionalized using metal coordination, pseudorotaxane formation, and hydrogen bond arrays. A graphical representation of the noncovalent functionalization strategy is shown in Figure 4.1. This approach towards terpolymer synthesis provides an attractive alternative to traditional terpolymer functionalization strategies based on covalent synthesis. It is an approach that (1) allows for rapid side-chain modification, (2) avoids lengthy post-polymerization purification steps, and (3) is reversible and therefore amenable to the rapid optimization of materials.

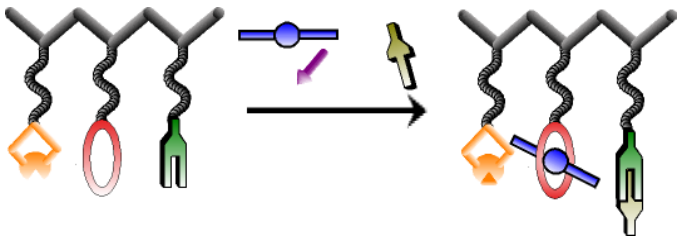

Figure 4.1. Diagram depicting noncovalent terpolymer functionalization.

The metal coordination unit we have employed is based on the palladated Sulfur-Carbon-Sulfur (SCS) pincer complex.[11-13] Secondly, pseudorotaxane formation, based on the threading of dibenzylammonium ions into dibenzo[24]crown-8 (DB24C8) rings, is employed.[14-23] The third noncovalent recognition motif is based on the diaminopyridine and thymine donor-acceptor-donor hydrogen bonding recognition pair that has already been used extensively in supramolecular polymer science.[5,10,13,24-26] The combination of these three recognition motifs along an architecturally controlled polymer backbone allows for fast and precise site-specific functionalization with a limited number of purification steps.

4.3 Results and Discussions

4.3.1 Polymer Synthesis

The terpolymers are based on norbornene monomers **1**-**3** bearing recognition motifs suitable for subsequent noncovalent modification. The synthesis and homopolymerization behavior by ring-opening metathesis polymerization (ROMP) of the three individual monomers have been reported before.[13,27] All terpolymers were synthesized according to Scheme 4.1 using the ruthenium initiator **4**, with varying amounts of monomers **1-3** resulting in terpolymers with varying densities of each recognition motif expressed along the polymer backbone. The recognition unit density was varied in order to determine if the orthogonality of the noncovalent functionalization strategy is dependent on the individual functional group densities along the polymer backbone. The molecular weights of all the terpolymers were determined using gel-permeation chromatography (GPC). Controlled molecular weights were observed for all

polymers regardless of the monomer feed ratios. GPC traces of all the terpolymers revealed monomodal distributions, ruling out the possibilities of homopolymerizations. Additionally, polydispersity indices (PDIs) ranged from 1.3-1.5 (Table 4.1) indicating well-behaved copolymerizations.

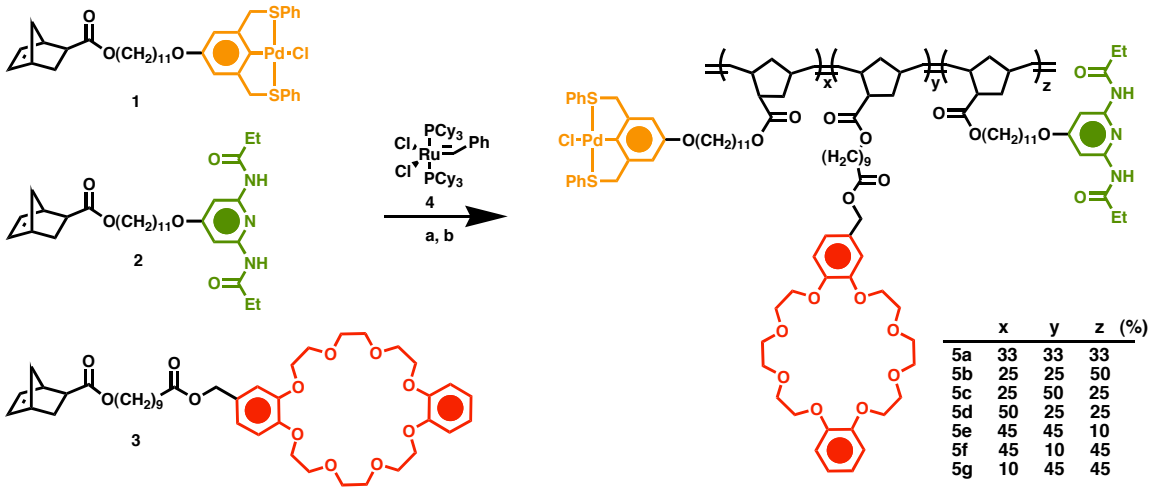

Scheme 4.1. Terpolymer Synthesis; [a](a) CH_2Cl_2, 4 h, 25 ºC; (b) ethyl vinyl ether, 10 min. Ph- and EtO- end groups are omitted for clarity.

Table 4.1. GPC Data for Terpolymers: solvent, DCM

Terpolymer	M_n	M_w	PDI
5a	42,500	56,000	1.32
5b	32,400	44,700	1.38
5c	30,600	43,600	1.42
5d	31,400	44,400	1.41
5e	21,200	30,000	1.42
5f	30,700	44,600	1.45
5g	30,000	41,500	1.38

The statistical nature of the resulting terpolymers was examined on the basis of the polymerization kinetics of individual monomers as well as from the point of view of the terpolymerization kinetics. The rate of the polymerization for the DB24C8 monomer **3** was determined by *in situ* ^{1}H NMR spectroscopy and then compared to the previously measured rates of polymerization for the monomers **1** and **2**.[13] The polymerization of a 20:1 ratio of monomer **3** to initiator **4** was complete after 20 minutes as indicated by the shift of the norbornene olefin signals originating from δ = 6.17 ppm (monomer) to δ = 5.38 ppm (polymer). Figure 4.2 displays the kinetic plot for percentage conversion with time (top) and the corresponding logarithm plot (bottom) used to calculate the rate constant for the polymerization of monomer **3** in $CHCl_3$, using ruthenium initiator **4**.

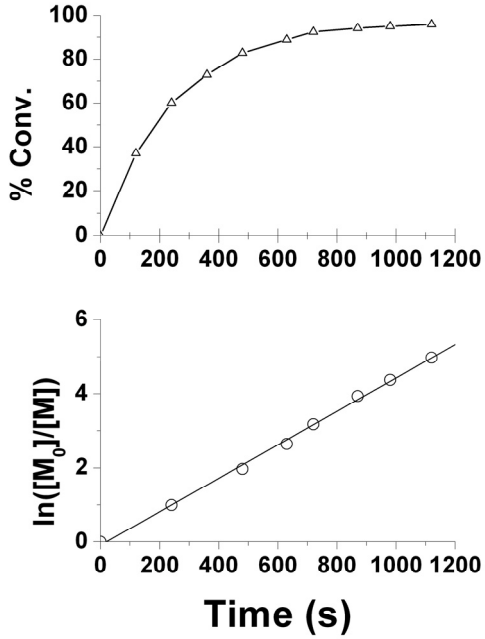

Figure 4.2. Polymerization conversion of monomer **3** over time (top); corresponding logarithmic plot (bottom).

The pseudo-first order rate constant for the polymerization of monomer **3** with [M] = 0.222 M and [I] = 0.0111 M was found to be 5.0 x 10^3 s^{-1}, a value which is comparable to the rate constants for the homopolymerizations of pincer monomer **1** (6.27 x 10^3 s^{-1}) and diaminopyridine monomer **2** (6.51 x 10^3 s^{-1}).[13] In addition, the *in situ* monitoring of terpolymerization by ^{1}H NMR spectroscopy revealed that all three monomers had undergone copolymerization within 20 minutes. Taking into account the fact that the polymerizable moiety for all three monomers is the same, these results prove that the copolymerization proceeded randomly instead of in a block copolymerization.

4.3.2 Molecular Recognition Studies

Terpolymers **5a**-**g** used in this study are capable of undergoing molecular recogntion with their complementary substrates **6**-**8**, shown in Figure 4.3. The DB24C8 recognition moiety undergoes high-yielding pseudorotaxane formation with the dibenzylammonium ions **6-H•BAr$_F$**. The BAr_F anion increases the binding affinity of the dibenzylammonium ion for the DB24C8 ring by forming a weakly associating salt with the ion, thereby increasing the charge density around the ammonium center. Pyridine (**7**) was chosen as the ligand for coordination with the Pd pincer complex because the coordination event can be characterized easily by ^{1}H NMR spectroscopy.[10] Finally, *N*-butylthymine (**8**) was chosen as the complementary substrate for the diaminopyridine receptor (**2**) because of the ease of characterizing the complex formed[10] and the increase in solubility compared to non-functionalized thymines.

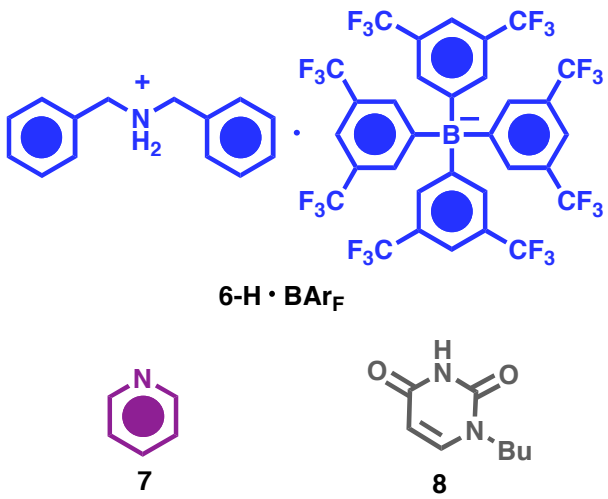

Figure 4.3. Substrates loaded onto terpolymers.

Scheme 4.2 shows the step-wise functionalization of terpolymer **5a**. First, one equivalent of pyridine (**7**) is added relative to the amount of Pd pincer complex in the terpolymer **5a**, followed by the addition of 1 equiv of $AgBF_4$. Upon the formation of the cationic[12-13] Pd species, *i.e.* the availability of an open coordination site on the Pd, the pyridine unit coordinates rapidly to the Pd-pincer complex, forming the monofunctional terpolmer $\mathbf{\{5a•(7•BF_4)_n\}^{n+}}$. Subsequently, the dibenzylammonium salt $\mathbf{6\text{-}H•BAr_F}$ is added to terpolymer $\mathbf{\{5a•(7•BF_4)_n\}^{n+}}$, and pseudorotaxane formation ensues, forming the bifunctional $\mathbf{\{5a•[(6\text{-}H•BAr_F)(7•BF_4)]_n\}^{2n+}}$. Finally, after the addition of *N*-butylthymine (**8**) to terpolymer $\mathbf{\{5a•[(6\text{-}H•BAr_F)(7•BF_4)]_n\}^{2n+}}$, the trifunctional terpolymer $\mathbf{\{5a•[(6\text{-}H•BAr_F)(7•BF_4)(8)]_n\}^{2n+}}$, is obtained.

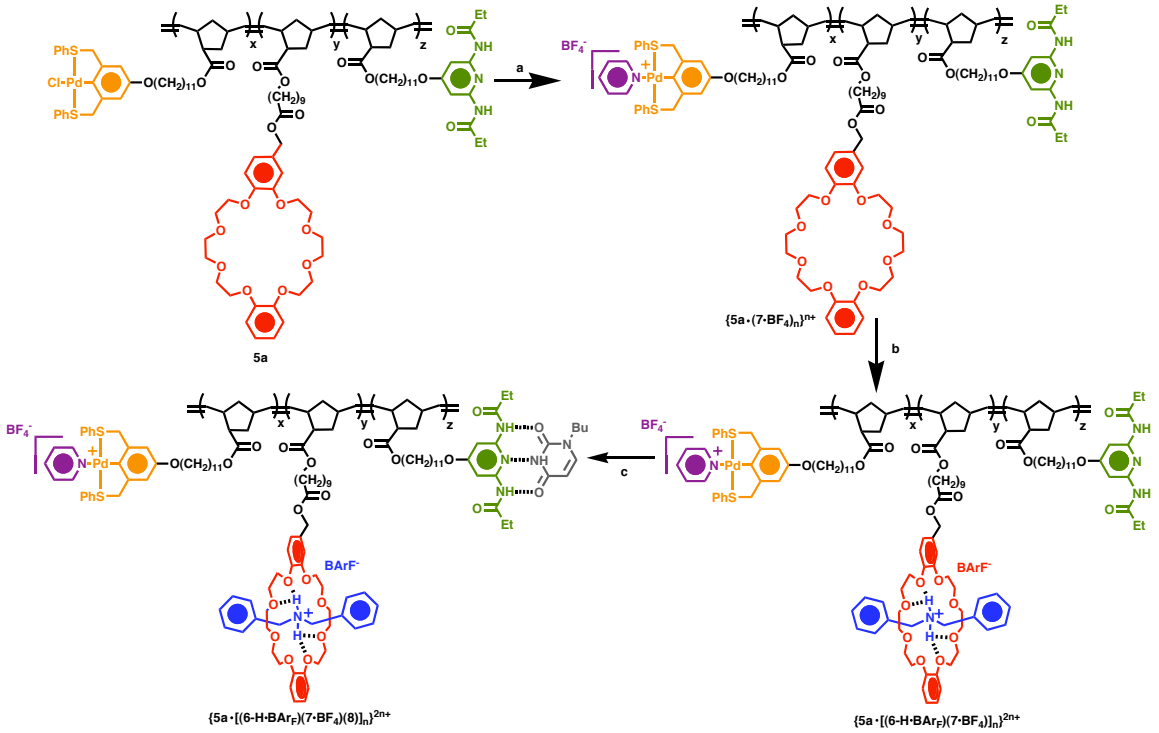

Scheme 4.1. Noncovalent terpolymer functionalizatition: (a) 7, $AgBF_4$; (b) **6-H• BAr_F**; (c) 1.5 eq. of **8** (solvent = CD_2Cl_2).

Proton NMR spectroscopy was used to monitor the self-assembly processes. Figure 4.4A shows the ^{1}H NMR spectrum of terpolymer **5a**, while Figure 4B shows a mixture of terpolymer **5a** and pyridine (**7**) which are present in a 1:1 ratio with the pincer complexes present along the terpolymer. Initially, no signal shifts are observed after the addition of pyridine **7** to **5a**. Subsequently, after the addition of $AgBF_4$ to the mixture, **7** coordinates quantitatively to the Pd centers to form the monofunctional terpolymer **{5a•(7•BF_4)$_n$}$^{n+}$** (Figure 4.4C). The coordination of the pyridine ligands to the terpolymer **5a** is reflected in the characteristic upfield shift of the α-pyridyl signal (H_b) from δ = 8.59 ppm to δ = 8.14 ppm.[28] In addition to this diagnostic shift of the α-pyridyl proton signals, the signal of the methylene arms on the pincer (labeled H_a in Figure 4.4) sharpens and shifts downfield (Figure 4C) from δ = 4.62 ppm to δ = 4.75 ppm. Furthermore, after the

addition of 1 equiv of **6-H•BAr$_F$** to the monofunctional terpolymer **{5a•(7•BF$_4$)$_n$}$^{n+}$**, pseudorotaxane formation ensues, and the bifunctional terpolymer **{5a•[(6-H•BAr$_F$)(7•BF$_4$)]$_n$}$^{2n+}$** forms (Figure 4.4D). The threading event results in diagnostic shifts of numerous of proton resonance signals in the ^{1}H NMR spectrum (Figure 4.4D). The signals of the α, β, and γ protons in the DB24C8 ring shift upfield from δ = 4.18, 3.88, and 3.79 ppm to δ = 4.13, 3.85, and 3.41 ppm, respectively. Moreover, the benzylic methylene protons (labeled H_c in Figure 4.4) adjacent to the ammonium center appear at δ = 4.62 ppm, indicating that the dibenzylammonium ions are encircled by the DB24C8 rings.[29] Furthermore, upon pseudorotaxane formation, a slight upfield shift of the α-pyridyl signal from δ = 8.14 to 7.99 ppm and a downfield shift of the pincer methylene protons from δ = 4.74 to 4.65 ppm occurs (Figure 4.4D). These shifts are indicative of a stronger coordinative bond between the pyridine ligand and the pincer complex,[28] a situation which is presumably a result of BF_4^- / BAr_F^- counterion exchange, since the nature of the outer-sphere anion present in Pd-pincer complexes has been shown to create conformational changes in the coordinated ligand, thereby affecting its magnetic environment.[30] To verify this hypothesis, control experiments on homopolymer **1** were carried out in which NaBAr$_F$ and/or dibenzylammonium BAr$_F$ were added to the polymer after the coordination of **7**. In both cases, upfield shifts of the α-pyridyl signals and downfield shifts of the pincer methylene proton signals were observed. These shifts are analogous to the shifts observed during the noncovalent terpolymer functionalization. These results indicate that counterion exchange occurs along the polymer backbone during functionalization. However, such an exchange does not interfere with the integrity

of the Pd-pyridine bond during the formation of pseudorotaxanes, proving the orthogonality of these two noncovalent interactions along the terpolymers.

Finally, in order to obtain the fully loaded functional terpolymer **{5a•[(6-H•BAr$_F$)(7•BF$_4$)(8)]$_n$}$^{2n+}$**, 1 equiv of *N*-butylthymine (**8**) is added to the bifunctional terpolymer **{5a•[(6-H•BAr$_F$)(7•BF$_4$)]$_n$}$^{2n+}$**. The ^{1}H NMR spectrum (Figure 4.4F) of the resulting functional terpolymer **{5a•[(6-H•BAr$_F$)(7•BF$_4$)(8)]$_n$}$^{2n+}$** (Figure 4.4E-F) shows a downfield shift of the imide signal of *N*-butylthymine from δ = 9.40 ppm to δ = 10.81 ppm (Figure 4.4E-F). Moreover, the amide signals of the diaminopyridine units, which were not resolved in the bifunctional terpolymer **{5a•[(6-H•BAr$_F$)(7•BF$_4$)]$_n$}$^{2n+}$**, appear (Figure 4.4F) characteristically[24] upon hydrogen bonding at δ = 9.85 ppm (Figure 4.4F). Consequently, the ^{1}H NMR spectroscopic studies reveal that the step-wise terpolymer functionalization is achieved without affecting the molecular recognition of the next receptor. Analogous chemical shifts upon the stepwise functionalization of all the terpolymers, *i.e.* **5b-g**, were observed in the ^{1}H NMR spectra.

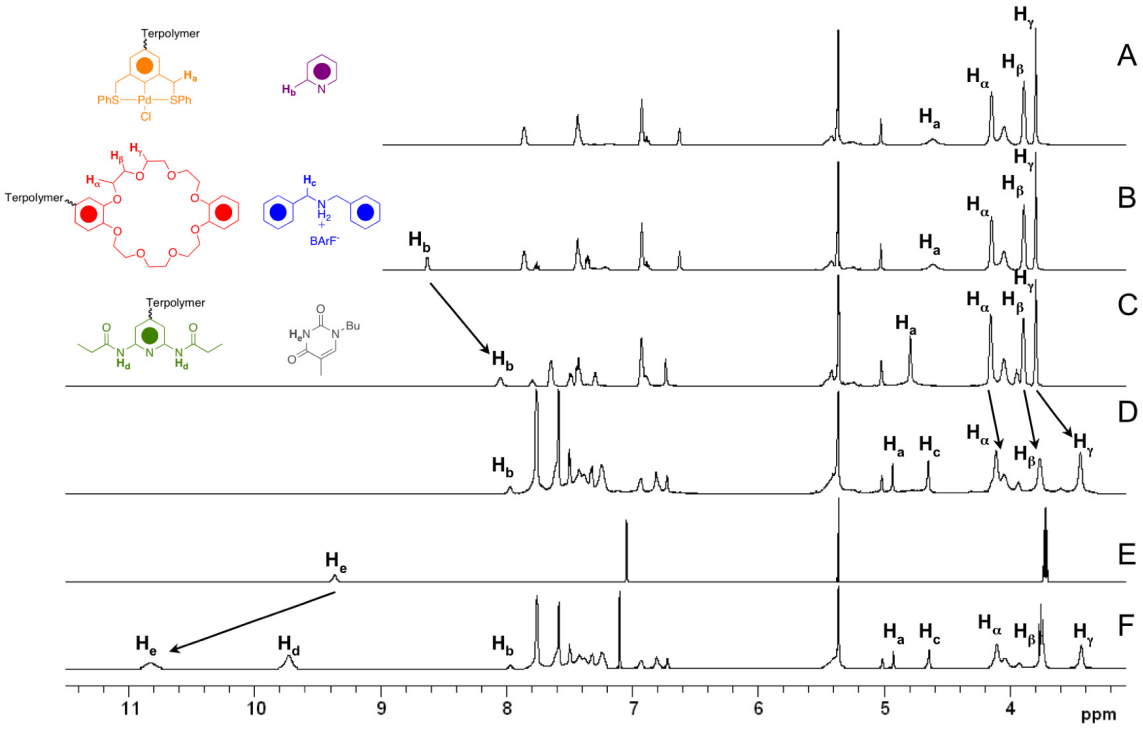

Figure 4.4. ^{1}H NMR spectra (500 MHz) with the corresponding legend depicting the self-assembly of terpolymer **5a** in CD_2Cl_2 at 25 °C. (A) Terpolymer **5a**; (B) terpolymer **5a** with 1 equiv of pyridine (**7**) (not assembled); (C) monofunctional terpolymer $\{\mathbf{5a{\bullet}(7{\bullet}BF_4)_n}\}^{n+}$ (after the addition of $AgBF_4$ to the mixture of **5a** and **7**); (D) bifunctional terpolymer $\{\mathbf{5a{\bullet}[(6\text{-}H{\bullet}BAr_F)(7{\bullet}BF_4)]_n}\}^{2n+}$ (after the addition of $\mathbf{6\text{-}H{\bullet}BAr_F}$ to $\{\mathbf{5a{\bullet}(7{\bullet}BF_4)_n}\}^{n}$); (E) reference spectra of N-butylthymine (**8**); (F) fully trifunctionalized terpolymer $\{\mathbf{5a{\bullet}[(6\text{-}H{\bullet}BAr_F)(7{\bullet}BF_4)(8)]_n}\}^{2n+}$ after the addition of 1.5 equiv of **8** to $\{\mathbf{5a{\bullet}[(6\text{-}H{\bullet}BAr_F)(7{\bullet}BF_4)]_n}\}^{2n}$.

Isothermal titration calorimetry (ITC) was attempted to determine the relative binding affinities for the three different self-assembly processes. The single-site binding constant for a ligand X binding to a polymer is given by the equation, K_a = [unfilled sites]/([filled sites][X]).[31] Each binding event along the terpolymer is therefore treated as independent, and apparent single-site association constants can be calculated using the thermodynamic parameters obtained from ITC measurements. Using this analysis, a single site association constant can be calculated from integrated heats of injection and an appropriate fit line. An example ITC isotherm with fitted heats of injection is shown in Figure 4.5. It is apparent from the isotherm that a strong binding event is occurring upon the titration of **6-H BArF** into terpolymer **5a**. If the first seven heats of injection are excluded, a single site association constant of 2 x 10^5 M^{-1} is obtained. On the other hand, if the first seven injections are included in the calculation, a best fit line is obtained assuming a two-site association model, with K_2 = 1.9 x 10^5 M^{-1} ~ K from the single association model (Figure 4.6). In either model, however, the heats of injection do not stabilize at the conclusion of the titration. Thus, the observed endothermic effect (Figures 4.5-4.6) could be occurring throughout the titration. This possibility makes our ITC data for the stronger binding components of the terpolymer largely inconclusive, regardless of the model fit. Such an endothermic effect was not observed in the case of the weaker binding event between n-butyl thymine and the terpolymers. An example ITC isotherm probing this binding event is shown in Figure 4.7; the remaining binding constants for the weaker binding event are shown in Table 4.2.

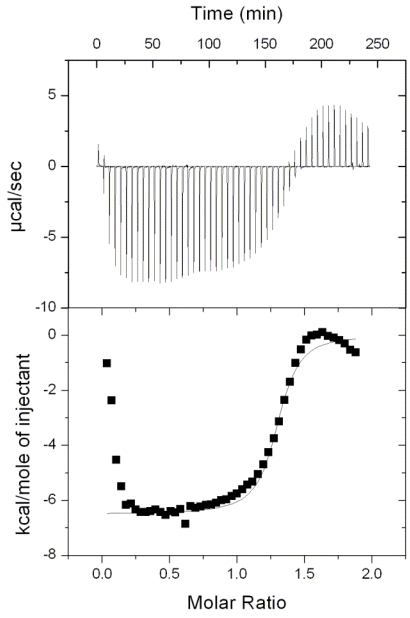

Figure 4.5. Raw ITC Isotherm (top) and fitted heats of injection (bottom); note that the first seven heats were excluded from this calculation. $K_a = 2 \times 10^5\ M^{-1}$

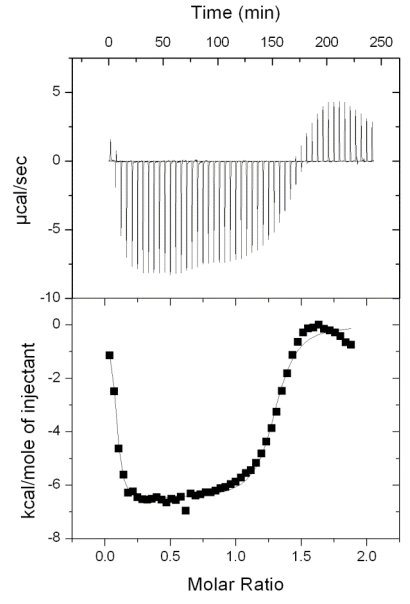

Figure 4.6. Raw ITC Isotherm (top) and fitted heats of injection (bottom) assuming a two-site association model; $K_2 = 1.9 \times 10^5\ M^{-1}$

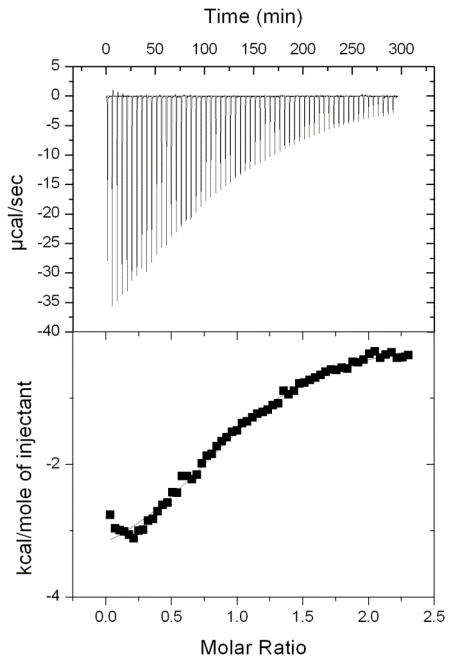

Figure 4.7. Raw ITC Isotherm (top) and fitted heats of injection (bottom) assuming a single-site association model for the titration of the thymine substrate into terpolymer **5g**; $K_a = 1.3 \times 10^3\ M^{-1}$

For terpolymers **5a-g**, the K_a value for coordinating pyridine (**7**) to the Pd-pincer complexes was found to be larger than $10^9\ M^{-1}$. Upon the titration of pyridine (**7**) into terpolymers **5a-g**, a heat saturation curve was observed, indicating the upper sensitivity level ($> 10^9\ M^{-1}$) on the ITC instrument has been reached. Strong binding isotherms are also observed upon the titration of **6-H•BAr$_F$** with the terpolymers **5a-g**. In all cases, the binding of the dibenzylammonium ion of the salt **6-H•BAr$_F$** with the DB24C8 rings on the terpolymers resulted in very tight binding, indicating near quantitative functionalization.

Table 4.2. Association Constants measured by ITC[a]

Terpolymer	K_a[b] (M^{-1})
5a	1,600
5b	1,520
5c	1,760
5d	1,650
5e	1,440
5f	1,260
5g	1,400
$\{$**5a**•**[(6-H•BAr$_F$)(7•BF$_4$)]$_n$**$\}^{2n+}$	1,570

[a]Values determined in CH_2Cl_2 at 298 K; [b]K_a for the complexation with **8**.

Nonetheless, given that association constants retrieved from binding isotherms resulting from the titration of **6-H•BAr$_F$** into terpolymers may be inconclusive given a background endothermic reaction, we attempted to establish a lower limit of binding for this process using an independent method. A precedent for establishing lower limits of binding has been established by Wilcox and coworkers.[32] The experiment involves making a 1:1 complex of the substrate: receptor pair and monitoring the chemical shift of a diagnostic proton resonance as the 1:1 complex is diluted. In simple terms, if the diagnostic proton resonance in question does not shift toward the corresponding resonance value of the same proton on the free species at a given dilution, then one can say that the association constant is above the inverse of the solution concentration. More precisely, however, the K_d value can be accurately determined by fitting a plot of δ_{obs} of

the diagnostic proton versus the solution concentration of the 1:1 complex to Equation 4.1.

Equation 4.1.

$$\delta_{obs} = \delta_s + \Delta\delta[1 + K_d/2C_o - \sqrt{(K_d/2C_o)^2 + (K_d/C_o)}]$$

Thus, an experiment was carried out in $CDCl_3$ in which terpolymer **5c** (chosen because of greater density of DB24C8 on the backbone) and **6-H•BAr$_F$** were mixed in a 1:1 ratio and monitored by ^{1}H NMR spectroscopy. The best diagnostic proton was determined to be H_c (Figure 4.4) on the dibenzylammonium cation. The δ_s value, or the resonant frequency of this proton on the free cation was determined to 4.14 ppm, whereas the $\Delta\delta$ value, or the difference in ppm(δ) between the proton resonance on the bound and unbound species, was determined to be 0.44 ppm. Spectra were taken starting from an intitial C_o value of 7 x 10^{-3} M^{-1} until a concentration of approximately 10^{-5} M^{-1} was reached, after which point resonance signals could not be resolved on a 500 MHz instrument. The results are plotted in Figure 4.8 along with a theoretical plot for an association constant of 10^5 M^{-1} based on Equation 4.1. The results strongly indicate that the association constant for this system is at least 10^5 M^{-1} not only because the complexed species diagnostic resonance does not shift toward to the unbound resonance value, but also because the plot clearly shows a divergence from the theoretical plot and the observed results. In other words, since diagnostic resonances shown in Figure 4.8 do not shift upfield during the course of the dilution (as would be expected with an association constant as low as 10^5 M^{-1}), it can be reasonably concluded that this system associates at a

value greater than or equal to 10^5 M^{-1}. Likewise, since our ITC experiments showed no major difference in association constants between terpolymers **5a-g**, we can reasonably conclude that the association constant for all terpolymers binding with **6-H•BAr$_F$** is at least 10^5 M^{-1}. The NMR spectra used to obtain these results are shown in Figure 4.9.

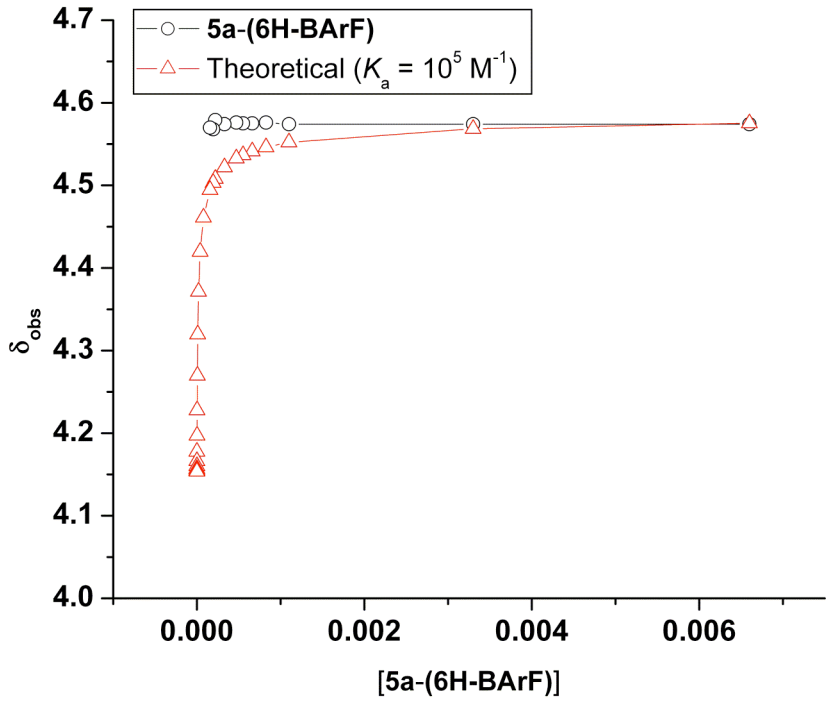

Figure 4.8. NMR titration experiment in which **6-H•BAr$_F$:5c** was diluted and chemical shifts were monitored.

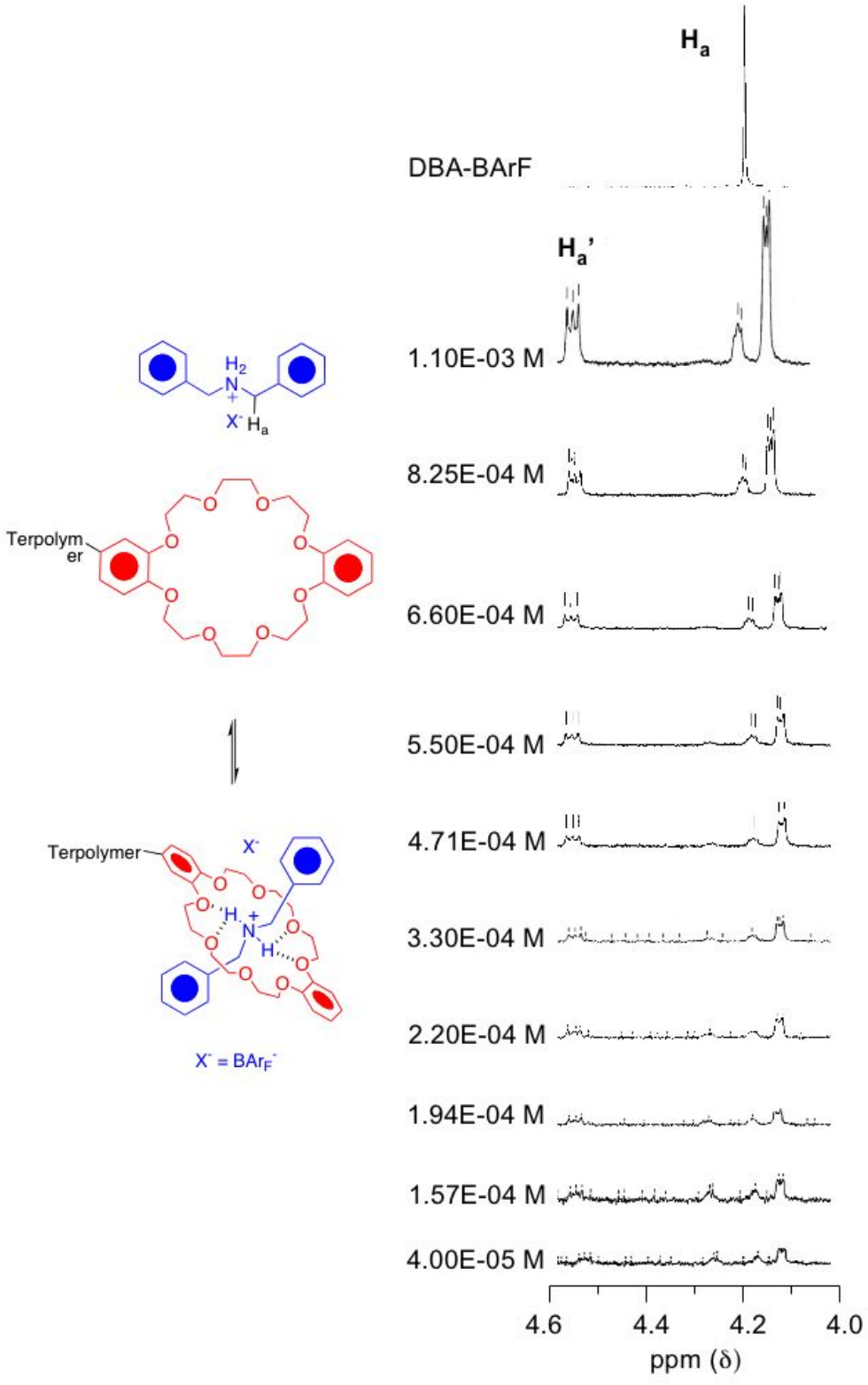

Figure 4.9. Partial stacked ^{1}H NMR spectra acquired through dilution experiment.

Lower K_a values are observed for the self-assembly process between **8** and the diaminopyridines on the terpolymers. For this self-assembly process, association constants ranging from 1,400 M^{-1} to 1,700 M^{-1} with only slight changes in association constants between terpolymers **5a-g** were measured. The small changes observed are within the experimental error limits suggesting that the K_a value for the hydrogen bonding event is independent of the terpolymer composition. Importantly, once both strong substrates like **7** and **6-H•BAr$_F$** are assembled onto terpolymer **5a**, the subsequent binding of *N*-butylthymine (**8**) with the diaminopyridine receptor to produce the fully functional terpolymer **{5a•[(6-H•BAr$_F$)(7•BF$_4$)(8)]$_n$}$^{2n+}$** is not affected (Table 4.2) by either of these two binding events. The measured association constant for the hydrogen bonding self-assembly was 1,570 M^{-1}, a value close to the K_a values measured for non-functionalized systems. These results indicated that the terpolymers can be functionalized in an orthogonal and stepwise fashion without compromising the integrity of neighboring interactions.

4.4 Conclusions

A noncovalent functionalization strategy for terpolymers based on self-assembly processes has been developed. The highly controlled terpolymerization of three different functional norbornene monomers bearing recognition motifs was successfully achieved by ROMP. An investigation of the kinetics of the polymerization of the three monomers revealed that statistical random terpolymers are formed during the controlled polymerization. Noncovalent functionalization of the terpolymers was achieved by the introduction of (i) pyridine units into Pd-pincer complexes, (ii) dibenzylammonium ions

into DB24C8 rings and (iii) *N*-butylthymines to the diaminopyridines. ^{1}H NMR spectroscopic characterization of the self-assembly events indicates that the three noncovalent interactions act independently of each other and demonstrate that the functionalization strategy can be applied to terpolymers in a stepwise fashion. Isothermal titration calorimetry and NMR spectroscropy were employed to determine the strength of these noncovalent interactions. The results show that the binding of recognition pairs is not affected by the composition of the terpolymer backbone and that functionalization can be achieved in an orthogonal manner without decreasing the binding affinities of the receptors attached to the polymer backbone. Eventually, this noncovalent functionalization strategy will be useful for creating materials for various applications that require extensive screening and rapid materials optimization. The approach we are describing requires polymer characterization of only a single, generic backbone that can be shelved and used for several different purposes. Such a generic backbone may provide a gateway to a combinatorial approach to polymer synthesis.

4.5 Experimental Section

4.5.1 General Methods

All reagents were purchased either from Acros Organics, Aldrich, or Strem Chemicals and used without further purification unless otherwise noted. CH_2Cl_2 was dried via passage through copper oxide and alumina columns. NMR spectra were recorded using a 500 MHz Bruker DRX spectrometer (^{1}H NMR: 500 MHz, ^{13}C NMR: 125 MHz). Spectra were referenced from the residual proton of the deuterated solvent. Gel-permeation chromatography analyses were carried out at room temperature using a

Waters 1525 binary pump coupled to a Waters 2414 refractive index detector with CH_2Cl_2 as the eluant and a flow rate of 1 mL/minute on American Polymer Standards 10 μm particle size, linear mixed bed packing columns. Gel-permeation chromatograms were calibrated using poly(styrene) standards. Isothermal titration calorimetry was performed on a Microcal VP-ITC Isothermal Calorimeter. Degassed, HPLC grade CH_2Cl_2 was used for all ITC experiments. Monomers **1**,[13] **2**,[13] and **3**,[27] and compounds **6-H•BAr$_F$**[27] and **8**[24] were synthesized according to the previously published procedures. The preparation chemistry involving terpolymer **5a** is given as an example for all copolymerizations and polymer functionalizations.

4.5.2 Synthesis

Terpolymer 5a.

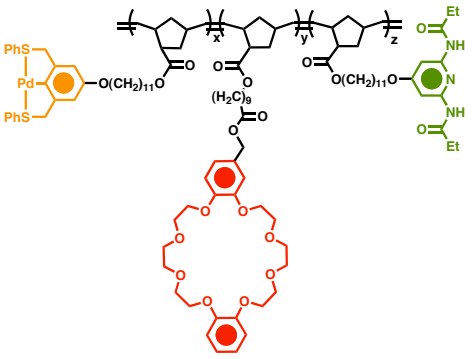

Monomers **1** (20 mg, 0.03 mmol), **2** (14 mg, 0.03 mmol), and **3** (20 mg, 0.03 mmol) were dissolved in anhydrous, degassed CH_2Cl_2 under an Argon atmosphere. The ruthenium initiator **4** (2.47 mg, 0.003 mmol) was added as a solution in CH_2Cl_2. Upon complete polymerization, a drop of ethyl vinyl ether was added to quench the polymerization. The terpolymer **5a** was isolated by repeated precipitations into cold MeOH (52 mg, 97%). ^{1}H NMR (CD_2Cl_2): δ = 8.00 (m, 4H), 7.58 (m, 6H), 7.37 (s, 2H),

7.01 (m, 7H), 6.69 (m, 2H), 5.55-5.31 (m, 6H), 5.12 (s, 2H), 4.77 (s, 4H), 4.31 (m, 8H), 4.10 (m, 6H), 3.98 (m, 8H), 3.83 (m, 8H), 3.22-3.00 (m, 6H), 3.05-1.87 (m, 83H). ^{13}C NMR ($CDCl_3$): δ = 176.0, 173.8, 150.5, 149.4, 149.3, 133.0, 131.8, 130.3, 129.9, 121.9, 121.8, 114.9, 114.7, 114.2, 109.2, 71.4, 70.2, 70.2, 69.7, 69.6, 68.5, 66.2, 64.8, 52.2, 50.0, 34.6, 29.9, 29.8, 29.7, 29.5, 29.1, 26.4, 26.3, 25.3.

Terpolymer {5a•(7•BF_4)$_n$}$^{n+}$.

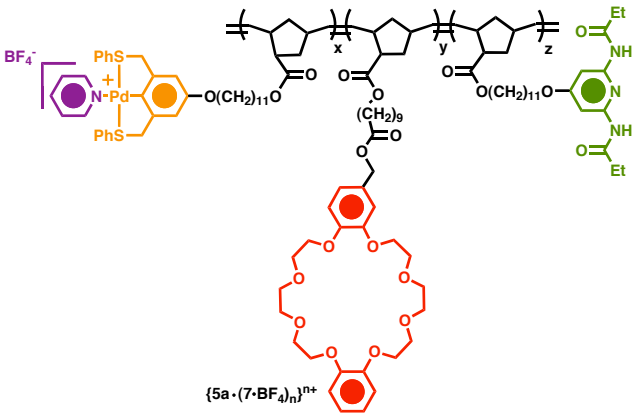

Terpolymer **5a** (50 mg) was dissolved in CH_2Cl_2 or CD_2Cl_2 and pyridine (**7**) was added until a 1:1 equivalency was reached in relation to the Pd pincer complexes as determined by ^{1}H NMR spectroscopy. One equivalent of $AgBF_4$ dissolved in $MeNO_2$ was added to the reaction mixture. After stirring for 5 min, the precipitated AgCl(s) was removed by centrifugation. The supernatant liquid was filtered through a plug of celite and subsequently through a 0.45 μm syringe filter. The solvent was removed *in vacuo* to yield the monofunctional terpolymer **{5a•(7•BF_4)$_n$}$^{n+}$** as an orange solid (yield: 100%). ^{1}H NMR (CD_2Cl_2): δ = 8.14 (s, 2H), 7.89 (m, 3H), 7.73 (m, 4H), 7.56 (m, 6H), 7.37 (s, 2H), 7.04 (m, 6H), 6.79 (m, 2H), 5.55-5.31 (m, 6H), 5.09 (s, 2H), 4.91 (s, 4H), 4.31 (m, 8H), 4.10 (m, 6H), 3.98 (m, 8H), 3.83 (m, 8H), 3.22-3.00 (m, 6H), 3.05-1.87 (m, 83H). ^{13}C NMR ($CDCl_3$): δ = 176.0, 173.8, 150.5, 149.5, 149.4, 149.3, 133.0, 130.8, 130.7,

130.3, 129.9, 121.8, 121.7, 121.5, 114.9, 114.7, 114.2, 109.2, 71.5, 70.2, 70.1, 69.7, 69.6, 68.5, 66.2, 64.8, 52.2, 50.0, 34.6, 29.9, 29.8, 29.6, 29.5, 29.1, 26.4, 26.3, 25.3.

Terpolymer {5a•[(6-H•BAr$_F$)(7•BF$_4$)]$_n$}$^{2n+}$.

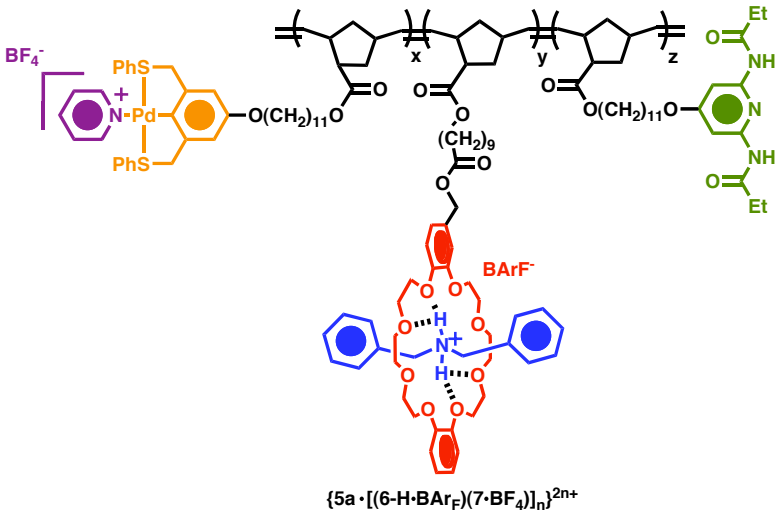

{5a•[(6-H•BAr$_F$)(7•BF$_4$)]$_n$}$^{2n+}$

Terpolymer **{5a•(7•BF$_4$)$_n$}$^{n+}$** (50 mg) was dissolved in CH_2Cl_2 and one equivalent of the dibenzylammonium salt **6-H•BAr$_F$** was added. Upon stirring the solution for 10 min, the solvent was removed *in vacuo* to yield the bifunctional terpolymer **{5a•[(6-H•BAr$_F$)(7•BF$_4$)]$_n$}$^{2n+}$** as an orange solid (yield: 100%). ^{1}H NMR (CD_2Cl_2): δ = 8.08 (s, 2H), 7.89 (m, 11H), 7.73 (m, 4H), 7.70 (m, 4H) 7.54 (m, 6H), 7.36 (s, 2H), 7.02 (s, 6H), 6.86 (m, 2H), 6.75 (m, 2H), 5.55-5.31 (m, 6H), 5.07 (s, 2H), 4.95 (s, 4H), 4.73 (s, 4H), 4.32 (m, 8H), 4.10 (m, 6H), 3.85 (m, 8H), 3.61 (m, 8H), 3.22-3.00 (m, 6H), 3.05-1.87 (m, 83H). ^{13}C NMR (CD_2Cl_2): δ = 176.0, 173.8, 150.5, 149.5, 149.4, 149.3, 147.8, 135.2, 133.0, 132.1, 130.8, 130.7, 130.2, 130.0, 129.6, 129.0, 122.0, 121.8, 121.7, 121.5, 114.9, 114.7, 114.2, 109.2, 71.5, 71.0, 70.6, 70.2, 70.2, 69.7, 69.6, 68.6, 68.5, 66.2, 64.8, 52.2, 50.0, 34.6, 29.9, 29.8, 29.6, 29.5, 29.1, 26.4, 26.3, 25.3.

Terpolymer {5a•[(6-H•BAr$_F$)(7•BF$_4$)(8)]$_n$}$^{2n+}$.

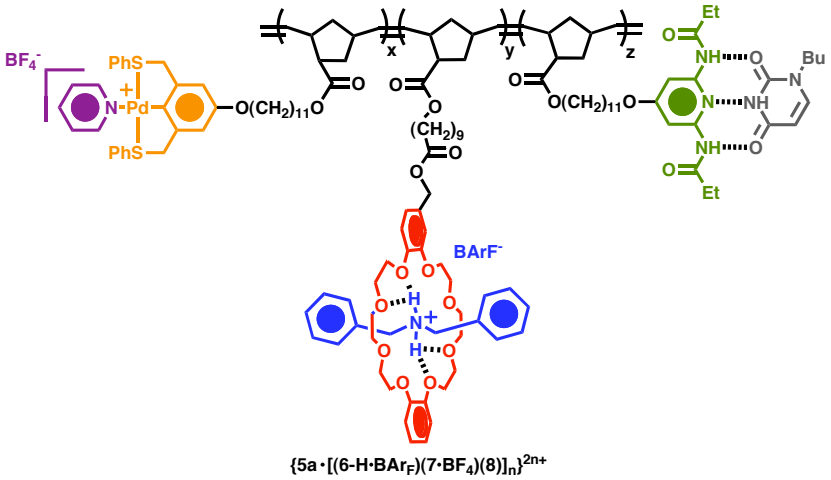

Terpolymer $\{5a\bullet[(6\text{-}H\bullet BAr_F)(7\bullet BF_4)]_n\}^{2n+}$ (50 mg) was dissolved in CH_2Cl_2 and 1.5 equiv of *N*-butylthymine (8) were added. Upon stirring the solution for 10 min, the solvent was removed *in vacuo* to yield the trifunctional terpolymer $\{5a\bullet[(6\text{-}H\bullet BAr_F)(7\bullet BF_4)(8)]_n\}^{2n+}$ as an orange solid (yield: 100%). ^{1}H NMR (CD_2Cl_2): δ = 10.80 (s, 1H), 9.65 (s, 2H), 8.08 (s, 2H), 7.89 (m, 11H), 7.73 (m, 4H), 7.70 (m, 4H) 7.54 (m, 6H), 7.36 (s, 2H), 7.15 (m, 2H) 7.02 (s, 6H), 6.86 (m, 2H), 6.75 (m, 2H), 5.55-5.31 (m, 6H), 5.07 (s, 2H), 4.95 (s, 4H), 4.73 (s, 4H), 4.32 (m, 8H), 4.10 (m, 6H), 3.85 (m, 8H), 3.76 (t, 2H, *J* = 6.5 Hz), 3.61 (m, 8H), 3.22-3.00 (m, 6H), 3.05-1.87 (m, 89H). ^{13}C NMR (CD_2Cl_2): δ = 177.0, 176.0, 173.8, 164.9, 162.7, 162.3, 161.9, 161.5, 151.4, 150.6, 147.8, 146.3, 141.1, 135.1, 132.3, 131.8, 131.5, 130.7, 130.3, 129.6, 129.4, 129.1, 129.0, 128.2, 126.5, 126.1, 123.9, 122.1, 117.9, 113.4, 113.1, 112.8, 110.5, 94.6, 71.0, 70.6, 68.7, 68.6, 68.6, 66.0, 64.8, 53.1, 48.5, 34.6, 31.4, 30.5, 30.1, 29.9, 29.7, 29.1, 26.3, 26.1, 25.3.

4.6 References

1. Wamsley, A.; Bhaskara, J.; Phiasivongsa, P.; Xiaoling, L. Synthesis of random terpolymers and determination of reactivity ratios of N-carboxyanhydrides of leucine, beta-benzyl aspartate, and valine. *J. Polym. Sci., Part A: Polym. Chem.* **2004**, *42*, 317.

2. El-Ghayoury, A.; Harald, H.; de-Ruiter, B.; Schubert, U. S. Combining Covalent and Noncovalent Cross-Linking: A Novel Terpolymer for Two-Step Curing Applications. *Macromolecules* **2003**, *36*, 3955.

3. Krzysztof, S.; Jankowska, M.; Nowakowska, M. "Smart" polymeric nanospheres as new materials for possible biomedical applications. *J. Mater. Sci.: Mater. Med.* **2003**, *14*, 699.

4. Bratcher, M. S.; DeClue, M. S.; Grunnet-Jepsen, A.; Wright, D.; Smith, B. R.; Moerner, W. E.; Siegel, J. S. Synthesis of Bifunctional Photorefractive Polymers with Net Gain: Design Strategy Amenable to Combinatorial Optimization. *J. Am. Chem. Soc.* **1998**, *120*, 9680.

5. Pollino, J. M.; Weck, M. Non-covalent side-chain polymers: design principles, functionalization strategies, and perspectives. *Chem. Soc. Rev.* **2005**, *34*, 193.

6. Brunsveld, L.; Folmer, B.; Meijer, E. W.; Sijbesma, R. P. Supramolecular Polymers. *Chem. Rev.* **2001**, *101*, 4071.

7. Lehn, J.-M. *Supramolecular Chemistry*; Wiley-VCH, 1995.

8. Philp, D.; Stoddart, J. F. Self-Assembly in Natural and Unnatural Systems. *Angew. Chem., Int. Ed. Engl.* **1996**, *35*, 1154.

9. Burd, C.; Weck, M. Self-sorting in Polymers. Self-Sorting in Polymers. *Macromolecules* **2005**, *38*, 7225.

10. Pollino, J. M.; Stubbs, L. P.; Weck, M. One-Step Multifunctionalization of Random Copolymers via Self-Assembly. One-Step Multifunctionalization of Random Copolymers via Self-Assembly. *J. Am. Chem. Soc.* **2004**, *126*, 563.

11. For discussions of pincer-type complexation see: (a) Crabtree, R. H. Carbenes. Pincers, chelates, and abnormal binding modes. *Pure App. Chem.* **2003**, *75*, 435.

    (b) van Manen, H.-J.; Nakashima, K.; Shinkai, S.; Kooijman, H; Spek, A. J.; van Veggel, F. C. J. M.; Reinhoudt, D. N. Coordination Chemistry of SCS PdII Pincer Systems. *Eur. J. Inorg. Chem.* **2000**, 2533.

12. (a) Albrecht, M.; Lutz, M.; Antoine, M. M.; Lutz, E. T. H.; Spek, A. L.; van Koten, G. Self-assembled organoplatinum(II) supermolecules as crystalline, SO2 gas-triggered switches. *J. Chem. Soc., Dalton Trans.* **2000**, 3797.

(b) Albrecht, M.; van-Koten, G. Platinum Group Organometallics Based on ldquoPincerrdquo Complexes: Sensors, Switches, and Catalysts. *Angew. Chem., Int. Ed.* **2001**, *40*, 3750.

13. For examples of Pd pincer complexes in supramolecular chemistry see: (a) Pollino, J. M.; Weck, M. Tandem Catalysis and Self-Assembly: A One-Pot Approach to Functionalized Polymers. *Org. Lett.* **2002**, *4*, 753.

(b) Pollino, J. M.; Stubbs, L. P.; Weck, M. Living ROMP of exo-Norbornene Esters Possessing PdII SCS Pincer Complexes or Diaminopyridines. *Macromolecules* **2003**, *36*, 2230.

(c) Pollino, J. M.; Stubbs, L. P.; Weck, M. One-Step Multifunctionalization of Random Copolymers via Self-Assembly. *J. Am. Chem. Soc.* **2004**, *126*, 563.

(d) Yount, W. C.; Loveless, D. M.; Craig, S. L. Strong Means Slow: Dynamic Contributions to the Bulk Mechanical Properties of Supramolecular Networks. *Angew Chem., Int. Ed.* **2005**, *44*, 2746.

(e) Meijer, M. D.; Mulder, B; van Klink, G. P. M.; van Koten, G. Synthesis of C60-attached SCS pincer palladium(II) complexes. *Inorg. Chim. Acta.* **2003**, *352*, 247.

(f) Huck, W. T. S.; Prins, L. J.; Fokkens, R. H.; Nibbering, N. M. M.; van Veggel, F. C. J. M.; Reinhoudt, D. N. Convergent and Divergent Noncovalent Synthesis of Metallodendrimers. *J. Am. Chem. Soc.* **1998**, *120*, 6240.

14. (a) Ashton, P. R.; Chrystal, E. J. T.; Glink, P. T.; Menzer, S.; Schiavo, C.; Spencer, N.; Stoddart, J. F.; Tasker, P. A.; White, A. J. P.; Williams, D. J. Pseudorotaxanes formed between secondary dialkylammonium salts and crown ethers. *Chem. Eur. J.* **1996**, *2*, 709;

(b) Ashton, P. R.; Fyfe, M. C. T.; Raymo, F. M.; Spencer, N.; Stoddart, J. F.; White, A. J. P.; Williams, D. J. Rotaxane or Pseudorotaxane? That Is the Question! *J. Am. Chem. Soc.* **1998**, *120*, 2297;

(c) Ashton, P. R.; Ballardini, R.; Balzani, V.; Baxter, I.; Credi, A.; Fyfe, M. C. T.; Gandolfi, M. T.; Gómez-López, M; Martínez-Díaz, Morosini, M.; Schiavo, C.; Shibata, K.; Stoddart, J. F.; White, A. J. P.; Williams, D. J. Selective Self-Assembly and Acid-Base Controlled De-/Rethreading of Pseudorotaxanes Constructed Using Multiple Recognition Motifs. *Chem. Eur. J.* **1998**, *4*, 2332;

(d) Fitzmaurice, D.; Rao, S. N.; Preece, J. A.; Stoddart, J. F.; Wenger, S.; Zaccheroni, N. Heterosupramolecular Chemistry: Programmed Pseudorotaxane Assembly at the Surface of a Nanocrystal. *Angew. Chem., Int. Ed.* **1999**, *38*, 1147.

15. (a) Glink, P. T.; Schiavo, C.; Stoddart, J. F.; Williams, D. J. The genesis of a new range of interlocked molecules. *Chem. Commun.* **1996**, 1483;

(b) Fyfe, M. C. T.; Stoddart, J. F. *Adv. Supramol. Chem.* **1999**, *5*, 1;

(c) Fyfe, M. C. T.; Stoddart, J. F. Interwoven supramolecular arrays via the noncovalent polymerization of pseudorotaxanes. *Coord. Chem. Rev.* **1999**, *183*, 139;

(d) Fyfe, M. C. T.; Stoddart, J. F.; Williams, D. J. X-ray Crystallographic Studies on the Noncovalent Syntheses of Supermolecules. *Struct. Chem.* **1999**, *10*, 243;

(e) Cantrill, S. J.; Pease, A. R.; Stoddart, J. F. A molecular meccano kit. *J. Chem. Soc., Dalton Trans.* **2000**, 3715.

16. (a) Hubin, T. J.; Kolchinski, A. G.; Vance, A. L.; Busch, D. H. *Adv. Supramol. Chem.* **1999**, *5*, 237;

(b) Hubin, T. J.; Busch, D. H. Template routes to interlocked molecular structures and orderly molecular entanglements. *Coord. Chem. Rev.* **2000**, *200-202*, 5;

(c) Clifford, T.; Abushamleh, A.; Busch, D. H. Supramolecular Chemistry And Self-assembly Special Feature: Factors affecting the threading of axle molecules through macrocycles: Binding constants for semirotaxane formation. *Proc. Natl. Acad. Sci. USA* **2002**, *99*, 4830.

17. (a) Takata, T.; Kawasaki, H.; Kihara, N.; Furusho, Y. Synthesis of Side-Chain Polyrotaxane by Radical Polymerizations of Pseudorotaxane Monomers Consisting of Crown Ether Wheel and Acrylate Axle Bearing Bulky End-Cap and Ammonium Group. *Macromolecules* **2001**, *34*, 5449;

(b) Tachibana, Y.; Kihara, N.; Furusho, Y.; Takata, T. Is the tert-Butyl Group Bulky Enough to End-Cap a Pseudorotaxane with a 24-Crown-8-ether Wheel? *Org. Lett.* **2004**, *6*, 4507-4509.

18. (a) Yamaguchi, N.; Hamilton, L. M.; Gibson, H. W. Dendritic Pseudorotaxanes. *Angew. Chem., Int. Ed.* **1998**, *37*, 3275;

(b) Bryant, W. S.; Guzei, I. A.; Rheingold, A. L.; Merola, J. S.; Gibson, H. W. A Study of the Complexation of Bis(m-Phenylene) Crown Ethers and Secondary Ammonium Ions. Crown-Linked Porphyrin Systems. *J. Org. Chem.* **1998**, *63*, 7634;

(c) Yamaguchi, N.; Gibson, H. W. Formation of Supramolecular Polymers from Homoditopic Molecules Containing Secondary Ammonium Ions and Crown Ether Moieties. *Angew Chem., Int. Ed.* **1999**, *38*, 143;

(d) Gibson, H. W.; Yamaguchi, N.; Hamilton, L.; Jones, J. W. Supramolecular Pseudorotaxane Polymers from Complementary Pairs of Homoditopic Molecules. *J. Am. Chem. Soc.* **2003**, *125*, 3522;

(f) Jones, J. W.; Huang, F. H.; Bryant, W. S.; Gibson, H. W. A cautionary note regarding the investigation of supramolecular complexes involving secondary ammonium salts in acetone. *Tetrahedron Lett.* **2004**, *45*, 5961.

19. (a) Montalti, M.; Prodi, L. A supramolecular assembly controlled by anions: threading and unthreading of a pseudorotaxane. *Chem. Commun.* **1998**, 1461;

(b) Ishow, E.; Credi, A.; Balzani, V; Spadola, F.; Mandolini, L. A Molecular-Level Plug/Socket System: Electronic Energy Transfer from a Binaphthyl Unit Incorporated into a Crown Ether to an Anthracenyl Unit Linked to an Ammonium Ion. *Chem. Eur. J.* **1999**, *5*, 984.

20. (a) Duggan, S. A.; Fallon, G.; Langford, S. J.; Lau, V. L.; Satchell, J. F.; Paddon-Row, M. N. Crown-Linked Porphyrin Systems. *J. Org. Chem.* **2001**, *66*, 4419;

(b) Langford, S. J.; Lau, V. L. *Aust. J. Chem.* **2004**, *57*, 29.

21. Kawano, S. I.; Fujita, N.; Shinkai, S. Novel host–guest organogels as stabilized by the formation of crown–ammonium pseudo-rotaxane complexes. *Chem. Commun.* **2003**, 1352.

22. (a) Chiu, S.-H.; Liao, K. S.; Su, J. K. Substituent effects in the binding of bis(4-fluorobenzyl)ammonium ions by dianilino[24]crown-8. *Tetrahedron Lett.* **2004**, *45*, 213;

(b) Cheng, P. N.; Hung, W. C.; Chiu, S.-H. A new macrocycle that forms pseudorotaxane-like complexes with dibenzylammonium ions. *Tetrahedron Lett.* **2005**, *46*, 4239.

23. Feng, D. J.; Li, X. Q.; Wang, X. Z.; Jiang, X. K.; Li, Z. T. Highly stable pseudo[2]rotaxanes co-driven by crown ether–ammonium and donor–acceptor interactions. *Tetrahedron* **2004**, *60*, 6137.

24. Stubbs, L. P.; Weck, M. Towards a Universal Polymer Backbone: Design and Synthesis of Polymeric Scaffolds Containing Terminal Hydrogen-Bonding Recognition Motifs at Each Repeating Unit. *Chem. Eur. J.* **2003**, *9*, 992.

25. Thilbault, R. J.; Hotchkiss, P. J.; Gray, M.; Rotello, V. M. Thermally Reversible Formation of Microspheres through Non-Covalent Polymer Cross-Linking. *J. Am. Chem. Soc.* **2003**, *125*, 11249.

26. Ilhan, F.; Gray, M.; Rotello, V. M. Reversible Side Chain Modification through Noncovalent Interactions. "Plug and Play" Polymers. *Macromolecules* **2001**, *34*, 2597.

27. South, C. R.; Higley, M. N.; Leung, K. C.-F.; Lanari, D.; Nelson, A.; Grubbs, R. H.; Stoddart, J. F.; Weck, M. Self-Assembly with Block Copolymers through Metal Coordination of SCS-PdII Pincer Complexes and Pseudorotaxane Formation. *Chem. Eur. J.* **2006**, *12*, 3789.

28. Albrecht, M.; van Koten, G. Platinum Group Organometallics Based on ldquoPincerrdquo Complexes: Sensors, Switches, and Catalysts. *Angew. Chem., Int. Ed.* **2001**, *40*, 3750.

29. Ashton, P. R.; Campbell, P. J.; Chrystal, E. J. T.; Glink, P. T.; Menzer, S.; Philp, D.; Spencer, N.; Stoddart, J. F.; Tasker, P. A.; Williams, D. J. Dialkylammonium Ion/Crown Ether Complexes: The Forerunners of a New Family of Interlocked Molecules. *Angew. Chem., Int. Ed. Engl.* **1995**, *34*, 1865.

30. Miecznikowski, J. R.; Gruendemann, S.; Albrecht, M.; Megret, C.; Clot, E.; Faller, J. W.; Eisenstein, O.; Crabtree, R. H. Outer sphere anion participation can modify the mechanism for conformer interconversion in Pd pincer complexes. *Dalton Trans.* **2003**, *5*, 831.

31. We assume that the dissociation of the **6-H•BAr$_F$** salt into separated ions would be almost complete in CH_2Cl_2 since the soft BAr_F^- anions are only very weakly associated with the dibenzylammonium cations in **6-H•BAr$_F$** at low dilution. Hence, we report K_a values obtained directly from the ITC experiments on the assumption that ion-pair formation is not prevalent under the reaction conditions. When ion-pairing is significant, it is necessary to invoke a more involved treatment of the ITC data. See: Jones, J. W.; Gibson, H. W. Ion Pairing and Host-Guest Complexation in Low Dielectric Constant Solvents. *J. Am. Chem. Soc.* **2003**, *125*, 7001.

32. Wilcox, C.S., in *Frontiers in Supramolecular Organic Chemistry and Photochemistry*, Weinheim, New York, **1991**, p. 123.

CHAPTER 5

Templated Ring-closing and Cross Metathesis

5.1 Abstract

Olefin metathesis, a versatile carbon-carbon bond forming and breaking reaction, has recently found widespread use in the templated synthesis of entropically constrained and topologically interesting structures such as catenanes, rotaxanes, and macrocycles, as well as other many other synthetic targets such as asymmetric olefins, ADMET trimers, and lactams. This chapter examines several strategies to reach difficult synthetic targets using templated olefin metathesis. Additionally, several research examples are presented in which Pd and Pt based pincer-type complexes were used as the mediator between a templated olefin cross-metathesis reaction. The results acquired from this research demonstrate the potential for using a template to confine molecules such that an enhanced concentration can enhance the reaction rate and regioselectivity of a particular reaction.

5.2 Introduction

In previous chapters, strategies for placing functional groups onto polymers in a precise manner using molecular recognition have been examined. This chapter marks the transition into applications of molecular recognition. Specifically, this chapter is devoted to small molecular templated synthesis, with an ultimate goal of applying lessons learned from small molecules to polymers.

Again looking toward Nature as a guide, we see that both regioselectivity and stereoselectivity of chemical tranformations are influenced and controlled by templates

that manipulate reactive groups through noncovalent interactions, molecular recognition, and self-assembly.[1] The high-fidelity replication of information rich sequences by DNA and RNA are hallmark examples of biochemical templated synthesis that operate under an umbrella of complexity unprecedented in conventional chemical laboratories.[1] Nonetheless, synthetic chemists are increasingly motivated by Nature, and the reliance on templates during difficult chemical transformations is on the rise.[1]

With the advancement of template-directed synthetic protocols, olefin metathesis[2] has quickly emerged as a powerful tool for the covalent bond forming step(s) required during many templated reactions. What makes olefin cross metathesis (CM) and ring-closing metathesis (RCM) particularly suited for template-directed synthesis is the dynamic nature of these reactions,[3] in which the covalent bond making and breaking steps are reversible, providing for an internal error checking mechanism similar to Nature's synthetic machinery. Aside from being dynamic covalent reactions, olefin CM and RCM using ruthenium alkylidene catalysts (Figure 5.1) are tolerant of a wide array of functional groups, allowing for easy noncovalent manipulation of pre-organized and thermodynamically stable templates prior to the covalent bond forming step(s).

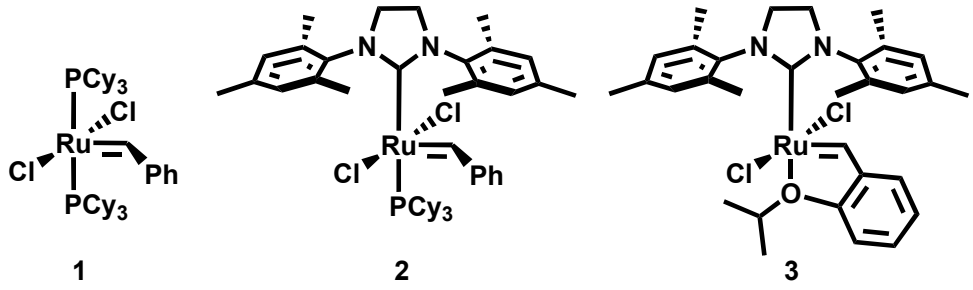

Figure 5.1. Ruthenium-alkylidene initiators commonly employed in template-directed synthesis. **1** is a phosphine based benzylidene, while **2**-**3** are heterocyclic carbene based benzylidenes.

5.3 Templated Ring-Closing Metathesis

An excellent illustration of both the dynamic and tolerant nature of olefin CM is the so-called "magic ring" formation developed by Grubbs, Stoddart, and coworkers.[5c] In these systems, a preorganized template was formed through supramolecular4 assistance provided by the interaction between dibenzylammonium cations and crown ether macro-rings or precursors to crown ether macro-rings. The mechanism for these "magic" transformations can be illustrated by the catenane formation example (Scheme 5.1) which presumably proceeds through a ring-opening metathesis of **4** to form a linear oligoether species, which then threads through **5** to form a [2]-pseudorotaxane after which a ring-closing metathesis reaction occurs to form catenane **6**. Similar approaches were used for the synthesis of rotaxanes,[5a] catenanes,[5c] and an otherwise inaccessible "molecular bundle,"[5b] under thermodynamic control.

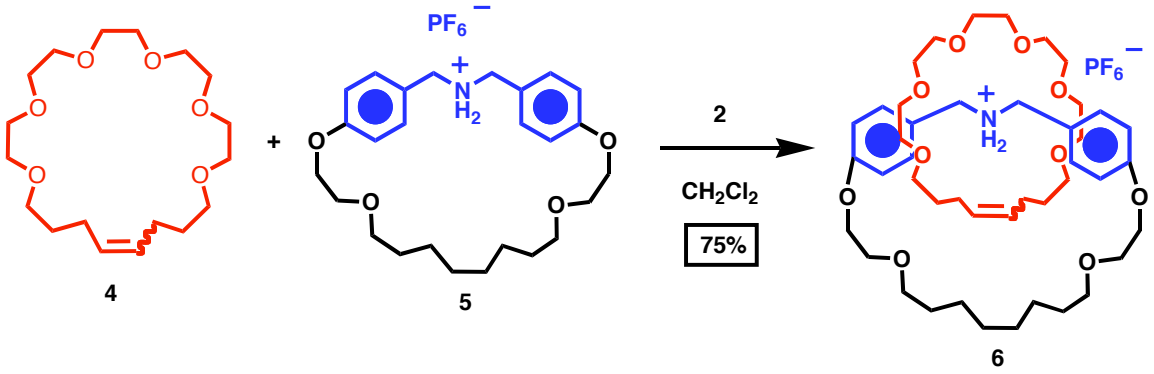

Scheme 5.1. "Magic Ring" catenation by Grubbs and Stoddart

Mechanically interlocked structures, such as the "magic" catenane **6** shown in Scheme 1, provide not only for aesthetically pleasing molecular structures that are

interesting from a historical and philosophical viewpoint[6] but have also been tested[7a] as memory and logic elements in electronic devices. An example[7b] has emerged from the Stoddart group in which rotaxanes have been used as the key element in a memory device with a density of 1011 bit/cm^2, a density predicted for commercial devices in 2020. As the successful utility of interlocked molecules continues to be demonstrated in materials science, the need for straightforward synthetic approaches to these structures will increase, and templated olefin metathesis approaches are at the forefront of many of these efforts.

Supramolecular interactions other than electrostatic and hydrogen bonding interactions have been used in similar examples of template-assisted catenane synthesis. Namely, metal complexes based on a number of transition metal complexes involving Zn[8d] (Scheme 2A), Rh,[8b] Ru,[8c] and Cu[8a] (Scheme 5.2B) to name a few, have mediated several successful catenane syntheses. In some cases, a linear species bearing two terminal olefins is threaded through a preformed macrocycle and held in place by a coordination bond. Subsequently, RCM forms the second ring, producing an interlocked [2]-catenane, such as **7a** shown in Scheme 5.2A. Alternatively, two linear segments can be brought together using metal-ligand interactions, and a two-fold RCM reaction can be used to form both rings at once. A [2]-catenane **8a** produced in this fashion is shown in Scheme 2B.

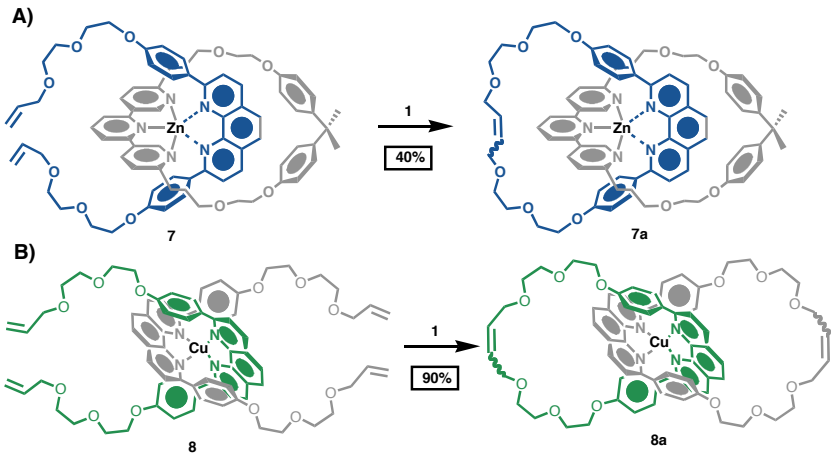

Scheme 5.2. Two approaches to catenanes mediated by metal-ligandiInteractions. A) RCM around a preformed ring and B) RCM of two connected linear segments.

Several other topologically interesting and otherwise hard to reach structures have been synthesized by templated RCM and templated CM. The van Koten group has utilized a templated metathesis approach to synthesize huge macrocycles based on Pt NCN pincer-type complexes.[9] In one elegant example, three different linear segments each consisting of di-olefins are combined with a trifurcate Pt template, and the metathesis of all three segments proceeds around the template in one-pot to produce a large macrocycle **9a** in 67% yield (Scheme 5.3). It is important to note that the synthesis of such macrocycles from multiple components *without* a template has thus far not been possible. Likewise, similar macrocycles have been produced by templated CM and RCM mediated by metal-ligand based calixarenes,[10b] and porphyrins.[10a, c-d]

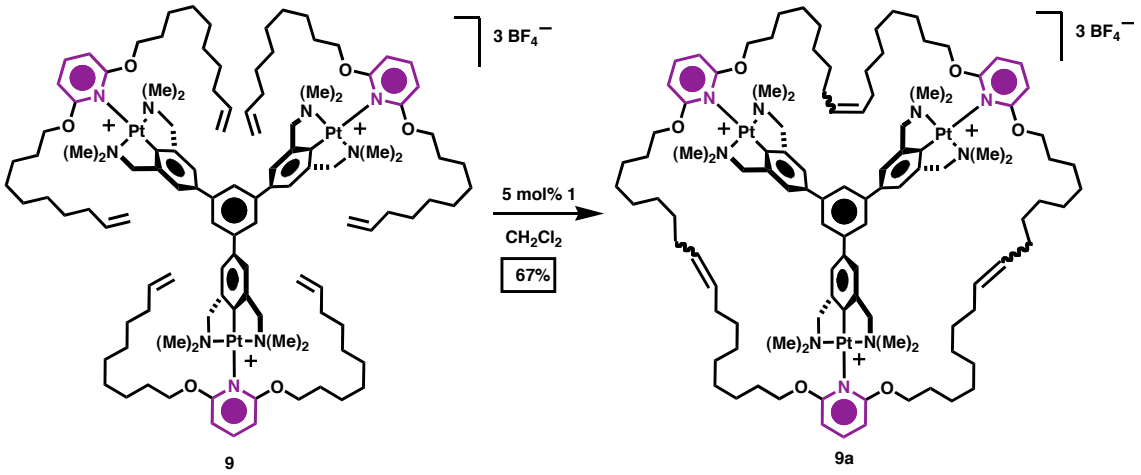

Scheme 5.3. Templated multimacrocycle synthesis.

5.4 Templated Cross Metathesis

Another unique element that is often seen in Nature's templated syntheses is the ability to achieve different transformations on the same substrate under different environments, i.e. by utilizing different templates.[1] To be able to alter reactivity in this way in conventional chemical laboratories would open up endless possibilities for dynamic and combinatorial approaches to diverse libraries of compounds. A proof-of-principle example has recently emerged in the literature demonstrating that by varying the template used during an olefin metathesis reaction, one mechanism can be favored over the other, creating two different products from the same starting material and the same catalyst (Scheme 5.4). This example is based on pseudorotaxane interactions between dibenzylammonium cations and dibenzo[24]crown-8 (DB24C8) macrorings.

As shown in Scheme 5.4, if a dimer, **DBA**$^{2+}$, is used as the template for metathesis with the di-olefin containing DB24C8 monomer **10**, then the CM mechanism is predominately enabled, producing mainly a dimer (**10a**) (70% yield) of monomer **10**, and

largely disabling the production of higher order products which would be expected if acyclic diene metathesis (ADMET) would be the dominant mechanism.[11a] On the other hand, if the trifurcate template, **DBA**$^{3+}$, is used, then ADMET is enabled and the cyclic trimer **10b** is formed in 50% yield.[11b] Neither exclusively dimer or trimer is formed with monomer **10** under metathesis conditions in the *absence* of a template. These results can be explained largely on the basis of effective concentrations. When only the dimer template, **DBA**$^{2+}$, is used under dilute (10 mM) conditions, the effective concentration is only sufficient to allow for the formation of a corresponding dimer based on the pre-organization of two monomers on a dimeric template. When the trimer template, **DBA**$^{3+}$, is used, however, three olefin bearing monomers are in close enough proximity to react *via* ADMET, producing a cyclic trimer replicated from the trimeric template. Multivalency[5c] and binding cooperativity[12] may have also promoted olefin metathesis of the DB24C8 monomers (**10**) situated on either dimer or trimer template. In both cases, binding cooperativity has been observed for the binding of multiple DB24C8 rings with **DBA**$^{n+}$ templates (i.e. $K_{a1} < K_{a2}$ or $K_{a1} < K_{a2} < K_{a3}$).[11a] Future studies will hopefully highlight an example where binding cooperativity is not required for switching mechanisms of olefin metathesis as well as probe the relationship between olefin reactivity and the association strength (and even association and dissociation kinetics) of the preorganized template.

Influencing regioselectivity and, most importantly, sequence are also important goals among synthetic chemists. Nature's approach to synthesizing sequence-specific biopolymers is based exclusively on templated synthesis. A few biomimetic examples have recently emerged in the literature based on templated olefin metathesis. Gong and

coworkers succesfully synthesized a heterodimer from CM on a sacrificial template that alligned two olefin containing monomers **11a** in the desired geometry (Scheme 5.5) sufficient for hetero-CM.[13]

In this case, complementary oligoamide strands bearing terminal olefins were designed to form a heterodimeric hydrogen bonded duplex that situated the two olefin arms on the same side of the duplex. Using initiator **1**, CM covalently connects the two strands. Upon hydrolysis of the ester linkages, a heterodimeric product **11b** is obtained in high overall yield. *Without* a template, two unwanted homodimeric products mixed with the desired heterodimeric product are formed.

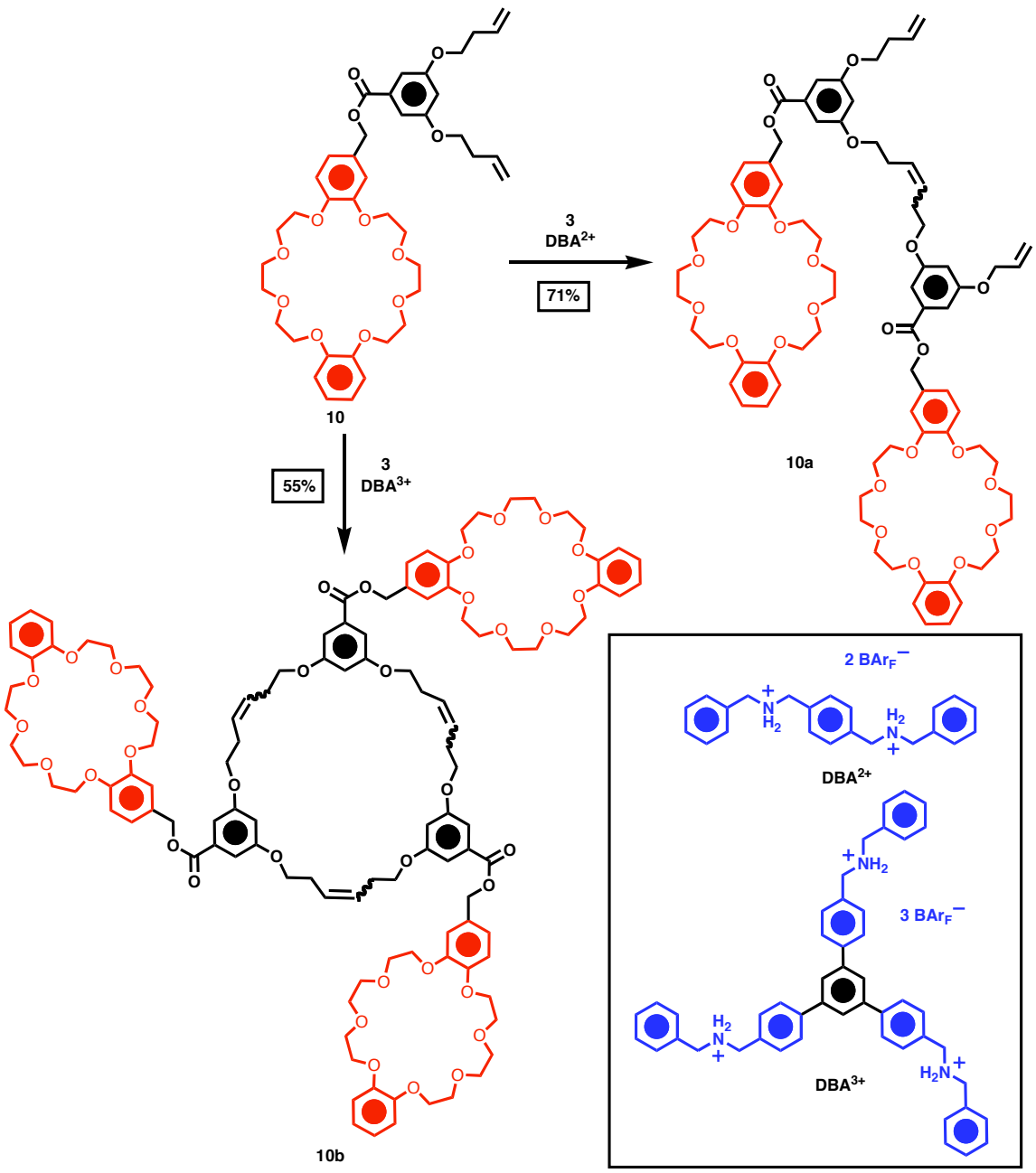

Scheme 5.4. Enabling CM or ADMET with different templates.

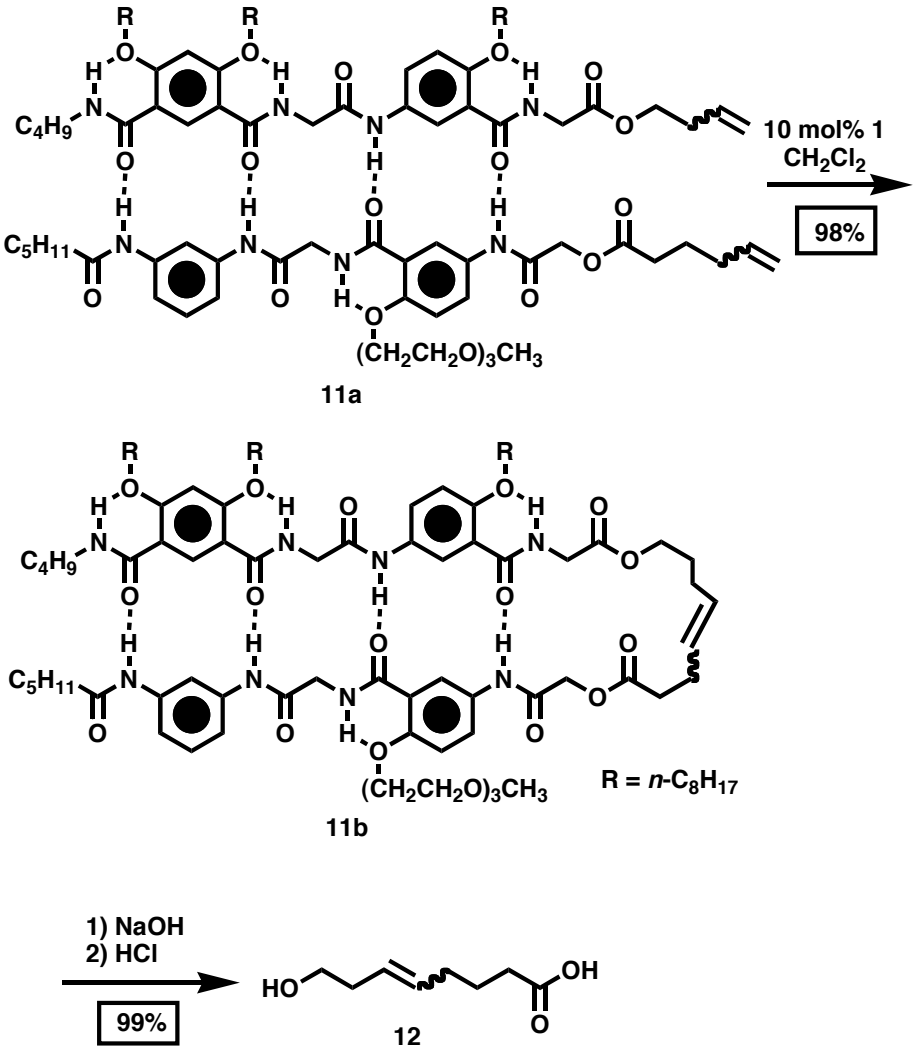

Scheme 5.5. Templated synthesis of a heterodimer

5.5 Template Metathesis in Natural Products and Medicinal Chemistry

While most examples of templated olefin metathesis fall under the umbrella of supramolecular chemistry involving self-assembly and molecular recognition with various noncovalent interactions, templated CM and RCM have become prolific among medicinal and total synthetic laboratories. A clever approach[14] taken by Maarseveen and coworkers utilizes a covalently bound sacrificial template to efficiently synthesize medium-sized lactams (Scheme 5.6). Salicylaldehyde is used as an auxiliary, sacrificial template for the synthesis of lactams. Salicylaldehyde serves two roles as a template: (i) it promotes the RCM reaction between the amine and the aryl ester olefinic containing arms by keeping the olefins in close proximity to one another, and (ii) it provides the correct spatial positioning of the secondary amine and the carbonyl functional group during the transannular ring-contraction reaction. After ring-contraction, the benzyl protecting group is removed, and the desired lactam is obtained (Scheme 5.6).

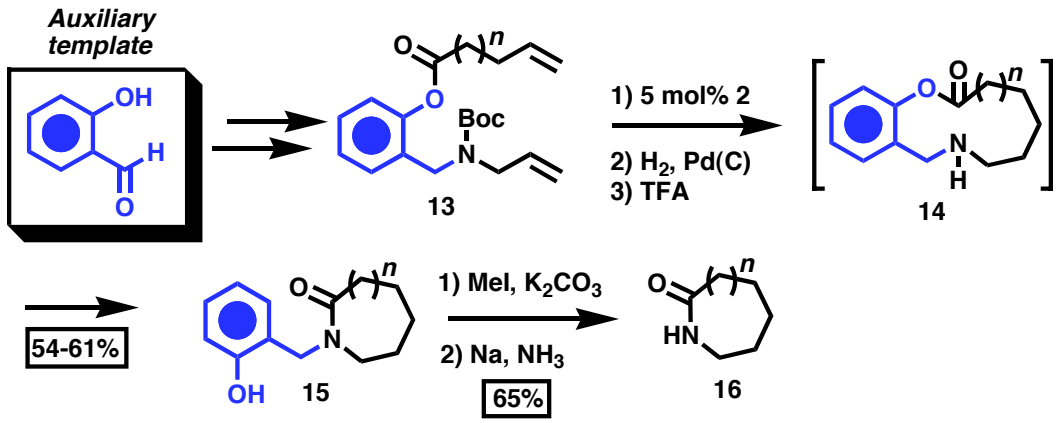

Scheme 5.6. Templated synthesis of lactams.

Other approaches have utilized a similar internal template that is part of the desired synthetic final target and is *not* sacrificed after use. For example, γ-lactones have been used[15] as templates for RCM in the enantioselective synthesis of medium-sized carbocycles fused to butyrolactones, a functional motif common to many natural products.[16] Similarly, macrocyclic helical peptides have been used as templates for RCM between the *i* and *i+4* amino acid residues within the helix. In this case, the helix is the template, and the resulting templated product is more stable than the helical precursor.[17a] The Arora group has optimized this approach by replacing one of the hydrogen bonds between *i* and *i+4* residues in small alpha helices with a covalent bond formed by templated RCM to produce "hydrogen-bond surrogate helices."[17b] This approach has been applied in medicinal chemistry, as the surrogate helices produced by templated metathesis are more stable and are hence more successful at regulating protein-protein interactions (Scheme 5.7).[17c]

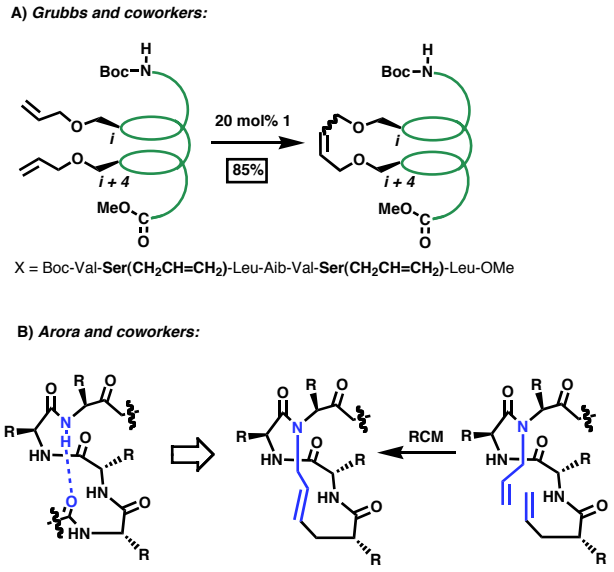

Scheme 5.7. Protein stabilization using olefin CM.

5.6 Our Attempts at Dimer and Heterodimer Synthesis from a Template

The previous sections of this Chapter presented a literature review of small-molecule based templated olefin metathesis. The remaining portion of this Chapter will present research carried out in the Weck, Grubbs, and Stoddart labs based on metal-coordination based templated synthesis. Our interest in templated synthesis primarily arises from an interest and long-term goal to template polymer synthesis (Chapter 6). Ultimately, a major goal in synthetic polymer chemistry is to control sequence, tacticity, etc. in a similar way Nature does during templated biosynthesis. While it is likely that synthetic chemists will not be able to rival Nature's complexity with purely abiotic polymer systems, it might be possible to at the very least template the sequence of a polymer or control the information embedded within a polymer. This is quite a lofty goal, and we reasoned that lessons learned from small-molecule based templated metathesis would be valuable as we advanced a templated synthetic methodology to polymer systems.

Our initial approach was to template the formation of a dimer from a dimeric template using molecular recognition. Motivated by van Koten's work on templated metathesis involving pincer-type complexes,[9] we investigated templated dimer synthesis using similar organometallic pincer-type complexes. We utilized both Pt and Pd pincer-type complexes as monomers and attempted to form dimers of these monomers from a pyridyl based template, which acts as a strong receptor for the Pt or Pd monomers.

We first attempted dimer formation of a Pd pincer monomer from a bipyridyl template. The pincer complex was initially attached to the bipyridyl template **17** after precipitation of the Cl atom on the pincer complex assisted by $AgBF_4$ (Scheme 5.7). The

resulting dicationic complex exposed to ruthenium initiators **1-3**, and in each case, isomerization of the double bond was observed with little CM (Scheme 5.8).

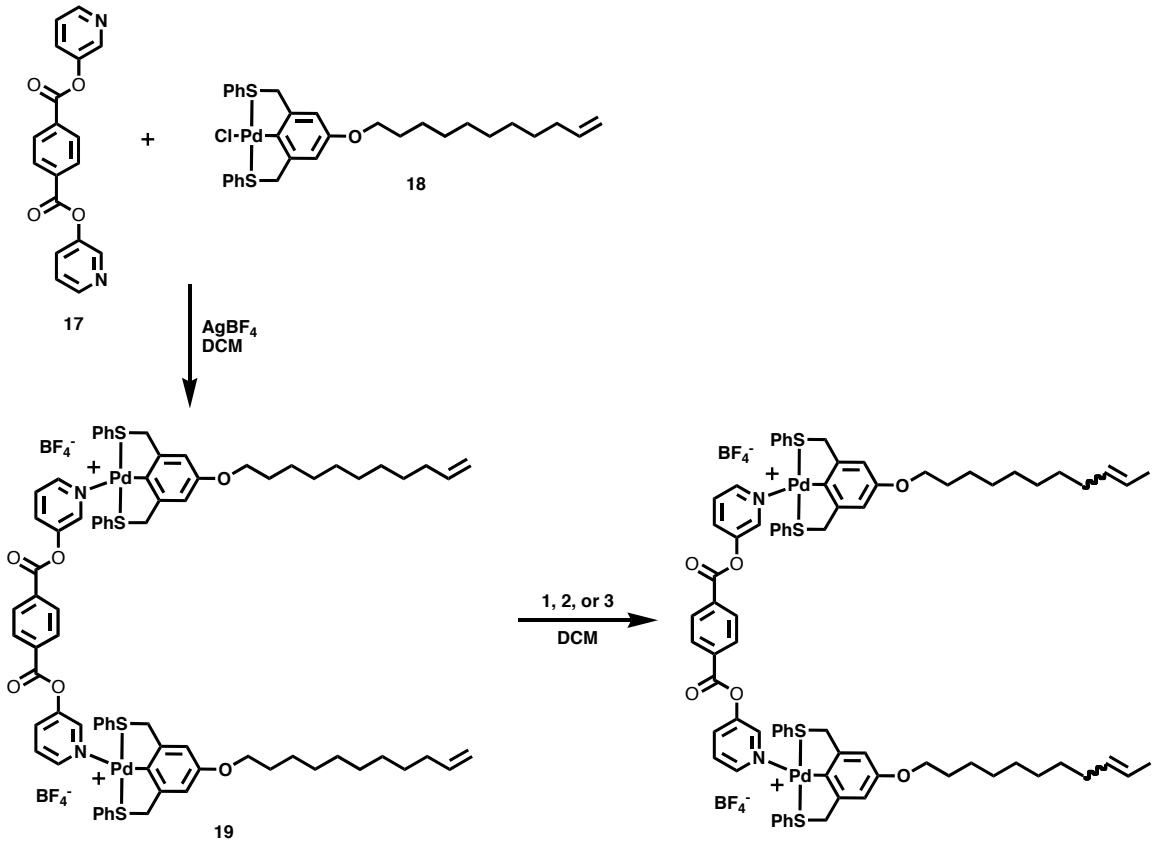

Scheme 5.7. Attachment of a Pd Pincer containing olefin to a bipyridal template and observed isomerization during attempted CM of **19** using ruthenium initiators **1-3**.

Van Koten had previously observed similar results during the attempted macrocycle formation using the corresponding Pd based Pincer complex.[9] A proposed explanation for the observed results is that the dissociation rate of complex **19** is such that

neighboring pincer complexes **18** are able to react with one another, leading to olefin insertion and subsequently isomerization.

A solution to the observed isomerization that took place during the attempted dimer synthesis of pincer complex **18** is to use another metal complex with greater stability (higher association constant and lower disassociation rate). Van Koten successfully applied this hypothesis to macrocycle synthesis and observed good yields with Pt pincer complexes.[9] Thus, we synthesized a series of Pt pincer complexes to use as monomers for a similar templated synthesis as that outlined in Scheme 5.7. The synthesis of the starting materials for our templated synthesis is outline in Scheme 5.9. The synthesis of intermediate **20** is known[9] and will not be discussed in detail. In comparison to the synthesis of Pd pincer complex analogues, however, Pt pincer complexes are generally easier to purify relative to the Pd complexes. Thus, a variety of Pt pincer complex analogues could be synthesized relatively easily from the common intermediate **20**.

Starting from the protected pincer complex **20**, olefins with a variety of carbon spacer lengths and incorporated heteroatoms were synthesized (Scheme 5.10). Olefins containing Pt pincer complexes were readily accessible upon deprotection of the protected Pt pincer complex **20** followed by reaction of the phenol (not isolated) with a suitable alkyl halide or akyl tosylate. Yields for these reactions ranged from 38-70%.

The first attempted templated dimerization reaction was investigated by attaching Pincer complex **21** to template **17** analogously to Scheme 5.7. Once this complex (**17:21**) was purified, the metathesis reaction was attempted with initiators **1-3**. In each case, the presence of an internal olefin was not observed by ^{1}H NMR spectroscopy indicating that

the desired product did not form. Additionally, the molecular ion peak for the desired product was not observed. In lieu of the results of our experiments with longer olefin tethers (*vide supra*), we attributed the observed lack of reactivity to the lack of spacer length on the olefin (**17**). While the catalyst initiated with at least one of the olefins, the other olefin was probably not in close enough proximity to react in the metathetical exchange reaction to produce the desired product.

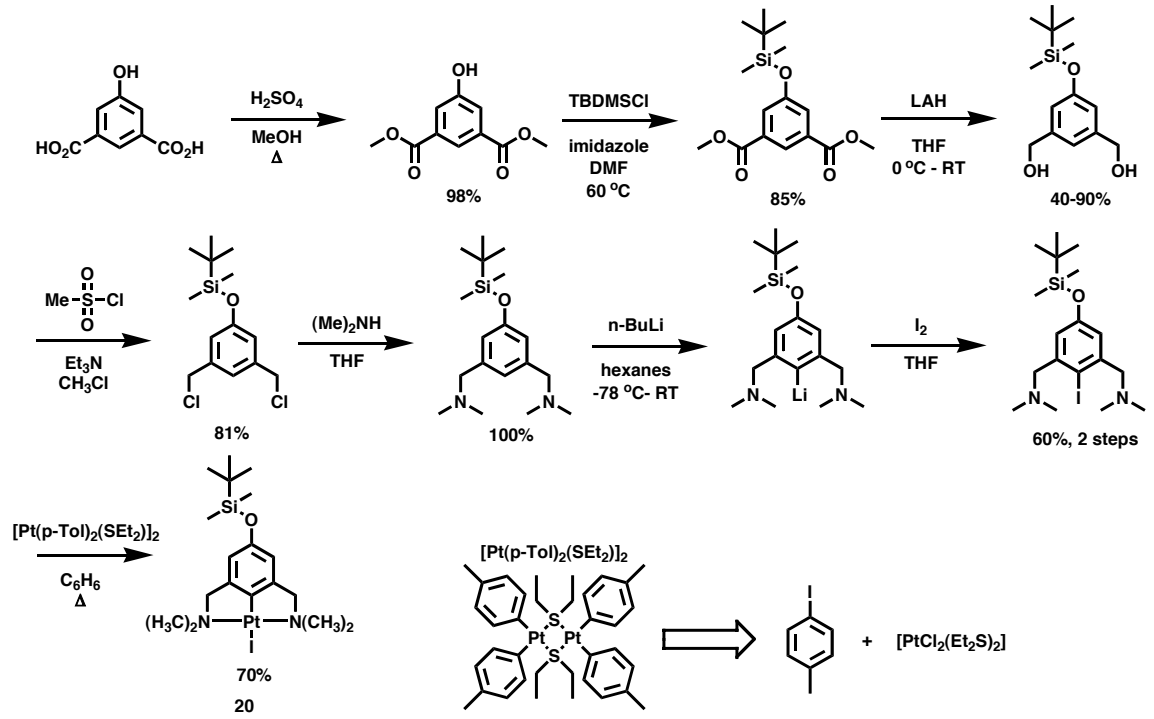

Scheme 5.9. Synthesis of Pt pincer complex starting material.

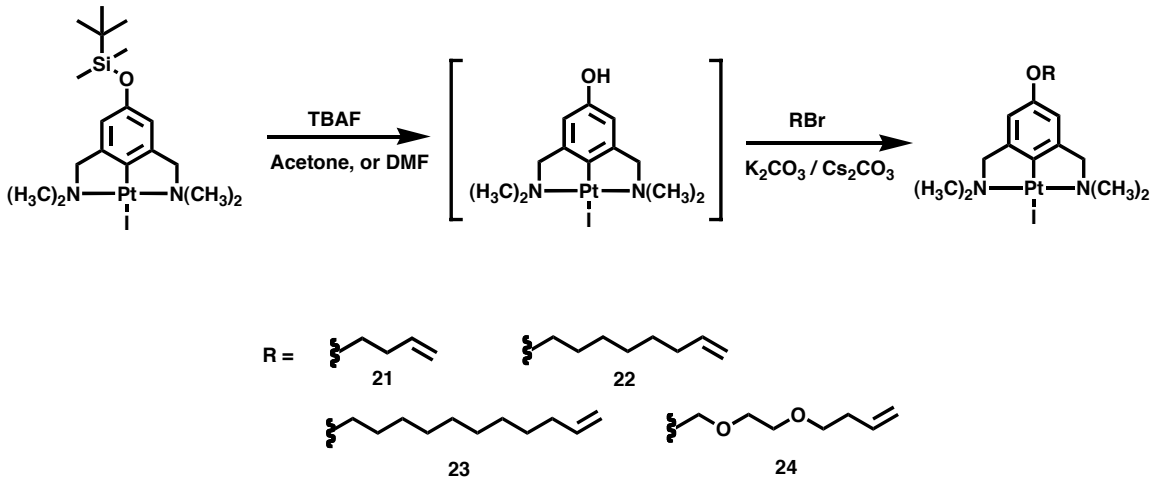

Scheme 5.10. Synthesis olefin bearing Pt Pincer complexes from intermediate **20**.

We viewed the results of our metathesis attempts on complex **17:21** as a positive result. It is likely that the lack of reactivity is due to a template "confinement" effect, meaning that the template is at least playing a role in the observed reactivity (or lack thereof). Several control experiments were carried out to help verify this hypothesis. First, a free olefin (hexene) was added to the reaction mixture including complex **17:21** and the initiator (**1**, **2**, or **3**). Upon the addition of hexene, an internal olefin peak appeared in the ^{1}H NMR spectrum. While the product of this reaction was not isolated, this result verified that our catalyst was active and did not decompose after exposure to complex **17:21**. Second, olefin **21** was subjected to metathesis conditions using initiators **1**, **2**, and **3**. In each case, olefin **21** promptly initiated the corresponding catalyst, and olefin CM was subsequently observed. The dimerized products in these cases were isolated. These results indicate that olefin **21** is at least capable of undergoing olefin cross metathesis. Our results could be characterized as a likely template de-cooperative effect that prevents olefin CM. While our desired product did not form, these results suggest that it might be possible to use this approach or a similar approach to *protect* two

neighboring olefins from reacting with one another during an adjacent *desired* olefin CM reaction, so long as the proximity of the targeted olefins was not close enough to induce metathesis at the *protected* site.

Our next approach was to lengthen the carbon tether length on the olefin and see if this helped to induce reactivity on the template. Complexes **22** and **23** were attached to template **17** to form complexes **17:22** and **17:23**, respectively, analogously to Scheme 5.7. When complex **17:22** was subjected to metathesis conditions using initiators **1**, **2**, or **3**, the reaction was slow, but the presence of an internal olefin was observed by ^{1}H NMR spectroscopy. The molecular ion of the desired product was observed by mass spectrometry (MS). Likewise, when complex **17:23** was subjected to metathesis conditions using intiators **1**, **2**, or **3**, the presence of an interal olefin was observed by ^{1}H NMR spectroscopy, and the product molecular ion was observed by MS. Coinciding with our hypothesis of a "template suppression effect," the reactivity of the olefins with initiators **1**, **2**, or **3**, was faster with complex **17:23** compared to that of complex **17:22**. These results further suggest that it is likely that the template is suppressing the reactivity of shorter tethered olefins. In both cases, however, the desired product was not isolated but only observed by ^{1}H NMR spectroscopy and MS. Accompanying the desired products of these reactions were substantial quantities of cross-metathesized isomerized products, all with the same or very similar polarities such that the purification of the final reaction mixture was too difficult to achieve using conventional purification techniques.

We attempted further to achieve a cleaner templated olefin CM reaction by utilizing a homoallylic olefin containing heteroatoms for increased flexibility. Likewise, we observed similar results when complex **17:24** was subjected to metathesis conditions

using initiators **1**, **2**, or **3**. However, the molecular ion of the desired product was observed by MS. We also attempted additives which are known by the Grubbs group to minimize olefin isomerization during CM. Among the additives used were benzoquinone, and acetic acid, both of which served, in this case, to reduce the reactivity of the initiator with our template organized olefins. We suspect that our results are likely due to isomerization resulting from olefin insertion into the Pt complex, and the competition of this process with the metathesis event involving the Ru catalyst.

Table 5.1. Summary of results of dimerization reactions.

Entry	Template:Complex	Initiator	Obs. Mol. Ion[a] (yes/no)
1	**17:18**	**1-3**	no
2	**17:21**	**1-3**	no
3	**17:22**	**2, 3**	yes
4	**17:23**	**1, 3**	yes
5	**17:24**	**3**	yes

[a]Molecular Ion refers to molecular ion of dimerized product still attached to the template.

5.7 Conclusion

In conclusion, templated olefin metathesis provides straightforward routes to many otherwise inaccesible molecular structures such as catenanes, rotaxanes, and multi-macrocycles, heterodimers, and natural product moeties. Olefin metathesis is particularly suited for templated synthesis because of its reversibility, which permits templates to engage in error checking mechanisms throughout the bond forming or breaking steps.

Much like enzymes in biochemistry, templates can readily engage or disengage different metathetical pathways depending on the pre-organization of substrates around a template. Most of the examples discussed in this Chapter are probably more aptly defined as "template-assisted synthesis," i.e. a catalyst is needed to form a new chemical bond; whereas true "templated synthesis" should not require a catalyst or additional reagent. But rather, the structure of the template itself should induce a new chemical transformation.[18] Nonetheless, template assisted synthesis offers alternatives to typical and generally more conventional protecting group strategies that can be cumbersome. Our interest in templated synthesis stemmed from a goal to apply concepts learned in small molecule templated synthesis to polymeric systems. Generally, the use of an organometallic complex in templated synthesis involving a metathesis initiator has advantages and disadvantages. On one hand, the stability of such complexes is typically greater than the stability of complexes based purely on hydrogen bonding or ionic interactions allowing a tight and thermodynamically preorganized template structure to form. On the contrary, the use of an organometallic template during a catalytic organometallic reaction can be met with compatibility problems, as we observed. The interest in templated synthesis and template-directed synthesis is growing among those in the art, and it is probable that in the near future, we will see many more examples of how reaction yield, reaction rates, and various forms of selectivity can be controlled through templated olefin metathesis.

5.8 Experimental

5.8.1 General Methods

Reagents were purchased either from Acros Organics, Aldrich Company, or Strem Chemicals and used without further purification unless otherwise noted. CH_2Cl_2 was dried via passage through copper oxide and alumina columns. Routine NMR spectra were recorded using a 300 MHz (^{1}H, 300 MHz; ^{13}C, 75 MHz) or 500 MHz (^{1}H, 500 MHz; ^{13}C, 125 MHz) Varian Mercury spectrometer; spectra were referenced to residual proton solvent. The Georgia Tech Mass Spectrometry Facility provided mass spectral analysis using a VG-70se spectrometer.

5.8.2 Synthesis

dimethyl 5-(tert-butyldimethylsilyloxy)isophthalate

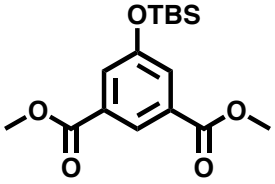

A modification to the literature procedure[9] was used. Dimethyl 5-hydroxyisophthalate (25 g, 0.12 mol), *tert*-butyl dimethyl silyl chloride (TBDMS) (19.7 g, 0.13 mol), and imidazole (17.7 g, 0.26 mol) were dissolved in anhydrous DMF (250 mL), and the solution was heated to reflux for 24 h. The reaction mixture was cooled; diethyl ether (150 mL) was added along with H_2O (200 mL). The organic layer was separated, and the remaining aqueous layer was extracted with diethyl ether (3 x 100 mL). The combined organic layers were washed with H_2O and dried ($MgSO_4$). The dried organic layer was filtered, and the solvent was removed under reduced pressure to yield a

white solid. The isolated solid was purified by column chromatography (Silica gel, 4:1 Hexanes: EtOAc) to yield a white solid. The purified product was dried over CaH_2 under reduced pressure. (30 g, 78%). Characterization data are consistent with literature reports.[19]

(5-(tert-butyldimethylsilyloxy)-1,3-phenylene)dimethanol

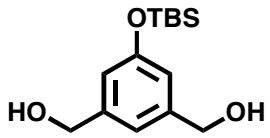

Lithium Aluminum Hydride (LAH) (2.81 g, 0.074 mol) was suspended in dry THF, and dimethyl 5-(tert-butyldimethylsilyloxy)isophthalate (10 g, 0.031 mol) was added as a solution in THF *via* cannula filtration at O ºC over a period of 30 min. The solution was gradually warmed to ambient temperature and stirred overnight. The reaction mixture was poured over ice and stirred for 30 min until a white sludge was obtained. The sludge was extracted with DCM to yield a white solid (5.5 g, 66%). Characterization data are consistent with literature reports.[19]

(3,5-bis(chloromethyl)phenoxy)(*tert*-butyl)dimethylsilane

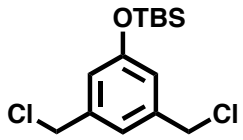

(5-(tert-butyldimethylsilyloxy)-1,3-phenylene)dimethanol (11.23 g, 0.042 mol) and Et_3N (12 mL, 0.126 mol) were dissolved in dry DCM at 0 ºC. Mesyl Chloride (14.43 g, 0.126 mol) was slowly added at 0 ºC. Upon complete addition, the reaction mixture was refluxed overnight. The reaction mixture was added to a separatory funnel and washed with 1N NaOH, 1N HCl, and H_2O. The organic layer was evaporated under reduced pressure to yield a yellow oil. The oil was purified using a column chromatography

(SiO_2, Hexanes: EtOAc, 3:1) to yield a light yellow oil (11.41 g, 89% yield). Characterization data are consistent with literature reports.[20]

1,1'-(5-(*tert*-butyldimethylsilyloxy)-1,3-phenylene)bis(*N*,*N*-dimethylmethanamine)

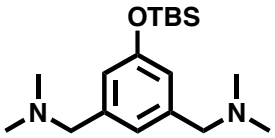

(3,5-bis(chloromethyl)phenoxy)(*tert*-butyl)dimethylsilane (11.41 g, 0.0373 mol) and Et_3N (16.64 g, 0.164 mol, 21 mL) were dissolved in dry DMF (200 mL) and $(Me)_2NHCl$ was subsequently added. The mixture was stirred overnight at ambient temperature. The mixture was filtered; H_2O was added to the mixture, and the organic layer was extracted with Et_2O. The solvent was removed to yield a light brown oil which was flash distilled to give a clear oil (11 g, 91%). Characterization data are consistent with literature reports.[21]

1,1'-(5-(*tert*-butyldimethylsilyloxy)-2-iodo-1,3-phenylene)bis(*N*,*N*-dimethylmethanamine)

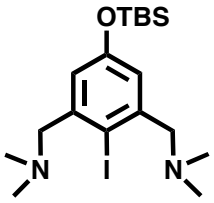

1,1'-(5-(*tert*-butyldimethylsilyloxy)-1,3-phenylene)bis(*N*,*N*-dimethylmethanamine) (3.44 g, 0.011 mol) was dissolved in dry hexanes (100 mL), and *n*-BuLi (1.6 M in Hexanes, 1.16 eq., 7.7 mL) was slowly added at -78 ºC at which time the solution turned blue indicating the presence of the newly formed Lithium salt. The solution was allowed to warm to ambient temperature, and I_2 (3.63 g, 0.0143 mol) was added via cannula filtration from an ethereal solution (to produce a final 1:1 Hexanes:Ether reaction

mixture). The solution was stirred at ambient temperature for 3 h. The solution was filtered to remove any salts, and the organic layer was washed with H_2O. The Ether was evaporated to give a light red oil. The oil was filtered through celite to remove colored impurities to give a clear oil. (4 g, 81%). Characterization data are consistent with literature reports.[21]

[$PtCl_2(SEt_2)_2$]

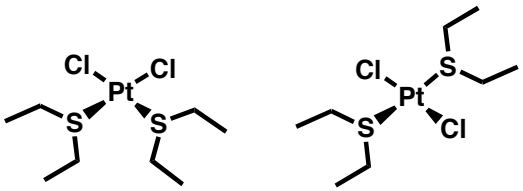

cis *trans*

$PtCl_2$ (5.61 g, 0.021 mol), and Et_2S (7.6 g, 0.084 mol, 9.0 mL) were suspended / dissolved in dry benzene, and the mixture was stirred for 4 h after which time the solution became homogenous. The solvent was evaporated, and the product was washed extensively with Hexanes and cold E_2O to give a light yellow solid (85%). Characterization data are consistent with literature reports.[21]

[Pt(p-Tol)2(SEt2)]2

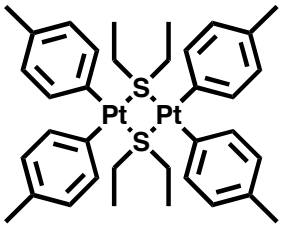

[$PtCl_2(SEt_2)_2$], and *p*-Iodotoluene were dissolved in benzene. *N*-BuLi was slowly added at -78 ºC. The solution was warmed to ambient temperature. The solvent was removed under reduced pressure, and the resulting solid was washed extensively with cold Et_2O. Characterization data are consistent with literature reports.[21]

Pt Pincer Complex

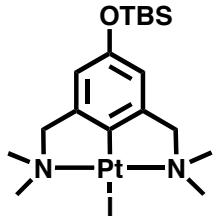

The Diamine (1.43 g, 0.0032 mol), and $[Pt(p\text{-tolyl})_2(SEt_2)]_2$ were dissolved in dry benzene and refluxed for 3 h under an Ar atmosphere. The solvent was removed after 3 h, and the yellow solid was washed with Ether to yield a white solid (0.91 g). The remaining brown solid recovered from the filtrate was purified by column chromatography (SiO_2, Hexanes: EtOAc, 3:1) to yield a light yellow solid (1.44 g total, 70%). Characterization data are consistent with literature reports.[21]

Pt Pincer 4C tethered olefin

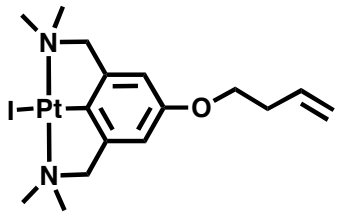

TBS protected Pincer complex (500 mg, 0.777 mmol), TBAF (270 mg, 0.8 mmol), Cs_2CO_3 (2.5 g, 7.97 mmol), and alkyl halide (0.224 g, 1.17 mmol) were dissolved in dry Acetone. The mixture was stirred at ambient temperature until deprotected was deemed complete according to TLC analysis. The mixture was then heated to 50 ºC, and the reaction was stopped after conversion was determined by TLC. The solvent was removed under reduced pressure, and the crude product was dissolved in DCM and washed with H_2O. The solvent was removed to yield a brown solid which was purified by

column chromatography (SiO_2, 4:1 Hexanes: EtOAc) to yield a light brown solid (0.25 g, 55%) as the product. See Appendix C for characterization.

Pt Pincer 11C tethered olefin

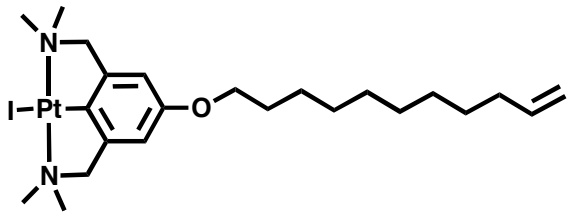

TBS protected Pincer complex (100 mg, 0.155 mmol), TBAF (54 mg, 0.1705 mmol), K_2CO_3, alkyl halide (1.5 eq) and 18-crown-6 (cat. Amount) were dissolved in dry DMF. The mixture was stirred at ambient temperature until deprotected was deemed complete according to TLC analysis. The mixture was then heated to 50 ºC, and the reaction was stopped after conversion was determined by TLC. The mixture was poured over ice water and stirred. The H_2O layer was extracted with Et_2O. The solvent was removed from the combined organic layers, and the resulting brown solid was purified by column chromatography (SiO_2, 2:1 Hexanes: EtOAc) to yield a light brown solid (40 mg, 38%) as the product. The remaining phenol was recovered by eluting the column with EtOAc (20 mg recovered). Yield based on reacted phenol was 80%. See Appendix C for characterization.

Pt Pincer 11C tethered olefin

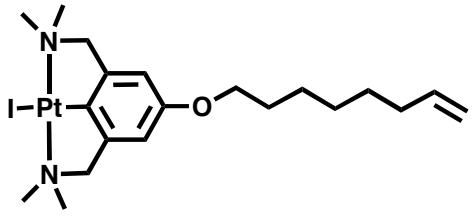

TBS protected Pincer complex (500 mg, 0.777 mmol), TBAF (270 mg, 0.8 mmol), Cs_2CO_3 (2.5 g, 7.97 mmol), and alkyl halide (0.224 g, 1.17 mmol) were dissolved in dry Acetone. The mixture was stirred at ambient temperature until deprotected was deemed complete according to TLC analysis. The mixture was then heated to 50 ºC, and the reaction was stopped after conversion was determined by TLC. The solvent was removed under reduced pressure, and the crude product was dissolved in DCM and washed with H_2O. The solvent was removed to yield a brown solid which was purified by column chromatography (SiO_2, 2:1 Hexanes: EtOAc) to yield a light brown solid (0.34 g, 68%) as the product. See Appendix C for characterization.

2-(2-(but-3-enyloxy)ethoxy)ethanol

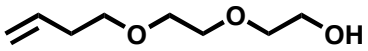

1-Bromo-4-butene (3.93 g, 0.029 mol) and diol (12.36 g, 0.12 mol) were dissolved in H_2O (50 mL). NaOH (2.33g, 0.058 mol) was slowly added. The reaction mixture was heated to 80 ºC overnight. The mixture was extracted with DCM. The solvent was removed under reduced pressure to yield a brown oil which was purified by column chromatography (SiO_2, Et_2O) to yield a clear oil (0.77 g, 17%). See Appendix C for characterization.

2-(2-(but-3-enyloxy)ethoxy)ethyl 4-methylbenzenesulfonate

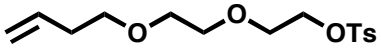

TsCl (1.8 g, 9.4 mmol) was added to a solution of Et_3N (2.3 g, 22.5 mmol), DMAP (cat. amount), and alcohol (0.72 g, 4.49 mmol) over a period of 2 h. The resulting mixture was stirred overnight at ambient temperature. The mixture was washed with H_2O. The H_2O washes were back extracted with DCM and Et_2O (extensively). The

combined organic layers were dried ($MgSO_4$). The solvent was removed to give a brown oil which was purified by gradient column chromatography (SiO_2, Et_2O: Hexanes, 1:2) followed by elution with pure Et_2O to yield a clear oil (1.0 g, 70%). See Appendix C for characterization.

Pt Pincer Homoallylic olefin

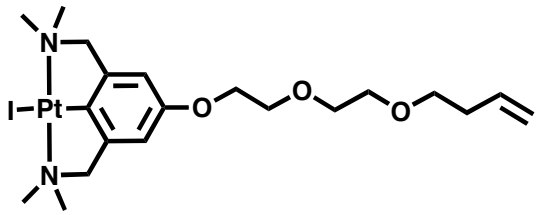

TBS protected Pincer complex (0.6 g, 0.93 mmol), TBAF (0.32 g, 1.03 mmol), Cs_2CO_3 (3.04 g, 9.32 mmol), and tosylated olefin (0.44 g, 1.4 mmol) were dissolved in dry Acetone. The mixture was stirred at ambient temperature until deprotected was deemed complete according to TLC analysis. The mixture was then heated to 50 ºC for 16 h. The solvent was removed under reduced pressure, and the crude product was dissolved in DCM and washed with H_2O. The solvent was removed to yield a brown oil which was purified by column chromatography (SiO_2, 2:1 Hexanes: EtOAc) to yield a brown oil which solidified under reduced pressure (0.42 g, 67%). See Appendix C for characterization.

5.9 References

1. Diederich, F., Stang, P. J.; Eds. *Templated Organic Synthesis*; Wiley-VCH: Weinheim, **2000**.

2. (a) Fürstner, A. Olefin Metathesis and Beyond. *Angew. Chem. Int. Ed.* **2000**, *39*, 3012.

   (b) Trnka, T. M.; Grubbs, R. H. The Development of L2X2Ru=CHR Olefin Metathesis Catalysts: An Organometallic Success Story. *Acc. Chem. Res.* **2001**, *34*, 18.

   (c) Grubbs, R. H. Olefin metathesis. *Tetrahedron* **2004**, *60*, 7117.

3. For a discussion of dynamic covalent chemistry, see: Chichak, K. S.; Cantrill, S. J.; Pease, A. R.; Chiu, S.-H.; Cave, G. W. V.; Atwood, J. L.; Stoddart, J. F. Molecular Borromean Rings. *Science* **2004,** 304, 1308.

4. Lehn, J.-M. *Supramolecular Chemistry*; VCH: Weinheim, 1996.

5. (a) Kilbinger, A. F. M.; Cantrill, S. J.; Waltman, A. W.; Day, M. W.; Grubbs, R. H. Magic Ring Rotaxanes via Olefin Metathesis. *Angew. Chem. Int. Ed.* **2003**, *42*, 3281.

   (b) Badjic, J. D.; Cantrill, S. J.; Grubbs, R. H.; Guidry, E. N.; Orenes, R.; Stoddart, J. F. The Exclusivity of Multivalency in Dynamic Covalent Processes. *Angew. Chem. Int. Ed.* **2004**, *43*, 3273.

   (c) Guidry, E. N.; Cantrill, S. J.; Stoddart, J. F.; Grubbs, R. H. Magic Ring Catenation by Olefin Metathesis. *Org. Lett.* **2005**, *7*, 2129.

6. Molecular Catenanes, Rotaxanes, and Knots; Sauvage, J.-P., Dietrich-Buchecker, C., Eds.; Wiley-VCH: Weinheim, **1999**.

7. For a selected examples, see: (a) Collier, C. P.; Mattersteig, G.; Wong, E. W.; Luo, Y.; Beverly, K.; Sampaio, J.; Raymo, F. M.; Stoddart, J. F.; Heath, J. R. A [2]Catenane-Based Solid State Electronically Reconfigurable Switch. *Science* **2000**, *289*, 1172.

   (b) Green, J. E.; Choi, J. W.; Boukai, A.; Bunimovich, Y.; Johnston-Halperin, E.; Delonno, E.; Luo, Y.; Sheriff, B. A.; Xu, K.; Shin, Y. S.; Tseng, H.-R.; Stoddart, J. F.; Heath, J. R. A 160-kilobit molecular electronic memory patterned at 1011 bits per square centimeter. *Nature* **2007**, *445*, 414.

8. (a) Mohr, B.; Weck, M.; Sauvage, J.-P.; Grubbs, R. H., High-Yield Synthesis of [2] Catenanes by Intramolecular Ring-Closing Metathesis. *Angew. Chem. Int. Ed. Engl.* **1997**, *36*, 1308.

(b) Mobian, P.; Kern, J.-M.; Sauvage, J.-P. A [2]Catenane Constructed around a Rhodium(III) Center Used as a Template. *Inorganic Chemistry*, **2003**, *42*, 8633.

(c) Mobian, P.; Kern, J.-M.; Sauvage, J.-P. A [2]Catenane Constructed around a Ru(Diimine)32+ Complex Used as a Template. *J. Am. Chem. Soc.* **2003**, *125*, 2016.

(d) Hamann, C.; Kern, J.-M.; Sauvage, J.-P. Zinc(II)-Templated Synthesis of a [2]-Catenane Consisting of a 2,2',6',2' '-Terpyridine-Incorporating Cycle and a 1,10-Phenanthroline-Containing Ring. *Inorganic Chemistry*, **2003**, *42*, 1877.

9. Chase, P. A.; Lutz, M.; Spek, A. L.; van Klink, G. P. M.; van Koten, G. *J. Mol. Cat. A: Chem.* **2006**, *254*, 2.

10. (a) Vyotsky, M. O.; Bogdan, A.; Wang, L.; Böhmer, V. Template synthesis of multi-macrocycles by metathesis reaction. *Chem. Commun.* **2004**, 1268.

(b) Cao, Y.; Wang.; Bolte, M.; Vysotsky, M. O.; Böhmer, V. Synthesis of huge macrocycles using two calix[4]arenes as templates. *Chem. Commun.* **2005**, 3132.

(c) Wakabayashi, R.; Kubo, Y.; Hirata, O.; Takeuchi, M.; Shinkai, S. Allosteric function facilitates template assisted olefin metathesis. *Chem. Commun.* **2005**, 5742.

(d) van Gerven, P. C. M.; Elemans, J. A. A. W.; Gerritsen, J. W.; Speller, S.; Nolte, R. J. M.; Rowan, A. E. Dynamic combinatorial olefin metathesis: templated synthesis of porphyrin boxes. *Chem. Commun.* **2005**, 3535.

(d) Wakabayashi, R.; Kubo, Y.; Kaneko, K.; Takeuchi, M.; Shinkai, S. Olefin Metathesis of the Aligned Assemblies of Conjugated Polymers Constructed through Supramolecular Bundling. *J. Am. Chem. Soc.* **2006**, *128*, 8744.

11. (a) Cantrill, S. J.; Grubbs, R. H.; Lanari, D.; Leung, K. C.-F.; Nelson, A.; Poulin-Kerstien, K. G.; Smidt, S.; Stoddart, J. F.; Tirrell, D. A. Template-Directed Olefin Cross Metathesis. *Org. Lett.* **2005**, *7*, 4213.

(b) Hou, H.; Leung, K. C.-F.; Lanari, D.; Nelson, A.; Stoddart, J. F.; Grubbs, R. H. Template-Directed One-Step Synthesis of Cyclic Trimers by ADMET. *J. Am. Chem. Soc.* **2006**, *128*, 15358.

12. Conners, K. A. *Binding Constants*; Wiley: New York, **1987**.

13. Gong, B.; Yang, X. Template-Assisted Cross Olefin Metathesis. *Angew. Chem. Int. Ed.* **2005**, *44*, 1352.

14. Bieräugel, H.; Jansen, T. P.; Schoemaker, H. E.; Hiemstra, H.; van Maarsevaan, J. H. A Novel Strategy for the Synthesis of Medium-Sized Lactams. *Org. Lett.* **2002**, *4*, 2673.

15. Ravelo, J. L.; Rodríguez, C. M.; Martín, V. S. -Lactones as templates in ring-closing metathesis: Enantioselective synthesis of medium sized carbocycles fused to butyrolactones. *J. Organomet. Chem.* **2006**, *691*, 5326.

16. Corey, E. J.; Cheng, X. M., Eds. *The Logic of Chemical Synthesis*, Wiley: New York, **1989**.

17. (a) Blackwell, H. E.; Sadowsky, J. D.; Howard, R. J.; Sampson, J. N.; Chao, J. A.; Steinmetz, W. E.; O'Leary, D. J.; Grubbs, R. H. Ring-Closing Metathesis of Olefinic Peptides: Design, Synthesis, and Structural Characterization of Macrocyclic Helical Peptides. *J. Org. Chem.* **2001**, *66*, 5291.

(b) Chapman, R. N.; Arora, P. S. Optimized Synthesis of Hydrogen-Bond Surrogate Helices: Surprising Effects of Microwave Heating on the Activity of Grubbs Catalysts. *Org. Lett.* **2006**, *8*, 5825.

(c) Wang, D.; Chen, K.; Kulp, J. L. III; Arora, P. S. Evaluation of Biologically Relevant Short -Helices Stabilized by a Main-Chain Hydrogen-Bond Surrogate. *J. Am. Chem. Soc.* **2006**, 128, 9248.

18. Stoddart, J.F., in *Frontiers in Supramolecular Organic Chemistry and Photochemistry* Weinheim: New York, **1991**, p. 262.

19. Felder, D; Nava, Gutierrez, M; Maria, D.P.C.; Eckert, J-F.; Luccisano, M.; Schall, C.; Masson, P.; Gallani, J-L.; Heinrich, B.; Guillon, D.; Nierengarten, J-F. Synthesis of Amphiphilic Fullerene Derivatives and Their Incorporation in Langmuir and Langmuir-Blodgett Films. *Helvetica Chimica Acta* **2002**, *85*, 288.

20. Davies, P. J.; Veldman, N.; Grove, D. M.; Spek, A. L.; Lutz, B. T. G.; van Koten, G. Organoplatinum Building Blocks for One-Dimensional Hydrogen-Bonded Polymeric Structures. *Angew. Chem., Int Ed Eng.* **1996**, *35*, 1959.

21. Davies, P. J.; Grove, D. M.; van Koten, G. Advances in the Synthesis of Multimetallic Systems: Hydroxyl Group Protection in (Aryldiamine)platinum Species. *Organometallics* **1997**, *16*, 800.

CHAPTER 6

Template Enhanced Ring-Opening Metathesis Polymerization

6.1 Abstract

The template enhanced ring-opening metathesis polymerization (ROMP) of a norbornene-based thymine monomer was examined. The template, based on diaminopyridine functionalized norbornenes that are designed to recognize thymine substrates with high fidelity, was synthesized via ROMP. The resulting template was used to harness the polymerization of the thymine monomer producing a bis-poly(norbornene) complex. Using ^{1}H NMR spectroscopy, we determined that the polymerization conditions do not disrupt the hydrogen bonding. In addition, the template enhances the rate of the polymerization by inducing an increase in local monomer concentration. To examine whether the polymerization is controlled, we synthesized a solid-supported diaminopyridine template. After the polymerization off this solid-supported template, we extracted the daughter polymer from the support. Detailed analysis of the daughter template proved that the templated polymerization was controlled, and that the supported template produces a well-defined daughter polymer.

6.2 Introduction

In the previous chapter, strategies to template dimeric and oligimeric structures from templates were surveyed. Ultimately, however, our goal is to template complex polymer structures in a similar way that Nature templates biopolymers.[1] This chapter

presents our initial attempts at this goal and provides more insight into the complexity of a biomimetic approach to polymers.

An enduring goal in synthetic polymer chemistry is to both understand and potentially harness Nature's templation strategies to produce abiotic polymers with controlled lengths, tacticities, and sequences. Polymer chemists have studied the effects of templates on various types of polymerization methods including condensation, addition, step, and chain polymerization.[2] Arguably the most impressive examples are the use of DNA templated synthesis (DTS)[3] and nucleic acid templated synthesis[4] to either elongate DNA and oligonucleotide strands or to polymerize daughter monomers from a predefined DNA sequence.[4c] While DTS provides an attractive platform for the production of monodisperse and even sequence defined polymers, it has thus far been limited to biopolymers.[3] While synthetically templated biopolymers provide insight into and perhaps even rival Nature's complexity, similar strategies for the production of synthetically templated abiotic polymers are still in their infancy. Advances in templation using synthetic polymers would be highly desirable, since they might provide a harness to control and even tune polymer properties. A few examples of influencing polymer properties through templation have recently emerged in the literature in which tacticity[5] and chain organization[6] can be controlled with a template. In addition, template polymerizations appear to be an excellent route to ladder and ladder-like polymers,[7] the properties of which are still not widely understood. Other potential applications include surface based template polymerizations for the production of intertwined structures and free-standing two–dimensional polymers.[8]

Nature's mechanisms have undoubtedly inspired the development of template-directed synthesis[9-10] mediated by molecular recognition and supramolecular self-assembly[11] for the production of topologically interesting small molecules and oligimeric structures[12-21] (Chapter 5). The success of templated olefin metathesis, in particular, is attributed to both functional group tolerance, namely catalyst tolerance toward a wide variety of noncovalent interactions, and the dynamic nature of the metathesis reaction.[22] During templated RCM and CM, both the template recognition event and the covalent bond formation step(s) is(are) reversible, which enables full thermodynamic control[10c] analogous to the proofreading mechanisms of DNA and RNA. Motivated by many small-molecule templated syntheses based on metathesis, we decided to investigate template effects on ROMP since the polymerization of bis-norbornene structures has been shown to be an efficient means for generating bridged polymer architectures.[23] While ROMP is not a dynamic covalent process, it is a highly functional group tolerant process, and thus well suited for template polymerizations. In the previous Chapters, the compatability of ROMP with a variety molecular recognition partners has been shown.[24] We utilize the molecular recognition process between the complementary recognition pair thymine (THY) **1** and diaminopyridine (DAP) **2** (Figure 6.1). Our design involves the use of a DAP based poly(norbornene) template that recognizes THY containing norbornene monomers, followed by the polymerization of the resulting template:monomer complex via ROMP.

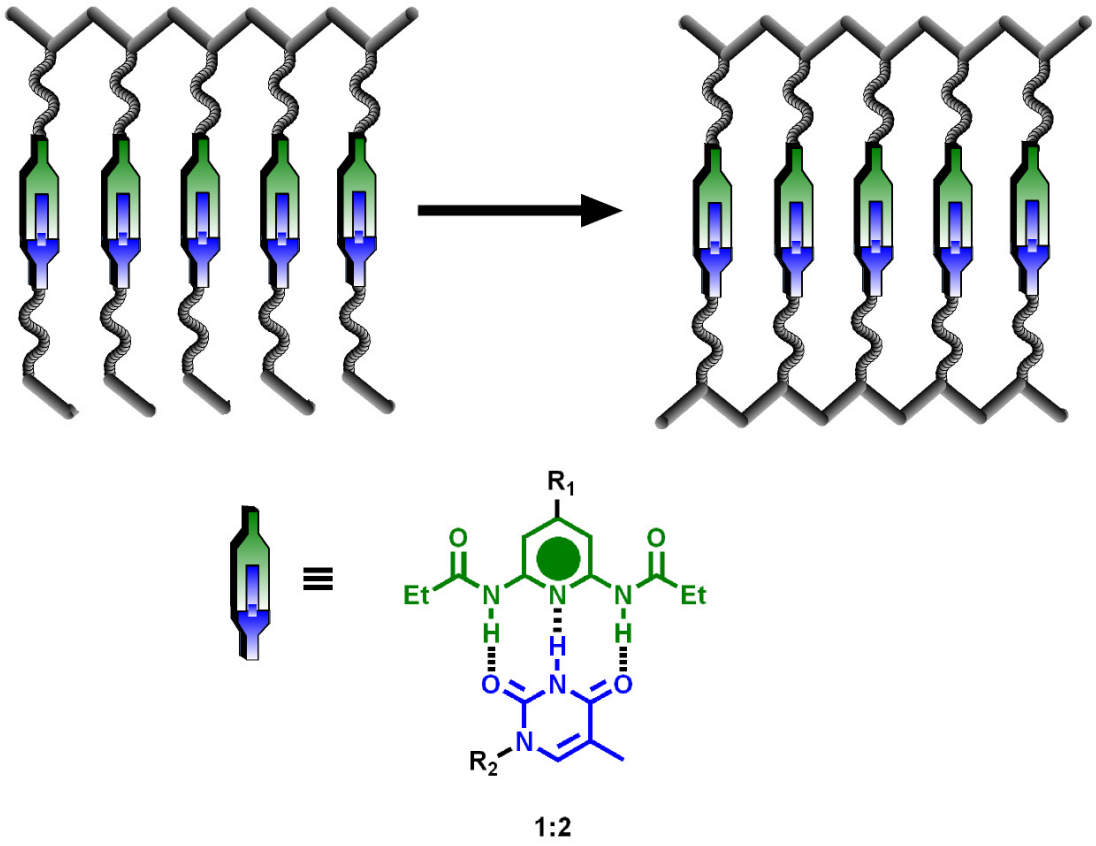

Figure 6.1. Schematic representation of the template polymerization investigated in this contribution.

6.3 Results and Discussion

6.3.1 Template Synthesis

In order to fully understand templated ROMP mediated by DAP:THY interactions, we investigated both solution and solid support-based templates. DAP was chosen as the recognition motif for the polymeric template because the dimerization constant of a polymeric DAP scaffold is lower than the dimerization constant of a THY scaffold, resulting in higher association constants (K_as) for small molecule THY substrates with DAP polymers relative to K_as for small molecule DAP substrates with THY polymers.[24c-d] The synthesis of the solution based template is outlined in Scheme

6.1 and was accomplished by the polymerization of the DAP-based monomer **5** using Grubbs' first generation catalyst. The polymer characterization data of **poly(3)** is outlined in Table 6.1. The support based template synthesis was carried out in close analogy to recent work by Kiessling and coworkers.[25] They demonstrated that the immobilization of poly(norbornene)s onto poly(styrene) resins is more successful when block copolymers consisting of one reactive block are used relative to strategies that utilize reactive polymer endgroups.[25] In our case, the reactive block contains a carboxylic acid group that is used to couple the template to the resin. Because of the uncontrolled nature of the polymerization of **4** using Grubbs' first generation catalyst, the carboxylic acid monomer was protected using a benzyl group through a DCC assisted esterification (Scheme 6.2). The resulting benzyl protected acid **5** polymerized in a controlled fashion, with molecular weights of the resulting polymers **poly(5a)** linearly dependent on the initiator loading (Appendix D).

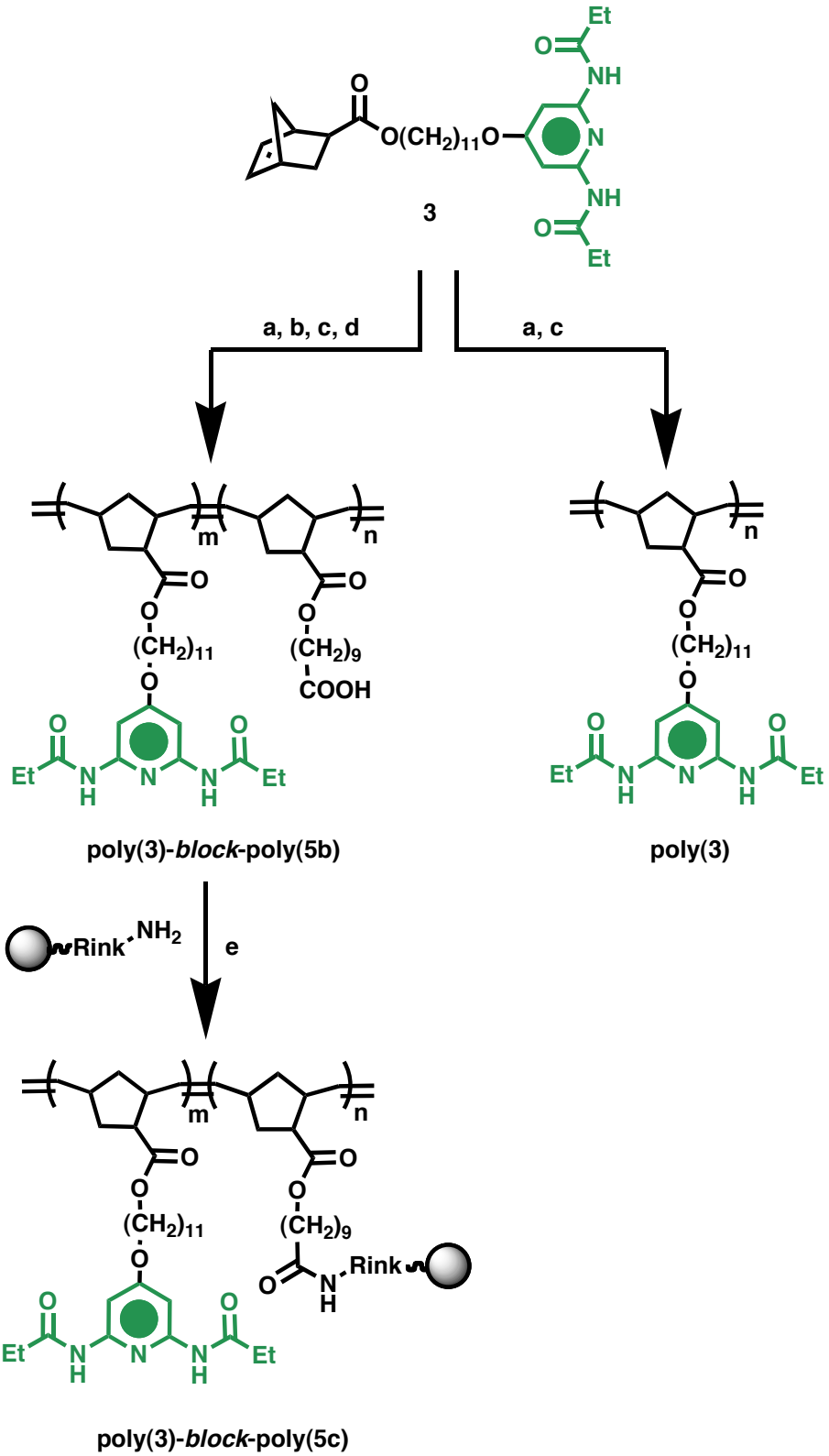

Scheme 6.1.[a] Synthesis of solution and solid support-based templates. [a]Reagents and Conditions: (a) Grubbs' 1st generation catalyst; (b) **4**; (c) Ethyl vinyl ether; (d) H_2 Pd/C; (e) Rink amine resin, HATU, DIEA, followed by acetic anhydride.

Table 6.1. GPC Data for template and daughter polymers.

Entry	M_w	M_n	M_w / M_n	m	n
poly(3)	11,800	9,150	1.29		20
poly(3)-*block*-poly(5b)	21,200	17,200	1.23	20	5
poly(3)-*block*-poly(5b)[a]	17,900	13,800	1.30	20	5
poly(6)	8,100	4,700	1.73		20
poly(6):(2)	10,200	8,000	1.28		20
poly(6)[b]	9,800	8,200	1.19		20

[a] after deprotection, [b]polymerized from template (at 10 mM in CH_2Cl_2).

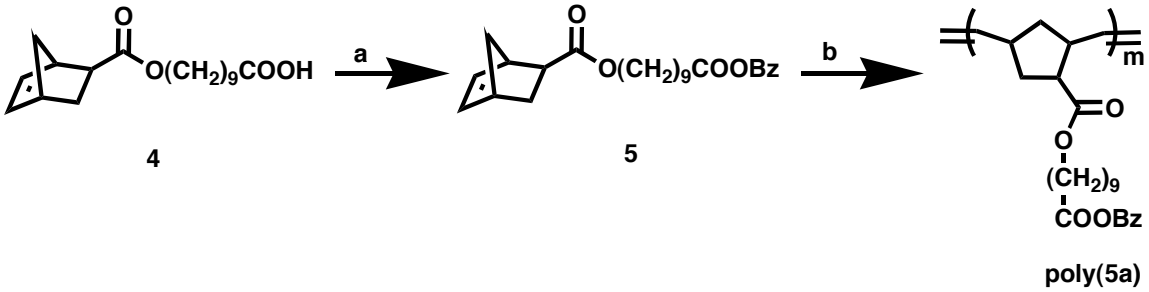

Scheme 6.2.[a] Synthesis and polymerization of protected carboxylic acid monomer.[a]Reagents and Conditions: (a) Benzyl alcohol, DCC, DMAP, 12 h, 80%; (b) Grubbs' 1st generation catalyst, 2 h, then ethyl vinyl ether.

Having demonstrated that monomer **5** can be polymerized in a controlled fashion, block copolymers consisting of both a DAP-based block and a protected carboxylic acid block were synthesized (Scheme 6.1). DAP-based monomer **3** has previously been found to polymerize in a living fashion[26] and thus was polymerized first. After complete consumption of **3** as evidenced by thin-layer chromatography (TLC), **5** was added to the

reaction mixture. The polymerization was terminated upon complete consumption of **5**. Upon hydrogenolysis of the benzyl protecting group, **poly(3)-*block*-poly(5b)** was obtained. The polymer characterization data before and after deprotection of **poly(3)-*block*-poly(5b)** is outlined in Table 6.1. The resulting block copolymer was coupled to a poly(styrene) Rink amine resin using HATU and DIEA (Scheme 6.1). Since a three-fold excess of polymer to resin (based on reactive carboxylic groups) was used, quantitative polymer attachment was achieved. Evidence of polymer attachment could be determined visually, as the color of the resin retained the dark brown polymer color after repeated washes. Additionally, a negative ninhydrin test indicated that surface amine reactive groups were consumed. Any residual amine groups were capped following the addition of acetic anhydride.

6.3.2 Template Polymerizations

Our hypothesis was that the DAP:THY interactions would be particularly suited for template polymerizations since the binding constant for this interaction is sufficiently high to result in an increase in local monomer concentrations, while low enough to allow for sufficient flexibility to retain full solubility of the noncovalently cross-linked polymers during the template polymerization. As a benchmark and control experiment, a non-templated polymerization analogue was investigated (Scheme 6.4). For the non-templated polymerization, the small molecule DAP-based compound **2** was added to monomer **6** to (a) reduce the dimerization behavior of this monomer, which ordinarily prevents a controlled polymerization in non-polar solvents (*vide infra*) and (b) mimic the

templation polymerization experiment as close as possible by having the same functional groups present in solution during the polymerization.

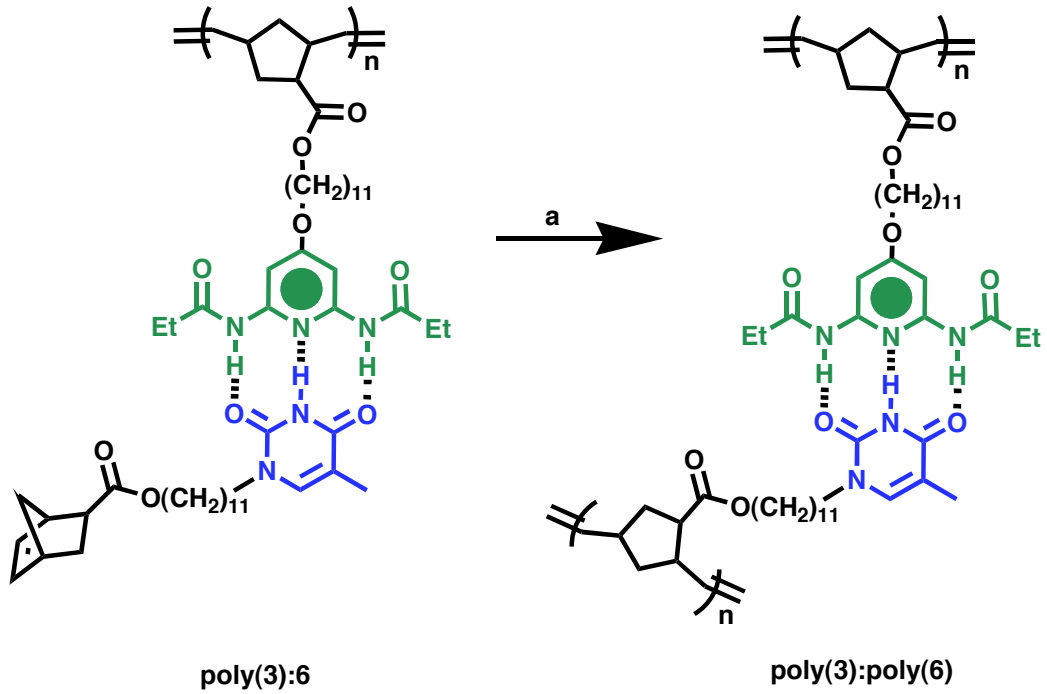

Scheme 6.3.[a] Solution based templated polymerization. [a]Reagents and Conditions: (a) Grubbs' 1st generation catalyst, $CDCl_3$ followed by ethyl vinyl ether.

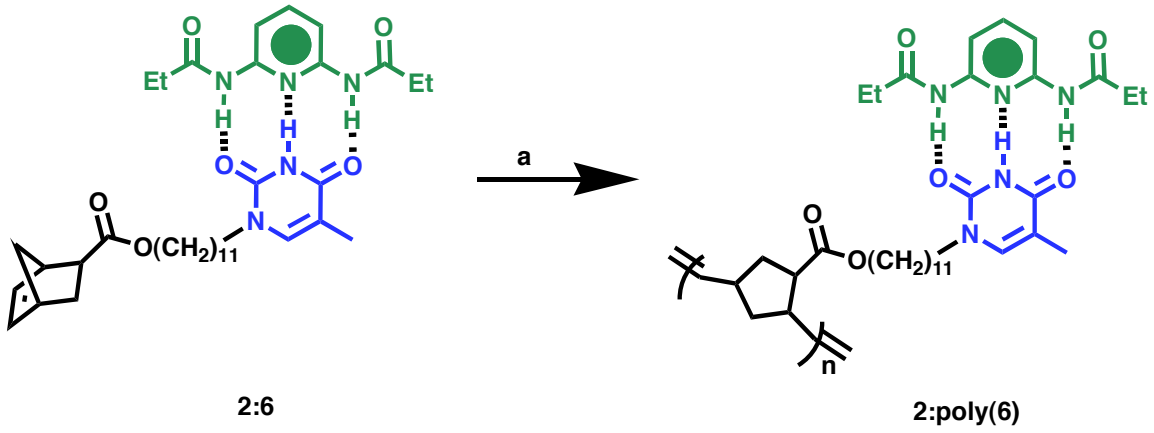

Scheme 6.4. Non-templated polymerization control experiment. [a]Reagents and Conditions: (a) Grubbs' 1st generation catalyst, $CDCl_3$ followed by ethyl vinyl ether.

Detailed ^{1}H NMR spectroscopic studies were performed to monitor the templated polymerization *in situ* (Figure 6.3). The amide proton resonances originating from **poly(3)** and the imide proton resonance originating from **6** and **poly(6)** are diagnostic signals for identifying the presence (or absence) of the hydrogen bonded complex.[24a, 24d] Signals originating from the amide protons present in the hydrogen bonded complex **poly(3):6** appear at 9.25 ppm, while the imide proton resonates downfield at 11.44 ppm. The presence of these signals provides good evidence for the formation of a polymeric DAP:THY hydrogen bonded complex, since the uncomplexed amide proton resonance typically appears around 8 ppm, while the complexed amide proton resonates downfield past 9 ppm in $CDCl_3$.[24d] Furthermore, the uncomplexed imide proton typically resonates at or upfield of 10 ppm, while the complexed analogue resonates downfield of 10.4 ppm,[24d] although the precise location of this proton usually depends on the ratio of DAP to THY present in the mixture.[24a] The ^{1}H NMR spectra (Figure 6.3) provide sufficient evidence to conclude that a hydrogen bonding complex between the polymeric DAP receptor (**poly(3)**) and THY monomer (**6)** is present. Once the presence of the hydrogen bonded complex was established, the important question to address was whether the hydrogen bonded species resides unaffected during the templated polymerization. Thus, we recorded ^{1}H NMR spectra at different intervals during a sample polymerization. We found that the nature of the hydrogen bonded complex does not appear to be affected by the formation of the polymer:polymer complex (**poly(3):poly(6)**) and that the hydrogen bonded species is not disrupted by the polymerization conditions. Both the amide proton resonance and the imide proton resonance remain at 9.25 and 11.44 ppm, respectively, throughout the polymerization (Figure 6.3). Additionally, the ^{1}H NMR spectra clearly

show the complete consumption of monomer **6** over time. The olefinic proton resonance originating from monomer **6** at 6.15 ppm disappears while the signal corresponding to the olefin-containing polymer at 5.28 ppm increases throughout the polymerization (Figure 6.3).

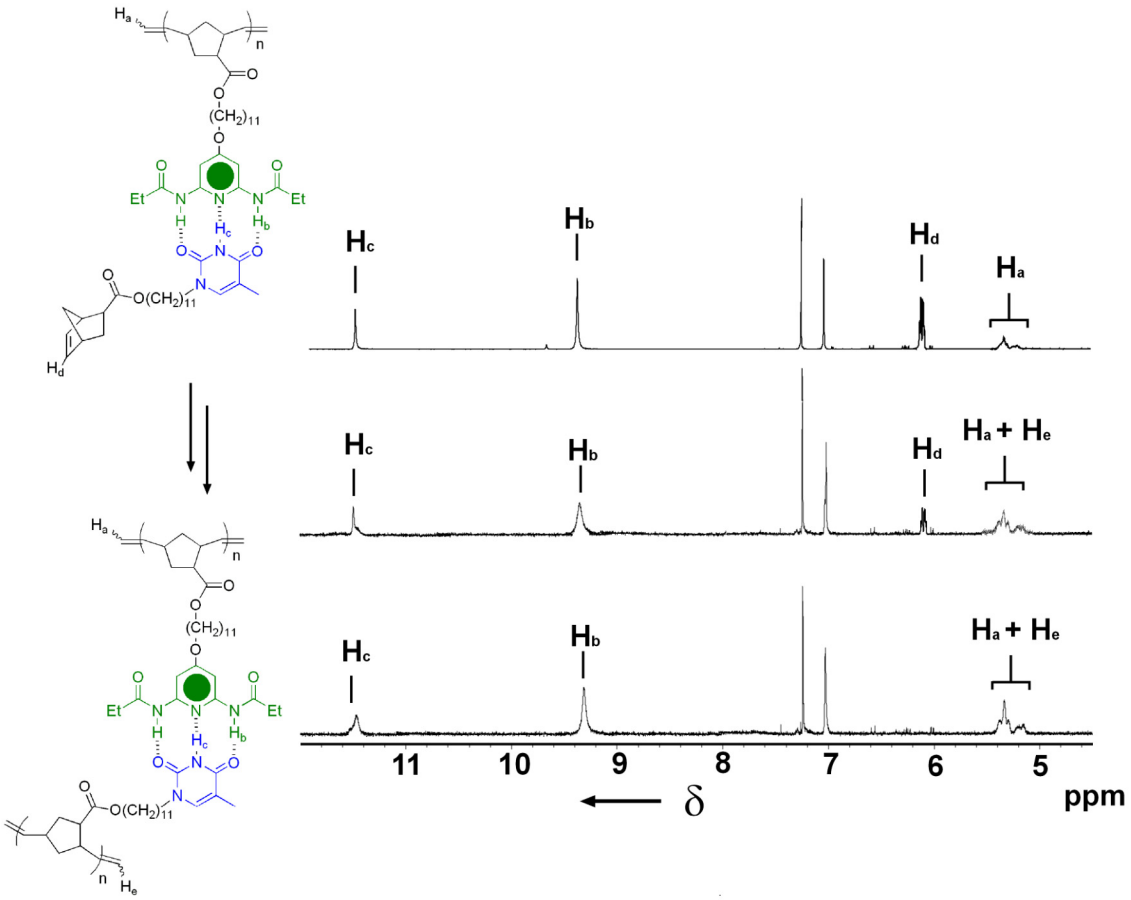

Figure 6.3. Stacked plot of partial ^{1}H NMR spectra (10 mM, $CDCl_3$, 298K) and corresponding peak assignments displaying the polymerization progress of monomer **6** bound to template **poly(3)** *in situ*.

We then investigated the kinetics of the template polymerization in detail to determine whether or not the polymer based template (**poly(3)**) could enhance the rate of polymerization. Such a phenomenon has been observed before during ionic and

hydrogen bond based free-radical template polymerizations.[2] Furthermore, kinetic enhancements are also seen during many examples of DTS and nucleic acid based templated polymerizations; in some cases, the template is *required* for polycondensation to ensue at dilute concentrations.[4b] We studied kinetics of both templated polymerizations and non-templated polymerization analogues at 10 mM, 50 mM, and 100 mM using ^{1}H NMR spectroscopy. Our hypothesis, based on many examples of DTS, was that the greatest template effect would be observed at the lowest concentration. In this case, 10 mM was the lowest concentration we investigated, since concentrations below 10 mM resulted in errors in the rate constants originating from baseline noise that were too high to properly assess the data. In order to compare templated and non-templated analogues, we chose to use a small molecule DAP substrate (**2**) to protect THY monomer **6** during the non-templated polymerization. We assumed that this would ensure the comparison of truly analogous systems, since THY monomer **6** has been shown to aggregate due to self-dimerization of polymer chains in non-polar solvents at moderate degrees of polymerization (DP > 50).[24a]

Pseudo-first order rate constants (k_{obs}) for the polymerization (in $CDCl_3$) of monomer **6** bound to template **poly(3)** or protected with small molecule **2** were measured by monitoring the decrease in peak height of the signal originating from the monomeric olefin protons. In the solution-based polymerization examples with or without a template (Schemes 6.3 and 6.4), exponential decreases in monomer concentrations were observed, indicating that the polymerizations follow expected pseudo-first order kinetics, in which all cases reached 100% conversion (Figures 6.4-6.6). The greatest rate enhancement was observed at 10 mM, the most dilute concentration studied. An approximate three-fold

increase in the rate constant was observed when the template was used relative to the non-templated analogue (Table 6.2). A result that was not entirely expected was observed at higher concentrations. The effect of the template seems to decrease exponentially as concentration decreases (Figure 6.7). At 10 mM, a three-fold template enhancement effect was observed, while at 50 mM, the enhancement was only two-fold, and at 100 mM, no enhancement was observed. These results suggest that at high dilution, a local concentration enhancement induced by the template is sufficient to speed up the rate of polymerization. At higher concentrations, however, this effect probably still exists, yet has little effect on the observed kinetics of the polymerization. Thus, at concentrations approaching 100 mM, the bulk solution molarity seems to dictate the rate of polymerization, rather than any local concentration effects induced by the template.

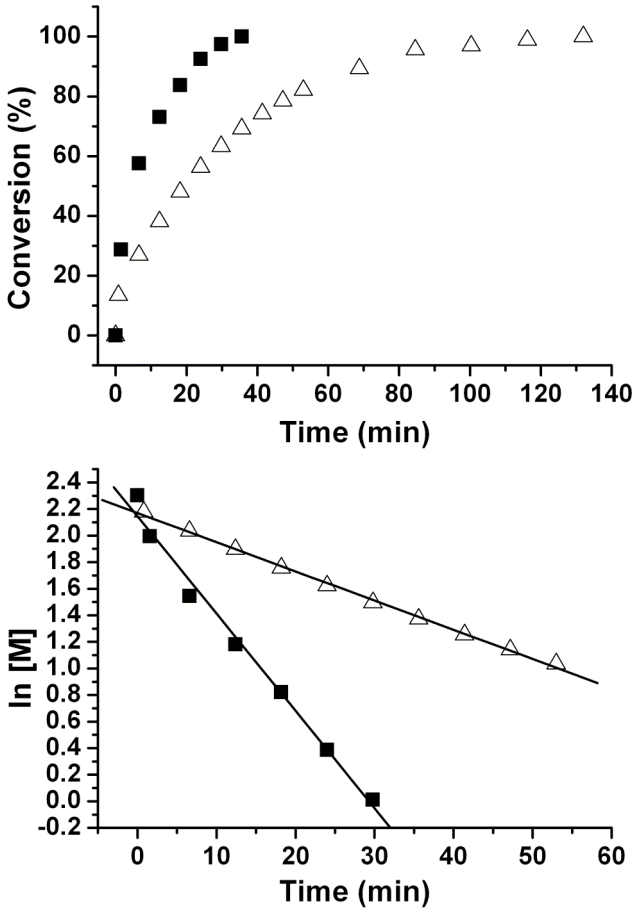

Figure 6.4. Polymerization kinetics at 10 mM ($CDCl_3$, 298 K): plot of conversion vs. time (top) and corresponding 1st order kinetics plot (bottom) for the polymerization of **2:6** (Δ) and **poly(3):6** ( ).

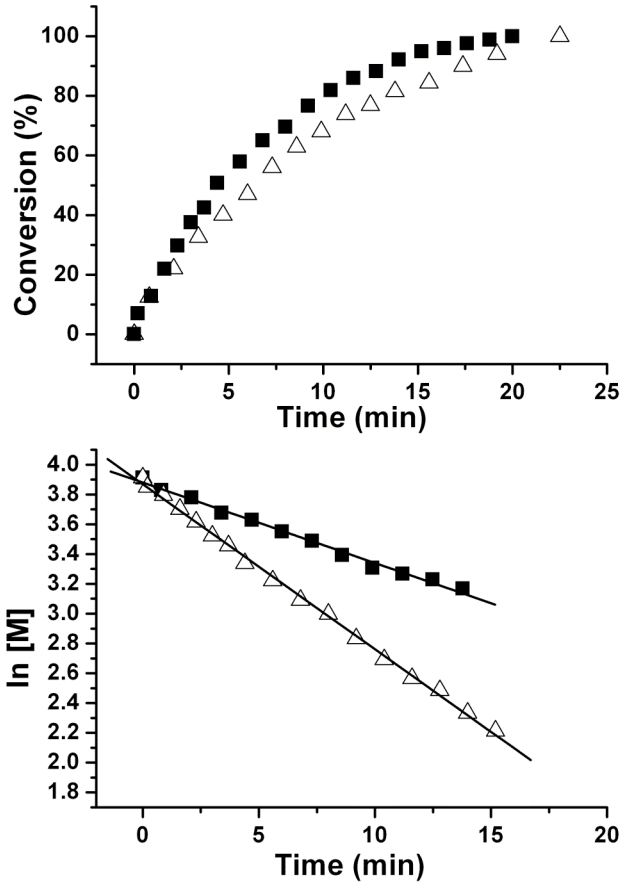

Figure 6.5. Polymerization kinetics at 50 mM ($CDCl_3$, 298 K): plot of conversion vs. time (top) and corresponding 1st order kinetics plot (bottom) for the polymerization of **2:6** (Δ) and **poly(3):6** ( ).

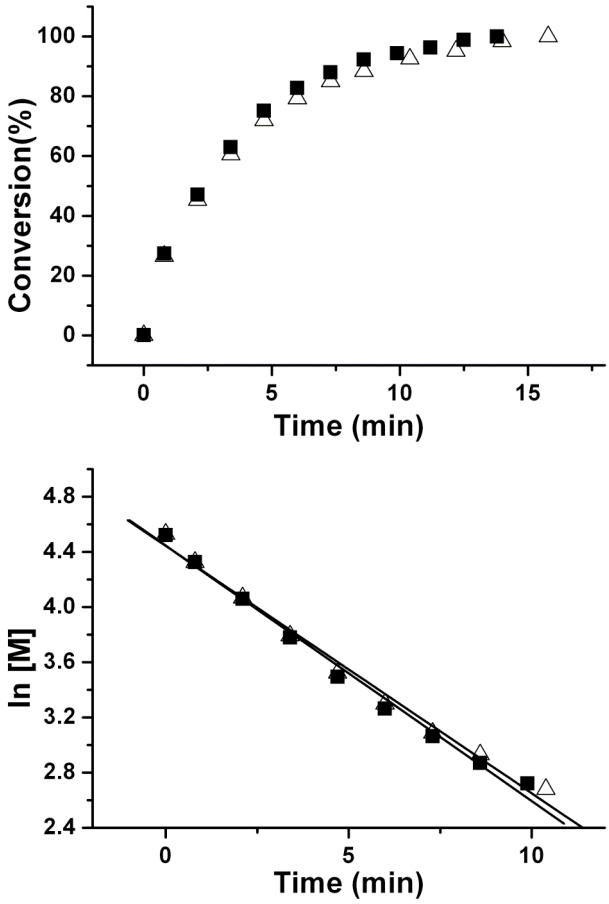

Figure 6.6. Polymerization kinetics at 100 mM ($CDCl_3$, 298 K): plot of conversion vs. time (top) and corresponding 1st order kinetics plot (bottom) for the polymerization of **2:6** (Δ) and **poly(3):6** ( ).

Table 6.2. Kinetic Data for template polymerizations and control polymerizations.

Entry	Concentration (mM)	k_{obs} (10^3 s^{-1})
2:6	10	0.37 ± 0.01
poly(3):6	10	1.22 ± 0.06
6	10	0.36 ± 0.01
2:6 + p(**NBE**)	10	0.41 ± 0.02
2:6	50	0.90 ± 0.03
poly(3):6	50	1.85 ± 0.02
6	50	0.82 ± 0.04
2:6 + p(**NBE**)	50	0.91 ± 0.02
2:6	100	2.99 ± 0.12
poly(3):6	100	3.09 ± 0.12
6	100	2.67 ± 0.09
2:6 + p(**NBE**)	100	2.65 ±0.06

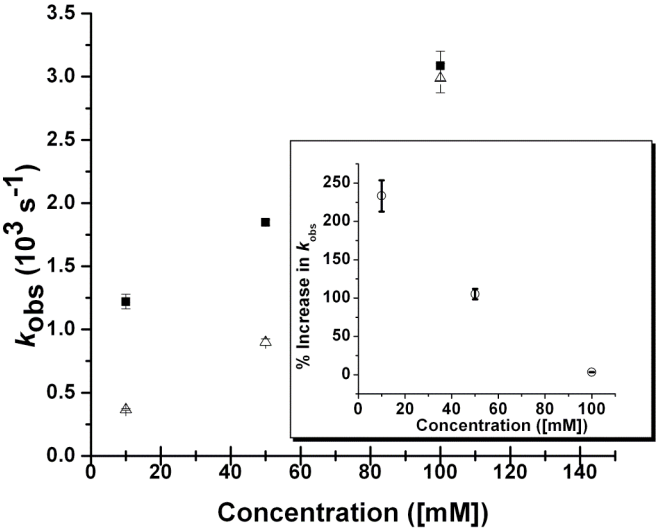

Figure 6.7. Rate constant dependence on concentration for templated (square) and non-templated (diamond) polymerizations. The corresponding inset plot displays the percent increase in k_{obs} induced by the polymeric template at varying concentrations.

Several control experiments were carried out to verify our hypothesis. First, it is plausible that the template prevents the *slowing* of the polymerization by reducing the aggregation behavior of monomer **6**, rather than actually *speeding* up the polymerization by inducing a local concentration effect, especially since aggregation behavior of monomer **6** has been observed when attempts were made to polymerize monomer **6** with a desired DP of greater than 50 (in CH_2Cl_2).[24a] This aggregation behavior would presumably be mitigated by protecting the THY moiety with the corresponding DAP (**2**) substrate, but it is possible that aggregation might still exist in competition with the protecting group, since we are considering an equilibrium process. Thus, we examined the polymerization of unprotected monomer **6** at varying concentrations in the hopes of quantifying how large of an effect aggregation might have on the rate constant. To our surprise, unprotected monomer **6** does not visibly aggregate at low concentrations (10-

100 mM), and no effect on the rate constant was observed relative to the rate constant observed for the polymerization of **2:6** (Table 6.2, Appendix D). Monomer **6** only tends to aggregate as initiator loading is decreased with desired DPs of greater than 50. It is important to note that when aggregation is observed while trying to polymerize monomer **6** with higher DPs, the polymerization only tends to proceed to around 50% conversion. Thus, these results indicate that the rate constants for the non-templated analogue polymerizations of monomer **6** are not hampered by aggregation. Most importantly, these data provide strong evidence that the template is not an aggregation suppressant, but rather an inducer of a local concentration increase.

The role of the polymer backbone during the template polymerization might also be important, since the template is based on a poly(olefin) and ROMP is used as the polymerization method. While we predicted that the polymer backbone would not interfere with subsequent template polymerizations since the first generation Grubbs catalyst is active primarily toward strained olefins, we nevertheless carried out control experiments in which monomer **2:6** was polymerized in the presence of poly(norbornene) (DP = 20, M_w = 2000, M_n = 1850, PDI = 1.08). The rate constant measurements were independent of the presence of the polymer backbone (Table 6.2, Appendix D). These results support the conclusion that the poly(olefin) backbone is not a nuisance during the polymerization, and if minimal back-biting is occurring, this has no noticeable effect on k_{obs}.

Next, we investigated the nature and the control of the templated polymerization. Since the daughter polymer (**poly(6)**) formed could not be separated easily from **poly(3)**, we utilized the support based template **poly(3)-*block*-poly(5c)** (Scheme 6.5). Once

monomer **6** was polymerized completely from the support based template, DMF was added to the reaction mixture to break up the hydrogen bonded complex and to remove the daughter polymer (**poly(6)**) from the resin. The resulting polymer could then be analyzed by GPC and compared to its non-templated analogues.

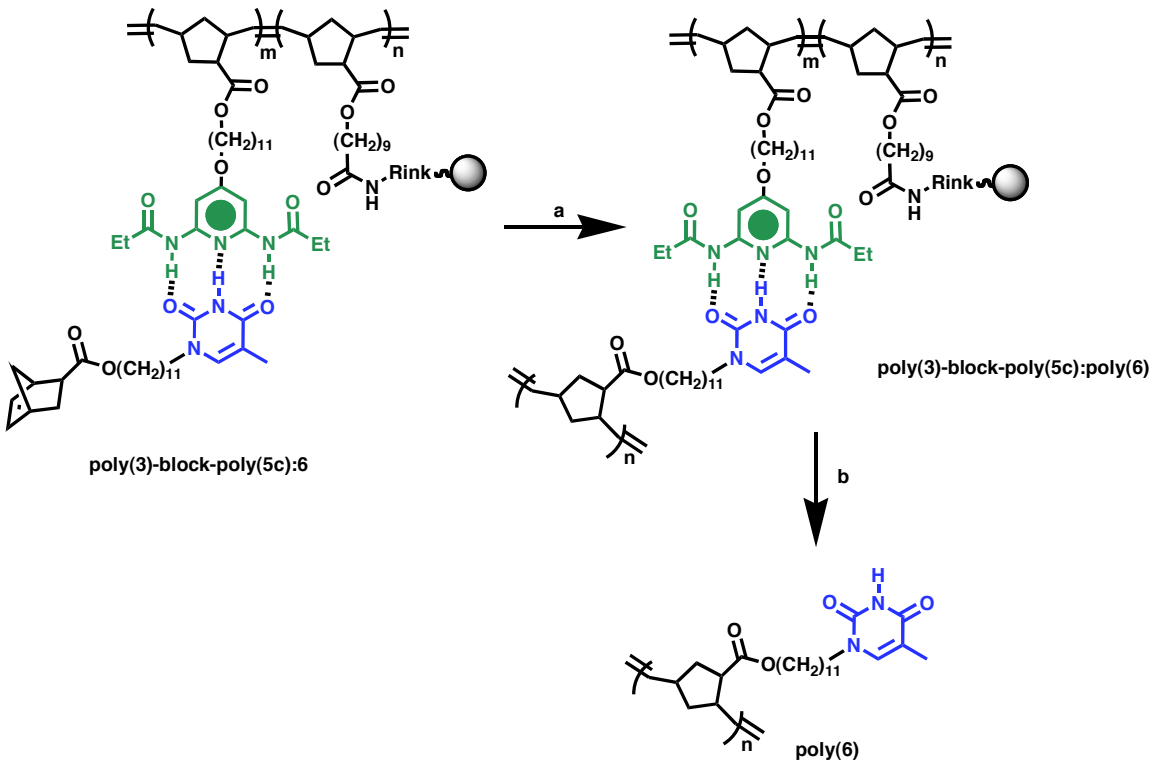

Scheme 6.5. Support-based template polymerization. [a]Reagents and Conditions: (a) Grubbs' 1st generation catalyst, CH_2Cl_2 followed by ethyl vinyl ether; (b) DMF.

The homopolymerization of monomere **6** in nonpolar solvents (CH_2Cl_2, $CHCl_3$) results in a rather uncontrolled polymerization with the formation of larger molecular weight species (Figure 6.8, Table 6.1). Our kinetic studies indicate that aggregation is not a problem during the polymerization of monomer **6** with DP < 50, so this is probably not a contributing factor to the uncontrolled polymerization. It is possible, however, that monomer **6** may interfere with the catalyst in some way, and this interference may have not been detectable during our ^{1}H NMR spectroscopy studies. Another factor may be the solubility of monomer **6** in CH_2Cl_2. Under dilute conditions, the limited solubility of monomer **6** in CH_2Cl_2 did not have a noticeable effect on the kinetics of the polymerization, but this still could potentially have an effect on the control of the polymerization. These are merely assumptions, however, as the exact reason why monomer **6** polymerizes in an uncontrolled fashion is not fully understood. Nevertheless, the addition of a small molecule DAP substrate (**2)** to monomer **6** clearly allows for a more controlled polymerization (Figure 6.8, Table 6.1). The resulting polymer has a lower polydisperity index (PDI) (1.28) than the analogue polymer formed without the addition of the THY additive, which has a PDI of 1.73 (Table 6.1).

Likewise, the polymer formed from the support based template **poly(3)-*block*-poly(5c)** has a PDI of 1.19. Such a narrow PDI indicates a controlled polymerization, and the GPC results indicate a monomodal distribution of molecular weights. A small amount of high molecular polymer is present according to the GPC results (Figure 6.8). However, significantly less high molecular weight polymer is formed during the templated polymerization relative to the homopolymerization of **6** (Figure 6.8). It is clear from these results that the support based template does not interfere with the

polymerization, a satisfactory result since we did not see the evidence of cross-linking at dilute conditions. Furthermore, upon washing with DMF, a solvent that is able to disrupt the hydrogen bonds between the template and the daughter polymer thereby releasing the daughter polymer, polymer was recovered. Based on initial monomer loading to the supported template, we found that 96% of the resulting polymer was recovered after the DMF wash. This rules out the possibility of higher molecular weight species being retained on the template after the wash. Our results from the supported template experiments indicate that the template is capable of providing an environment in which monomer **6** can polymerize in a controlled fashion. However, when the small molecule protecting group (DAP **2**) is used, similar results are obtained. Thus, the supported template does not appear to be significantly advantageous over the small molecule **2** in providing a controlled polymerization environment.

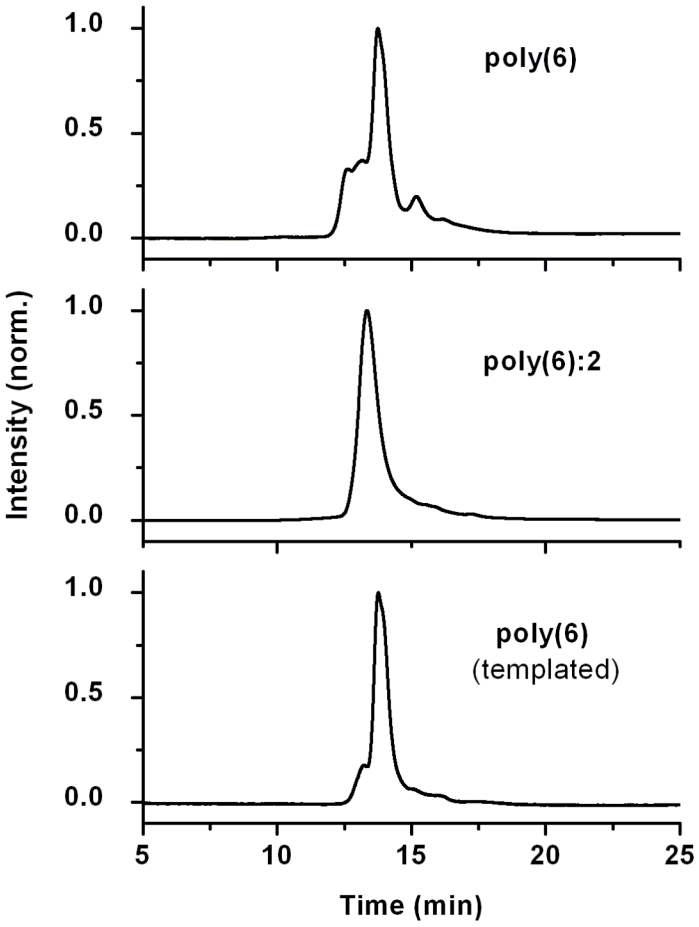

Figure 6.8. GPC traces of **poly(6)** without any template, **poly(6)** in the presence of **2**, and **poly(6)** released from the template.

We also investigated the effect of the template on the degree of polymerization (DP) of the daughter polymer and found no relationship between the DP of the template with the DP of the daughter polymer. Rather, the DP was based on initiator loading. Regardless of the DP of the template, the initiator loading was the only factor that seemed to affect the DP of the daughter polymer. Although relationships between template DP and daughter DP have been observed during radical polymerizations,[27] these results cannot be generalized and applied to our system. The observed control during the

support based template polymerization is most likely the result of the protection of the thymine moiety, analogous to the effect of the small molecule DAP (**2**) protecting group. Another possibility, however, is that the template speeds up the polymerization such that catalyst death is minimized, and the larger molecular weight species are not produced, a result that we have previously observed during the polymerization of similar monomers.[26]

6.4 Conclusion

Template polymerizations are of great interest because they mimic the impressive polymerization techniques found in Nature thereby allowing for a high degree of control during the polymerization and might permit for the realization of applications to which templated polymers are key. Most of the prior studies on templated polymerizations, however, deal with uncontrolled polymerization methods that have difficulties separating the daughter polymer from the template. In this contribution, we present that both a controlled polymerization method can be performed from a polymeric template and that the daughter polymer can be separated from a support-based template easily. We find that a polymeric template enhances both polymerization kinetics under dilute conditions and the control of the resulting polymerization. These results are satisfactory for our next challenge to apply templated ROMP to materials applications, such as surface templated polymerizations or polymerizations from nanoparticle assemblies.

6.5 Experimental Section

6.5.1 Materials

Grubbs' 1st generation catalyst was purchased from Aldrich. *N,N'*-dicyloclohexylcarbodiimide (DCC) and dimethylaminopyridine (DMAP) was purchased from Alfa Aesar. Benzyl alcohol was purchased from Alfa Aesar and distilled prior to use. 2-(7-Aza-1H-benzotriazole-1-yl)-1,1,3,3-tetramethyluronium hexafluorophosphate (HATU) was purchased from Oakwood Products, West Columbia, South Carolina. Rink Amide AM Resin (200-400 mesh, 0.71 mmole/g) was purchased from Novabiochem. Ethyl vinyl ether (stabilized) and dry *N,N*-Dimethylformamide (DMF) was purchased from Acros Organics. 5% palladium on carbon powder, 50% water wet, was purchased from Aldrich. $CHCl_3$ purchased from Fischer was dried ($CaCl_2$), distilled, and degassed prior to use. CH_2Cl_2 purchased from Fischer was dried via passage through copper oxide and alumina columns. Compounds **3**,[26] **4**,[24f] and **6**,[24a] were synthesized according to literature procedures. *N*-diisopropylethylamine purchased from Avocado Research Chemicals was distilled over CaH prior to use.

6.5.2 Methods

Reactions were carried out under an Argon atmosphere unless otherwise noted. Thin-layer chromatography (TLC) was performed on Silica XHL TLC glass backed plates (Sorbent Technologies). Column chromatography was performed on premium R_f grade silica gel (Sorbent Technologies, 40-75μm). Nuclear magnetic resonance (NMR) spectra were recorded using a 500 MHz Bruker DRX spectrometer (^{1}H NMR: 500 MHz, ^{13}C NMR: 125 MHz) or a 300 MHz Varian Vx 300 spectrometer (^{1}H NMR: 300 MHz, ^{13}C NMR: 75 MHz). Spectra were referenced from the residual proton resonance of the

deuterated solvent. Chemical shifts are reported as parts per million (ppm) downfield from the signal origination of Me_4Si as an internal standard for ^1H and ^{13}C NMR spectroscopy. Kinetic experiments for polymerizations were conducted using ^1H NMR spectroscopy (298° K) by monitoring the decay in proton resonances originating from monomer. The peak heights were subsequently fitted to a decreasing exponential function (pseudo-first order) from which rate constants were extrapolated. Gel-permeation chromatography (GPC) analyses were carried out using a Shimadzu pump, a Shimadzu UV detector with THF or DMF as the eluants and a set of American Polymer Standards columns (100,1000,100,000 Å linear mixed bed). The flow rate used for all the measurements was 1 mL/min. All GPC measurements were calibrated using poly(styrene) standards and were carried out at room temperature. M_w, M_n and PDI represent weight average molecular weight, number average molecular weight and the polydispersity index, respectively. Isothermal titration calorimetry was performed on a Microcal VP-ITC Isothermal Calorimeter using degassed $CHCl_3$ as the solvent with a cell concentration of 1 mM and a syringe (titrant) concentration of 10 mM.

6.5.3 Synthesis

Monomer 5.

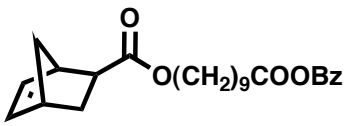

5

Carboxylic acid monomer **4** (100 mg, 0.325 mmol), benzyl alcohol (35 mg, 0.325 mmol), DCC (74 mg, 0.358 mmol) and DMAP (cat) were dissolved in dry CH_2Cl_2, and the reaction mixture was refluxed overnight. The precipitate was filtered off, and the

solvent was removed using rotary evaporation under reduced pressure. The resulting oil was purified using column chromatography (Hexanes/EtOAc = 9:1) to give a clear oil (120.5 mg, 93%). ^{1}H NMR ($CDCl_3$): δ = 7.37 (m, 5H), 6.12 (m, 2H), 5.12 (s, 2H), 4.08 (t, *J* = 6.7 Hz, 2H), 3.01 (m, 1H), 2.98 (m, 1H), 2.35 (t, *J* = 7.6 Hz, 2H), 2.22, (m, 1H), 1.81-0.90 (m, 18H). ^{13}C NMR ($CDCl_3$): δ = 174.0, 171.1, 140.3, 136.0, 135.9, 128.5, 128.0, 127.3, 70.3, 68.9, 50.6, 48.3, 43.0, 34.2, 31.3, 30.2, 29.5, 29.1, 29.0, 28.6, 25.4, 24.7. Anal. Calcd for $C_{25}H_{34}O_4$: C, 75.34; H, 8.60. Found: C, 75.59; H, 8.74.

General Procedure for the Synthesis of Poly(3) and Poly(5a).

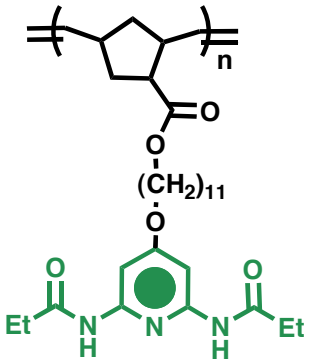

poly(3)

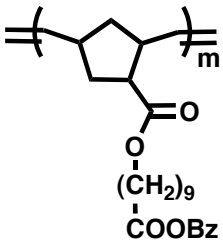

poly(5a)

The desired amount of monomer was weighed into a glass vial with a rubber septum cap, placed under an Argon atmosphere and dissolved in anhydrous, degassed CH_2Cl_2. A stock solution of the catalyst (in the corresponding solvent) was prepared, and the desired volume was added to the polymerization vessel. Upon complete polymerization, ethyl vinyl ether was added to quench the polymerization. The polymer was isolated and purified by repeated precipitations into MeOH.

Poly(3). All analytical data are consisted with previously published results.[47]

Poly(5a). ^{1}H NMR ($CDCl_3$): δ = 7.37 (m, 5H), 5.39 (m, 2H), 5.12 (s, 2H), 4.08 (t, *J* not resolved, 2H), 2.80-2.60 (m, 2H), 2.36 (t, *J* = 7.7 Hz, 2H), 1.90-1.20 (m, 18H). ^{13}C NMR

($CDCl_3$): δ = 174.3, 170.1, 140.3, 137.0, 134.0, 133.1, 130.2, 128.5, 128.0, 127.3, 70.3, 67.6, 50.3, 48.0, 43.0, 34.2, 30.3, 30.2, 29.3, 29.1, 28.9, 28.6, 24.9, 24.3.

Poly(3)-*block*-poly(5b).

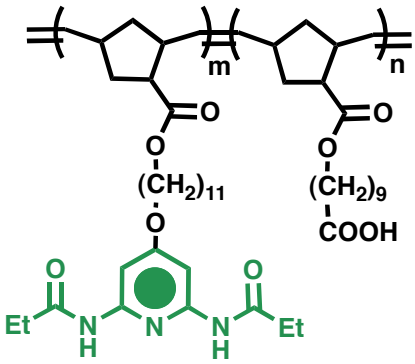

poly(3)-*block*-poly(5b)

Monomer **3** (44 mg, 0.083 mmol) was dissolved in anhydrous, degassed CH_2Cl_2. Grubbs' first generation catalyst (3.45 mg, 0.004 mmol) was added in a solution of CH_2Cl_2. The polymerization was monitored by TLC. Upon complete disappearance of **3**, **5** (8.3 mg, 0.021 mmol) was added as a solution in CH_2Cl_2. Upon complete consumption of **5**, the polymerization was terminated with ethyl vinyl ether. The polymer was isolated and purified by successive precipitations in cold methanol (50 mg, 96%). ^{1}H NMR ($CDCl_3$): δ = 7.80 (br m, 2H), 7.45 (m, 2H), 7.36 (m, 5H) 5.27 (m, 4H), 5.10 (s, 2H), 4.05 (m, 6H), 2.80 (m, 2H), 2.21 (m, 23H) 1.80-1.11 (m, 40H). ^{13}C NMR ($CDCl_3$): δ = 176.2, 173.9, 172.8, 169.3, 150.7, 136.3, 133.9, 128.8, 128.4, 96.3, 68.7, 66.3, 64.8, 49.8, 47.8, 42.1, 36.5, 34.5, 31.0, 29.7, 29.5, 29.1, 28.9, 27.2, 26.5, 26.1, 25.1.

The resulting polymer was dissolved in THF / MeOH = 3:1 and hydrogenated for 24 h to remove the benzyl protecting group using H_2 over Pd/C (60 p.s.i.). The reaction mixture was filtered over celite, and the solvent was removed using rotary evaporation under reduced pressured to yield **poly(3)-*block*-poly(5b)** as a light brown glassy solid (40

mg, 80%). ^{1}H NMR ($CDCl_3$): δ = 11.20, (br s, 1H), 7.80 (br m, 2H), 7.45 (m, 2H), 5.27 (m, 4H), 5.10 (s, 2H), 4.05 (m, 6H), 2.75 (m, 2H) 2.21 (m, 23H) 1.80-1.11 (m, 40H). ^{13}C NMR ($CDCl_3$): δ = 176.2, 173.9, 172.8, 169.3, 150.7, 136.3, 133.9, 96.3, 68.7, 66.3, 64.8, 49.8, 47.8, 42.1, 36.5, 34.5, 31.0, 29.7, 29.5, 29.1, 28.9, 27.2, 26.5, 26.1, 25.1.

Resin supported Poly(3)-*block*-poly(5c).

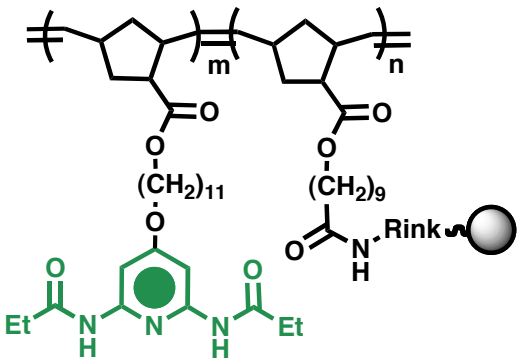

poly(3)-*block*-poly(5c)

Rink amide AM resin (121 mg, 0.71 mmol/g, 0.086 mmol) was added to a fritted filter equipped coupling vessel and swelled in CH_2Cl_2 for 45 min followed by DMF for 10 min with shaking using a WS180 º Shaker (Glas-Col). The resin was subsequently washed with MeOH and DMF. Piperidine (20% in DMF, 1mL) was added to remove the Fmoc protecting group. The mixture was agitated for 10 min and the resin was thoroughly washed with CH_2Cl_2, MeOH, and DMF. A ninhydrin test indicated the presence of free amine groups. **Poly(3)-*block*-poly(5b)** (3 eq, 135.5 mg, 0.258 mmol,), HATU (130 mg, 0.344 mmol), and DIEA (0.05 mL) were added to the resin as solutions in DMF and the coupling vessel was shaken overnight. The resin was filtered and washed thoroughly with DMF, MeOH, and CH_2Cl_2. A negative ninhydron test indicated the consumption of surface amine groups. Residual amine groups were capped with acetic anhydrid. The resin-supported polymer was dried under high vacuum for 24 h.

Solution-based Template Polymerization for Poly(3):poly(6). **Poly(3)** was dissolved in CH_2Cl_2 or $CDCl_3$ followed by the addition of **6**. The concentration of **6** was kept at 10 mM. The mixture was sonicated for 30 min to ensure complete dissolution followed by the addition of Grubbs' 1st generation catalyst. The polymerization was monitored by ^1H NMR spectroscopy. Upon complete conversion, the polymerization was quenched with ethyl vinyl ether. The resulting polymer:polymer complex **poly(3):poly(6)** was isolated by precipitation into cold MeOH.

Support-based Template Polymerization for Poly(3)-*block*-poly(5c):poly(6). Resin supported **poly(3)-*block*-poly(5c)** was swelled in CH_2Cl_2 for 45 min. Monomer **6** was then added to the vessel and the mixture was shaken for 1 h to ensure complete complexation. Then, Grubbs' 1st generation catalyst was added and the polymerization was allowed to proceed for 6 h, and the polymerization was terminated with ethyl vinyl ether. The resin was washed with CH_2Cl_2, and subsequently with DMF to remove the daughter polymer (**poly(6)**). Analytical data for **poly(6)** are consistent with previous reported values.[47]

6.6 References

1. Watson, J. D.; Crick, F. H. C., Molecular Structure of Nucleic Acids: A Structure for Deoxyribose Nucleic Acid. *Nature* **1953,** 171, 737.

2. Polowinski, S., *Template Polymerization*. ChemTec Publishing: Ontario, **1997**.

3. (a) Alemdaroglu, F. E.; Ding, K.; Berger, R.; Herrmann, A., DNA-templated synthesis in three dimensions: introducing a micellar scaffold for organic reactions. *Angew. Chem. Int. Ed.* **2006,** 45, 4206.

   (b) Calderone, C.; Liu, D. R., Small-molecule diversification from iterated branching reaction pathways enabled by DNA-templated synthesis. *Angew. Chem. Int. Ed.* **2005,** 44, 7383.

   (c) Kanan, M. W.; Rozenman, M. M.; Sakurai, K.; Snyder, T. M.; Liu, D. R., Reaction discovery enabled by DNA-templated synthesis and in vitro selection. *Nature* **2004,** 431, 545.

   (d) Li, X.; Liu, D. R., DNA-templated organic synthesis: Nature's strategy for controlling chemical reactivity applied to synthetic molecules. *Angew. Chem. Int. Ed.* **2004,** 43, 4848.

4. (a) Calderone, C. T.; Liu, D. R., Nucleic-acid-templated synthesis as a model system for ancient translation. *Curr. Opin. Chem. Biol.* **2004,** 8, 645.

   (b) Li, X.; Lynn, D. G., Polymerization on Solid Supports. *Angew. Chem. Int. Ed.* **2002,** 41, 4567.

   (c) Rosenbaum, D. M.; Liu, D. R. 1., Efficient and Sequence-Specific DNA-Templated Polymerization of Peptide Nucleic Acid Aldehydes. *J. Am. Chem. Soc.* **2003,** 125, 13924.

5. Hamada, K.-i.; Serizawa, T.; Akashi, M., Template Polymerization Using Artificial Double Strands. *Macromolecules* **2005,** 38, 6759.

6. Chandra, M. S.; Radhakrishnan, T. P., Polyelectrolyte Templated Polymerization in Langmuire Films: Nanoscopic Control of Polymer Chain Organization. *Chem. Eur. J.* **2006,** 12, 2982.

7. Zhang, T.; Deng, K.; Zhang, P.; Xie, P.; Zhang, R., Supramolecular Template-Directed Synthesis of Perfect Phenelenediimino-Bridged Ladderlike Polyphenylsiloxanes. *Chem. Eur. J.* **2006,** 12, 3630.

8. Stroock, A. D.; Kane, R. S.; Weck, M.; Metallo, S. J.; Whitesides, G. M., Synthesis of free-standing quasi-two-dimensional polymers. *Langmuir* **2003,** 19, 2466.

9. Diederich, F.; Stang, P. J., *Templated Organic Synthesis*. Wiley-VCH: Weinheim, 2000.

10. (a) Breault, G. A.; Hunter, C. A.; Mayers, P. C., Supramolecular Topology. *Tetrahedron* **1999,** 55, 5265.

(b) Busch, D. H.; Stephenson, N. A., Molecular Organization, portal to supramolecular chemistry. Structural analysis of the factors associated with molecular organization in coordination and inclusion chemistry, including the coordination template effect. *Coord. Chem. Rev.* **1990,** 100, 119.

(c) Furlan, R. L. E.; Otto, S.; Sanders, J. K. M., Supramolecular templating in thermodynamically controlled synthesis. *Proc. Nat. Acad. Sci. U.S.A.* **2002,** 99, 4801.

(d) Fyfe, M. C. T.; Stoddart, J. F., Synthetic Supramolecular Chemistry. *Acc. Chem. Res.* **1997,** 30, 393.

(e) Hoss, R.; Vögtle, F., Template Synthesis. *Angew. Chem., Int. Ed. Engl.* **1994,** 33, 375.

(f) Schalley, C. A.; Weilandt, T.; Brüggemann, J.; Vögtle, F., Hydrogen-Bond-Mediated Template Synthesis of Rotaxanes, Catenanes, and Knotanes. *Top. Curr. Chem.* **2004,** 248, 141.

(g) Stoddart, J. F.; Tseng, H.-R., Chemical synthesis gets a fillip from molecular recognition and self-assembly processes. *Proc. Nat. Acad. Sci. U.S.A.* **2002,** 99, 4797.

11. Lehn, J.-M., *Supramolecular Chemistry*. VCH Weinheim: 1995.

12. (a) Grubbs, R. H., Olefin Metathesis. *Tetrahedron* **2004,** 60, 7117.

(b) Ivin, K. J., *Olefin Metathesis*. Academic Press: London, 1996.

(c) Trnka, T. M.; Grubbs, R. H., The Olefin Metathesis Story. *Acc. Chem. Res.* **2001,** 34, 18.

13. Gerven, P. C. M. v.; Elemans, J. A. A. W.; Gerritsen, J. W.; Speller, S.; Nolte, R. J. M.; Rowan, A. E., Dynamic combinatorial olefin metathesis: templated synthesis of porphyrin boxes. *Chem. Commun.* **2005**, 3535.

14. (a) Chase, P. A.; Lutz, M.; Spek, A. L.; Klink, G. v.; Koten, G. v., Ring closing methathesis employing organometallic substrates and the templated synthesis of macrocyles. *J. Mol. Catal. A: Chem.* **2006,** 254, 2.

(b) Mohr, B. Weck, M.; Sauvage, J.-P.; Grubbs, R. H.; Weck, M., High-Yield Synthesis of [2] Catenanes by Intramolecular Ring-Closing Metathesis. *Angew. Chem. Int. Ed.* **1997,** 36, 1308.

(c) Weck, M.; Mohr, B.; Sauvage, J.-P.; Grubbs, R. H., Synthesis of Catenane Structures via Ring-Closing Metathesis. *J. Org. Chem.* **1999,** 64, 5463.

15. Vyotsky, M. O.; Bogdan, A.; Wang, L.; Böhmer, V., Template synthesis of multi-macrocyles by metathesis reaction. *Chem. Commun.* **2004**, 1268.

16. Yang, X.; Gong, B., Template-Assisted Cross Olefin Metathesis. *Angew. Chem. Int. Ed.* **2005,** 44, 1352.

17. Constable, E.; Housecroft, C. E.; Lambert, J. N.; Malarek, D. A., Supramolecular self-assembly on a solid support: metal-directed complementarity. *Chem. Commun.* **2005**, 3739.

18. (a) Cantrill, S. J.; Grubbs, R. H.; Lanari, D.; Leung, K. C.-F.; Nelson, A.; Poulin-Kerstien, K. G.; Smidt, S. P.; Stoddart, J. F.; Tirrell, D. A., Template-Directed Olefin Cross-Metathesis. *Org. Lett.* **2005,** 7, 4213.

(b) Hou, Hongyi, Leung, K. C.-F.; Lanari, D.; Nelson, A.; Stoddart, J. F.; Grubbs, R. H., Template-Directed One-Step Synthesis of Cyclic Trimers by ADMET. *J. Am. Chem. Soc.* **2006**, 128, 15358.

19. (a) Badjic´, J. D.; Balzani, V.; Credi, A.; Lowe, J. N.; Silvi, S.; Stoddart, J. F., A mechanically interlocked bundle. *Chem. Eur. J.* **2004,** 10, 1926.

(b) Badjic´, J. D.; Balzani, V.; Credi, A.; Silvi, S.; Stoddart, J. F., A Molecular Elevator. *Science* **2004,** 303, 1845.

(c) Badjic´, J. D.; Cantrill, S. J.; Grubbs, R. H.; Guidry, E. N.; Orenes, R., The Exclusivity of multivalency in dynamic covalent processes. *Angew. Chem. Int. Ed.* **2004,** 43, 3273.

(d) Badjic´, J. D.; Cantrill, S. J.; Stoddart, J. F., Can Multivalency Be Expressed Kinetically? The Answer is Yes. *J. Am. Chem. Soc.* **2004,** 126, 2288.

20. Kilbinger, A. F. M.; Cantrill, S. J.; Waltman, A. W.; Day, M. W.; Grubbs, R. H. ,Magic Ring Rotaxanes via Olefin Metathesis. *Angew. Chem. Int. Ed.* **2003,** 42, 3281.

21. Guidry, E. N.; Cantrill, S. J.; Stoddart, J. F.; Grubbs, R. H., Magic Ring Catenation by Olefin Metathesis. *Org. Lett.* **2005,** 7, 2129.

22. For discussions of dynamic covalent chemistry, see: (a) Aricó, F.; Chang, T.; Cantrill, S. J.; Khan, S. I.; Stoddart, J. F., Template-Directed Synthesis of Multiply Mechanically Interlocked Molecules Under Thermodynamic Control. *Chem. Eur. J.* **2005,** 11, 4655.

(b) Chichak, K. S.; Cantrill, S. J.; Pease, A. R.; Chiu, S.-H.; Cave, G. W. V.; Atwood, J. L.; Stoddart, J. F., Molecular Borromean Rings. *Science* **2004,** 304, 1308.

(c) Fuchs, B.; Nelson, A.; Star, A.; Stoddart, J. F.; Vidal, S. B., Amplification of dynamic chiral crown ether complexes during cyclic acetal formation. *Angew. Chem. Int. Ed.* **2003**, 42, 4220.

(d) Lehn, J.-M., Dynamic combinatorial chemistry and virtual combinatorial libraries. *Chem. Eur. J.* **1999,** 5, 2455.

(e) Rowan, S. J.; Cantrill, S. J.; Cousins, G. R. L.; Sanders, J. K. M.; Stoddart, J. F., Dynamic Covalent Chemistry. *Angew. Chem. Int. Ed.* **2002,** 41, 898.

(f) Corbett P. T.; Leclaire, J.; Vial, L.; Wietor, J.-L.; Sanders, J. K. M.; Otto, S., Dynamic combinatorial chemistry. *Chem. Rev.* **2006**, *106*, 3652.

23. (a) Yang, H.-C.; Lin, S.-M.; Liu, Y.-H.; Wang, Y.; Chen, M.-M.; Sheu, H.-S.; Tsou, D.-L.; Lin, C.-H.; Luh, T.-Y. , Ring opening metathesis polymerization of bisnorbornene derivatives linked by $Cp_2Ni_2(\mu\text{-}S)_2$ bridge. *J. Organomet. Chem.* **2006,** 691, 3196.

(b) Yang, H.-C.; Lin, S.-Y.; Yang, H.-C.; Lin, C.-L.; Tsai, L.; Huang, S.-L.; Chen, I. W.-P.; Chen, C.-h.; Jin, B.-Y.; Luh, T.-Y., ROMP of Bis-norbornene Derivatives. *Angew. Chem. Int. Ed.* **2006,** 45, 726.

24. (a) Burd, C.; Weck, M., Self-Sorting in Polymers. *Macromolecules* **2005,** 38, 7225.

(b) Gerhardt, W.; Crne, M.; Weck, M., Multifunctionalization of Synthetic Polymer Systems via Self-Assembly. *Chem. Eur. J.* **2004,** 10, 6212.

(c) Nair, K. P.; Pollino, J. M.; Weck, M., Non-Covalently Functionalized Block Copolymers Possessing Both, Hydrogen-Bonding and Metal-Coordination Centers *Macromolecules* **2006,** 39, 931.

(d) Pollino, J. M.; Stubbs, L. P.; Weck, M., One-Step Multi-Functionalization of Random Copolymers via Self-Assembly. *J. Am. Chem. Soc.* **2004,** 126, 563.

(e) Pollino, J. M.; Weck, M., Non-Covalent Side-Chain Polymers: Design Principles, Functionalization Strategies, and Perspectives *Chem. Soc. Rev.* **2005,** 34, 193.

(f) South, C. R.; Higley, M. N.; Leung, K. C.-F.; Lanari, D.; Nelson, A.; Grubbs, R. H.; Stoddart, J. F.; Weck, M., Self-Assembly With Block Copolymers Using SCS Pd(II) Pincer Metal Coordination and Pseudorotaxane Formation *Chem. Eur. J.* **2006,** 12, 3789.

(g) South, C. R.; Leung, K. C.-F.; Lanari, D.; Stoddart, J. F.; Weck, M., Noncovalent Side-Chain Functionalization of Terpolymers. *Macromolecules* **2006,** 39, 3738.

(h) South, C. R.; Burd, C.; Weck, M., Modular and Dynamic Functionalization of Polymeric Scaffolds. *Acc. Chem. Res.* **2007**, *40*, 63.

25. Pontrello, J. K.; Allen, M. J.; Underbakke, E. S.; Kiessling, L. L., Solid-Phase Synthesis of Polymers Using the Ring-Opening Metathesis Polymerization. *J. Am. Chem. Soc.* **2005,** *127*, 14536.

26. Pollino, J. M.; Stubbs, L. P.; Weck, M., Living ROMP of Exo-Norbornene Esters Possessing Pd(II) SCS Pincer Complexes or Diaminopyridines *Macromolecules* **2003,** *36*, 2230.

27. Ferguson, J.; Al-Alawi, S.; Granmayeh, R., Template molecular weight effects on the polymerization of acrylic acid *Eur. Polym. J.* **1982,** 19, 475.

CHAPTER 7

Erasable Coordination Polymer Multilayers on Gold

7.1 Abstract

In this chapter, the use of reversible coordination chemistry to assemble polymer multilayers on gold surfaces is examined. Such multilayers have potential application ranging from drug delivery to electro-optics. Our system (i) provides for uniform film deposition and control of multilayer thickness, (ii) allows for the integration of diverse polymer components embedded in alternating polymer bilayers, and (iii) affords stable, yet responsive multilayers that can be manipulated by chemical means using competing supramolecular interactions.

7.2 Introduction

Current methods to assemble multilayers on surfaces rely predominantly on Layer-by-Layer (LbL) deposition of polycations and polyanions to produce polyelectrolyte multilayers (PEMs)[1,2] that are stabilized primarily through polyvalent electrostatic interactions.[3] While PEMs have been employed successfully as key material in biological applications such as drug delivery,[4] their performance in applications that demand either long-term use or added stability toward heat and other solution conditions such as changes in salt concentrations, or even mild pH changes is limited.[5] To overcome these shortcomings, several groups have explored the use of covalently bound multilayers[6] as a robust alternative to PEMs for use in OLEDs,[7] etch resistant materials,[8a] dielectrics,[8a] and as feature replicants.[8b] These covalently bound multilayers

offer additional stability toward heat, solvent changes, pH, and other solution conditions, but the responsiveness afforded by PEMs is sacrificed.

A significantly less studied area is the use of metal-ligand interactions to integrate components within polymer multilayer thin films with the goal of enhancing stability and adding functionality.[9] Metal-ligand assisted lateral film growth has been achieved through Ru-pyridine complexation,[10a] while Fe-bipyridine complexes have been laterally integrated between poly(styrene sulfonate) and poly(ethylene imine) multilayers.[10b] Polyelectrolyte assembly has also been assisted by intermittent integration of metal cations, namely Cu^{2+}, allowing for the reductive formation of polymer / Cu nanocomposites.[11] Similarly, poly(oxometalate) nanoclusters have been integrated between poly(cations) within multilayered thin films.[12] Additionally, the use of polymer multilayers with embedded metal complexes have been explored in a variety of applications, including sensors that detect chemical toxicity[13a] and damaged DNA.[13b-c] Much like covalent multilayers, metal-coordination multilayers tend to increase multilayer stability while sacrificing responsiveness. A methodology that allows for the formation of metal-coordination multilayers that are stable with fully reversible formation has not been demonstrated.

7.3 Results and Discussion

Our system described herein combines the advantages offered by covalent multilayers, metal-bound multilayers, and PEMs by using strong, yet reversible noncovalent[14] metal-ligand interactions to create a new class of coordination polymer multilayers (CoPMs). It is based on the coordination of weak bases to palladium

complexes as the key noncovalent interaction to create stable, yet responsive CoPMs. We utilize Pd(II) pincer-type complexes[15] because of their strength (K_a > 109 M^{-1} in nonpolar solvents)[16] and inertness[14c] toward a variety of functionalities, including polar, nonpolar, charged, and even acidic groups. Furthermore, Pd(II) pincer complexes are tolerant toward many reaction conditions, including organometallic reactions,[17] yet responsive toward stronger coordinating ligands. In our study, the Pd(II) pincer complexes are supported on poly(norbornene)s, **PNBE+** (M_w = 30,000), creating a polymer with a metal complex on each repeating unit. The acetonitrile coordinated to the Pd(II) pincer complexes along the **PNBE+** can be displaced quantitatively by pyridine (Scheme 7.1).[18] Therefore, we employed commercially available poly(vinyl pyridine) (M_w = 20,000), **PVP**, as the complementary macroligand.

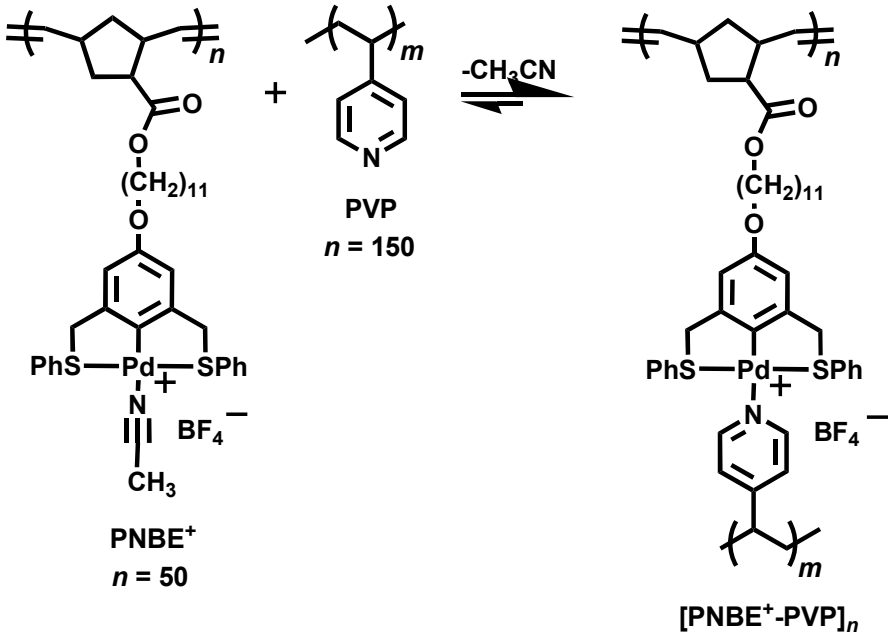

Scheme 7.1. Pincer-type coordination chemistry between **PNBE+** and poly(vinyl pyridine) **PVP** to yield **[PNBE+-PVP]**$_n$ coordination multilayers.

We began our study by functionalizing a gold surface with 4-mercaptopyridine. Upon exposure of the pyridyl functionalized surface to **PNBE+**, the acetonitrile ligands on the Pd(II) pincer complexes along the **PNBE+** are quantitatively and instantaneously displaced by surface pyridines forming a polyvalent layer upon which multilayers can be built. CoPM buildup then proceeded by simple alternation of **PVP** and **PNBE+** solution treatments (Scheme 7.2). Using this simple methodology, we were able to fabricate CoPMs based on coordination chemistry with up to 25 bilayers in less than three hours.

The multilayer buildup was initially monitored by UV-vis absorption spectroscopy. As multilayer buildup progressed, the absorption band attributable to the aromatic groups on both the **PNBE+** and the **PVP** (l_{max} = 254 nm) increased linearly with bilayer number (Figure 7.1A). Grazing angle FT-IR experiments additionally demonstrated peak intensity increases upon bilayer build-up (Figure 7.2). Additionally, XPS confirmed the presence of N, S, and Pd in our CoPMs.

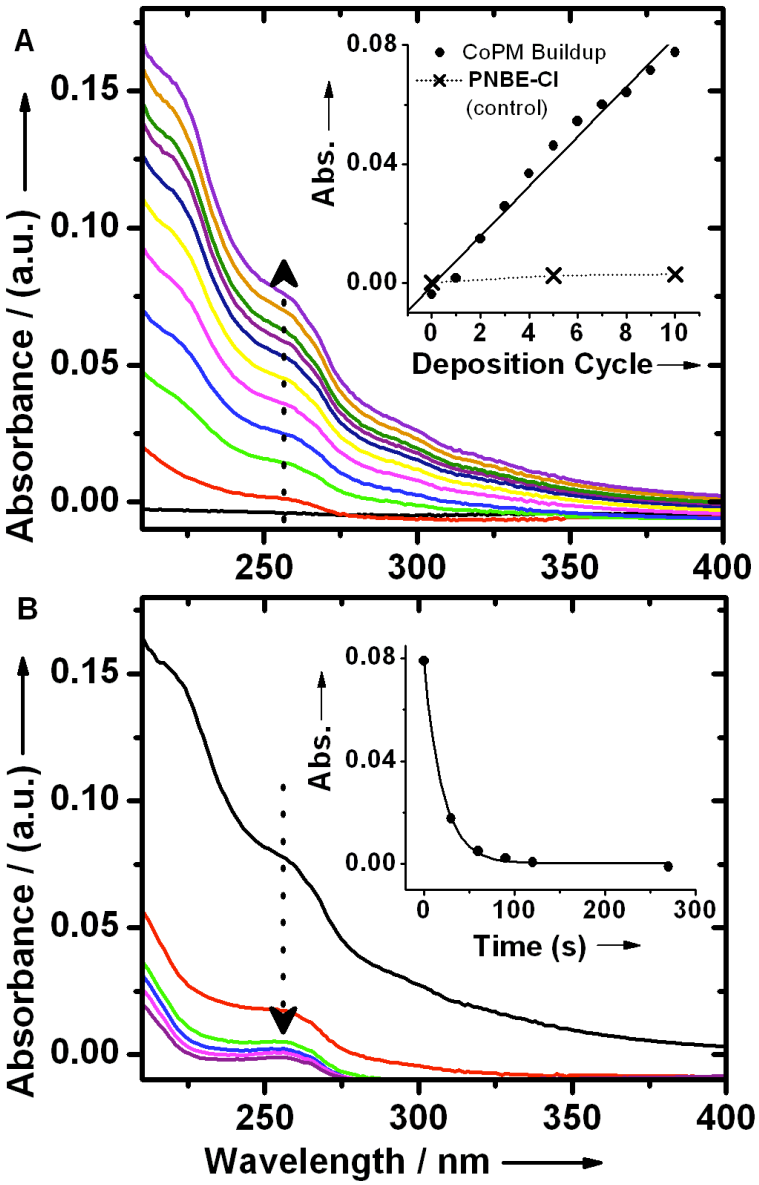

Figure 7.1. **(A)** UV-vis absorption spectra for CoPM buildup taken at every bilayer **(PNBE+-PVP)**$_n$ on a 20 nm Au layer deposited on quartz. The inset plot displays absorbance intensity at 254 nm vs. deposition cycle (R^2 = 0.98) and a corresponding control experiment to rule out non-specific adsorption in which a non-activated **PNBE-Cl** was used in place of **PNBE+** as the deposition polymer. (B) UV-vis absorption spectra for CoPM breakdown taken over time. The inset plot displays absorbance intensity at 254 nm vs. time.

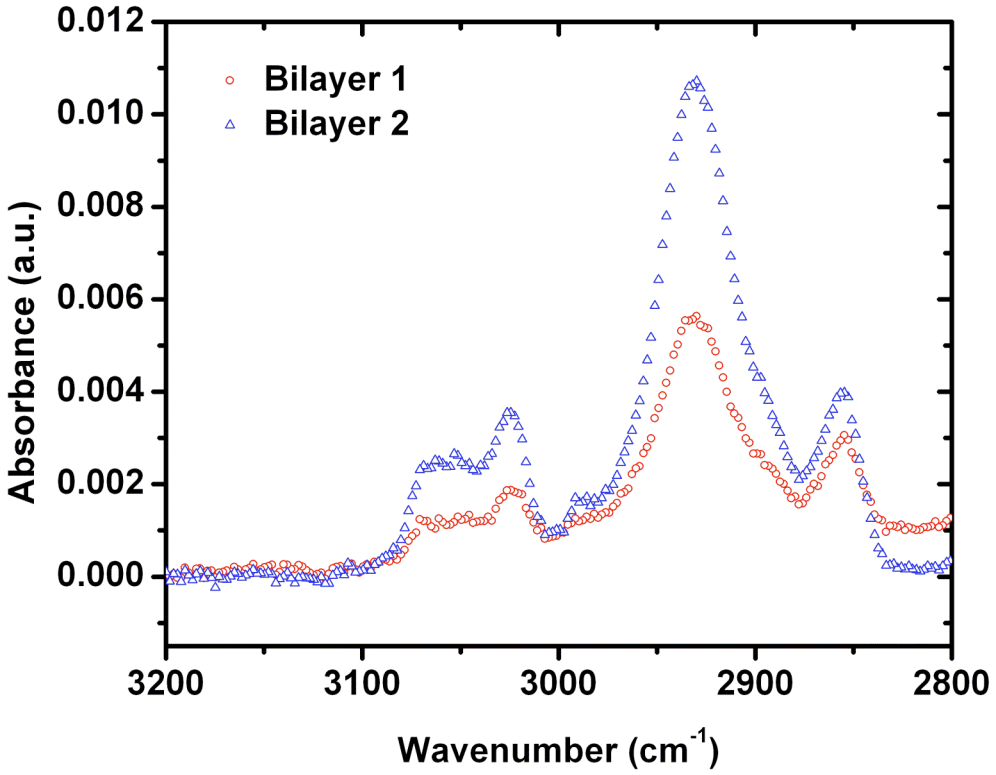

Figure 7.2. Partial RAS-FTIR spectra displaying absorbance intensity increases observed in the aliphatic C-H stretching region upon bilayer buildup.

Surface heights were measured using ellipsometry and AFM. Ellipsometry data indicate an average layer thickness of 28 nm and an average bilayer thickness of 58 nm. Linear trends between surface height and layer number were observed for both even and odd **(PNBE+-PVP)$_n$** layers (Figure 7.3A-B). Heights determined by ellipsometry for the eight and sixteen layer films were 199 (± 20) nm and 523 (± 50) nm, respectively. These values corresponded well with height values measured by AFM of 190 (± 10) nm and 451 (± 32) nm for the eight and sixteen layer films, respectively.

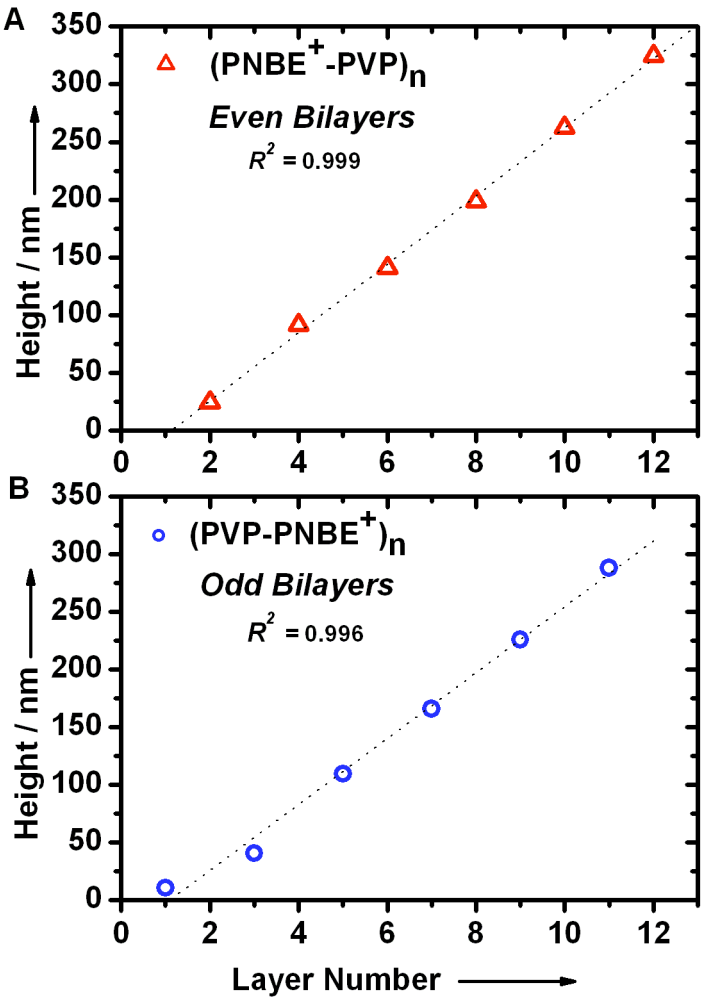

Figure 7.3. Plot of surface height determined by spectroscopic ellipsometry vs. even (A) and odd (B) bilayer number.

The observed heights for the multilayers are much thicker than expected. Molecularly thin PEMs can often be produced through LbL methods with layer thicknesses as small as a few nanometers.[19] Based on molecular mechanics energy minimized decamer models of **PNBE+** and **PVP**, we predict molecularly thin multilayers

to have bilayer thicknesses of about 7 nm, whereas the observed thicknesses correspond to about ten linear polymer molecules per bilayer. These models, however, are just rough predictions for perspective and do not take into account polymer folding and swelling. In reality, we believe that several factors contribute to the observed thicknesses.

First, while PEMs are often very thin due to counterion expulsion upon multilayer buildup resulting in greater multilayer packing through a process known as "intrinsic compensation," [21b] we would not expect the counterion on **PNBE+** to be expelled during the deposition process. The presence of the counterion within the multilayer contributes significantly to swelling, a phenomena known as "extrinsic compensation." [21b]

Second, the effect of electrostatic repulsion and charge compensation upon multilayer buildup is often cited as one key reason why PEMs are so thin.[21b] Since our deposition is not purely electrostatic, we would not expect our polymers to spread out as flat as PEMs (this is also evident by our roughness measurements).

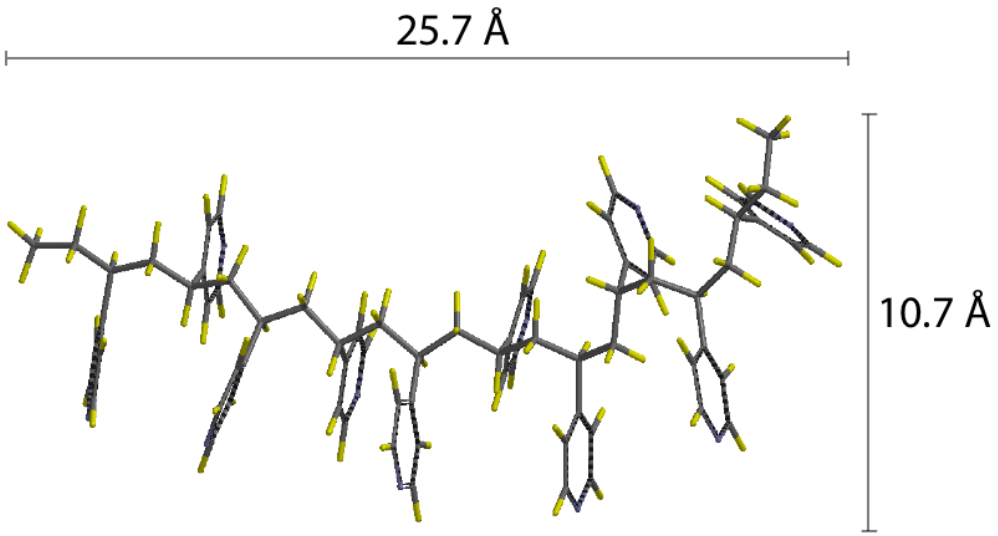

Figure 7.4. Molecular mechanics energy minimized simulation of PVP decamer using Spartan software.

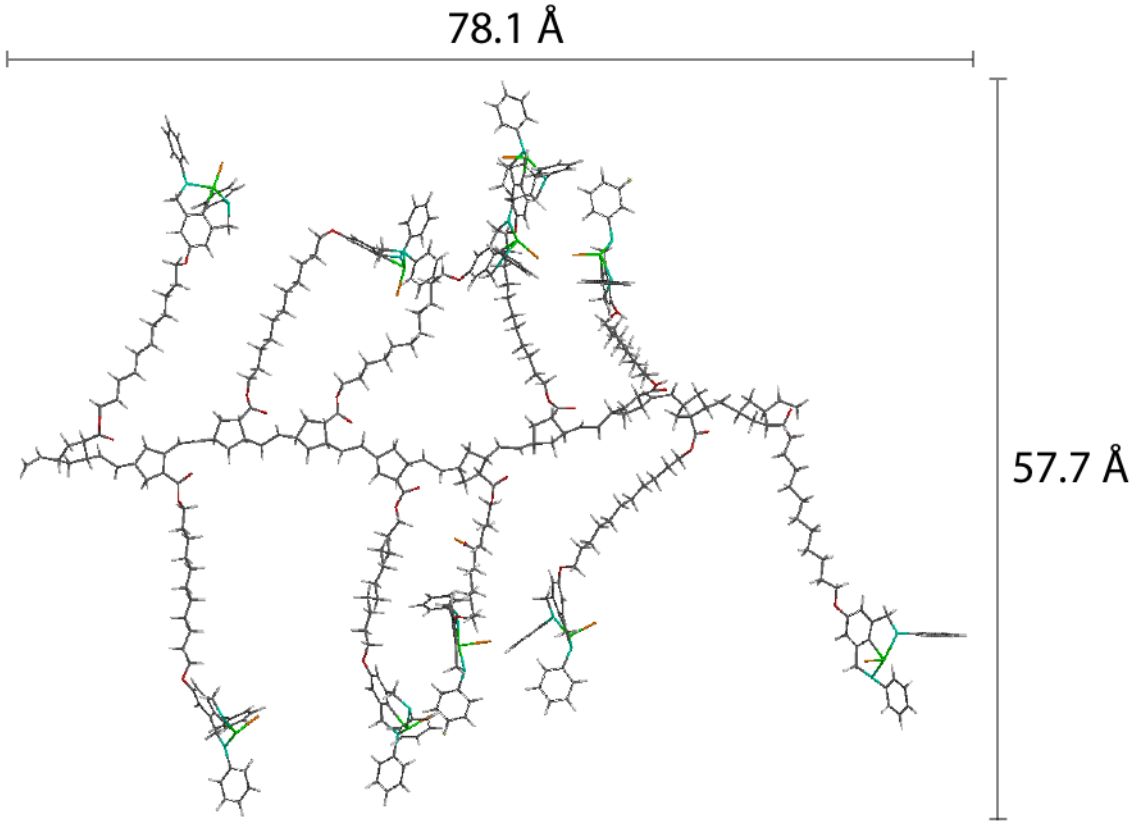

Figure 7.5. Molecular mechanics energy minimized simulation of $PNBE^{+}$-Cl decamer using Spartan software.

Third, we suspect that since our individual polymer recognition units have such a high association constant, entangled polymers are getting "dragged" to the surface. This should largely be an effect due to the deposition concentration. To test this hypothesis, we deposited an eight layer film at 5 mM concentrations, rather than 10 mM, since we reasoned that a lower concentration would reduce polymer entanglement in solution. The height of this film was measured by AFM to be 115 nm + 17 nm, a height about half as thick as the eight layer film deposited at 10 mM. While we suspect polymer entanglement to be the main source of this effect,[20] other concentration and kinetic effects might also be

contributing to the observed results. However, we are pleased that these results indicate that we might be able to modulate film thicknesses in a controlled manner by merely varying the deposition concentration (Figure 7.4).

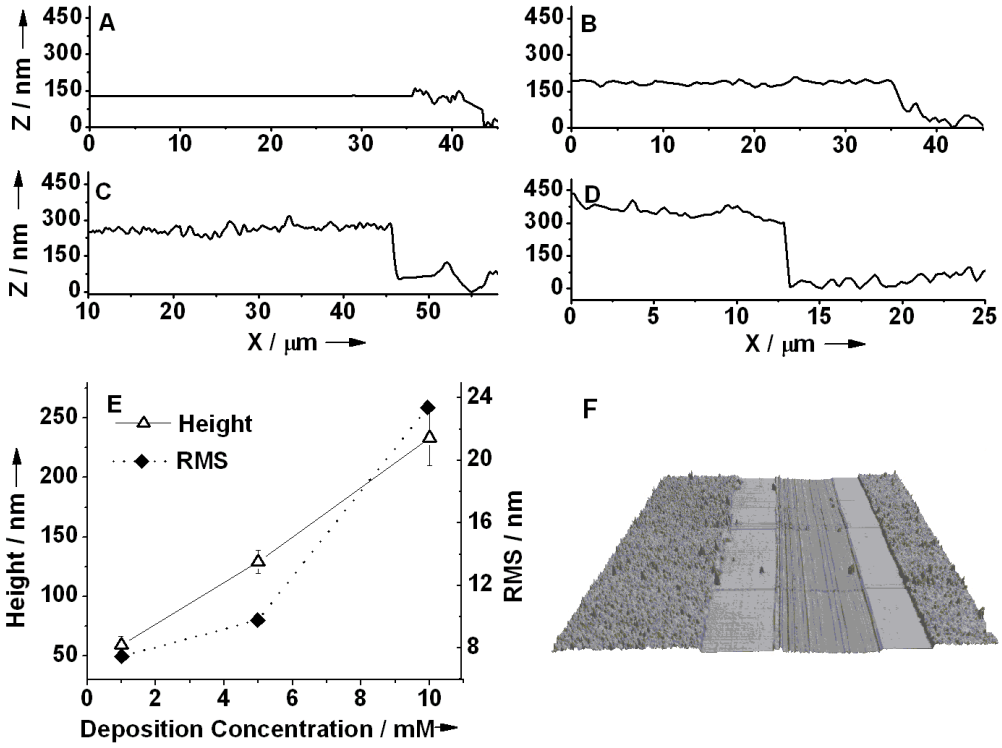

Figure 7.6. A-D) section line height profiles of scratched CoPMs (16 layers) on (A) gold plated slides for multilayers deposited at (B) 1 mM, (C) 5 mM, and (D) 10 mM; E) corresponding surface heights and RMS roughness measurements for the films deposited at 1 mM, 5 mM, and 10 mM. F) Example AFM image taken in air of a scratched 16 layer CoPM (x = y = 90 μm; z = 4 μm); rougher area is polymer; smooth areas are scratch edges defining center of scratch (deeper portion).

Nonspecific adsorption between the polymer and the surface was ruled out on the basis of a control experiment in which we employed non-activated PNBE instead of

PNBE+ where a Cl- ligand was in place of the more labile acetonitrile ligand. Deposition experiments analogous to the one described previously were carried out. After fifteen deposition cycles, no absorbance was observed demonstrating that no polymer was adsorbed to the gold surface. The stability of the multilayers to solvent changes, temperature in solution and the solid state as well as salts was examined. First, we exposed them to EtOH, THF, and DMF for short rinsing periods. In all cases, the absorbance intensity of the multilayer remained constant.

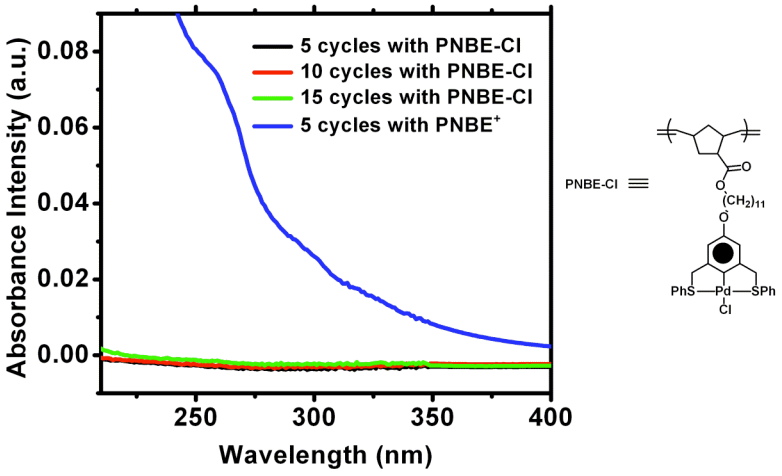

Figure 7.7. Control UV-vis absorption spectra: alternate deposition cycles were performed with **PVP** and **PNBE-Cl.** No absorption was observed after fifteen deposition cycles. For reference, a spectra (blue line) corresponding to a 10-bilayer film (after 5 deposition cycles) is included.

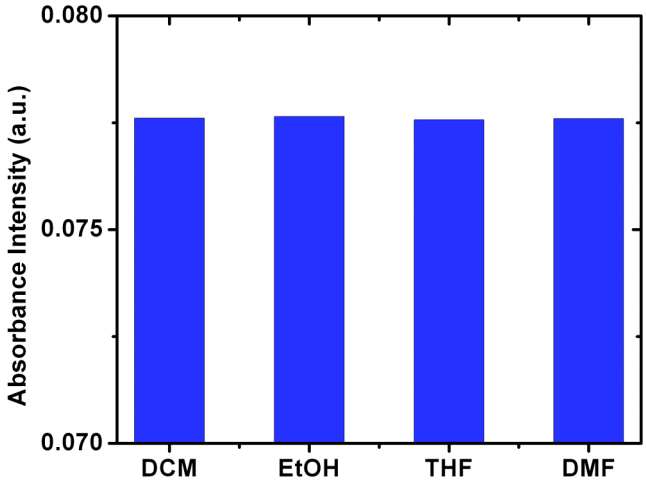

Figure 7.8. Plot of absorbance intensity after short rinsing periods with DCM, EtOH, THF, and DMF. No changes in absorption were observed.

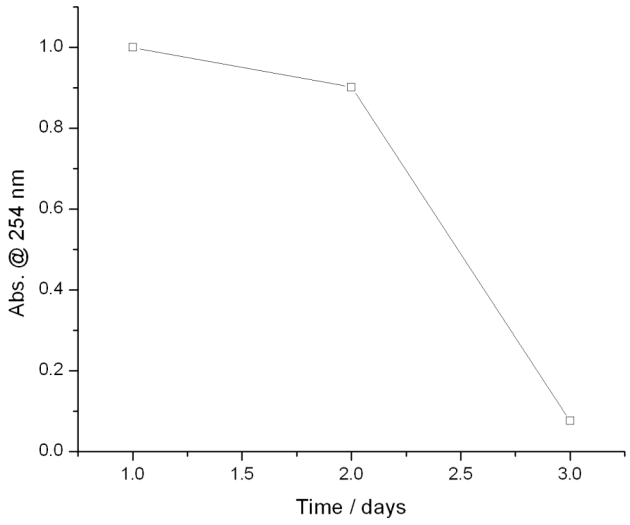

Figure 7.9. Plot of Absorbance intensity vs. time for Soxhlet DMF etch extraction experiment.

To further test the stability of our CoPMs toward solvent etching, we placed an eight layer CoPM in a DMF Soxhlet extractor and monitored the etching progress over time. The CoPM was completely etched in three days. We attribute the degradation to both solubility of the multilayers in DMF as well as decomposition of the metal complex at 153 °C in solution. It is important to note, however, that these CoPMs are far more stable than most PEMs towards polar solvents. Some of the most commonly used and stable PEMs based on poly(allylamine hydrochloride) (PAH) and poly(acrylic acid) or poly(styrene sulfonate) (PSS) are etched almost completely after 1 hr of DMF exposure at room temperature.[21] This problem is often circumvented by cross-linking the multilayers;[21] however, upon cross-linking, responsiveness if largely sacrificed.

Additionally, no significant etching was observed after oven heating the surfaces to 140 °C for two weeks and subsequently washing with $CHCl_3$ before analysis using UV-vis spectroscopy. The observed thermal stability is orders of magnitude greater than most PEMs, such as PAH-PSS or PAH-PAA, which typically either degrade or undergo crosslinking at these temperatures over short time periods.[21] To test the stability of our CoPM functionalized surfaces toward salt exchange, we placed the functionalized gold surfaces in a $CHCl_3$ solution of AgOTf, and no etching was observed by UV-vis spectroscopy. However, if the CoPMs are exposed to excess NaCl, the metal complexation is reversed, and the formation of **PNBE-Cl** most likely results effectively etching the multilayers. We believe this to be a positive finding, since a similar responsiveness to NaCl has recently been used to spatially pattern PEMs through controlled etching in a "top-down" approach.[22] We intend to investigate the possibility of controlled etching of our multilayers to produce patterned surfaces using NaCl solutions.

We subsequently tested the ability to etch our CoPMs chemoresponsively using competing ligands. Upon exposure of a multilayer to a 10 mM solution of PPh_3, a stronger base and a tighter coordinating ligand for the Pd(II) complexes along the **PNBE+**, the absorbance intensity decreased dramatically within a few minutes (Figure 7.1B) demonstrating the removal of our multilayers and their responsiveness to chemical stimuli and suggesting a possible trigger mechanism for surface applications, such as "top-down" patterning.[22]

7.4 Conclusion

In summary, we have demonstrated that coordination chemistry between palladium complexes and bases can be used to assemble CoPMs. The CoPMs produced in this fashion rival the stability of covalent multilayers, while retaining the responsiveness of PEMs. These appealing characteristics of our system makes CoPMs desirable for a variety of applications, specifically, as key materials in optical devices, delivery systems, catalytic systems, and templated[23] synthesis.

7.5 Experimental

7.5.1 Materials and General Methods

NMR and GPC. Nuclear magnetic resonance (NMR) spectra were recorded using a 500 MHz Bruker DRX spectrometer (^{1}H NMR: 500 MHz, ^{13}C NMR: 125 MHz) or a 300 MHz Varian Vx 300 spectrometer (^{1}H NMR: 300 MHz, ^{13}C NMR: 75 MHz). Spectra were referenced to residual proton resonances of the deuterated solvent.

Chemical shifts are reported as parts per million (ppm) downfield from the signal origination of Me_4Si as an internal standard for ^1H and ^{13}C NMR spectroscopy. Gel-permeation chromatography (GPC) analyses were carried out using a Shimadzu pump, a Shimadzu UV detector with THF or DMF as the eluants and a set of American Polymer Standards columns (100,1000,100,000 Å linear mixed bed). The flow rate used for all the measurements was 1 mL/min. All GPC measurements were calibrated using poly(styrene) standards and were carried out at room temperature. M_w, M_n and PDI represent weight average molecular weight, number average molecular weight and the polydispersity index, respectively.

Gold slide preparation. For UV-vis studies, we placed quartz slides (20 mm x 20 mm, ChemGlass) into a plasma cleaner for 20 min. Using Teflon coated tweezers, we removed the slides and placed them in a solution (2% by volume) of 3-mercaptopropyltrimethylsilane (MPTMS, Aldrich) in EtOH. After removal from this solution, we rinsed the slides with EtOH and dried the slides under a stream of N_2. We then vacuum deposited gold (gold shot, 99.999% pure, Alfa Aesar) at a rate of 0.10 nm/s until a desired thickness of 20 nm was reached. After removal from the gold evaporator, the slides were placed directly into the desired thiol solution or EtOH. For AFM, ellipsometry, and RAS-FTIR, we purchased gold slides (1 in. x 1 in.) from Evaporated Metal Films (EMF) and cleaned them using a DMF sonication and EtOH rinse prior to use. The purchased slides consisted of 100 nm of gold deposited onto 5 nm of Titanium deposited onto float glass.

Ellipsometry. Ellipsometry measurements were carried out using a J.A. Woollam Co. Inc. Spectroscopic Ellipsometry (M2000 VI). Spectra were collected at a 75° incidence angle from 372nm – 1000 nm using a Cauchy dispersion method to model the film. Errors for height measurements obtained by ellipsometry were less than 10% in all cases.

Grazing Angle FT-IR. FT-IR data were collected at 4 cm^{-1} resolution using a Digilab FT-IR equipped with an LN_2 cooled MCT detector. The measurements were taken using a Pike grazing angle apparatus. The chamber was purged with UHP N_2. A desiccant was used in the chamber to further minimize moisture.

XPS. We carried out XPS characterization on a Phi model SCA 1600 XPS with an Al K_a (1486.7eV) electron source. We probed an 800 micron spot size at a depth of 10 nm. We kept the chamber pressure at 3 x 10^{-9} Torr. We conducted alignment using a C1s peak. We analyzed our spectra were analyzed using Multipak 8.2.

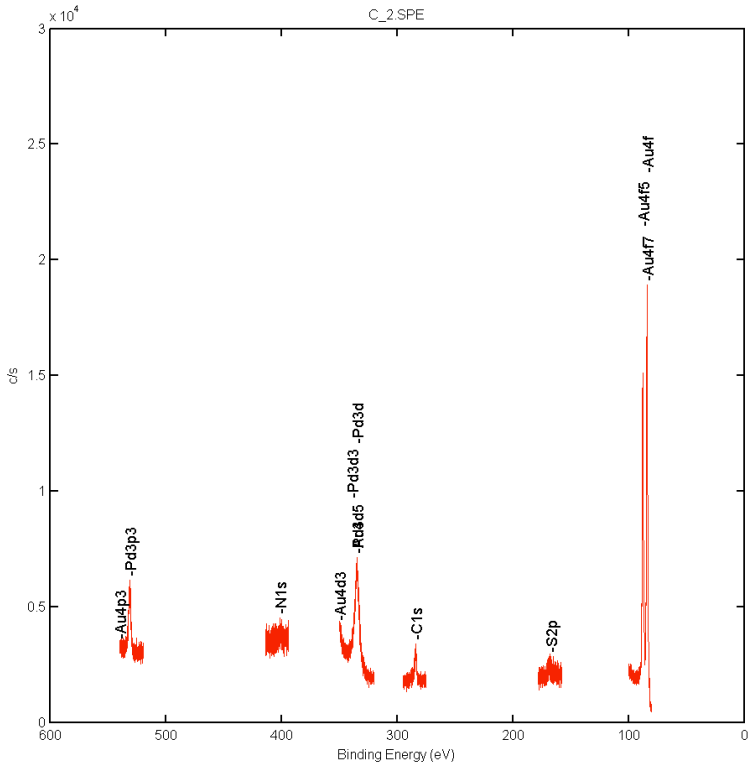

Figure 7.10. XPS Spectra for a five-bilayer CoPM.

AFM. AFM data were taken in air in AC mode on an Asylum Research MFP3D instrument. We processed all AFM images and analyzed surface heights using Asylum Research MFP3D software operating in IgorPro (WaveMetrics, Inc., Lake Oswego, OR). An Olympus cantilever (k = 42 N/m, f_0 = 377 kHz) was employed for imaging substrates, prelayers substrates, and multilayer films. The same cantilever was used for surface thickness determination. Images for surface analysis were taken over a 10 mm x 10mm scan range (512 x 512 pixels for each image). For absolute surface height measurements using AFM, we first scratched a blank gold slide with a razor blade and scanned (512 x 512 pixels for each image) this area on the gold slide (90 mm x 90 mm or 50 mm x 50 mm) so as to include enough area around. CoPM films were scratched and imaged in the same manner. To determine surface height, the AFM software was used to process the

image and perform an averaged line analysis over 100 lines for each image. A point along the averaged line corresponding to the top of the surface was selected, and from this height value was subtracted a value corresponding to a point at the bottom of the surface (step-etch from scratch). The thickness of the blank gold slide (125 nm) was subtracted from the height value determined for the multilayer films. Errors in these values were calculated from standard deviations in the averaged line height analyses.

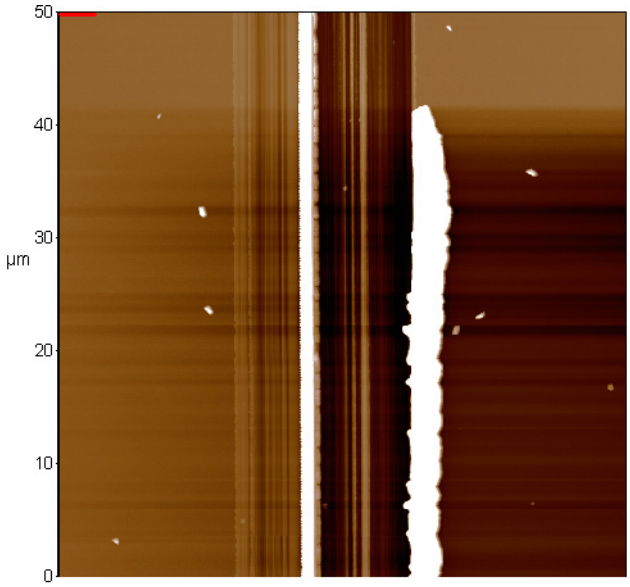

Figure 7.11. AFM image (90 mm x 90 mm) of a blank gold slide displaying a scratch used to calculate base thickness for subsequent CoPM thickness determinations.

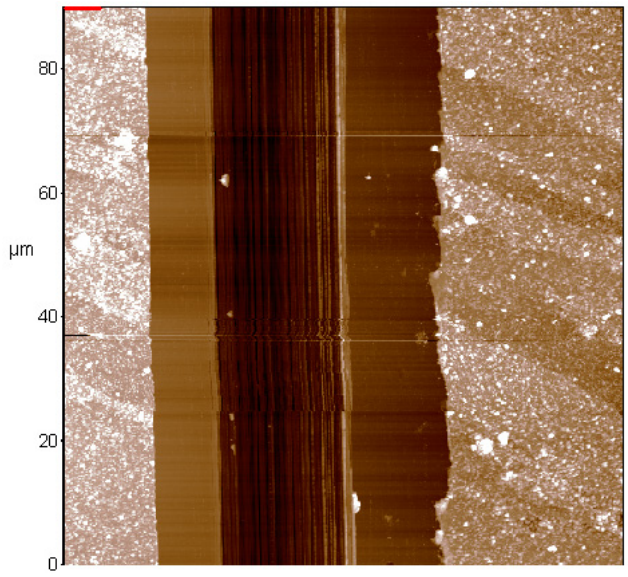

Figure 7.12. AFM image (90 mm x 90 mm) of **(PNBE$^+$-PVP)$_4$** and a scratch on a gold surface used to calculate thickness for the four bilayer CoPM.

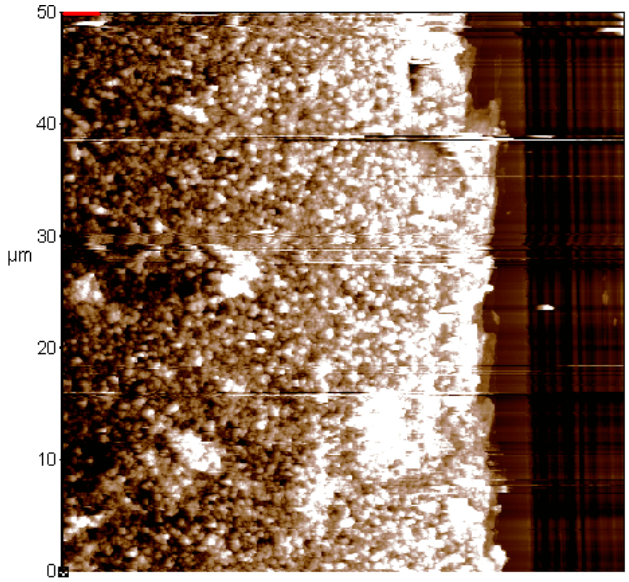

Figure 7.13. AFM image (50 mm x 50 mm) of **(PNBE$^+$-PVP)$_8$** and a scratch on a gold surface used to calculate thickness for the eight bilayer CoPM.

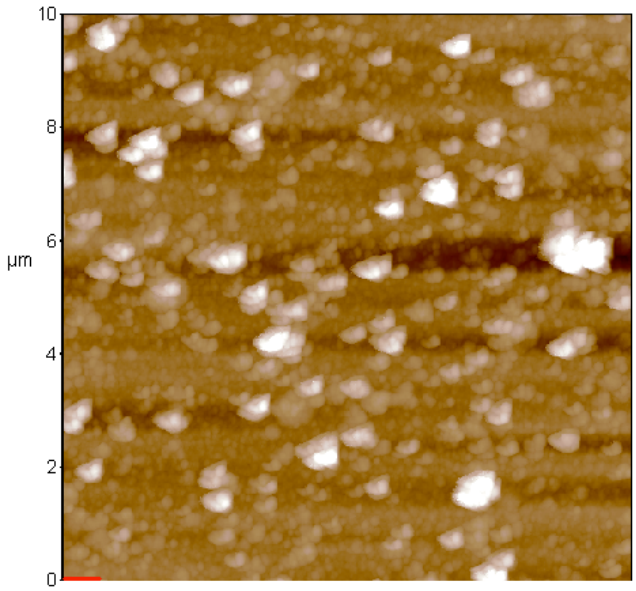

Figure 7.14. AFM image (10 mm x 10 mm) of **(PNBE$^+$-PVP)$_4$** on a gold surface used for the surface analysis.

UV-Vis spectroscopy. Solution and solid-state UV-vis absorption spectra were acquired using a Varian Cary 5A spectrometer. Solution-based absorption spectra were referenced to a blank containing the same solvent as the sample. Solid-state absorption spectra were referenced to a blank gold slide. For all solid-state measurements, transparent gold slides consisting of 18-20 nm of gold deposited on quartz were used.

7.5.2 Synthesis

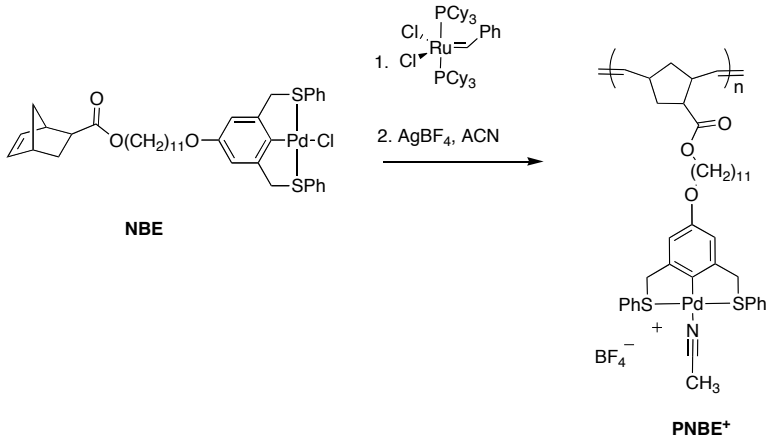

Scheme 7.2. Synthesis of **PNBE$^+$**

PNBE$^+$. We dissolved the **NBE** monomer (50 mg, 0.065 mmol) in dried (Na, benzophenone), degassed CH_2Cl_2 (1 mL). Then Grubbs 1st generation catalyst (1 mg dissolved in 0.1 mL of CH_2Cl_2) was added under Argon, and the resulting mixture was stirred for 30 min. We quenched the polymerization with the addition of ethyl vinyl ether and precipitated the resulting polymer out of CH_2Cl_2 using cold MeOH to give a yellow solid (48 mg, 96% yield). Characterization data are consisted with previous reports.[1] We dissolved the resulting polymer in acetonitrile and $AgBF_4$ (1 mg) was added. The solution was stirred in the dark for 15 min. The acetonitrile was removed under reduced pressure, the resulting residue dissolved in CH_2Cl_2, and the polymer precipitated out using cold MeOH to give a yellow solid (52 mg, 94%). ^{1}H NMR (500 MHz, CD_2Cl_2, d): 7.85 (m, 4H, SPh), 7.40, (m, 6H, SPh), 6.60 (s, 2H, OPh), 5.50-5.15 (m, 2H, -C*H*=C*H*-), 4.60 (br s, 4H, ArCH_2-), 4.05, (t, *J* not resolved, 2H, -OCH_2-), 3.85, (t, *J* not resolved, 2H, -OCH_2-), 3.13 (s, 1H, ring C*H*), 3.05 (s, 1H, ring C*H*), 2.80-2.40 (m, 2H), 2.15 (m, 2H), 1.80-1.53 (m, 4H), 1.50-1.25 (m, 15H). ^{13}C NMR (125 MHz, CD_2Cl_2, d): =174.4, 156.8, 151.3, 149.9, 132.3, 131.2, 129.6, 129.5, 108.7, 108.6, 67.9, 64.2, 51.5, 48.0, 45.4, 40.4, 39.7, 37.3, 36.0, 29.3, 29.2, 28.9, 28.6, 27.2, 26.0, 25.8. M_n = 28,500 M_w = 30,000 PDI = 1.05.

PYR Monolayer Formation and LbL deposition. The gold slides were placed into a 10 mM solution (in EtOH) of 4-mercaptopyridine for 24 hrs (Others have fully characterized PYR monolayers produced in this fashion[2]). We rinsed the resulting slides with EtOH, dried them under a stream of N_2 and placed the slides into a solution of **PBNE$^+$** (10 mM in CH_2Cl_2) for five min. Again, the resulting slides were rinsed

(CH_2Cl_2), dried under a stream of N_2, and placed into a solution of **PVP** (10 mM in CH_2Cl_2). This cycle was repeated until the desired layer number was reached.

7.6 References

1. Recent examples: (a) Krishnan, R. S.; Mackay, M. E.; Duxbury, P. M.; Pastor, A.; Hawker, C. J.; Horn, B. V.; Asokan, S.; Wong, M. S., Self-assembled multilayers of nanocomponents. *Nano Lett.* **2007**, *7*, 484.

   (b) Mertz, D.; Hemmerle, J.; Mutterer, J.; Ollivier, S.; Voegel, J.-C.; Schaaf, P.; Lavalle, P., Mechanically Responding Nanovalves Based on Polyelectrolyte Multilayers. *Nano Lett.* **2007**, *7*, 657.

   (c) Michel, M.; Arntz, Y.; Fleith, G.; Toquant, J.; Haikel, Y.; Voegel, J.-C.; Schaaf, P.; Ball, V., Layer-by-Layer Self-Assembled Polyelectrolyte Multilayers with Embedded Liposomes: Immobilized Submicronic Reactors for Mineralization. *Langmuir* **2006**, *22*, 2358.

   (d) Schneider, A.; Francius, G.; Obeid, R.; Schwinté, P.; Hemmerlé, J.; Frisch, B.; Schaaf, P.; Voegel, J.-C.; Senger, B.; Picart, C., Polyelectrolyte Multilayers with a Tunable Young's Modulus: Influence of Film Stiffness on Cell Adhesion. *Langmuir* **2006**, *22*, 1193.

2. Xia, Y.; Rogers, J. A.; Paul, K. E.; Whitesides, G. M., Unconventional Methods for Fabricating and Patterning Nanostructures. *Chem. Rev.* **1999**, *99*, 1823.

3. Decher, G., Fuzzy Nanoassemblies. *Science* **1997**, *277*, 1232.

4. Berg, M. C.; Zhai, L.; Cohen, R. E.; Rubner, M. F., Controlled Drug Release from Porous Polyelectrolyte Multilayers. *Biomacromolecules* **2006**, *7*, 357.

5. a) Cho, J.; Caruso, F., Polymeric Multilayer Films Comprising Deconstructible Hydrogen-Bonded Stacks Confined between Electrostatically Assembled Layers. *Macromolecules* **2003**, *36*, 2845.

   b) Sukhishvili, S. A.; Granick, S., Layered, Erasable Polymer Multilayers Formed by Hydrogen-Bonded Sequential Self-Assembly. *J. Am. Chem. Soc.* **2000**, *122*, 9550.

6. a) Major, J. S.; Blanchard, G. J., Strategies for Covalent Multilayer Growth. 2. Interlayer Linking Chemistry. *Chem. Mater.* **2002**, *14*, 2574.

   b) Such, G. K.; Quinn, J. F.; Quinn, A.; Tjipto, E.; Caruso, F., Assembly of Ultrathin Polymer Multilayer Films by Click Chemistry. *J. Am. Chem. Soc.* **2006**, *128*, 9318.

7. Kato, S.; Pac, C., Molecularly Thin Polymer Films That Function to Enhance Charge Injection Efficiency in Organic Light-Emitting Diodes *J. Phys. Chem. B* **2004**, *108*, 19932.

8. a) Huck, W. T. S.; Yan, L.; Stroock, A.; Haag, R.; Whitesides, G. M., Patterned Polymer Multilayers as Etch Resists. *Langmuir* **1999**, *15*, 6862.

b) Stroock, A. D.; Kane, R. S.; Weck, M.; Metallo, S. J.; Whitesides, G. M., Synthesis of Free-Standing Quasi-Two-Dimensional Polymers. *Langmuir* **2003**, *19*, 2466.

9. Molecular multilayers based on metal coordination have recently become a more widely investigated concept, for examples, see: a) Abe, M.; Michi, T.; Akira, S.; Kondo, T.; Zhou, W.; Ye, S.; Uosaki, K.; Sasaki, Y., Electrochemically Controlled Layer-by-Layer Deposition of Metal-Cluster Molecular Multilayers on Gold. *Angew. Chem. Int. Ed.* **2003**, *42*, 2912.

b) Kanaizuku, K.; Murato, M.; Nishimori, Y.; Mori, I.; Nishio, K.; Masuda, H.; Nishihara, H., Stepwise Preparation of Linear π-Conjugated Bis(terpyridine)metal Polymer Chains at Gold Surface. *Chem. Lett.* **2005**, *34*, 534.

c) Altman, M.; Shukla, A. D.; Zubkov, T.; Evmenenko, G.; Dutta, P.; van der Boom, M. E., Controlling Structure from the Bottom-Up: Structural and Optical Properties of Layer-by-Layer Assembled Palladium Coordination-Based Multilayers. *J. Am. Chem. Soc.* **2006**, *128*, 7374.

d) Wanunu, M.; Vaskevich, A.; Shanzer, A.; Rubinstein, I., Divergent Growth of Coordination Dendrimers on Surfaces. *J. Am. Chem. Soc.* **2006**, *128*, 8341-8349.

e) Kosbar, L.; Srinivasan, C.; Afzali, A.; Graham, T.; Copel, M.; Krusin-Elbaum, L., Self-Assembled Multilayers of Transition-Metal-Terpyridinyl Complexes; Formation, and Characterization. *Langmuir*, **2006**, *22*, 7631.

f) Nishimori, Y.; Kanaizuka, K.; Murato, M.; Nishihara, H., Synthesis of Molecular Wires of Linear and Branched Bis(terpyridine)-Complex Oligomers and Electrochemical Observation of Through-Bond Redox Conduction. *Chem. Asian J.* **2007**, *2*, 367.

10. a) Lin, C.; Kagan, C. R., Layer-By-Layer Growth of Metal-Metal Bonded Supramolecular Thin Films and Its Use in the Fabrication of Lateral Nanoscale Devices. *J. Am. Chem. Soc.* **2003**, *125*, 336.

b) Schütte, M.; Kurth, D. G.; Linford, M. R.; Cölfen, H.; Möhwald, H., Metallosupramolecular Thin Polyelectrolyte Films. *Angew. Chem.* **1998**, 110, 3058; *Angew. Chem. Int. Ed.* **1998**, *37*, 2891.

11. Xiong, H.; Cheng, M.; Zhou, Z.; Zhang, X.; Shen, J., A new approach to the fabrication of a self-organizing film of heterostructured polymer/Cu_2S nanoparticles. *Adv. Mater.* **1998**, *10*, 529.

12. Liu, S.; Kurth, D. G.; Bredenkötter, B.; Volkmer, D., he Structure of Self-Assembled Multilayers with Polyoxometalate Nanoclusters. *J. Am. Chem. Soc.* **2002**, *124*, 12279.

13. a) Wang, B.; Rusling, J. F., Voltammetric Sensor for Chemical Toxicity Using $[Ru(bpy)2poly(4\text{-}vinylpyridine)10Cl)]^+$ as Catalyst in Ultrathin Films. DNA Damage from Methylating Agents and an Enzyme-Generated Epoxide. *Anal. Chem.* **2003**, *75*, 4229.

b) Dennany, L.; Forster, R. J.; White, B.; Smyth, M.; Rusling, J. F., Direct Electrochemiluminescence Detection of Oxidized DNA in Ultrathin Films Containing $[Os(bpy)2(PVP)10]^{2+}$. *J. Am. Chem. Soc.* **2004**, *126*, 8835.

c) Mugweru, A.; Wang, B.; Rusling, J. F., Voltammetric Sensor for Oxidized DNA Using Ultrathin Films of Osmium and Ruthenium Metallopolymers. *Anal. Chem.* **2004**, *76*, 5557.

14. Selected examples: (a) Leung, K. C.-F.; Mendes, P. M.; Magonov, S. N.; Northrop, B. H.; Kim, S.; Patel, K.; Flood, A. H.; Tseng, H.-R.; Stoddart, J. F., Supramolecular Self-Assembly of Dendronized Polymers: Reversible Control of the Polymer Architectures through Acid-Base Reactions. *J. Am. Chem. Soc.* **2006**, *128*, 10707.

b) Pollino, J. M.; Weck, M., Non-covalent side-chain polymers: design principles, functionalization strategies, and perspectives. *Chem. Soc. Rev.* **2005**, *34*, 193.

c) South, C. R.; Burd, C.; Weck, M., Modular and Dynamic Functionalizatino of Polymer Scaffolds. *Acc. Chem. Res.* **2007**, *40*, 63.

d) Uzun, O.; Rotello, V. M., Recognition-Directed Orthogonal Self-Assembly of Polymers and Nanoparticles on Patterned Surfaces *J. Am. Chem. Soc.* **2006**, *128*, 3162.;

e) Dholakia, G.R.; Meyyappan, M.; Facchetti, A.; Marks, T.J., Monolayer to Multilayer Nanostructural Growth Transition in N-Type Oligothiophenes on Au(111) and Implications for Organic Field-Effect Transistor Performance. *Nano Lett.* **2006**, *6*, 2447.

15. Serpe, M. J.; Craig, S. L., Physical Organic Chemistry of Supramolecular Polymers. *Langmuir* **2007**, *23*, 1626.

16. South, C. R.; Higley, M. N.; Leung, K. C.-F.; Lanari, D.; Nelson, A.; Grubbs, R. H.; Stoddart, J. F., Self-Assembly With Block Copolymers Using SCS Pd(II) Pincer Metal Coordination and Pseudorotaxane Formation. *Chem. Eur. J.* **2006**, *12*, 3789.

17. Chase, P. A.; Lutz, M.; Spek, A. L.; Klink, G. P. M. v.; Koten, G., v., Ring closing metathesis employing organometallic substrates and the templated synthesis of macrocycles. *J. Mol. Catal. A: Chem.* **2006**, *254*, 2.

18. We have demonstrated that pyridines can displace nitriles, see: Gerhardt, W. W.; Zucchero, A. J.; Wilson, J. N.; South, C. R.; Bunz, U. H. F.; Weck, M., Supramolecular Cruciforms. *Chem. Commun.* **2006**, *20*, 2141. For the displacement of pyridines by phosphines in pincer-type complexes see ref. 11.

19. Park, Stella, Y.; Rubner, M. F.; Mayes, A. M., Free Energy Model for Layer-by-Layer Processing of Polyelectrolyte Multilayer Films. *Langmuir* **2002**, *18*, 9600 and references therein.

20. Entanglement effects have been implicated in PEM buildup, with control of the entanglement often mediate by ionic strength in solution, see ref. 21b.

21. a) Chen, J.; Huang, L.; Ying, L.; Lin, G.; Zhao, X.; Cao, W., Self-Assembly Ultrathin Films Based on Diazoresins. *Langmuir* **1999**, *15*, 7208.

b) *Multilayer Thin Films: sequential assembly of nanocomposite materials*, Eds. Decher, G.; Schlenoff, J. B.; Wiley-VCH, Weinheim **2003**.

c) Dai, X.; Zhang, Y.; Guan, Y.; Yang, S.; Xu, J., Mechanical properties of polyelectrolyte multilayer self-assembled films. *Thin Solid Films*, **2005**, *474*, 159.

22. Nolte, A.; Takane, N.; Hindman, E.; Gaynor, W.; Rubner, M.; Cohen, R. E., Thin Film Thickness Gradients and Spatial Patterning via Salt Etching of Polyelectrolyte Multilayers. *Macromolecules* **2007**, *40*, 5479.

23. Nanowires have recently been produced from a surfacial templated synthetic approach, see: Kovtyukhova, N.I.; Kelley, B.K.; Mallouk, T.E., Coaxially Gated In-Wire Thin-Film Transistors Made by Template Assembly. *J. Am. Chem. Soc.* **2004**, *126*, 12738.

CHAPTER 8

Bridged Coordination Polymer Multilayers with Tunable Properties

8.1 Abstract

Coordination multilayers consisting of Pd(II) pincer type complexes and poly(vinyl pyridine) were synthesized and characterized. Layer-by-layer Polymer deposition was carried out on a pyridyl functionalized quartz slide. Film properties were found to be dependent on, and could be tuned by varying, bath deposition concentrations, polymer molecular weights, and solution additives that compete with binding. Generally, smoother, thinner films were obtained with lower poly(vinyl pyridine) deposition bath concentrations. Likewise, film thickness and roughness could be reduced by employing a higher molecular weight poly(vinyl pyridine). Film properties were influenced by using acetonitrile as a solution additive, which effectively drives the binding equilibrium toward the free species.

8.2 Introduction

In the previous Chapter, an alternative[2,3] to traditional poly(electrolyte) multilayer (PEMs)[1] thin films was presented. While the previous work outlined a new method to produce thin films without the use of poly(electrolytes), other approaches to assemble thin films onto surfaces exist and include hydrogen bonding,[4-10] covalent chemistry,[2] halogen bonding,[11] and metal ion coordination,[18-27] to name a few. Of particular interest to us is the use of metal coordination, however, given that coordination polymer

multilayers (CoPMs) can be responsive to environmental stimuli, much like PEMs, while still being as robust as films formed through covalent bonding.[2]

The potential uses of metal coordination multilayers are arguably as widespread as uses envisioned and practiced with PEMs,[1] a few of which were briefly introduce in Chapter 7. Examples of already existing technologies include the use of polymer multilayers with embedded metal complexes in biological applications.[12-14] Likewise, CoPMs have potential uses in electrical and photoelectrical devices.[15] Moreover, a diverse range of functional components can be easily integrated into CoPMs to impart a desired property to the film.[16,17] For example, a light responsive azobenzene dye was periodically incorporated into a polyelectrolyte component, and ZrO_2 was used to cement the polymer layers.[18] We and others are also attracted to methods utilizing reversible coordination chemistry to assemble erasable multilayers[10,19] on surfaces, particularly since these approaches can yield thin films that are subject to top down lithography using a stimulus other than light.

Current strategies employing coordination chemistry to build polymer multilayers on surfaces typically rely on metal ion induced assembly in an aqueous environment. For example, terpyridine-based metal ion coordination chemistry has been used to fabricate surface anchored polyelectrolyte networks.[20] Other examples include the orthogonal use of both electrostatic and coordination chemistry, to assemble polymer multilayers.[21] Likewise, dendritic multilayers have been assembled onto surfaces using Ag(II),[22] Co(II)[23] and Zr(IV) metal ions.[24] Zirconium has also been used to assemble polymer multilayer thin films.[25] Other examples have utilized metal ion-based coordination chemistry to induce changes in polymer film properties, such as morphology,[26] by

exposing a PEM to an aqueous solution of metal ion. More common than coordination polymer multilayers are molecular multilayers based on coordination chemistry. Here too, however, aqueous metal ion coordination is typically the method of choice for the assembly of components onto a surface. For example, carboxylic acid ligands were assembled onto silica surfaces using aqueous Zn(II) complexes.[27] Similarly, a variety of charged and uncharged ligands have been assembled onto surfaces using metal ion coordination.[24,28-32]

The approach introduced in Chapter 7, in contrast to typical metal ion approaches, allow for both the build up and break down of a polymer multilayer in an organic solvent, while also imparting diverse functionality to the multilayer.[33] Such an approach allows for the integration of non-water soluble materials into thin films, such as optical dyes or other aliphatic materials. This approach can also allow for the use of multilayer films in applications that are sensitive to water or humidity such as electro-optical and hydrogen storage applications.[34]

The investigation detailed in Chapter 7 involved the assembly of a poly(norbornene) containing side-chain Pd(II) pincer type complexes onto a commercially available, complementary macroligand, poly(vinylpyridine) (PVP). We demonstrated the uniform build-up and subsequent eraseability of these polymer films.[33] Based on our positive result using coordination chemistry to fabricate multilayers, we extended our approach of coordination multilayers by using a simplified small molecule Pd(II) pincer complex assembled using reversible coordination chemistry as depicted in Scheme 8.1. The use of the small molecule Pd(II) pincer complex (**1**) allows us to employ non-aqueous deposition techniques and can optionally provide for the integration

of diverse ligands and functionalities into the films. Small molecule **1** is also compatible with a number of deposition parameters, including varying concentrations of **PVP** with deposition enabled at concentrations as low as 1 mM [**PVP**] and as low as 0.4 mM [**1**]. Additionally, **1**, because of its high association strength with **PVP**, can be deposited into or onto films and surfaces quickly (~ 2 minutes) and quantitatively, in contrast to weaker associating small molecules and metal ions that typically require longer deposition times and often strict deposition parameters.[22-23] Furthermore, **1** also results in thinner, smoother films, in comparison to the poly(norbornene) based analogue.[35] The use of **1** with **PVP** could also provide a versatile platform for the integration of other components, including hydrogen bonding materials such as poly(4-vinyphenol) (PSOH).[8] In light of the versatility of the system reported herein, we have extended upon our previous approach by tuning film properties by modulating various deposition parameters.

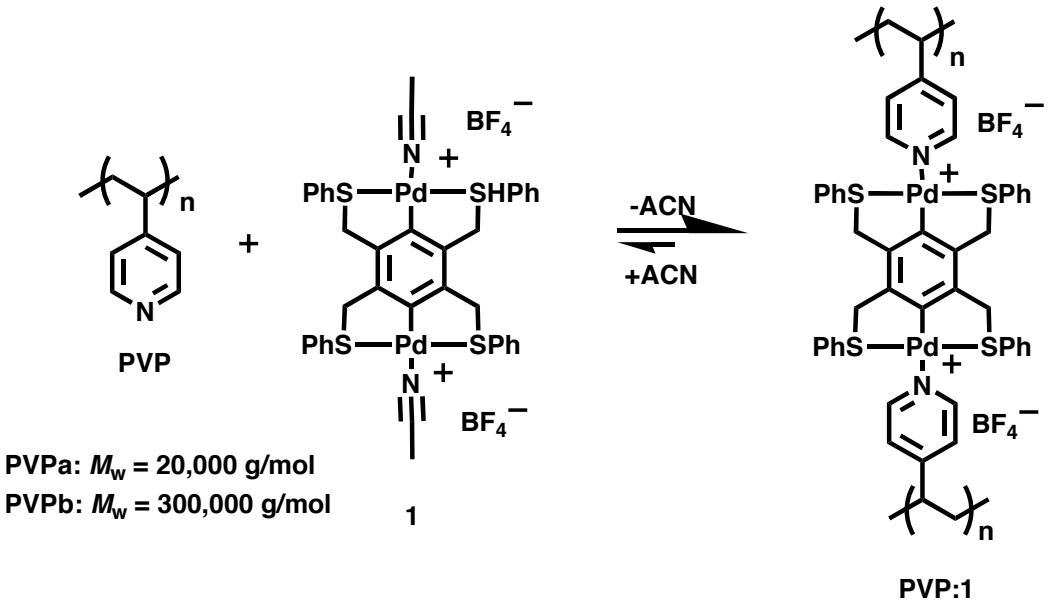

Scheme 8.1. Ligand displacement reaction between **PVP** and **1** used to build coordination polymer multilayers.

8.3 Results and Discussion

Quartz was chosen as the substrate of choice for the LbL deposition. We opted to use a prelayer template based on pyridine rather than attempting to attach **1** directly to a surface. The quartz slide was reacted with 4-(2-(trichlorosilyl)ethyl)pyridine **2** in analogy to a prior report under anhydrous conditions to yield a densely packed pyridine monolayer.[37] The molar surface density, Γ, was extrapolated using UV-vis spectroscopy[38] to be 1.5 x 10^{-9} mol/cm^2 (Figure E.1) assuming that the molar extinction coefficient in solution lies reasonably close to the molar extinction coefficient in the solid state. Our calculated Γ value agrees well with the Γ value (1.3 x 10^{-9} mol/cm^2) calculated by Paulson and coworkers for the same monolayer on quartz.[37] Assuming a moderately ordered monolayer is formed during the polymerization of the silyl chlorides as well as an average pyridine headgroup radius of about 4Å (calculated using molecular mechanics and Spartan software), a Γ value of 1.2 x 10^{-9} is expected, a value that closely corresponds with our and Paulson's results. These calculations correspond to about nine pyridine headgroups per 1 nm^2, suggesting a uniform, densely packed monolayer.

A common concern with the lateral polymerization of silyl chlorides is the formation of islands or large defects on the surface. Paulson and coworkers did not observe such defects on their monolayers during their earlier work.[37] We were able to verify their finding in our system by both optical microscopy (OM) and atomic-force microscopy (AFM). At 10,000 x's magnification, observed through OM, no defects were observed on our films. Likewise, AFM showed a smooth surface, with no obvious

defects observed at several locations on the slide and with a calculated roughness (rms) of 0.4 nm (Figure E.2). The rms value increased slightly, as expected, after the polymerization, from a value of 0.1 nm for the clean quartz slide (Table 8.1). We concluded, on the basis of these results, that our pyridine-functionalized surface was adequate as a prelayer for the LbL deposition of polymers.

Table 8.1. Surface characterization data.

Entry	Sample	[Polymer]/mM[a]	Height/nm[c]	Error /nm	A / a.u.	rms/nm[c]
1	**PVPa:1** film	1	40	6	0.02	6.3
2	**PVPa:1** film	5	150	30	0.10	29.9
3	**PVPa:1** film	10	370	17	0.15	17.3
4	**PVPb:1** film	1	30	1	0.007	1.3
5	**PVPb:1** film	5	90	9	0.03	8.7
6	**PVPb:1** film	10	150	14	0.07	13.8
7	**PVPb:1** film[b]	10	100	5	0.10	4.6
8	Quartz slide	-	-	-	-	0.09
9	**2** on quartz	-	-	-	-	0.35
10	**2:1** on quartz	-	-	-	-	0.41

[a]deposition solution concentration; [b]with acetonitrile additive in baths; [c]determined from AFM.

To modify the pyridine prelayer so that **PVP** is able to stick to the surface, we simply deposited compound **1** onto the slide. Deposition was monitored by UV-vis

spectroscopy. According to UV-vis data, layer deposition in using a 10 mM solution (CH_2Cl_2) of **1** is complete (no further increases in absorption intensity is observed after continued exposure of the film to a deposition solution) after about two minutes (Figure E.5). Roughness (rms) measurements of the modified prelayer were calculated to be between 0.3-0.4 nm (Table 8.1) for each prelayer produced. Subsequent multlilayer buildup was then accomplished by placing the functionalized surface into a bath of **PVP** and **1**, with thorough rinsing and sonication in between deposition cycles.

Our initial deposition experiments utilized 10 mM solutions (CH_2Cl_2) of both, **PVP** and **1**. UV-vis spectroscopy measurements revealed that the deposition of each layer is complete within two minutes (Figure E.5), which is consistent with our previous results.[33] UV-vis spectroscopy data also indicated uniform layer buildup, with a linear relationship between layer number, *n*, and absorption, *A*. However, AFM data taken of the films revealed rough films. The films were so rough, in fact, that a 20 μm x 20 μm area could not be scanned without either breaking an AFM tip or having tips irreversibly spring from the surface after encountering large defects. We have observed relatively rough surfaces before, using a similar system, and concluded that the deposition concentration is a critical parameter during the multilayer buildup of these coordination polymers.[33] Ultimately, through varying the concentration of **1** and measuring the resulting film roughness, we determined that the optimum concentration of **1** should be around 0.4 mM to achieve smooth thin films. We thus employed 0.4 mM concentrations of **1** for all remaining deposition experiments.

Based on our prior observation, originating from the hypothesis that a lower deposition concentration can minimize polymer entanglement,[33] we lowered the

deposition concentration of **PVP** first to 5 mM and subsequently to 1 mM. With deposition concentrations of 1, 5, and 10 mM, we observed uniform film buildup determined by UV-vis spectroscopy (Figure 8.1B-C), with final absorbance values of 10 layer films increasing proportionally with **PVP** concentration. By monitoring the absorbance band corresponding to the **PVP** π–π^* transition at 257 nm, we determined the deposition to be approximately linear with each layer being close to uniform. UV-vis spectroscopy data also revealed another important feature attributable to the high energy, nitrile complex absorption band at 217 nm, which is generally distinct at times when **1** is covering the surface as the terminal layer, and fades when **PVP** covers the surface as the terminal layer. This is consistent with our hypothesis that the acetonitrile ligand is released when **PVP** is coordinated to **1** (Scheme 8.1). This exchange of a weaker ligand (acetonitrile) with a stronger one (pyridine) has been well-established in solution experiments investigating similar chemistry.[35-36]

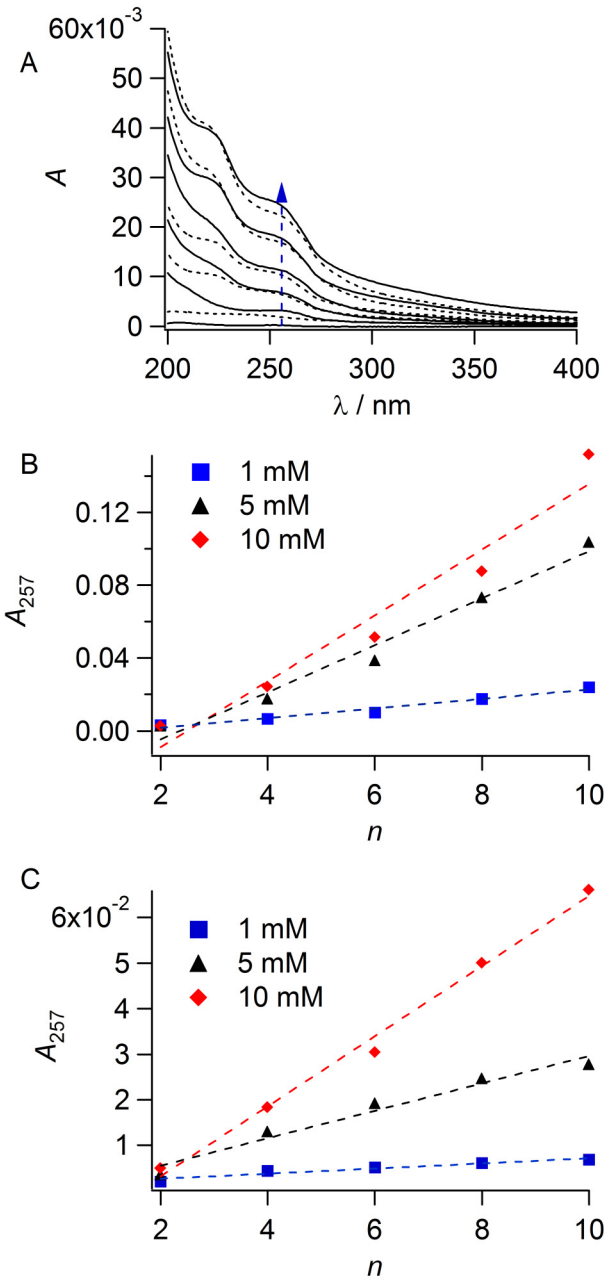

Figure 8.1. UV-vis data for polymer multilayers consisting of **1** and **PVPa**: (A) Example UV-vis absorption spectra taken at each deposition interval between **1** (0.4 mM in CH_2Cl_2) and **PVPa** (1 mM in CH_2Cl_2). Dotted lines represent odd buildup, with **1** on top of the film, while solid lines represent even buildup, with **PVPa** on top; (B) Plot of layer number, *n*, vs. absorption, *A*, for films deposited using **1** and **PVPa** at deposition solution concentrations of 1, 5, and 10 mM of **PVPa**; (C) Plot of layer number, *n*, vs. absorption, *A*, for films deposited using 1 and **PVPb** at deposition solution concentrations of 1, 5, and 10 mM of **PVPb**.

Our UV-vis results correlate well with more direct data probing the mechanism of deposition collected by infrared spectroscopy (IR) (Figure 8.2). We were interested in determining the existence and fate of the nitrile ligand on **1** after the initial deposition of **1** as well as during the deposition of **PVP** on top of **1**. For all IR experiments, we first spun cast a **PVP** film onto a CaF plate and subsequently deposited **1** and a layer of **PVP** using solution deposition. Generally, Figure 8.2 shows intensity increases, consistent with our UV-vis results, upon deposition of each layer. Specifically, after the deposition of **1** onto a **PVP** layer, one coordination site on **1** is coordinated to a nitrile ligand while the other coordination site is complexed to the **PVP** layer, as the band attributable to the nitrile stretching frequency at 2250 cm^{-1} is evident in the IR spectrum (Figure 8.2). After the subsequent deposition of **PVP** on top of this layer, the band attributable to the nitrile ligand disappears, presumably due to the displacement of the second nitrile ligand by the incoming **PVP** macroligand (Figure 8.2). These results suggest the chemistry of Scheme 8.1, well known in solution, is occurring at the surface interface. Further evidence for this conclusion was obtained by control experiments, in which a similar Pd pincer complex comprising a harder Cl ligand in place of the more labile nitrile ligand (**1**) was exposed to a pyridine monolayer (**2** on quartz) and a **PVP** layer. In this case, **PVP** is not capable of displacing the Cl ligand, and no deposition was evident by UV-vis spectroscopy. This observation is also consistent with our previous report.[33]

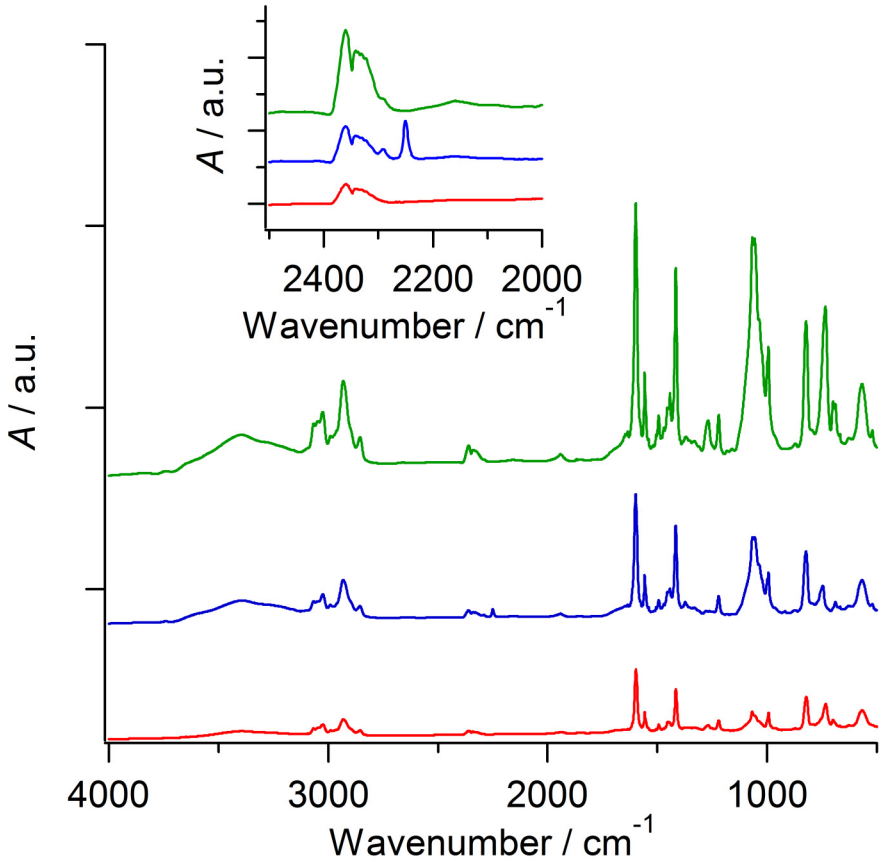

Figure 8.2. Transmission IR spectra of films consisting of **1** and **PVPb**: (Red spectrum) A **PVPb** film formed by spin casting the polymer onto a CaF plate; (Blue spectrum) after the deposition of **1** onto the **PVPb** film; the inset blowup of the nitrile region shows a resolved nitrile band at 2250 cm^{-1}; (Green spectrum) after the subsequent deposition of **PVPb** onto previous bilayer; the disappearance of the nitrile band is evident from the insent blowup plot. The H_2O broad peak past 3000 cm^{-1} may be due to residual water in the solvent or water adsorbed by PVP from the atmosphere. Likewise, we suspect the broad band at 2400 cm^{-1} to attributable to a complex OH stretching frequency due to water absorption frequently seen in solid state silica IR spectra.

AFM experiments were used to determined film morphology, height, and roughness. For a typical AFM experiment, we first gently scratched though the polymer film with a razor blade to form a step edge that served as an internal AFM height standard. During the process of scratching the surface, displaced polymer often builds up around the edges of the scratch to form "dog-ear" features evident most clearly from the section line height profiles of the final image (Figure 8.3). This area was excluded from the polymer film height and roughness calculations. Occasionally, we observed greater film trauma such as cracks in the films or film displacement during the scratch, exemplified in Figure 8.3E. Nonetheless, the AFM data were sufficient to calculate roughness and thickness values from the undisturbed film areas. We attempted to verify our surface height calculations through ellipsometry to obtain an independent measurement. Unfortunately, however, due to the opacity of our films, the ellipsometry data could not be succinctly fit to an appropriate model. We thus deemed our ellipsometry data largely inconclusive; although ellipsometry measurements also suggested, through comparisons of each film spectra, uniform layer buildup.

Most importantly, however, AFM results are consistent with our UV-vis data, rms roughness and film thickness measurements (Figure 8.3-8.4) suggesting a strong dependence of the dipping solution concentration on the film properties (Table 8.1). By varying the deposition concentration of **PVP**, we observed films with different morphology, rms roughness, and thickness (Table 8.1). In general, the lower the concentration of **PVP**, the thinner and smoother the desired film. The thickness of these films, for both low and high molecular weight **PVP** is approximately linearly related to the deposition concentration (Figure 8.4).

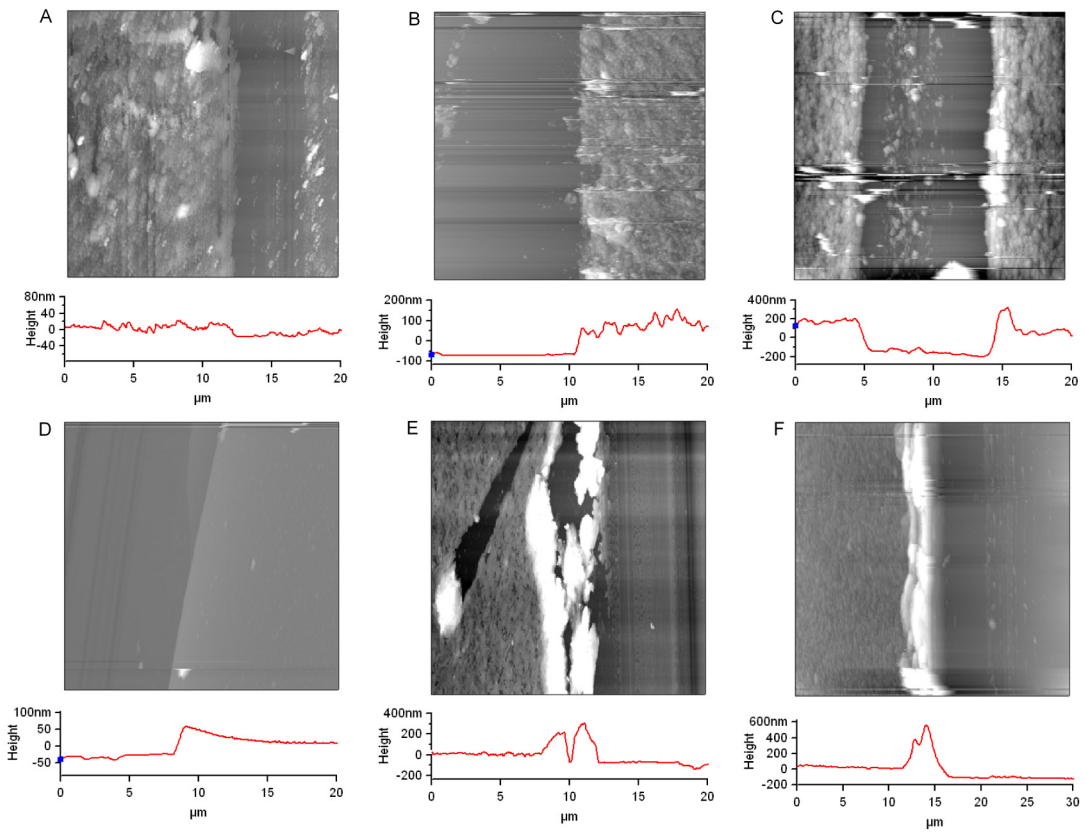

Figure 8.3. AFM images of scratched **PVP:1** films and corresponding section line height profiles: **PVPa:1** deposited at (A) 1 mM; (B) 5 mM; (C) 10 mM; **PVPb:1** deposited at (D) 1 mM; (E) 5 mM; (F) 10 mM.

While the deposition concentration can be varied to modulate the amount of polymer deposited onto the film, other deposition parameters can also be used to tune film properties. Our initial experiments used a low molecular weight **PVP** (**PVPa**, M_w = 20,000 g/mol). To investigate the influence of molecular weight on the film characteristics, we decided to investigate high molecular weight poly(vinyl pyridine) (**PVPb**, M_w = 300,000 g/mol). Interestingly, films comprising higher molecular weight **PVPb** were thinner and smoother in comparison to the lower molecular weight **PVPa** films. Films deposited with **PVPb** at 5 mM and 10 mM, for example, were almost half as thick (90 nm, 150 nm, respectively) as films deposited with **PVPa** under the same film

forming conditions (150 nm, 370 nm). Likewise, roughness measurements generally indicate smoother films when the higher molecular weight **PVPb** is used during deposition (Table 8.1). Our results also correlate well with the UV-vis data indicating that the amount of polymer absorbed is less when the high molecular weight polymer **PVPb** is used in comparison to when the low molecular weight polymer **PVPa** (Table 8.1).

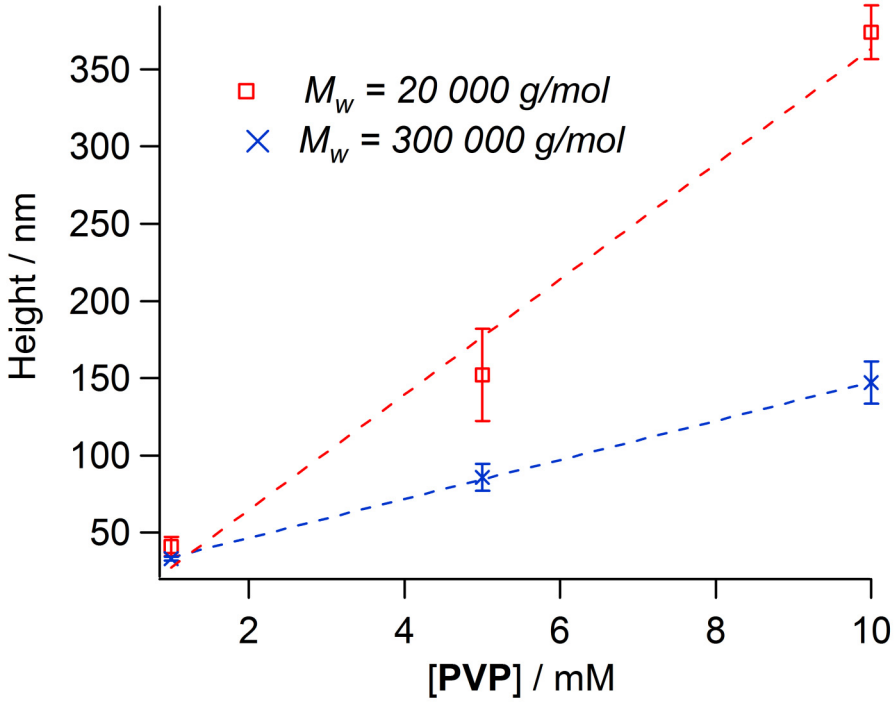

Figure 8.4. Plot of height, determined by AFM, vs. deposition concentration for low (**PVPa**) and high (**PVPb**) molecular weight PVP.

Our results obtained with the higher molecular weight **PVPb** agree well with previously published analyses[39-41] regarding the molecular weight dependence of thin film thicknesses and roughness values. Rubner and coworkers reported that while thicknesses of films of PEMs were independent of molecular weight due to segmental repulsion irregardless of molecular weight, thicknesses of films containing neutral

hydrogen bonded polymers were dependent on molecular weight of the polymer, with film thickness increasing as polymer molecular weight increased.[39] They reasoned that with a neutral, hydrogen bonding system, segmental chain repulsion is minimized resulting in more folded polymers during the film formation. On the other hand, Ito and coworkers reported that when stronger noncovalent interactions such as charge transfer interactions are used, little variations in layer thickness are observed as the molecular weight of the polymer increases. They attribute this result to the strength of the interaction, such that the polymer, when binding to the film, accrues a large enthalpic energy gain compared with the entropic loss in conformation energy. They further conclude that this energy balance can result in a chain extension during binding. Presumably, if films containing polymers with large differences in molecular weights were compared, one could reason that an enthalpic gain would be greater for the polymer with the most binding sites. In fact, this hypothesis was explored in detail by Schlenoff and coworkers; they observed that bound low molecular weight poly(electrolyte)s could even be *displaced* by poly(electrolyte)s with much larger molecular weights in a thin film.[42] In this context, and based on the analysis of Ito and coworkers, since the interaction that we have used is even stronger ($K_a > 10^9$ M^{-1} in nonpolar solvents)[43] we hypothesize that higher molecular weight chains have a larger enthalpic gain upon binding, and thus extend more in light of the relatively small entropic loss paid during unfolding.

We also reasoned, that since the metal coordination interaction we were using was so strong, that we could potentially reduce the amount of coiled polymer bound to the surface by lowering the association constant between the film and the polymer. We

initially attempted to carry out the deposition experiments in DMF. However, due to solubility limitations of **1** in DMF, very little deposition occurred. We next attempted the deposition in CH_2Cl_2 at 10 mM concentration of **PVPb**, and 0.4 mM concentration of **1**, with the addition of 3% (v/v) acetonitrile. Our hypothesis was that the acetonitrile would shift the equilibrium in the backward direction (Scheme 8.1), potentially allowing for more polymer reorganization after the binding event. Indeed, with the addition of 3% acetonitrile to the deposition solution, thinner and smoother films result (100 nm with an rms = 5 nm) (Figure 8.5, Table 8.1). Analogously, we have previously observed that similar films can be completely erased with a 5% solution of pyridine.[33] Noteworthy is that the amount of acetonitrile that could be added to the solution while still allowing for deposition seemed to be critical,. With more than about 3% acetonitrile, incomplete deposition results presumably due to the acetonitrile in solution erasing the polymer once it is bound.

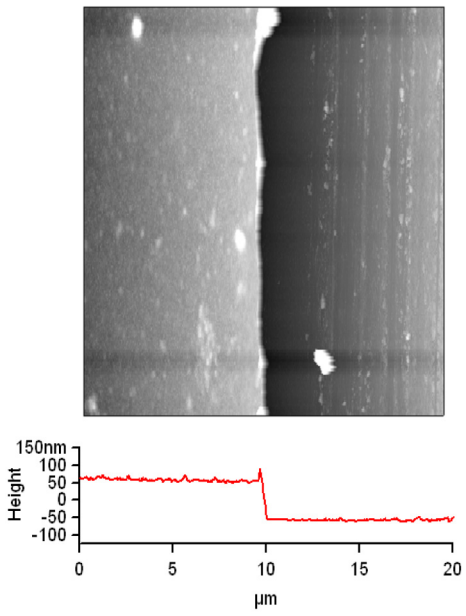

Figure 8.5. AFM image and corresponding section line height profile of a scratched film deposited using **PVPb** and **1** in a 10 mM solution of each component with acetonitrile (3%) as an additive.

8.4 Conclusion

Our results reported herein suggest a straightforward way to achieve multilayer thin films through metal coordination in a non-aqueous environment. Films produced in this manner could be useful in, for example, hydrogen storage materials that are extremely water sensitive. Additionally, based on our previous reported erasable metal coordination films involving analogous chemistry,[33] the films reported herein could have both diverse function and presumably form through appropriate top down lithographic engineering. Most importantly, however, we can also modify film properties using solution concentration, different molecular weight polymers, and additives that compete with binding, much like pH and salt additives are used to modulate the properties of PEMs. These results suggest that metal coordination films, and perhaps other non-traditional thin films, might be at least as versatile as the more common PEMs. While all of our films were thicker than "molecularly thin" films attainable through poly(electrolyte)s, we view our results as significant, especially given that a seemingly uncooperative deposition system can be tuned easily with various deposition parameters. Additionally, our surface height measurements and analysis should incite others, particularly theoreticians, to investigate more the physical chemistry of polymer deposition when the interaction used is not electrostatic in nature. Many models have been suggested and developed to explain PEMs,[1] particular since PEMs can often be modeled with well known methods involving electrostatics, but very little work has been

completed on understanding more complicated binding modes at surfacial interfaces, such hydrogen bonding and metal coordination.

8.5 Materials and Methods

Poly(vinylpyridine) was purchased from commercial sources and used without purification (M_w = 20,000 **PVPa** from Monomer-Polymer & Dajac Labs, Inc.; M_w = 300,000 **PVPb** from Sigma-Aldrich). Compound **1** was synthesized according to previously published methods.[36] Solvents were either distilled over Na and benzophenone or anhydrous solvents were purchased from Acros Organics or Sigma Aldrich. Quartz microscope slides (25 x 25 x 1 mm) were purchased from ChemGlass and plasma cleaned for at least 20 min prior to use.

Preparation of Quartz Prelayer. In a dry box, cleaned quartz slides were added to a solution of 4-(2-(trichlorosilyl)ethyl)pyridine (15% in toluene) as described by Paulson and coworkers.[37] After two hours of immersion, the slides were removed, rinsed, and sonicated with toluene. The slides were characterized by UV-vis spectroscopy prior to their use as substrates in multilayer buildup. The molar surface density of the prelayers was calculated from UV-vis spectroscopy data according to the analysis described by Durfor and coworkers.[38] The molar surface density was consistent with Paulson's report.[37] To verify that large islands did not form during the lateral polymerization of 4-(2-(trichlorosilyl)ethyl)pyridine, optical microscopy was utilized (10,0000 x magnification) to scan each slide for any defects. According to these characterization methods, no islands were formed. To determine the roughness of the prelayer, AFM was used.

Multilayer Buildup. A pyridine functionalized quartz slide was added to a freshly prepared solution of **1** (concentration varied) in a slide trough. The slide was kept immersed for 2 minutes (UV-vis spectroscopy verified saturation of the prelayer with **1** after 2 minutes). The slide was removed from the trough and rinsed thoroughly with the solvent used for deposition. The slide was then dried in a stream of nitrogen or argon. Subsequently, a similar process was used for the addition of **PVP** to the film, with the saturation point (2-3 minutes) determined again by UV-vis spectroscopy. These processes were repeated until the desired number of layers had been deposited. The resulting films were stored in air and were stable for extended periods of time (months).

Spectroscopy. Solution and solid-state UV-vis absorption spectra were acquired using a Varian Cary 5A spectrometer. Solution-based absorption spectra were referenced to a blank containing the same solvent as the sample. Solid-state absorption spectra were referenced to a blank quartz slide. For all solid-state measurements, 1 mm quartz slides (ChemGlass) were used. IR spectra were acquired with a Perkin-Elmer Spectrum 1000 spectrometer.

AFM. AFM data were taken in air on an Asylum Research MFP3D instrument. We processed all AFM images and analyzed surface heights using Asylum Research MFP3D software operating in IgorPro (WaveMetrics, Inc., Lake Oswego, OR). An Olympus cantilever (k = 42 N/m, f_0 = 377 kHz) was employed for imaging substrates, prelayers substrates, and multilayer films. The same cantilever was used for surface thickness determination. Images for surface analysis were taken over a predetermined scan range (512 x 512 pixels for each image). For absolute surface height measurements using AFM, we scratched through a multilayer deposited on a quartz slide with a razor

blade (care was taken not to scratch through the quartz) and scanned (512 x 512 pixels for each image) this area on the slide (90 mm x 90 mm or 50 mm x 50 mm) so as to include enough area around the scratch. To determine surface height, the AFM software was used to process the image and perform an averaged line analysis over at least 100 lines for each image. The averaged line corresponding to the top of the surface was selected, and from this height value was subtracted a value corresponding to a point at the bottom of the surface (step from scratch). Errors in these values were calculated from standard deviations in the averaged line height analyses.

8.6 References

1. Decher, G.; Schlenoff, J. B. *Multilayer Thin Films: Sequential Assembly of Nanocomposite Materials*; Wiley-VCH: Weinheim, 2003.

2. Such, G. K.; Quinn, J. F.; Quinn, A.; Tjipto, E.; Caruso, F. Assembly of Ultrathin Polymer Multilayer Films by Click Chemistry. *J. Am. Chem. Soc.* **2006**, *128*, 9318.

3. Cho, J.; Caruso, F. Polymeric Multilayer Films Comprising Deconstructible Hydrogen-Bonded Stacks Confined between Electrostatically Assembled Layers. *Macromolecules* **2003**, *36*, 2845.

4. Zeng, G.; Gao, J.; Chen, S.; Chen, H.; Wang, Z.; Zhang, X. Combining Hydrogen-Bonding Complexation in Solution and Hydrogen-Bonding-Directed Layer-by-Layer Assembly for the Controlled Loading of a Small Organic Molecule into Multilayer Films. *Langmuir* **2007**, *23*, 11631.

5. Hao, E.; Lian, T. Buildup of Polymer/Au Nanoparticle Multilayer Thin Films Based on Hydrogen Bonding. *Chem. Mater.* **2000**, *12*, 3392.

6. Wang, L.; Fu, Y.; Wang, Z.; Fan, Y.; Zhang, X. Investigation into an Alternating Multilayer Film of Poly(4-Vinylpyridine) and Poly(acrylic acid) Based on Hydrogen Bonding. *Langmuir* **1999**, *15*, 1360.

7. Zhang, H.; Wang, Z.; Zhang, Y.; Zhang, X. Hydrogen-Bonding-Directed Layer-by-Layer Assembly of Poly(4-vinylpyridine) and Poly(4-vinylphenol): Effect of Solvent Composition on Multilayer Buildup *Langmuir* **2004**, *20*, 9366.

8. Wang, L.; Cui, S.; Wang, Z.; Zhang, X.; Jiang, M.; Chi, L.; Fuchs, H. Multilayer Assemblies of Copolymer PSOH and PVP on the Basis of Hydrogen Bonding. *Langmuir* **2000**, *16*, 10490.

9. Fu, Y.; Bai, S.; Cui, S.; Qiu, D.; Wang, Z.; Zhang, X. Hydrogen-Bonding-Directed Layer-by-Layer Multilayer Assembly: Reconformation Yielding Microporous Films. *Macromolecules* **2002**, *35*, 9451.

10. Sukhishvili, S. A.; Granick, S. Layered, Erasable Polymer Multilayers Formed by Hydrogen-Bonded Sequential Self-Assembly. *Macromolecules* **2002**, *35*, 301.

11. Wang, F.; Ma, N.; Chen, Q.; Wang, W.; Wang, L. Halogen Bonding as a New Driving Force for Layer-by-Layer Assembly. *Langmuir* **2007**, *23*, 9540.

12. Dennany, L.; Forster, R. J.; White, B.; Smyth, M.; Rusling, J. F. Direct Electrochemiluminescence Detection of Oxidized DNA in Ultrathin Films Containing $[Os(bpy)2(PVP)10]^{2+}$. *J. Am. Chem. Soc.* **2004**, *126*, 8835.

13. Mugweru, A.; Wang, B.; Rusling, J. F. Voltammetric Sensor for Oxidized DNA Using Ultrathin Films of Osmium and Ruthenium Metallopolymers. *Anal. Chem.* **2004**, *76*, 5557.

14. Wang, B.; Rusling, J. F. Voltammetric Sensor for Chemical Toxicity Using $[Ru(bpy)2poly(4\text{-}vinylpyridine)10Cl)]^{+}$ as Catalyst in Ultrathin Films. DNA Damage from Methylating Agents and an Enzyme-Generated Epoxide. *Anal. Chem.* **2003**, *75*, 4229.

15. Kim, J.; Lee, L.; Niece, B. K.; Wang, J. X.; Gewirth, A. A. Formation of Ordered Multilayers from Polyoxometalates and Silver on Electrode Surfaces. *J. Phys. Chem. B* **2004**, *108*, 7927.

16. Hong, M. Inorganic-Organic Hybrid Coordination Polymers: A New Frontier for Materials Research. *Cryst. Growth Des.* **2007**, *7*, 10.

17. Mitzi, D. B. Thin-Film Deposition of Organic-Inorganic Hybrid Materials. *Chem. Mater.* **2001**, *13*, 3283.

18. Kang, E. H.; Bu, T.; Jin, P.; Sun, J.; Yang, Y.; Shen, J. Layer-by-Layer Deposited Organic/Inorganic Hybrid Multilayer Films Containing Noncentrosymmetrically Orientated Azobenzene Chromophores. *Langmuir* **2007**, *23*, 7594.

19. Sukhishvili, S. A.; Granick, S. Layered, Erasable, Ultrathin Polymer Films. *J. Am. Chem. Soc.* **2000**, *122*, 9550.

20. Sievers, T. K.; Vergin, A.; Möhwald, H.; Kurth, D. G. Thin Films of Cross-Linked Metallo-Supramolecular Coordination Polyelectrolytes. *Langmuir* **2007**, *23*, 12179.

21. Krass, H.; Papastavrou, G.; Kurth, D. G. Layer-by-Layer Self-assembly of a Polyelectrolyte Bearing Metal Ion Coordination and Electrostatic Functionality. *Chem. Mater.* **2003**, *15*, 196.

22. Cha, B. J.; Kang, Y. S.; Won, J. Preparation and Characterization of Dendrimer Layers on Poly(dimethylsiloxane) Films *Macromolecules* **2001**, *34*, 6631.

23. Blasini, D. R.; Flores-Torres, S.; Smilgies, D. M.; Abruña, H. D. Stepwise Self-Assembly of Ordered Supramolecular Assemblies Based on Coordination Chemistry. *Langmuir* **2006**, *22*, 2082.

24. Wanunu, M.; Vaskevich, A.; Cohen, S. R.; Cohen, H.; Arad-Yellin, R.; Shanzer, A.; Rubinstein, I. Branched Coordination Multilayers on Gold. *J. Am. Chem. Soc.* **2005**, *127*, 17877.

25. Byrd, H.; Holloway, C. E.; Pogue, J.; Kircus, S.; Advincula, R. C.; Knoll, W. Ultrathin Film Self-Assembly of Hybrid Organic-Inorganic Metal Coordination Polymers. *Langmuir* **2000**, *16*, 10322.

26. Cao, M.; Wang, J.; Wang, Y. Surface Patterns Induced by Cu2+ Ions on BPEI/PAA Layer-by-Layer Assembly *Langmuir* **2007**, *23*, 3142.

27. Shekhah, O.; Wang, H.; Strunskus, T.; Cyganik, P.; Zacher, D.; Fischer, R.; Woll, C. Layer-by-Layer Growth of Oriented Metal Organic Polymers on a Functionalized Organic Surface. *Langmuir* **2007**, *23*, 7440.

28. Abe, M.; Michi, T.; Akira, S.; Kondo, T.; Zhou, W.; Ye, S.; Uosaki, K.; Sasaki, Y. Electrochemically Controlled Layer-by-Layer Deposition of Metal-Cluster Molecular Multilayers on Gold. *Angew. Chem., Int. Ed.* **2003**, *42*, 2912.

29. Altman, M.; Shukla, A. D.; Zubkov, T.; Evmenenko, G.; Dutta, P.; Boom, M. E. v. d. Divergent Growth of Coordination Dendrimers on Surfaces. *J. Am. Chem. Soc.* **2006**, *128*, 8341.

30. Kanaizuki, K.; Murato, M.; Nishimori, Y.; Mori, I.; Nishio, K.; Masuda, H.; Nishihara, H. Stepwise Preparation of Linear π-Conjugated Bis(terpyridine)metal Polymer Chains at Gold Surface. *Chem. Lett.* **2005**, *34*, 534.

31. Kosbar, L.; Srinivasan, C.; Afzali, A.; Graham, T.; Copel, M.; Krusin-Elbaum, L. Self-Assembled Multilayers of Transition-Metal-Terpyridinyl Complexes; Formation, and Characterization. *Langmuir* **2006**, *22*, 7631.

32. Nishimori, Y.; Kanaizuka, K.; Murato, M.; Nishihara, H. Synthesis of Molecular Wires of Linear and Branched Bis(terpyridine)-Complex Oligomers and Electrochemical Observation of Through-Bond Redox Conduction. *Chem. Asian J.* **2007**, *2*, 367.

33. South, C. R.; Piñón III, V.; Weck, M. Erasable Coordination Polymer Multilayers on Gold. *Angew. Chem., Int. Ed. Eng.* **2008**, *47, in press.*

34. Kamineni, V. K.; Lvov, Y. M.; Dobbins, T. A. Layer-by-Layer Nanoassembly of Polyelectrolytes Using Formamide as the Working Medium. *Langmuir* **2007**, *23*, 7423.

35. Similar pincer complex chemistry has been used extensively in Steve Craig's laboratory to provide supramolecular polymer networks in solution: see, for example, Serpe, M. J.; Craig, S. L. Physical Organic Chemistry of Supramolecular Polymers. *Langmuir* **2007**, *23*, 1626.

36. Gerhardt, W. W.; Zucchero, A. J.; Wilson, J. N.; South, C. R.; Bunz, U. H. F.; Weck, M. Supramolecular Cruciforms. *Chem. Commun.* **2006**, 2141.

37. Paulson, S.; Morris, K.; Sullivan, B. P. A general preparative route to self-assembled monolayer surfaces of polypyridine ligands and their metal complexes *J. Chem. Soc., Chem. Commun.* **1992**, 1615.

38. For a detailed explanation of our calculation, see: Durfor, C. N.; Turner, D. C.; Georger, J. H.; Peek, B. M.; Stenger, D. A. Formation and naphthoyl derivatization of aromatic aminosilane self-assembled monolayers: characterization by atomic force microscopy and ultraviolet spectroscopy. *Langmuir* **1994**, *10*, 148.

39. Stockton, W. B.; Rubner, M. F. Molecular-Level Processing of Conjugated Polymers. 4. Layer-by-Layer Manipulation of Polyaniline via Hydrogen-Bonding Interactions. *Macromolecules* **1997**, *30*, 2717.

40. Anzai, J.; Kobayashi, Y.; Nakamura, N.; Nishimura, M.; Hoshi, T. Layer-by-Layer Construction of Multilayer Thin Films Composed of Avidin and Biotin-Labeled Poly(amine)s. *Langmuir* **1999**, *15*, 221.

41. Shimazaki, Y.; Nakamura, R.; Ito, S.; Yamamoto, M. Molecular Weight Dendence of Alternate Adsorption through Charge-Transfer Interaction. *Langmuir* **2001**, *17*, 953.

42. Sui, Z.; Salloum, D.; Schlenoff, J. B. Effect of Molecular Weight on the Construction of Polyelectrolyte Multilayers: Stripping versus Sticking. *Langmuir* **2003**, *19*, 2491.

43. South, C. R.; Higley, M. N.; Leung, K. C.-F.; Lanari, D.; Nelson, A.; Grubbs, R. H.; Stoddart, J. F.; Weck, M. Self-Assembly With Block Copolymers Using SCS PdII Pincer Metal Coordination and Pseudorotaxane Formation. *Chem. Eur. J.* **2006**, *12*, 3789.

CHAPTER 9

Molecular Recognition on the Side-Chains Of Polymers: Conclusions and Future Directions

9.1 Abstract

This final chapter summarizes the conclusions learned from the results reported in earlier parts of this thesis. Analysis regarding the advantages and disadvantages of the methods reported is included. A further presentation of the limitations of each approach presented herein is also provided. Finally, potential future directions and potential ideas to address the limitation of the results of this thesis are disclosed.

9.2 Introduction

The central hypothesis of this thesis is that molecular recognition can provide for new and easy ways for polymer functionalization, polymer synthesis, and provide a new platform for polymer applications, in contrast to typical synthetic polymer approaches that rely heavily on covalent bonding. Since polymer reactivity and polymer functionalization are often difficult to achieve using traditional covalent approaches, it is reasonable to predict that a noncovalent approach would allow for the error-checking and cleanliness required for polymer synthesis and polymer applications. Based on this central hypothesis, this thesis was designed to expand upon previous methods of noncovalent polymer functionalization by providing more efficient means of polymer synthesis and by using molecular recognition in polymers in applications toward the goal of demonstrating the promise of supramolecular side-chain polymers. This goal was met and the hypothesis was supported by the research results presented in this thesis.

Specifically, new and efficient polymer functionalization strategies were developed, new ways of controlling polymer synthesis were developed using a templated approach centered on molecular recognition, and finally, molecular recognition was used in multilayer thin films, demonstrating the vast possibility of molecular recognition based polymers.

9.3 Summary and Conclusions

Chapter 3 presents the results of using two strong molecular recognition components to functionalize polymers with architectural control. To demonstrate that an architecturally controlled copolymer could be used in conjunction with two strong molecular recognition components, we utilized a block copolymer based on norbornene, which can be easily polymerized using ROMP.[1] The results of this study were promising and advanced our original[2] noncovalently functionalized copolymers to include a copolymer with two recognition units that associated strongly with their small molecule counterparts, in comparison to the previous system in which one of the polymer recognition units required 10-fold excess of substrate to achieve saturation of the polymer backbone.[2] Furthermore, the use of both a pseudorotaxane and a metal complex along the backbone of a copolymer also enabled us to remove and replace functional groups on each side of the polymer using a distinct stimulus. We were able to remove the threaded component of the pseudorotaxane using a base stimulus, while the metal complex could be broken apart using a competing ligand.

Chapter 4 discusses yet another advancement of our noncovalent polymer functionalization strategy. To demonstrate that such a strategy could potentially have

broad appeal, we added another component to a random copolymer to produce a fully functional terpolymer similar to the block copolymer discussed in Chapter 3. Our incentive was simply to demonstrate that a noncovalent polymer functionalization strategy was not limited to only two recognition units, and if a particular application required the use of more than two functional groups, a noncovalent strategy could rise to the challenge.[3]

Chapter 5 presents results of extensive study on templated synthesis aided by molecular recognition. While our interest lies in templating architecturally controlled polymers, we decided to first begin our approach with small molecules with the use cross-metathesis to see if our molecular recognition partners could survive metathesis and vice-versa. Ultimately, it became obvious to us that the use of a metal complex as a template alongside an organometallic catalyst as a bond forming reagent was not a fruitful endeavor, despite several successful reports by van Koten and coworkers that might suggest the contrary.[4] However, important lessons were learned from these studies. For example, we observed that metathesis could be disabled if two olefins that were attached to a template were too far apart to react. We envision that such an approach in synthesis might be useful as a protected group strategy, especially given that olefin metathesis has emerged as the carbon-carbon bond forming reaction of choice for many chemists.[5]

In the next Chapter, results of our efforts in templated polymer synthesis are presented. Based on our small molecule studies, and the limitations of the metal complex we used for template attachement, we transitioned to a hydrogen bonding complex for our intitial polymer templating work.[6] The results of this study were positive, and we

were able to control an uncontrolled polymerization using a template. Importantly, we also observed moderate kinetic enhancements during polymerizations in which a template was utilized. We attributed this observation to an increase in local concentration via the template. Ultimately, the template we used for this study both prevented monomer aggregation as well as enhanced reaction kinetics.[6]

The last part of the thesis, Chapters 7-8, discusses a transition into materials science. We are interested in taking polymers with molecular recognition elements into a new more applied direction. Thus, for this goal we first investigated the use of noncovalent molecular recognition as a tool for building up polymer multilayers on surfaces. Our first approach utilized two different polymers that could recognize each other, and we depositied each polymer on top of the other to form a multilayer.[7] We found that these multilayers were both stable and responsive. Next, we simplified our approach and tuned multilayer properties using a poly(vinyl pyridine) polymer and a small molecule analog complex similar to the polymer discussed in Chapter 7. These results were even more promising, especially since we observed that films could be made thinner and smoother by varying deposition parameters. We observed that by the addition of an additive that shifted the equilibrium away from the bound metal complex, that a 10-layer film had roughness values of less than 5 nm.

The results of the surface science Chapters especially open up new areas for future study. Metal-ligand interactions are interesting when studied at a surface interface. In particular, metal-ligand interactions on polymers are unique because it seems from the results of our studies, that the interactions produce such a large enthalpic gain, that the entropic loss accrued during the polymer deposition is negligible. This results suggests a

mechanism quite different than that of typical poly(electrolyte) deposition, in which the individual interactions are very weak.

To summarize, this thesis demonstrate that noncovalent binding principles can be used to design and implement research strategies aimed at minimizing problems associated with traditional covalent bonding based strategies. For example, polymers can be functionalized with strongly associating substrates quantitatively and site-selectively without extensive purification (Chapters 3-4). Such an approach to polymer synthesis might not only enable the easy synthesis of polymeric libraries, but also might allow for the recycling of polymer backbones since each functionalization strategy relies on a reversible reaction. This concept can be applied to templated synthesis, wherein a template can control an otherwise hard-to-control polymerization (Chapter 6). Moreover, noncovalent binding strategies are not limited to methodology and/or proof-of-principle based research. Chapters 7-8 demonstrate that polymers with side-chain molecular recognition elements can be used in materials applications, such as polymer thin films.

9.4 Potential Future Directions

The work presented in this thesis, as a whole, resoundingly echoes the belief among many in the field that some of the key problems associated with covalent polymer synthetic strategies can be overcome by using noncovalent reactions in lieu of the more traditional approaches. Thus, in light of the results presented in this thesis, there are many possibilities for future work.

9.4.1 Complex Polymer Targets through Molecular Recognition

An area of polymer science that is quickly emerging as a promising field is the study of dendrimers, despite the fact that dendrimers are hard to reach molecular structures that require extensive purification after the attachment of each generation. Alternatives to dendrimers exist,[8] however, and linear dendronized polymers have been found to present a viable alternative to traditional dendrimers, particularly for applications that do not require polydispersity indeces of unity. The Hawker group established a fairly straightforward way to reach dendronized copolymers using click-chemistry.[8] While this approach worked well, a more generalized approach that would not require extensive monomer synthesis and polymer purification would be through the use of molecular recognition. The Stoddart group explored this area using a DB24C8 containing polymer.[9] They found that the supramolecular architecture could be shifted through the attachment of a dendron on the backbone of a polymer. A suitable new endeavor to explore would be the use of our strong, pincer-type complex as a vehicle to attach large dendrons onto the backbone of polymers. The polymers of choice could be random copolymers, block copolymers, or graft copolymers. Figure 9.1, taken from reference 9, shows this general approach in a covalent context. One can see that Route I, specifically, would likely be compatible with the use of molecular recognition for the dendron attachment step.

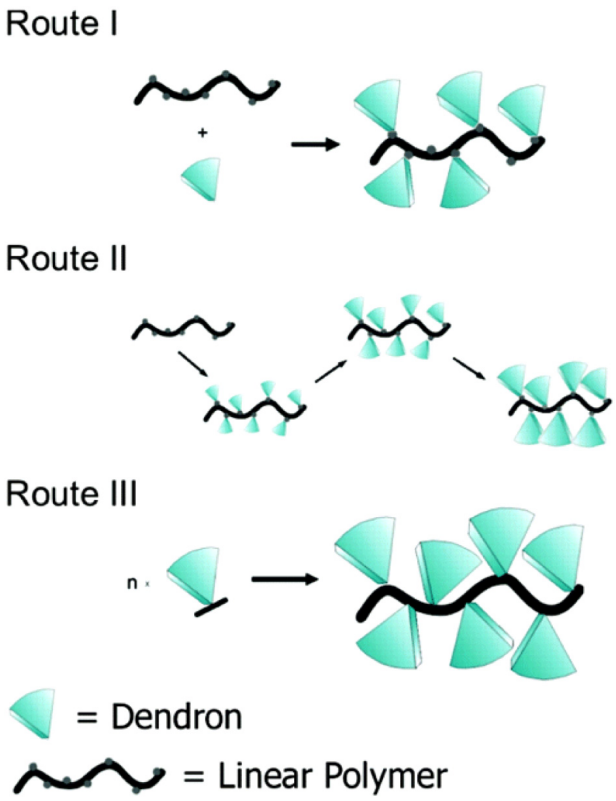

Figure 9.1. Routes to dendronized polymers.[8]

While dendronized polymers represent a suitable new target to work toward using molecular recognition, other complex polymers that require extensive purification are also ideal candidates.

9.4.2 Investigating effects of template structure during template-directed synthesis

Our initial efforts in templated synthesis involved the use of metal coordination as the binding force for keeping substrates on a template (Chapter 5). We chose this approach primarily because of the strength of the metal complex utilized. Ultimately, however, we found no conclusive evidence that the binding strength was critical during a template synthesis event. In light of this quandary, it would be ideal to investigate the effect of a weaker binding motif during a templated synthesis. A suitable template to

investigate would be a cyclobutane thymine photodimer, not only because of potential biological implications, but also because of the unique nature of this dimer. The Hamilton group reported the synthesis of a suitable thymine dimer[10] that would be ideal for a templated bond forming reaction, such as metathesis. They observed that **1** could assemble in a 1:2 ratio with diamidopyridine counterparts. In the context of templated synthesis, **1** would be unique because it is likely that once two diamidopyridine components formed a bond between one another while on the template, the resulting diamidopyridine dimer would bind less strongly to **1** than the individual monomers due to such a large entropic penalty paid after the reaction (Figure 9.2). Such a scenerio would potentially yield an autocatalytic system, or at the very least a unique example of product activation. This proposed project could also elucidate the effects of a template that associates less strongly with substrates than does a template based on metal coordination.

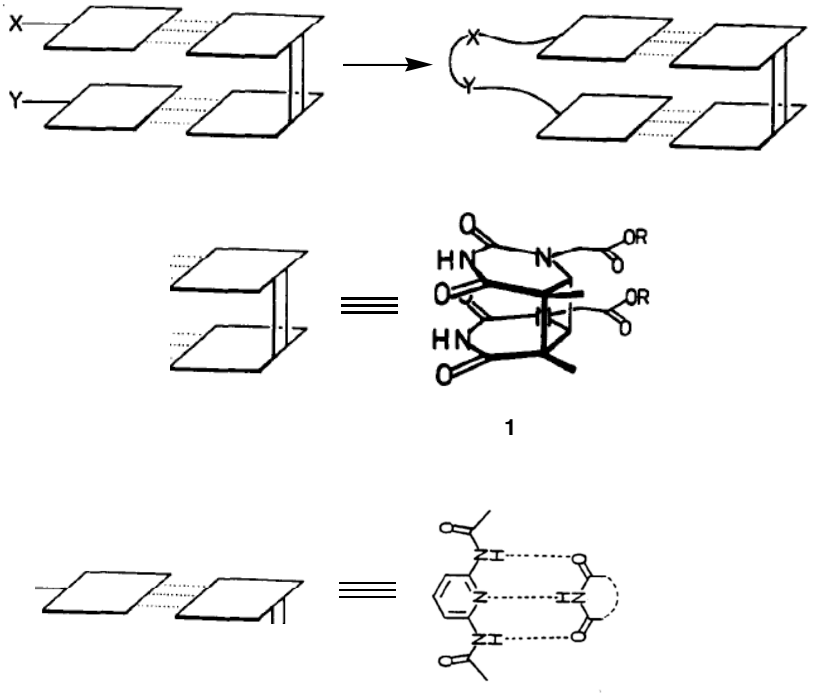

Figure 9.2. Template synthesis from a cyclobutane thymine dimer. Adapted from ref. 10.

9.4.3 New directions for Molecular Recognition on Surfaces

There are numerous possibilities for future work dealing with molecular recognition and multilayer thin films. However, the next logical step for this area of work would be two fold: (1) utilize more than one distinct recognition pattern to assemble polymer multilayer films, and (2) pattern these films using external stimuli through a "top-down" lithography approach. In general, for polymer multilayers, it is desirable to use cost-effective materials that do not require lengthy synthetic procedures. In particular since proper deposition of a polymer onto a surface or film usually requires a fresh deposition solution at each interval. Therefore, for the use of multiple recognition motifs, it would be desirable to design a system using commercially available, cheap materials. An straightforward example could use materials shown in Figure 9.3.

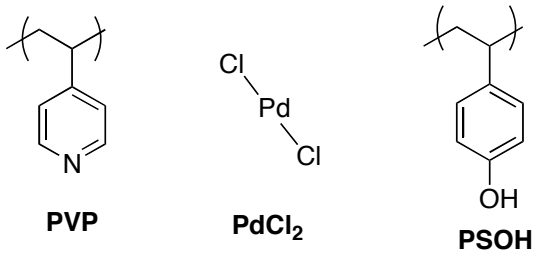

Figure 9.3. Materials for orthogonal multilayer build-up / break-down.

Poly(vinyl pyridine) (**PVP**) can be assembled through any commercially available *trans* Pd(II) complex, such as $PdCl_2$, which is formed in situ from K_2PdCl_4 and the exposure to a competing ligand. Likewise, **PVP** can also bind to poly(4-vinyl phenol) (**PSOH**) through hydrogen bonding. Thus, for example, an orthogonal multilayer could be built from these materials having a structure of **-(-PVP-$PdCl_2$-PSOH-)-$_n$**. Furthermore, such a multilayer could be patterned by first patterning a substrate and using a bottom-up

approach by orthogonally depositing each material onto the appropriate section of the surface. Or, a top-down approach could be utilized in which bits of the multilayer were washed away using, for example, a phosphine to erase the bonds between **$PdCl_2$** and **PVP**. The top-down approach is attractive because such a method could be compatible with user-friendly, cheap processes such as ink-jet printing.

9.5 Conclusion

While several examples of possible future work are presented in this Chapter, the possibilities for new ideas and uses of polymers containing molecular recognition elements are limitless. This thesis has demonstrated several unique examples of applications of molecular recognition in polymer science, all of which are seemingly very different. Yet in each example, the common thread of molecular recognition exists. Similarly, almost every biopolymer cooperates with other molecules through molecular recognition producing a vast library of bioapplications that all aid an orchestra of life. While the work presented in this thesis serves as a reminder of the complexity of molecular recognition, especially in biological systems, it also serves as a reminder of the level of complexity that we cannot yet attain in a conventional laboratory. Thus, in a giant scheme, this thesis is but a small step in advancing abiotic applications of molecular recognition in polymers. One day, however, we can hopefully fulfill the ultimate goal of rivaling natural processes with synthetic polymers.

9.6 References

1. South, C. R.; Higley, M. N.; Leung, K. C.-F.; Lanari, D.; Nelson, A.; Grubbs, R. H.; Stoddart, J. F.; Weck, M. Self-Assembly With Block Copolymers Using SCS PdII Pincer Metal Coordination and Pseudorotaxane Formation. *Chem. Eur. J.* **2006**, *12*, 3789.

2. Pollino, J. M.; Stubbs, L. P.; Weck, M. One-Step Multifunctionalization of Random Copolymers via Self-Assembly. *J. Am. Chem. Soc.* **2004**, *126*, 563.

3. South, C. R.; Leung, K. C.-F.; Lanari, D.; Stoddart, J. F.; Weck, M. Noncovalent Side-Chain Functionalization of Terpolymers. *Macromolecules* **2006**, *39*, 3738.

4. Chase, P. A.; Lutz, M.; Spek, A. L.; Klink, G. P. M. v.; Koten, G. v. Ring closing metathesis employing organometallic substrates and the templated synthesis of macrocycles *J. Mol. Cat. A: Chem.* **2006**, *254*, 2.

5. Fürstner, A. Olefin Metathesis and Beyond. *Angew. Chem. Int. Ed.* **2000**, *39*, 3012.

6. South, C. R.; Weck, M. Template Enhanced Ring-Opening Metathesis Polymerization. *Macromolecules* **2007**, *40*, 1386.

7. South, C. R.; III, V. P. Erasable Coordination Multilayers on Gold. *Angew. Chem. Int. Ed. Eng.* **2008**, *47*, in press.

8. Helms, B.; Mynar, J. L.; Hawker, C. J.; Frechet, J. M. J. Dendronized Linear Polymers via "Click Chemistry" *J. Am. Chem. Soc.* **2004**, *126*, 15020-15021.

9. Leung, K. C. F.; Mendes, P. M.; Magonov, S. N.; Northrop, B. H.; Kim, S.; Patel, K.; Flood, A. H.; Tseng, H. R.; Stoddart, J. F. Supramolecular Self-Assembly of Dendronized Polymers: Reversible Control of the Polymer Architectures through Acid-Base Reactions *J. Am. Chem. Soc.* **2006**, *128*, 10707-10715.

10. Hirst, S. C.; Hamilton, A. D. Molecular recognition: Cyclobutane thymine diners as rigid two-site receptors *Tet. Lett.* **1990**, *31*, 2401.

APPENDIX A

Supplemental Material for Chapter 3

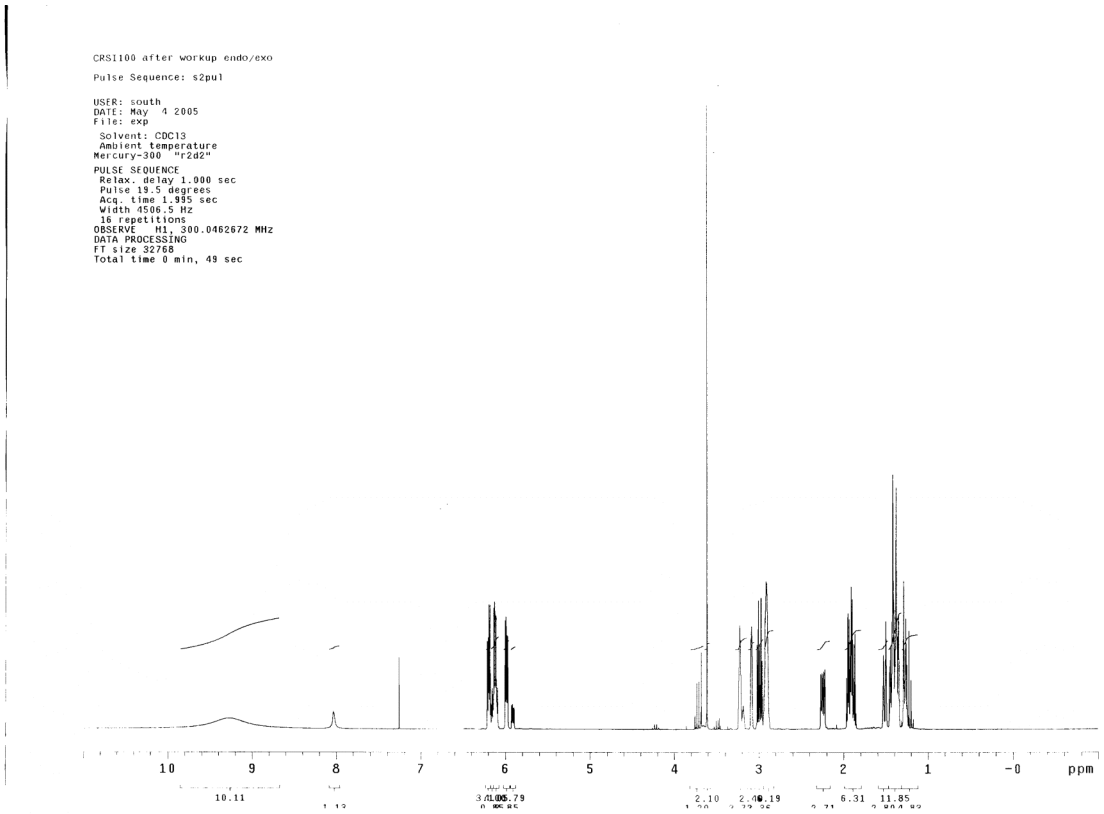

Figure A.1. ^{1}H NMR spectrum of an endo / exo mixture of compound **6** that can be be bought commercially or synthesized from cyclopentadiene and acrylic acid (this sample was synthesized according to this method); see refs. 54-56 in Chapter 3.

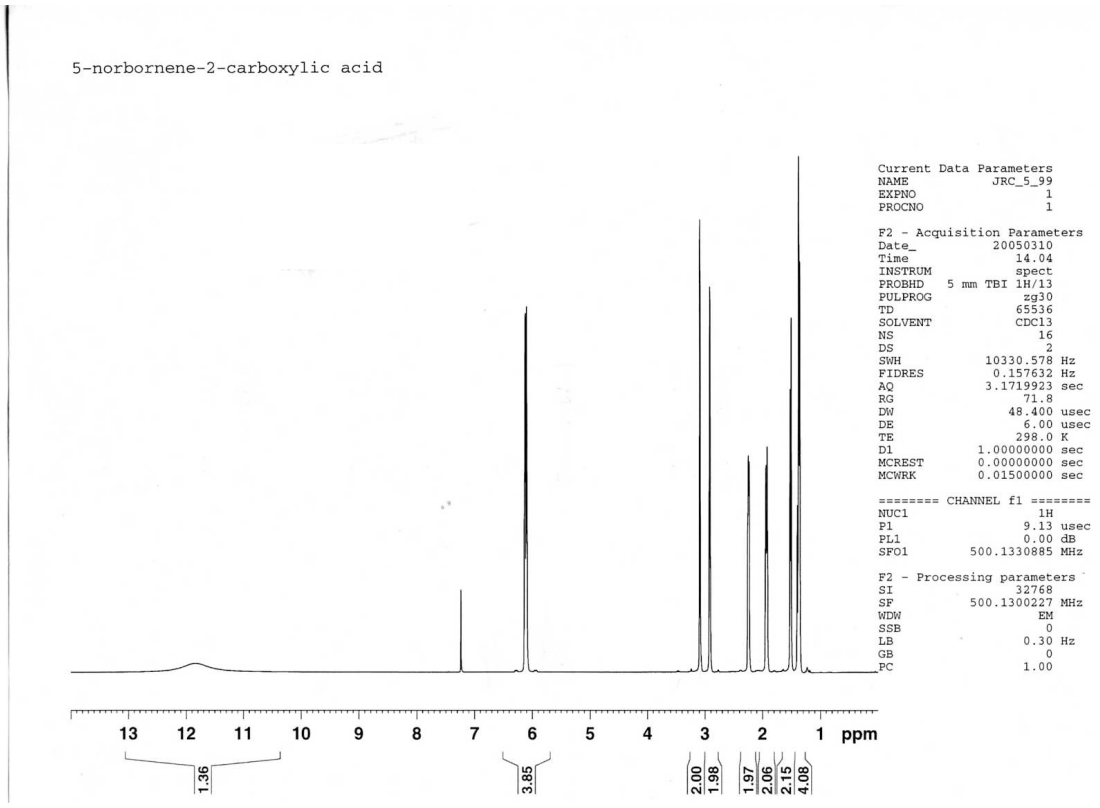

Figure A.2. ^{1}H NMR spectrum of 5-norbornene carboxylic acid (pure exo) after an iodolactonization reaction (see ref. 54 in Chapter 3) with an endo / exo mixture.

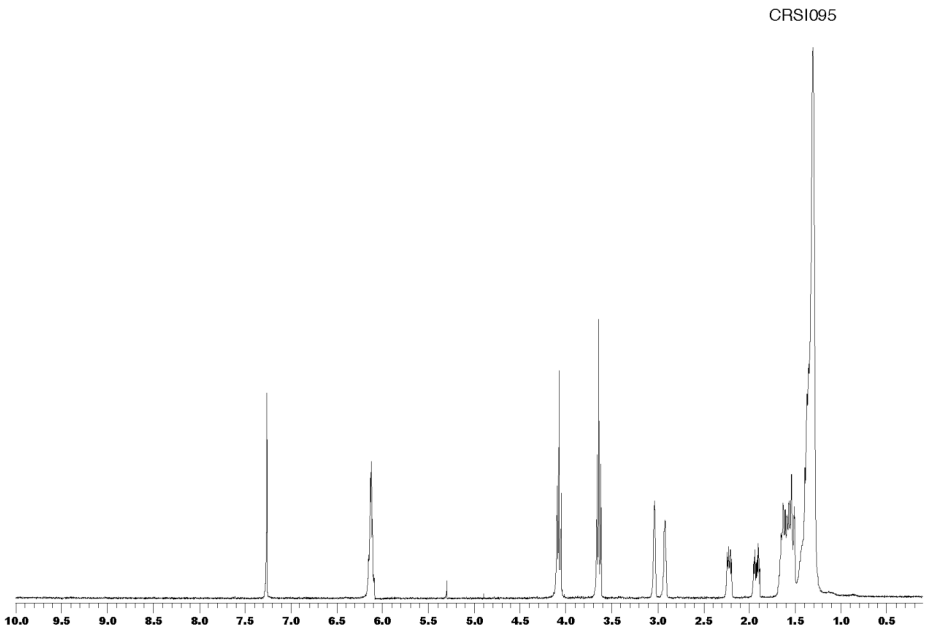

Figure A.3. ^{1}H NMR spectrum of compound **7** taken in $CDCl_3$.

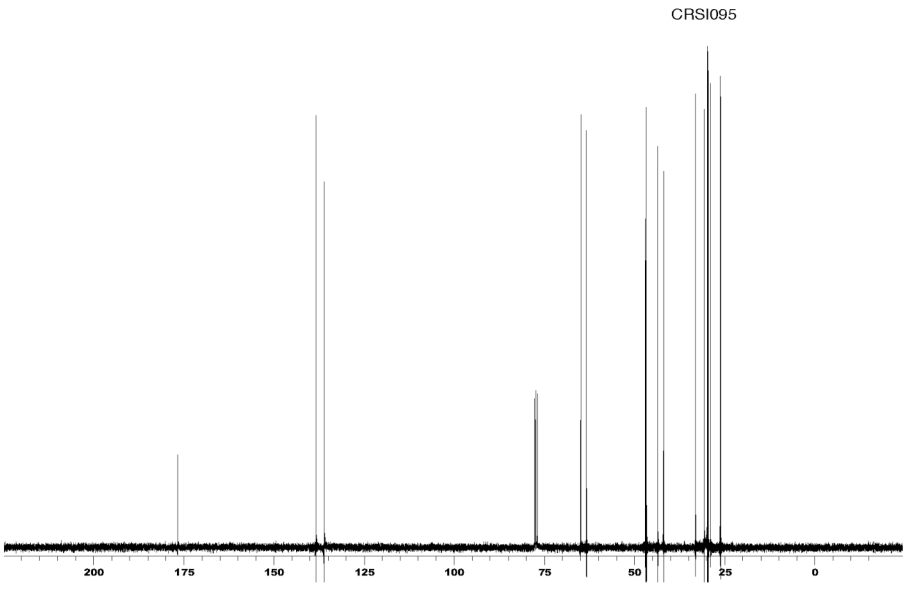

Figure A.4. ^{13}C NMR spectrum of compound **7** taken in $CDCl_3$.

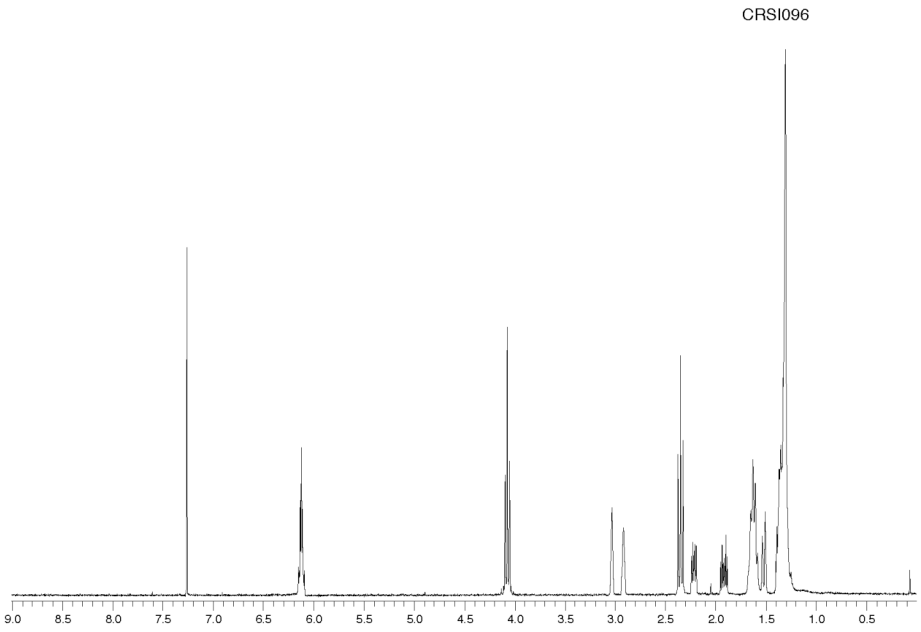

Figure A.5. ^{1}H NMR spectrum of compound **8** in $CDCl_3$.

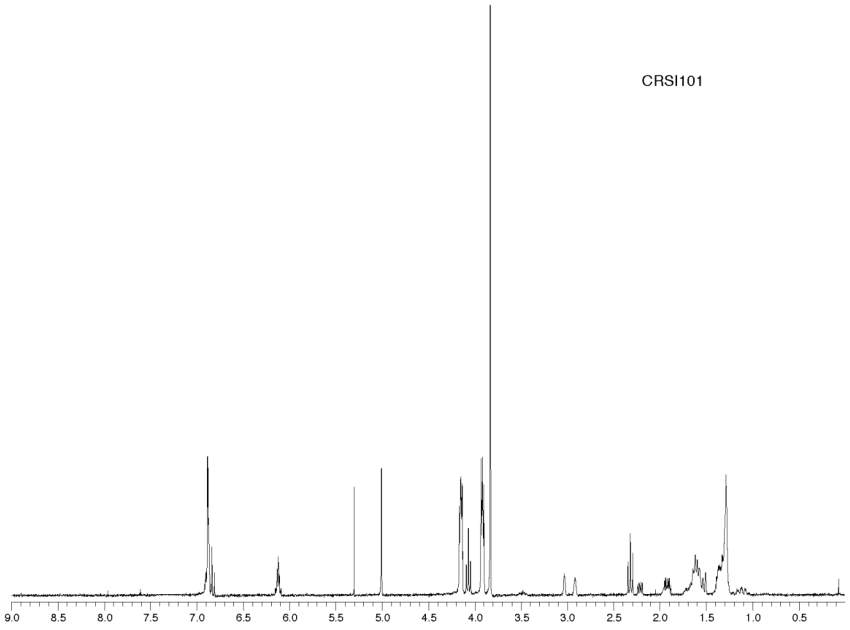

Figure A.6. ^{1}H NMR spectrum of compound **12** in CD_2Cl_2.

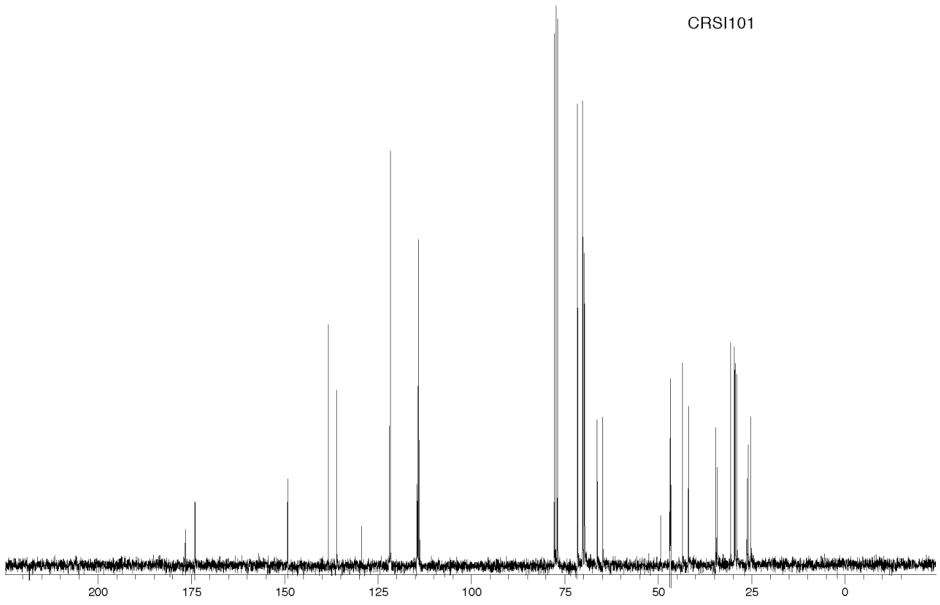

Figure A.7. ^{13}C NMR spectrum of compound **12** in $CDCl_3$.

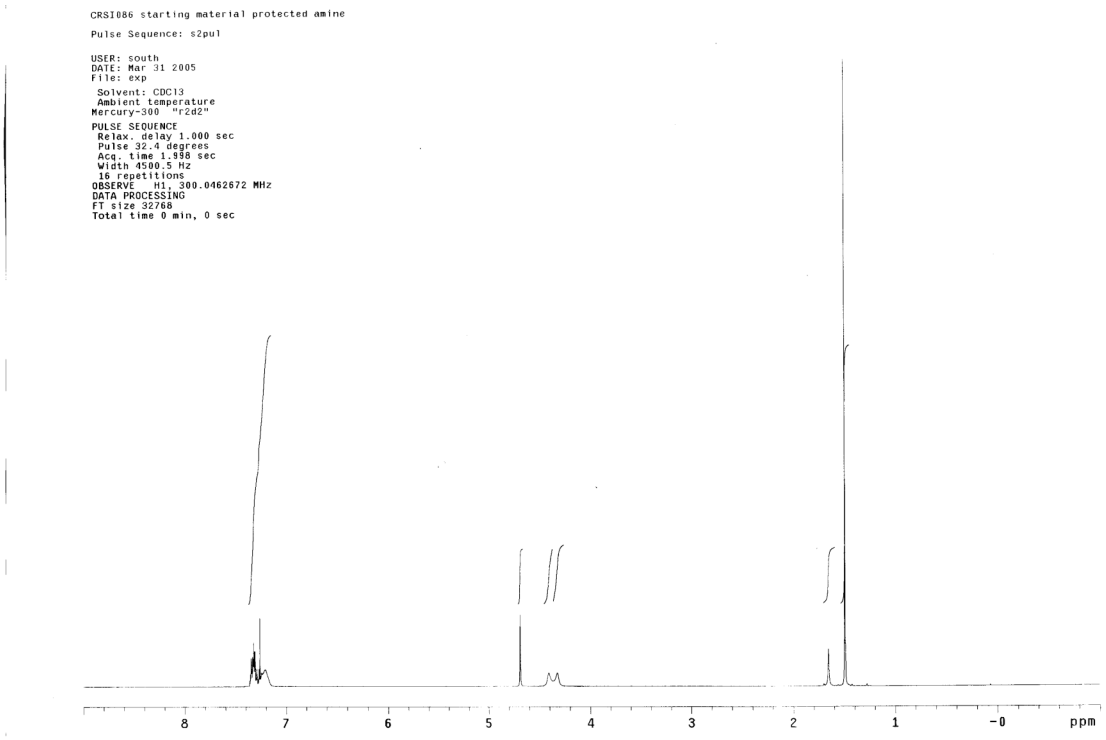

Figure A.8. ^{1}H NMR spectrum of compound **9** in $CDCl_3$.

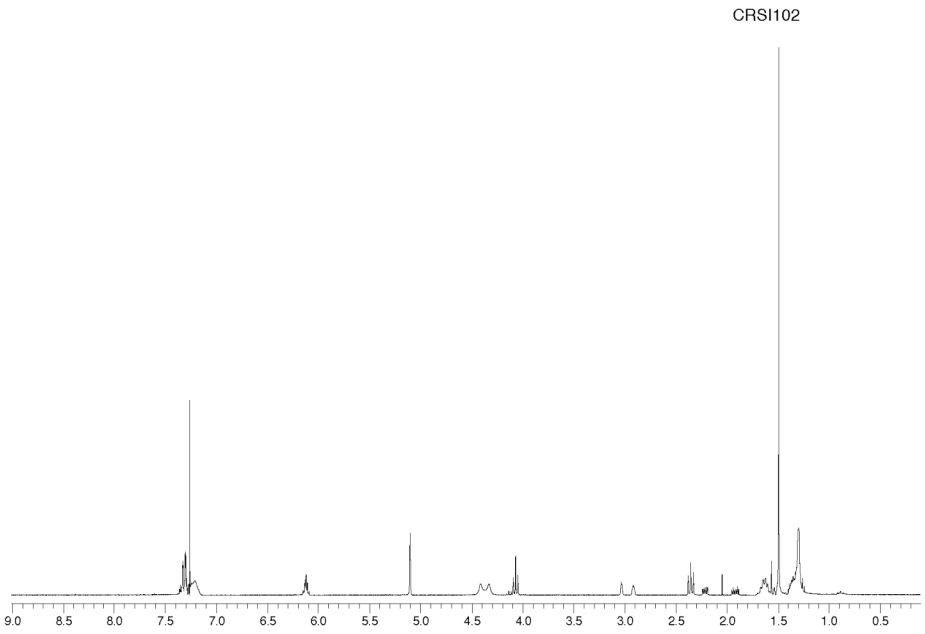

Figure A.9. ^{1}H NMR spectrum of compound **11** in $CDCl_3$.

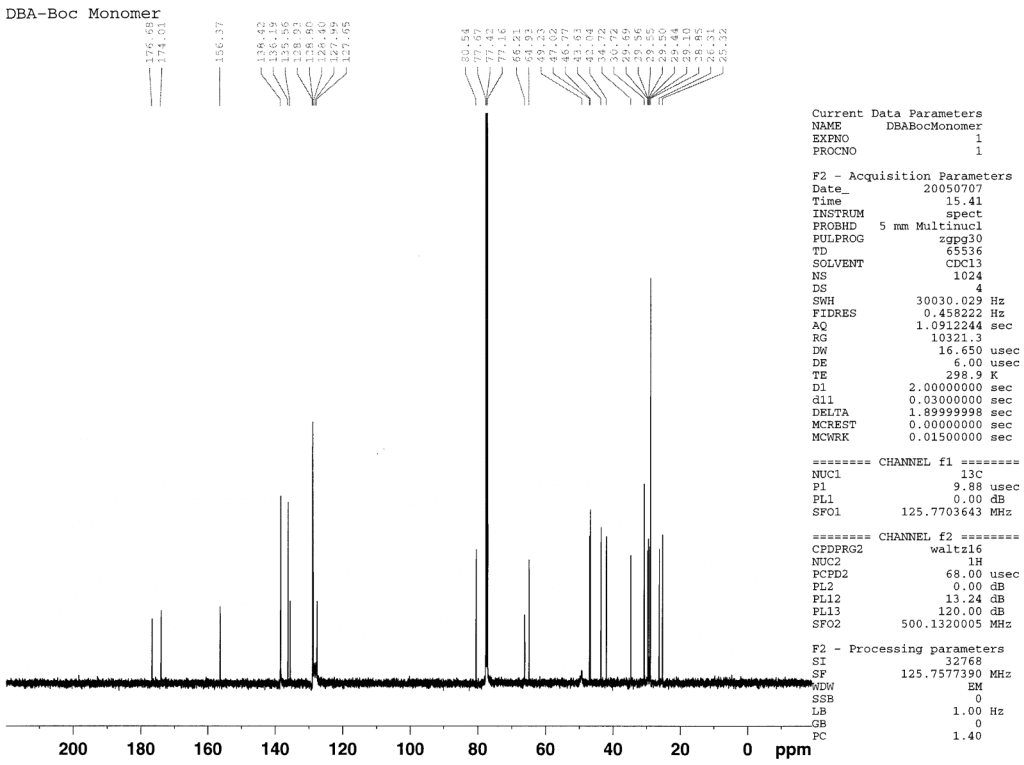

Figure A.10. ^{13}C spectrum of compound **11** in $CDCl_3$.

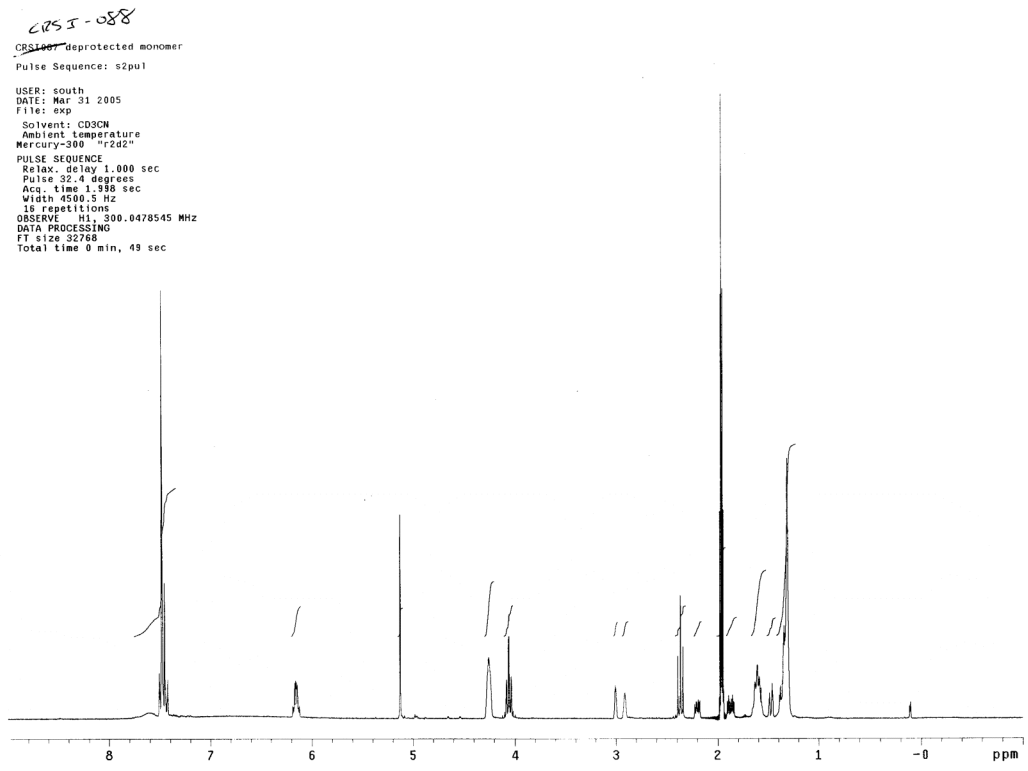

Figure A.11. ^{1}H NMR of compound **11** after deprotection with TFA (spectrum taken in $CDCl_3$).

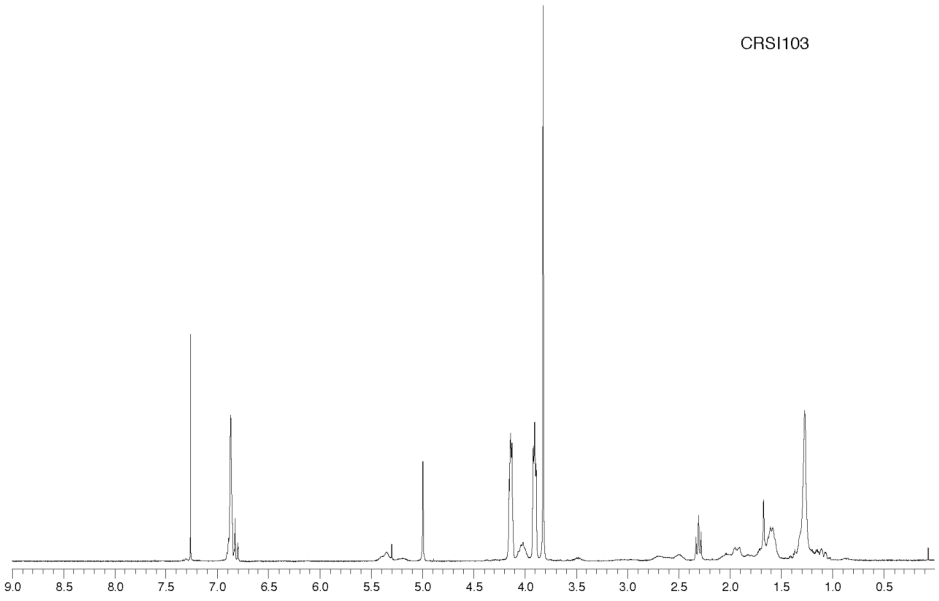

Figure A.12. ^{1}H NMR spectrum of polymer **14 (a-e)** in $CDCl_3$.

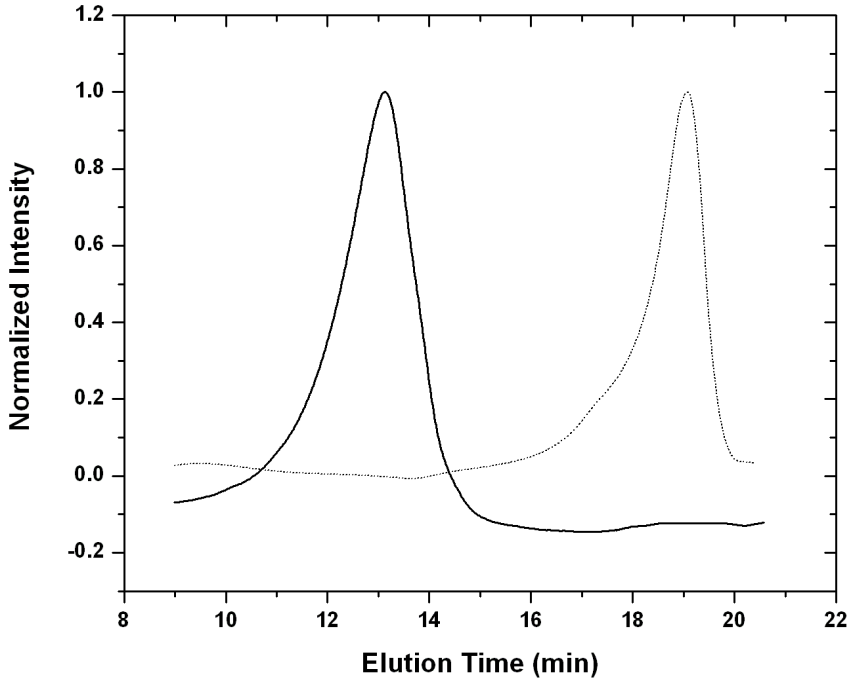

Figure A.13. Living Test for the polymerization of monomer **12**: GPC traces (eluant: CH_2Cl_2) of polymer **14** with [M]:[I] = 10:1 (dotted line) and polymer **14** with [M]:[I] = 210:1 (solid line). The solid-line GPC trace is the result of adding 200 equivalents of monomer **12** to a "living" solution of a decamer of **14** in CH_2Cl_2 (GPC trace shown as dotted line).

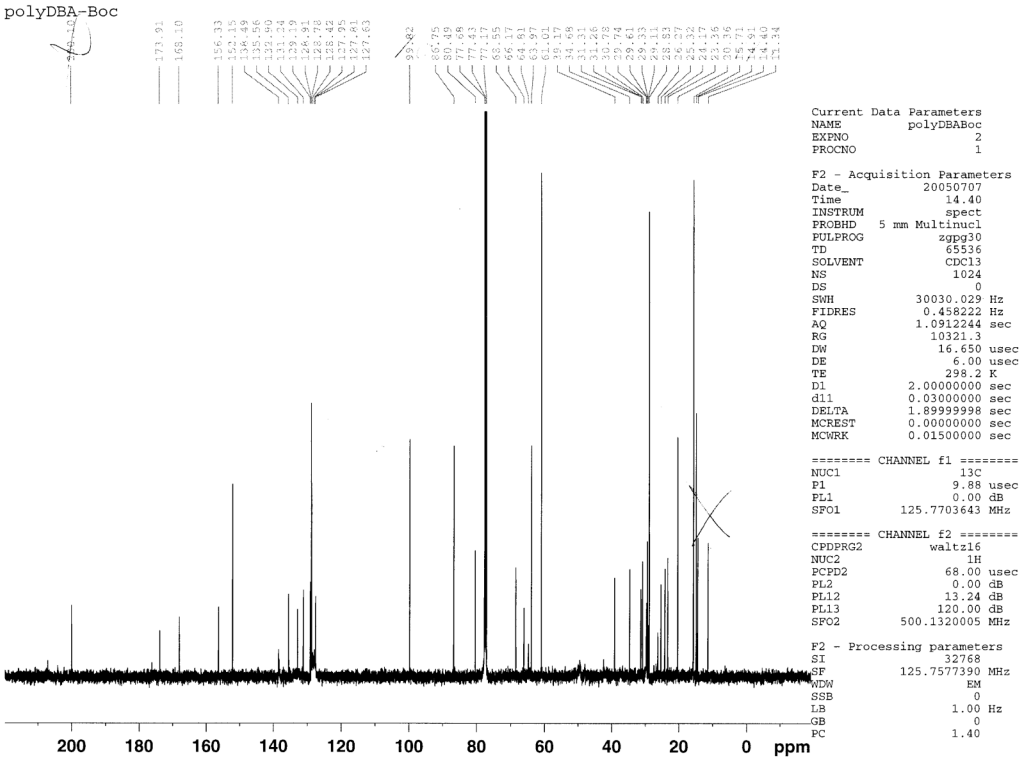

Figure A.14. ^{13}C NMR spectrum of polymer **13 (a-e)** in $CDCl_3$.

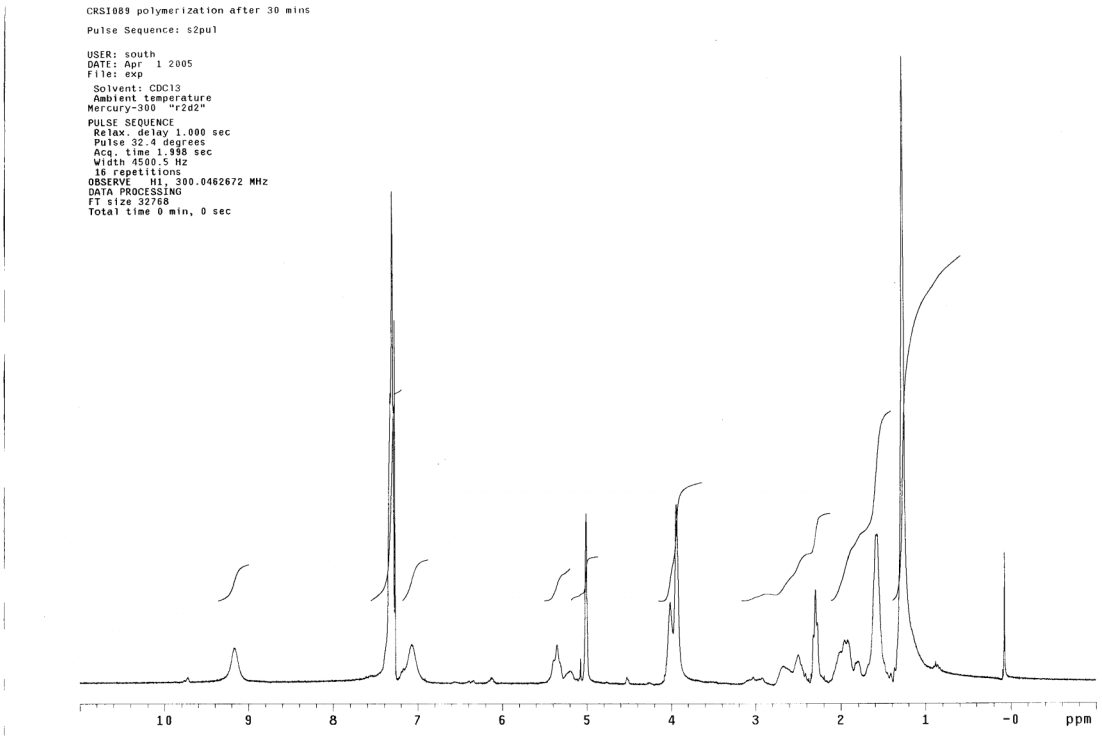

Figure A.15. ^{1}H NMR spectrum of polymer **15** taken in $CDCl_3$.

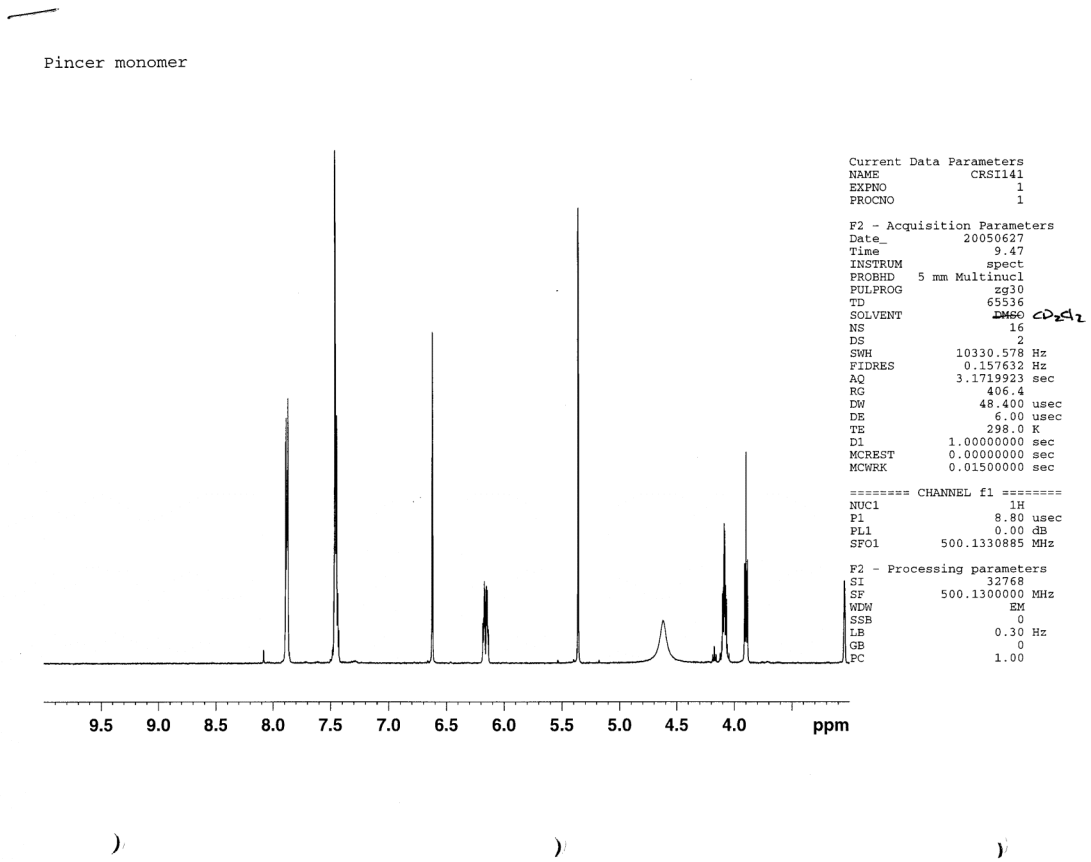

Figure A.16. ^{1}H NMR spectrum of monomer **16** taken in CD_2Cl_2.

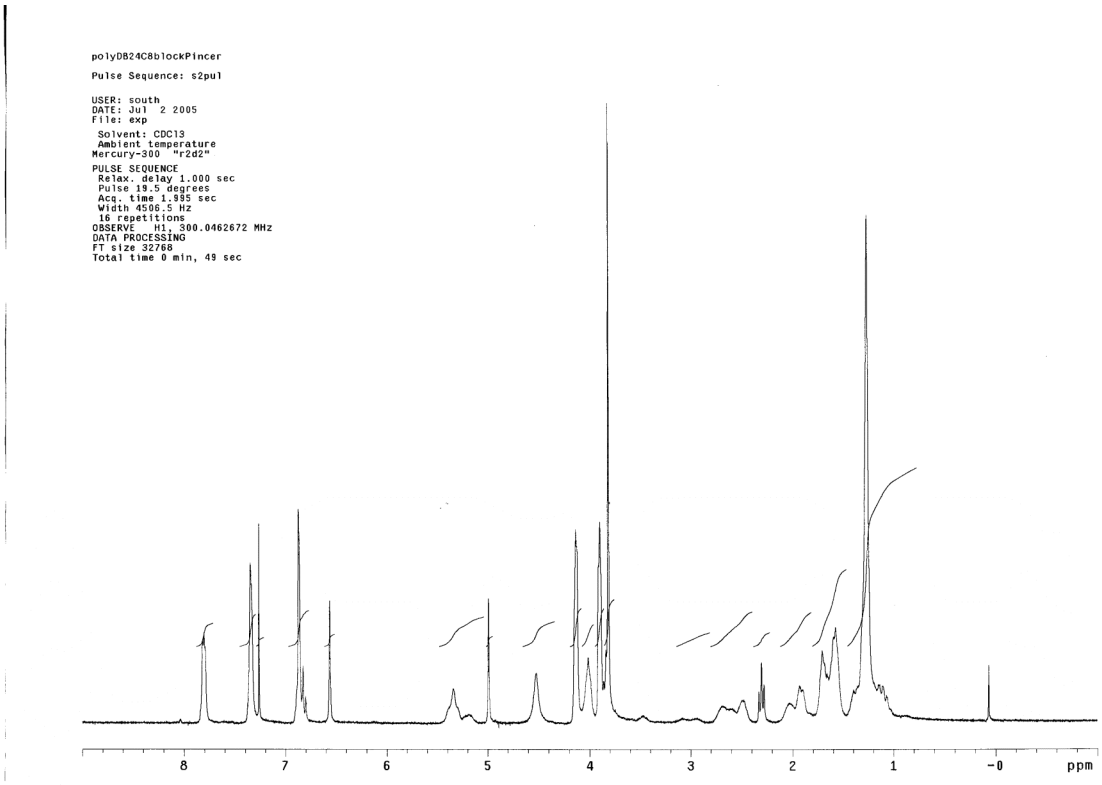

Figure A.17. ^{1}H NMR spectrum of polymer **18** taken in $CDCl_3$.

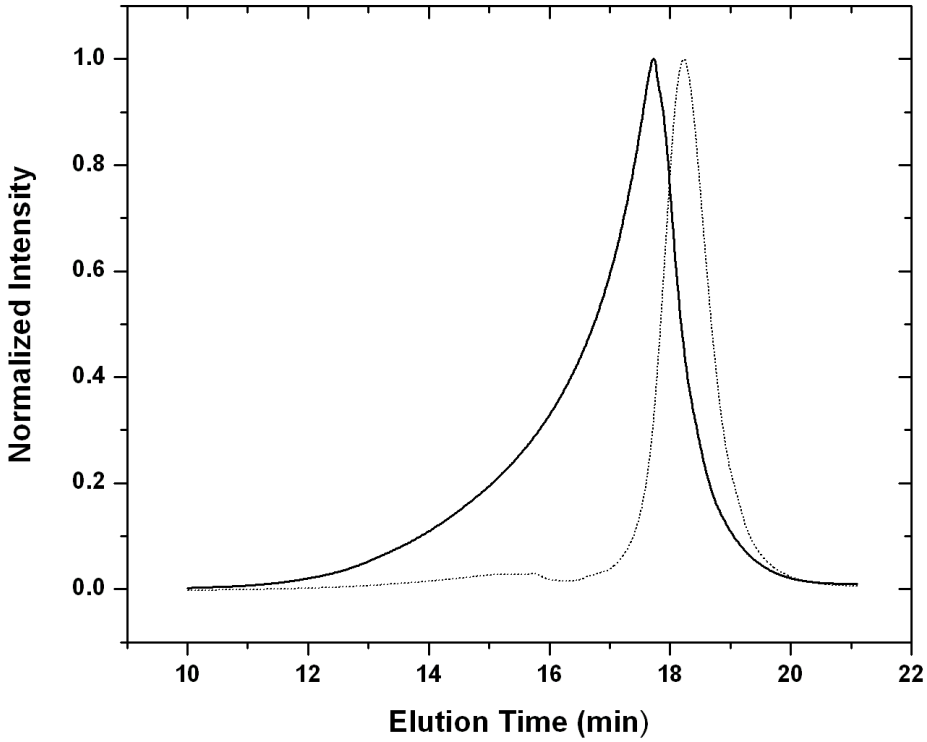

Figure A.18. GPC trace of block copolymer **18** (solid line) after the addition of **1** equivalent of monomer **12** to a living solution of polymer **17** in CH_2Cl_2 (GPC trace shown as dotted line).

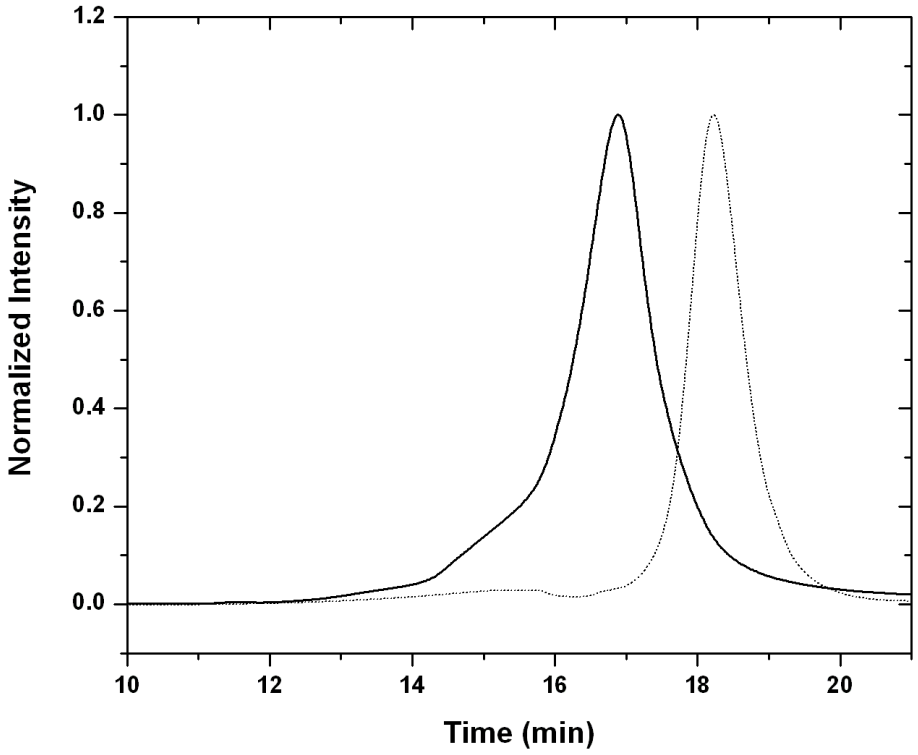

Figure A.19. GPC trace of block copolymer **19** (solid line) after the addition of **1** equivalent of monomer **11** to a living solution of polymer **17** in CH_2Cl_2 (GPC trace shown as dotted line).

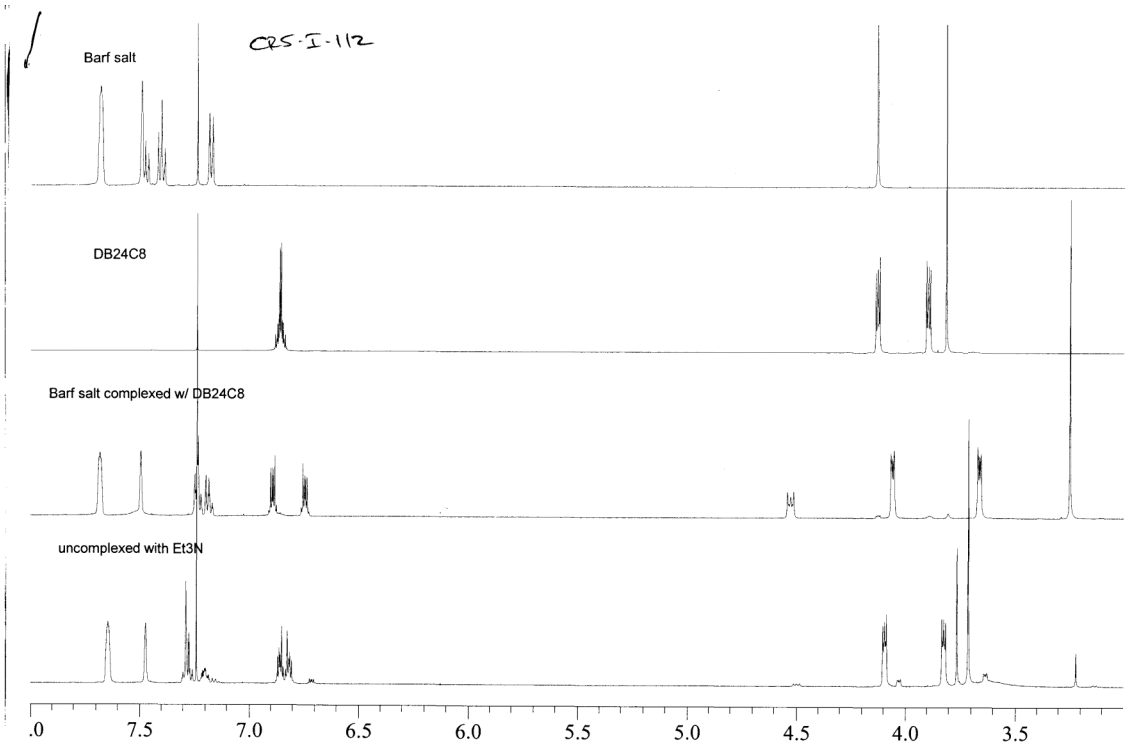

Figure A.20. Reference ^{1}H NMR spectra taken in CD_2Cl_2 for complexation studies. 1st spectrum (from top to bottom): compound **2-BArF**; 2nd spectrum: compound **3**; 3rd spectrum: 1:1 complex with **2-BArF** and **3**; 4th spectrum: decomplexed **2-BArF** and **3** after the addition of Et_3N.

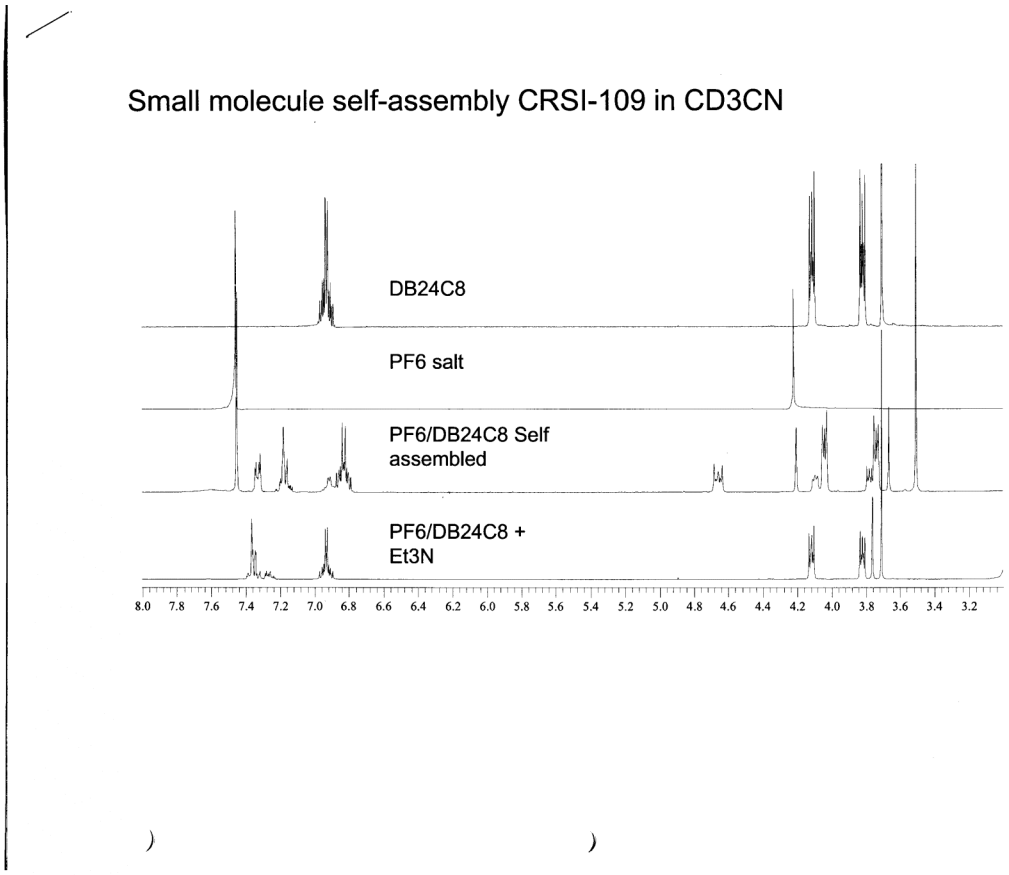

Figure A.21. Reference ^{1}H NMR spectra taken in CD_3CN for complexation studies (showing incomplete complexation). 1st spectrum (from top to bottom): compound **3**; 2nd spectrum: compound **2-PF$_6$**; 3rd spectrum: 1:1 complex with **2-PF$_6$** and 3; 4th spectrum: decomplexed **2-PF$_6$** and **3** after the addition of Et_3N.

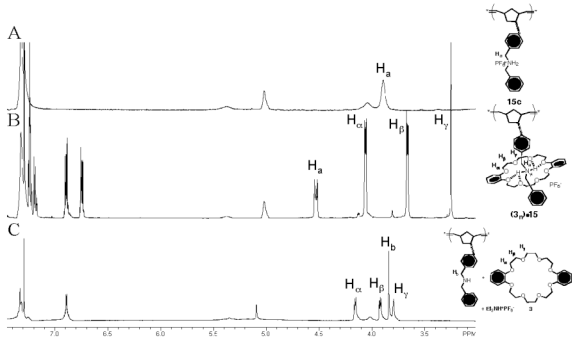

Figure A.22. ^{1}H NMR spectra displaying complexation studies with polymer **15** and compound **3** taken in $CDCl_3$**.**

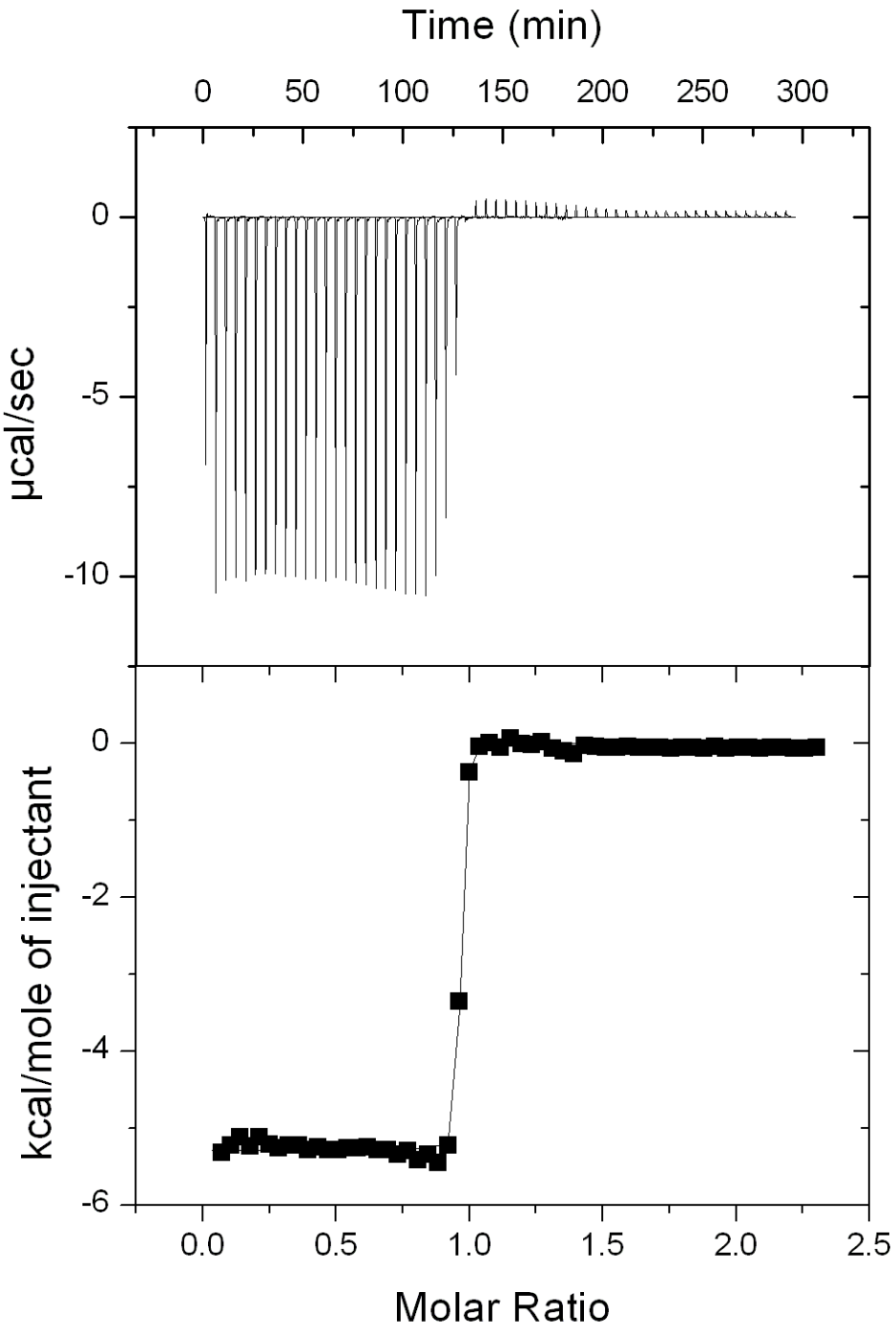

Figure A.23. ITC Data for the titration of **2-BArF** into polymer **14c**.

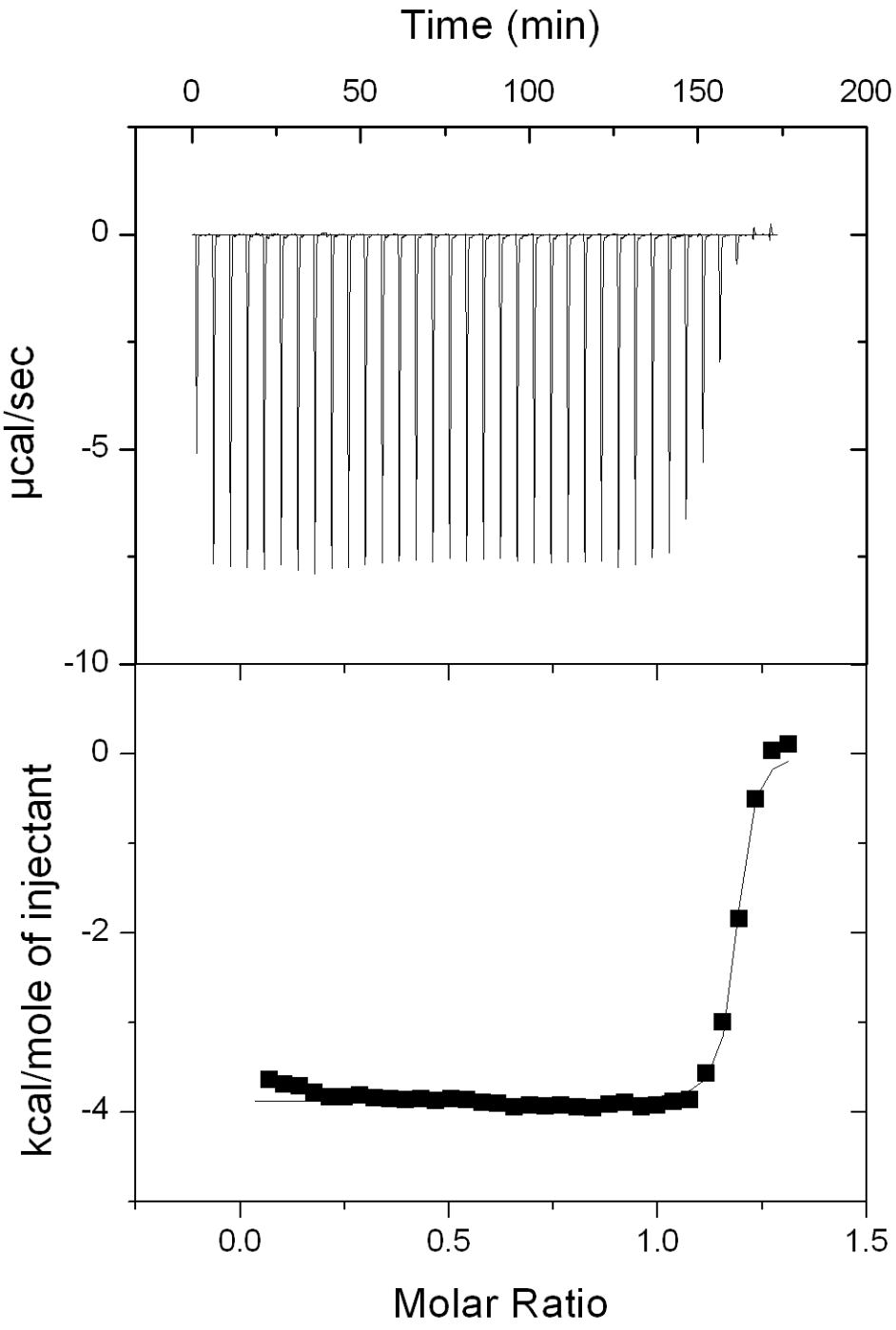

Figure A.24. ITC Data for the titration of **3** into polymer **15**.

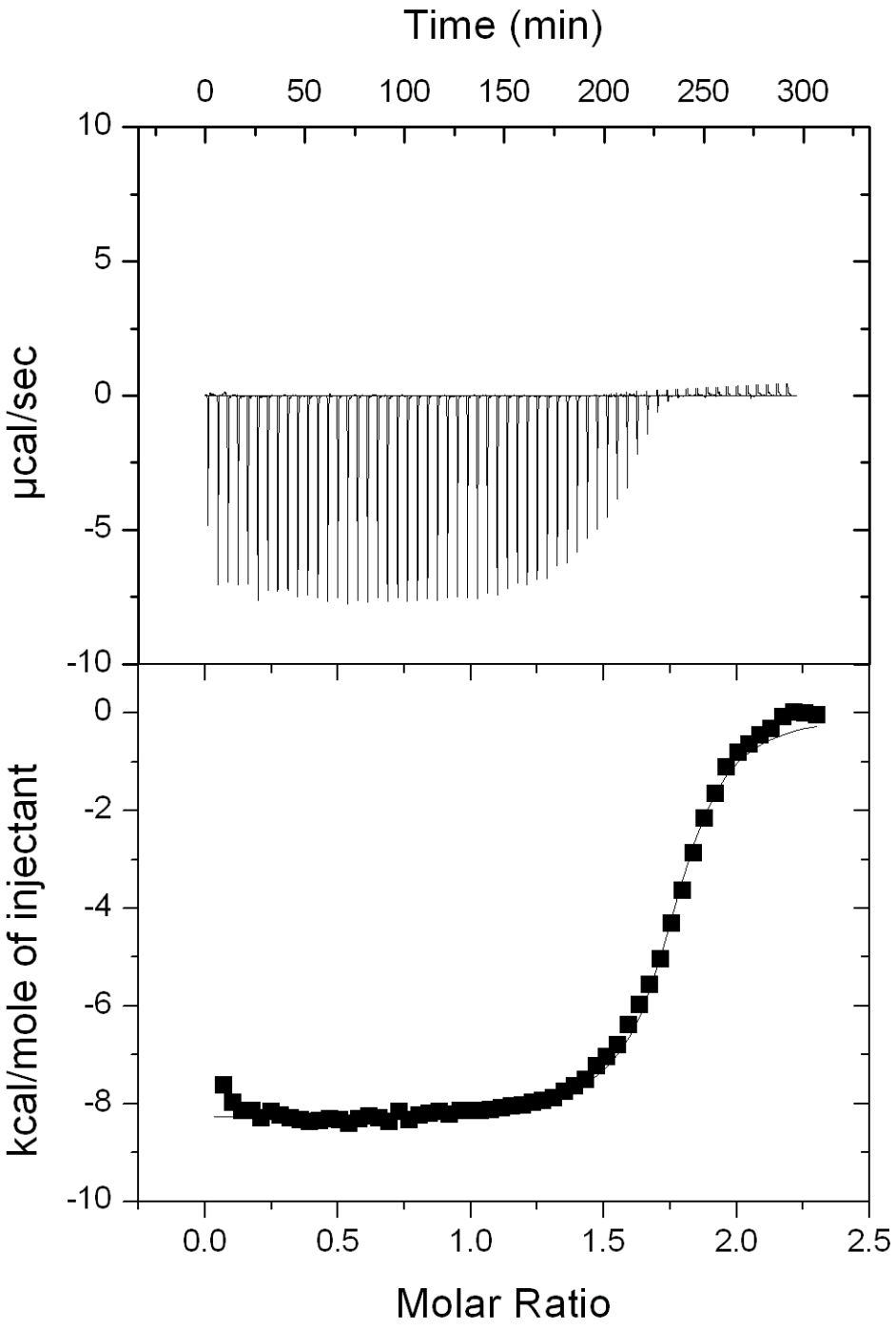

Figure A.25. ITC Data for the titration of **2-BArF** into polymer **18**.

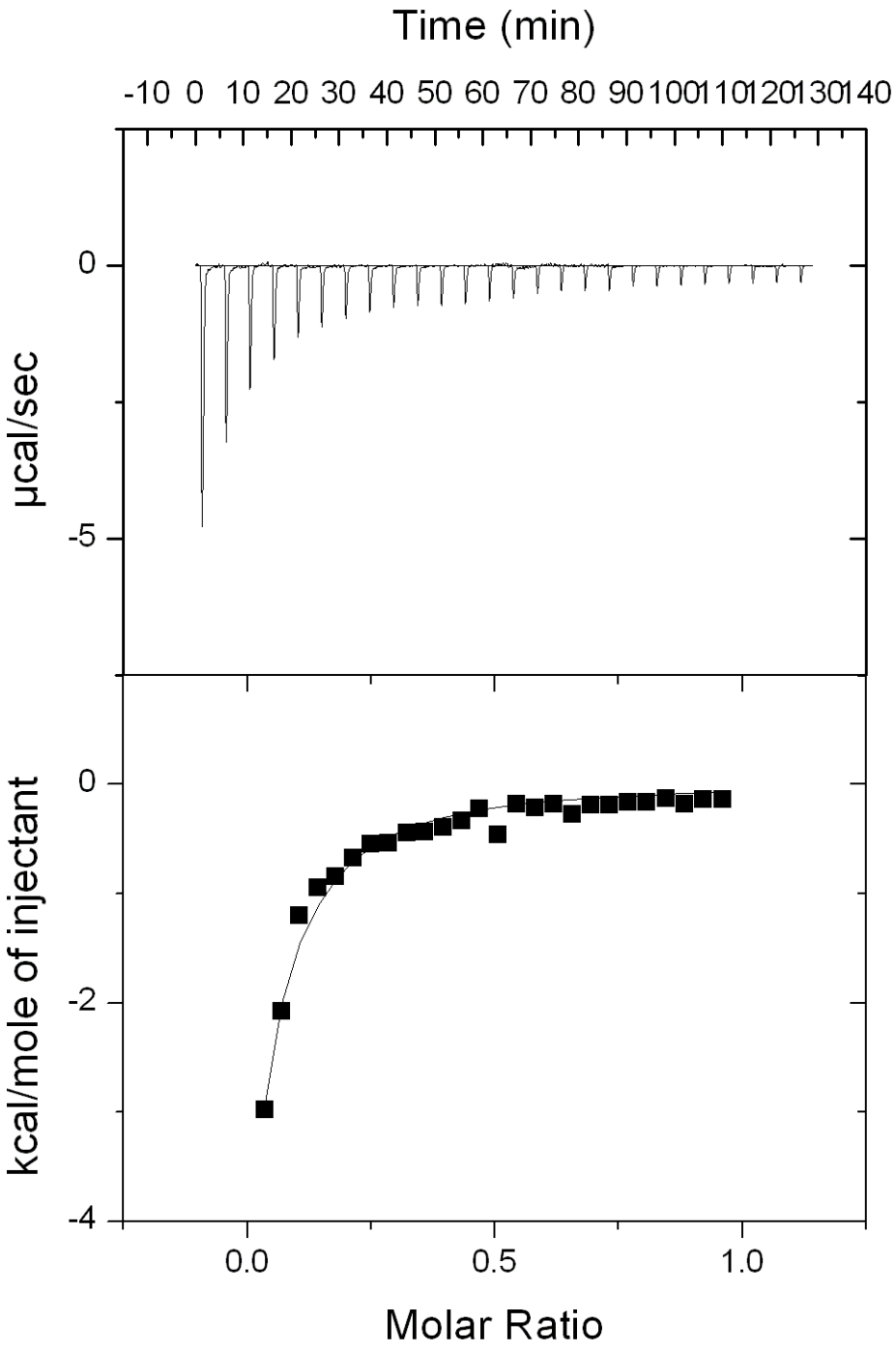

Figure A.26. ITC Data for the titration of **3** into polymer **5„-20**.

APPENDIX B

Supplemental Information for Chapter 4

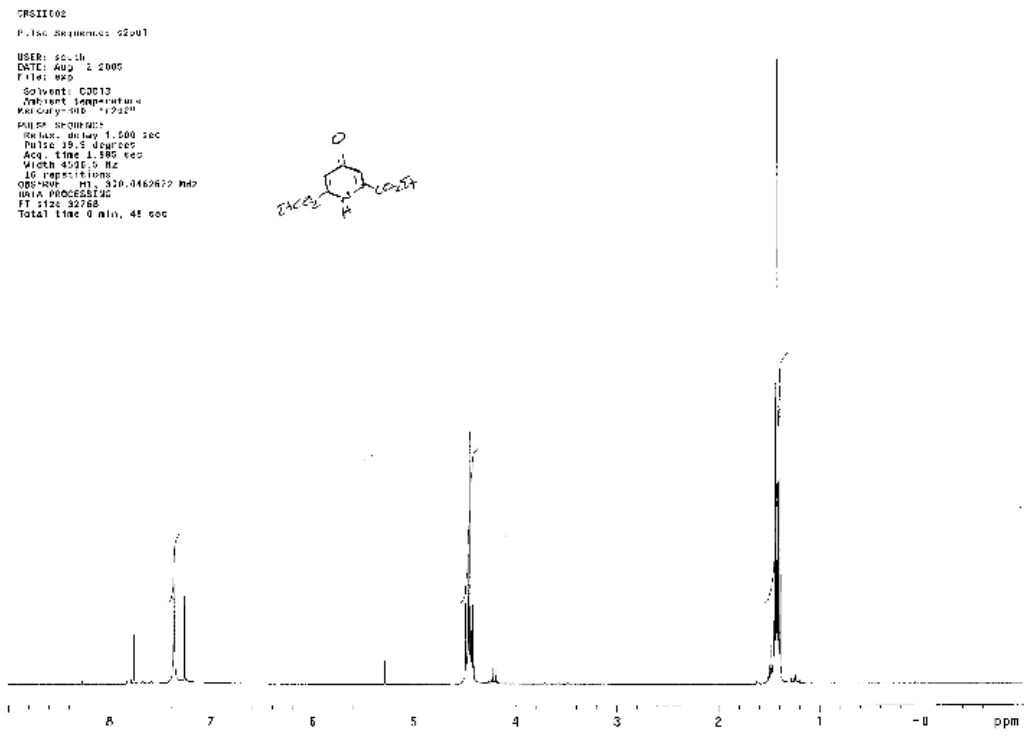

Figure B.1. Ethyl carboxylate used in DAP monomer synthesis.

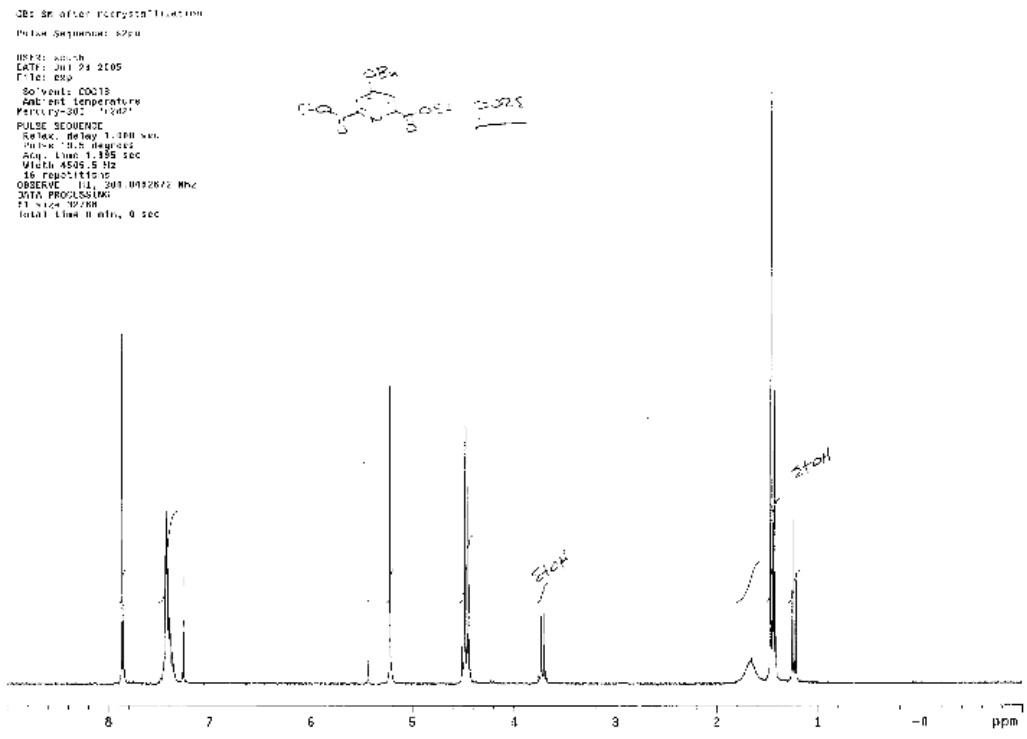

Figure B.2. Benzyl protected starting material used in DAP monomer synthesis.

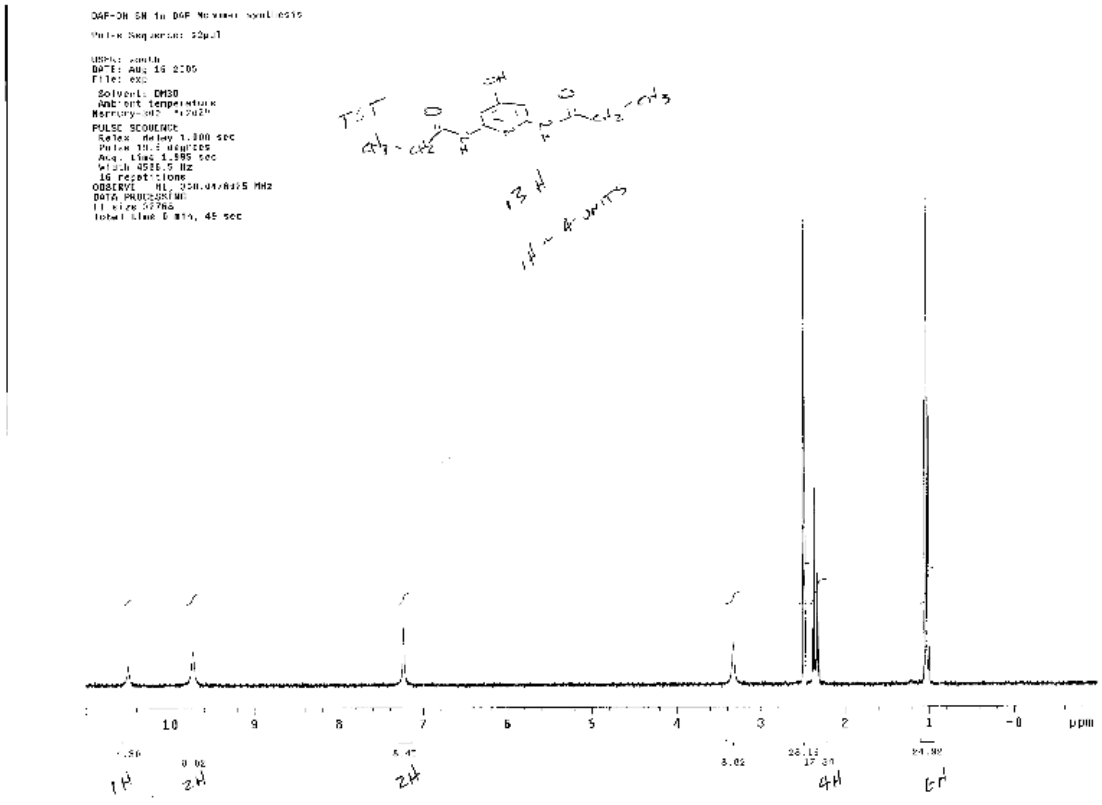

Figure B.3. Hydrogenated amide used in DAP monomer synthesis.

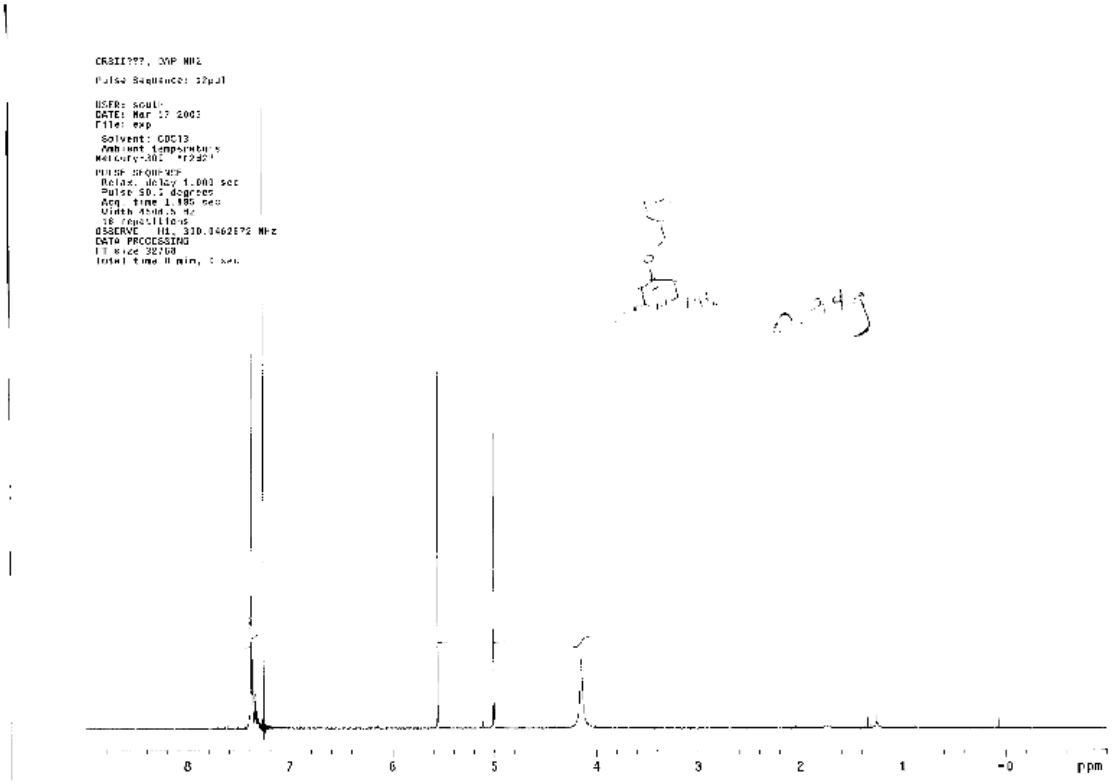

Figure B.4. Diamine used in DAP monomer synthesis.

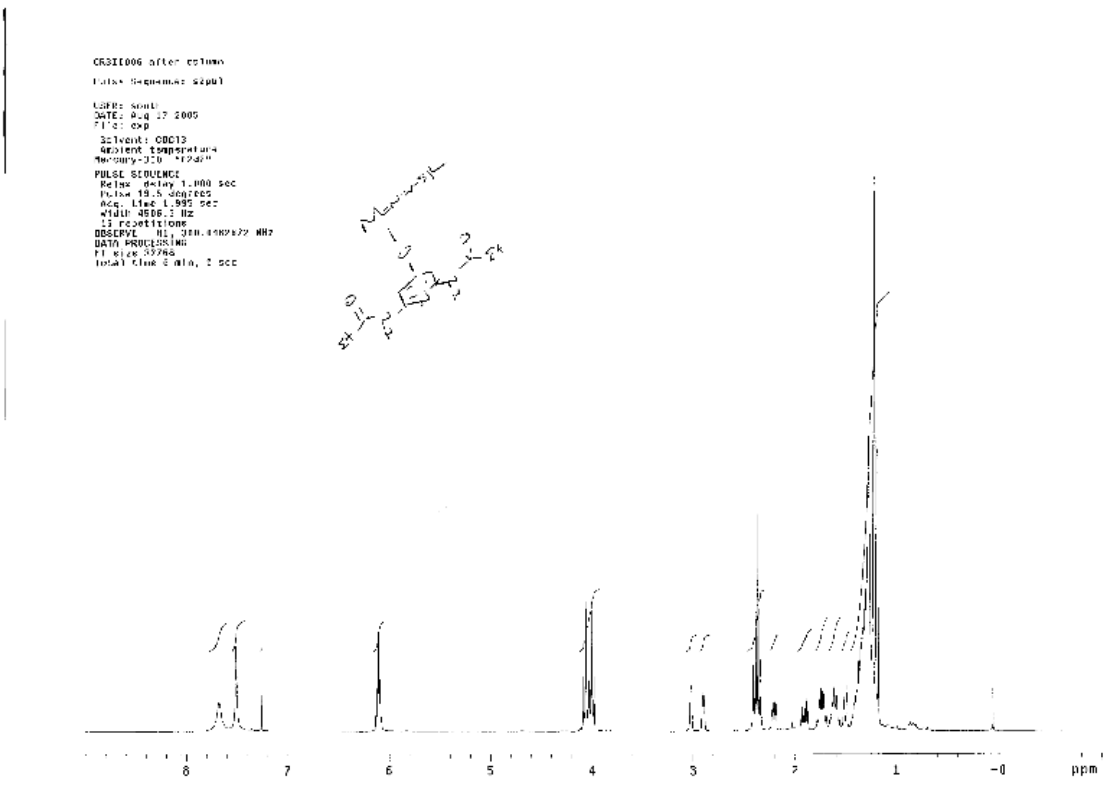

Figure B.5. Diamidopyridine norbornene monomer.

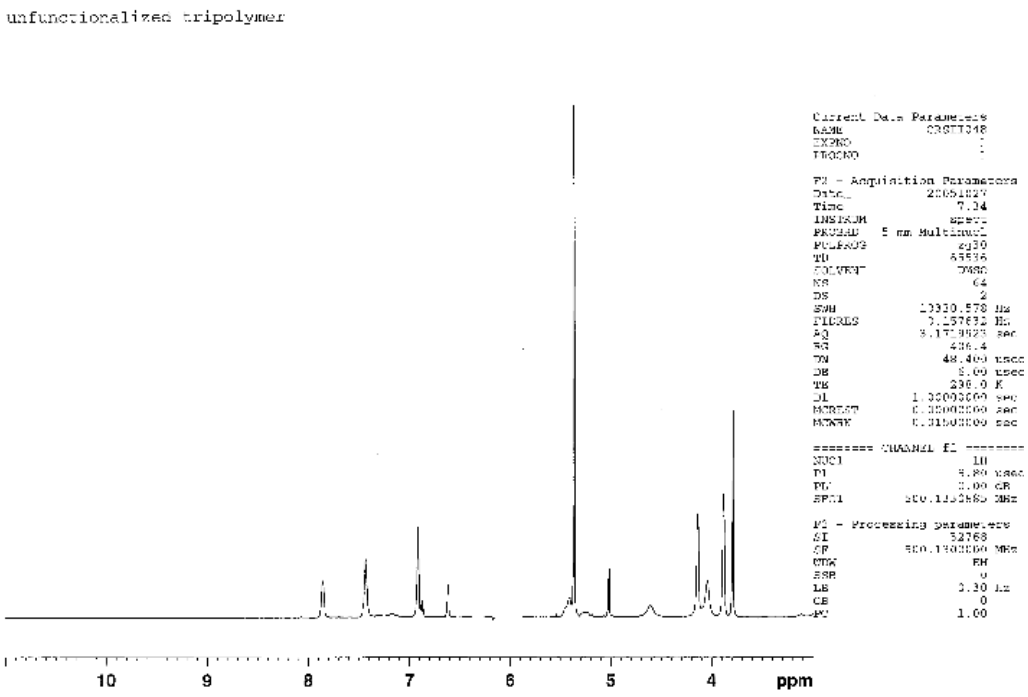

Figure B.6. Terpolymer **5a**.

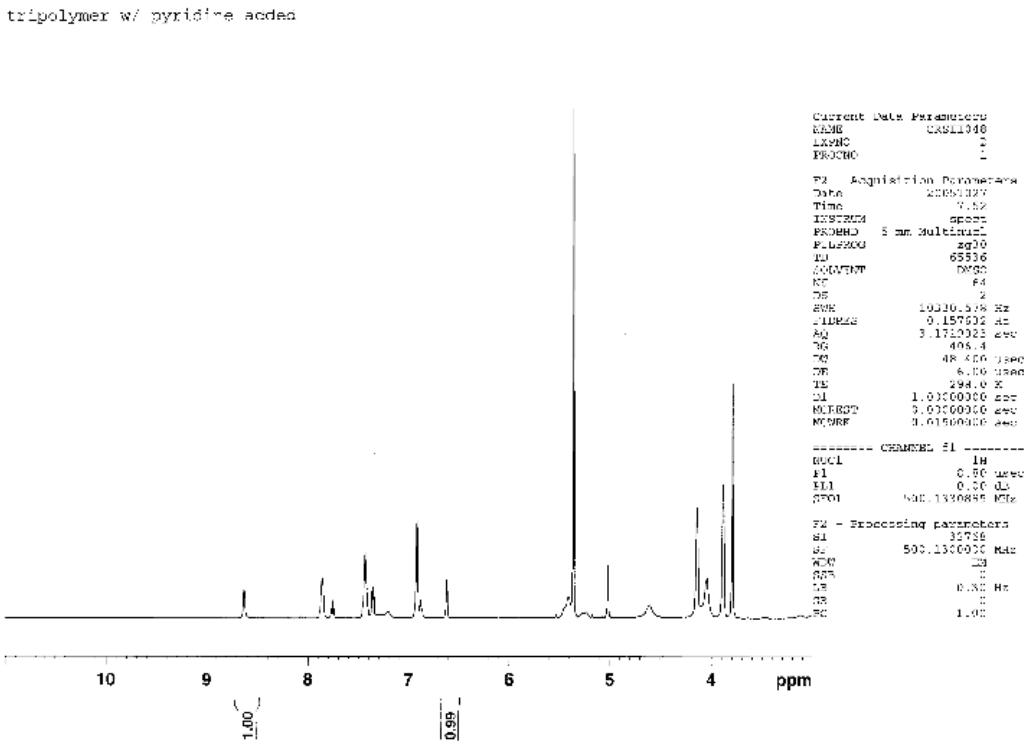

Figure B.7. Terpolymer with pyridine added.

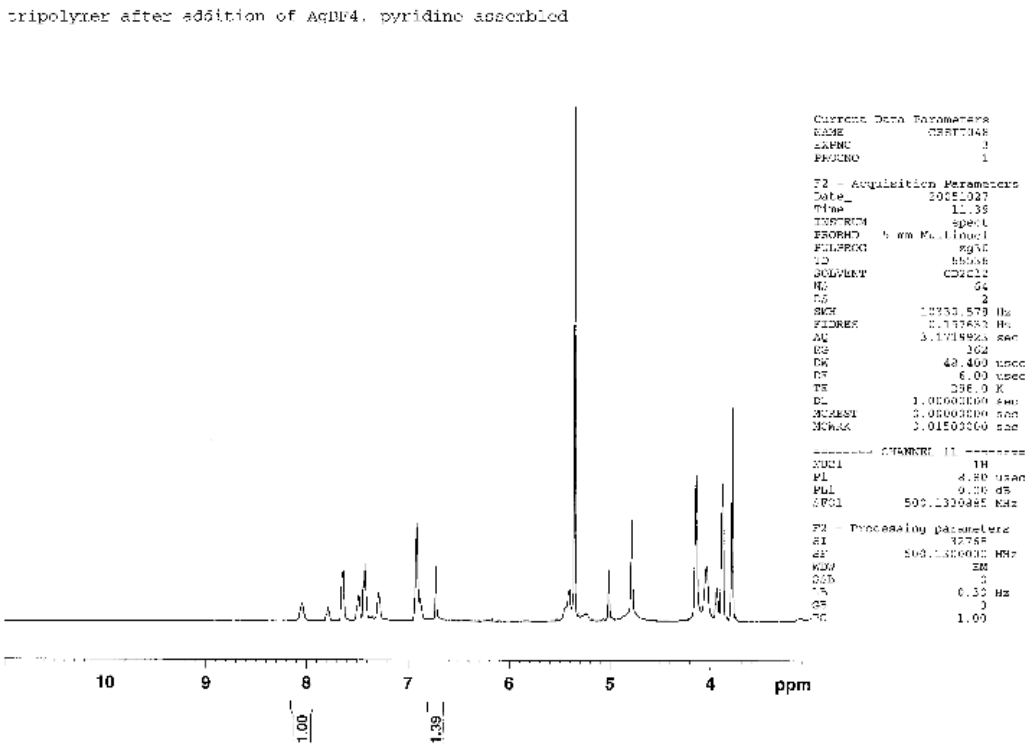

Figure B.8. Terpolymer with pyridine assembled.

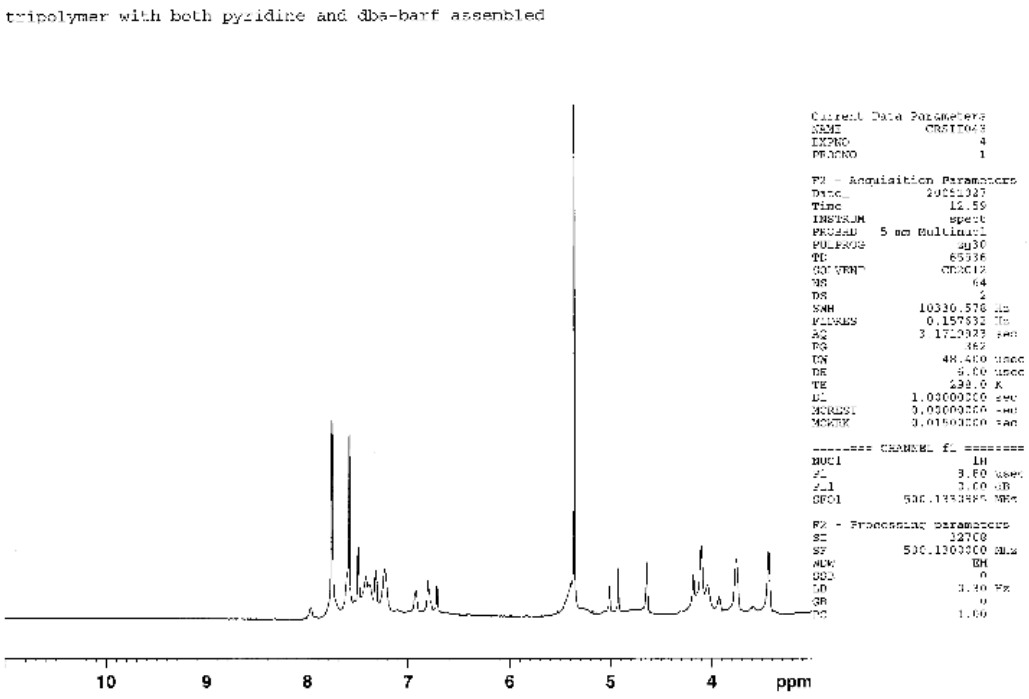

Figure B.9. Terpolymer with pyridine and DBA assembled.

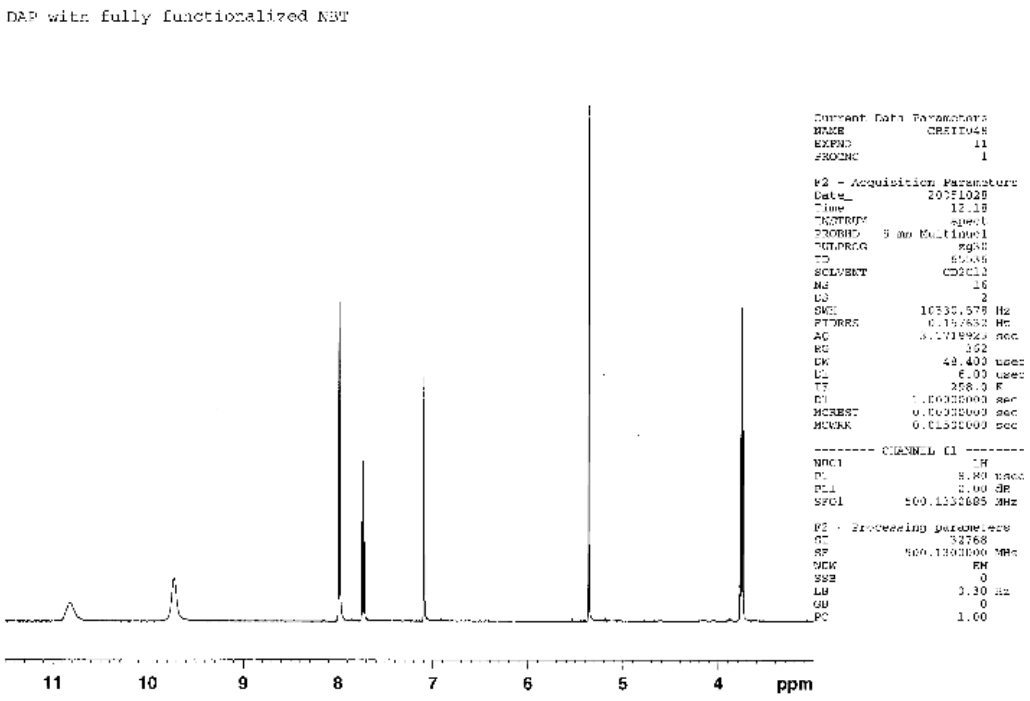

Figure B.10. Reference spectum with DAP bound to NBT.

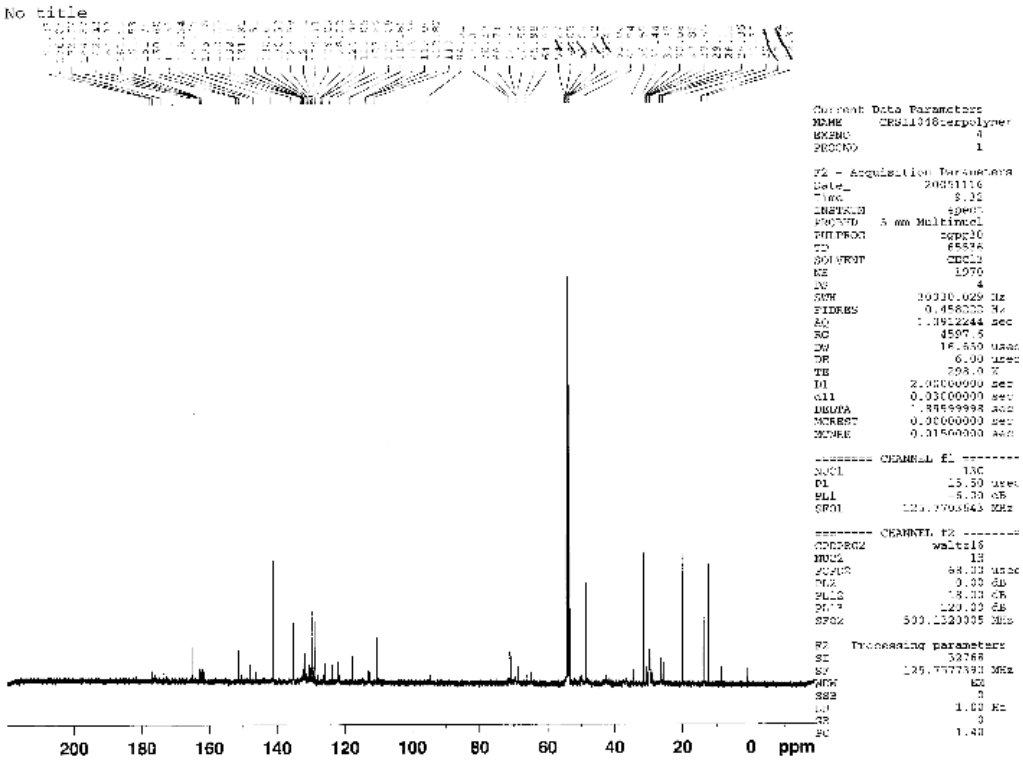

Figure B.11. Terpolymer ^{13}C NMR spectrum

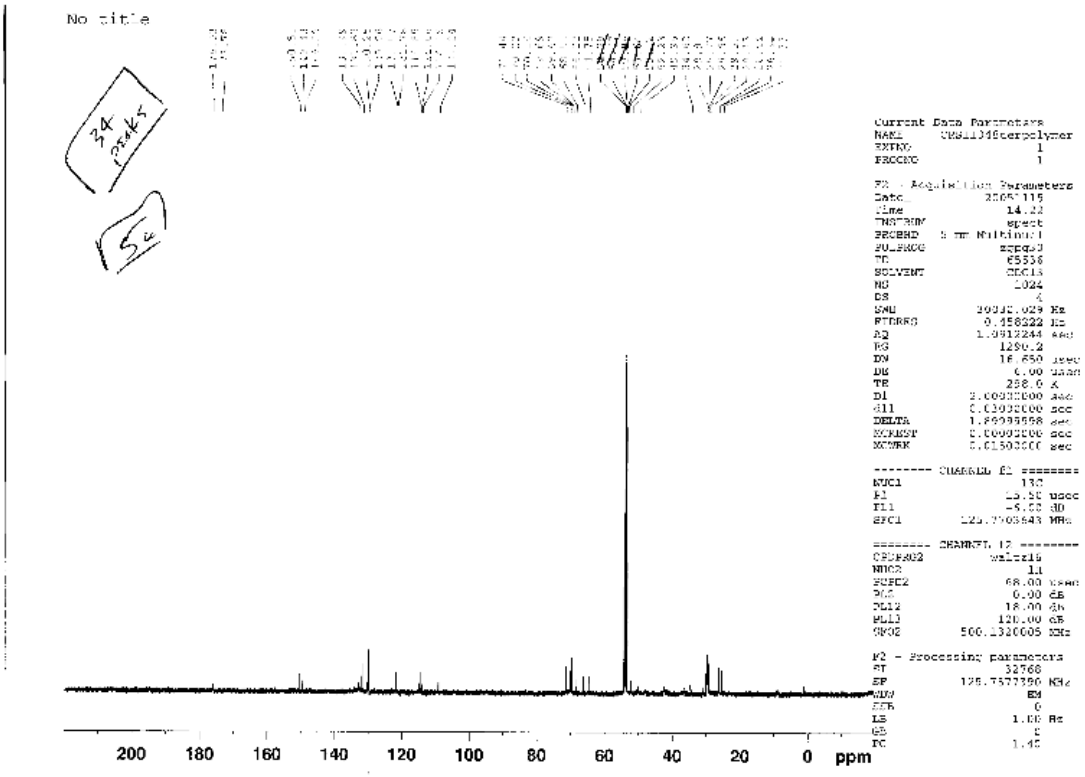

Figure B.12. Functionalized Terpolymer ^{13}C NMR spectrum.

APPENDIX C

Supplemental Information for Chapter 5.

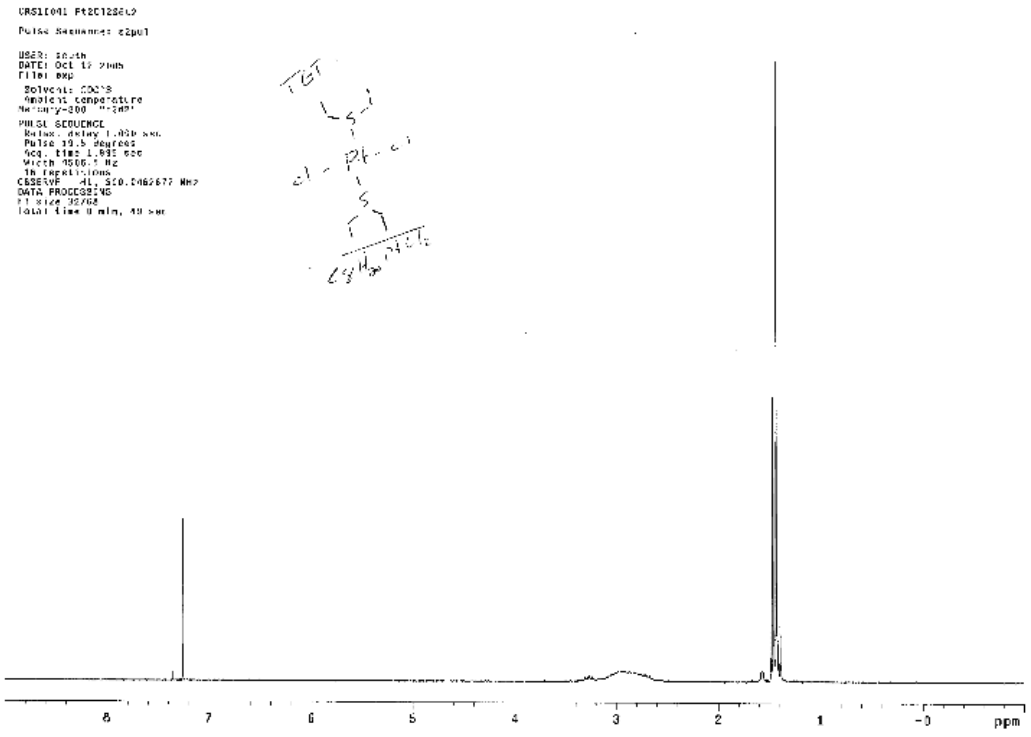

Figure C.1. $PtCl_2(SEt_2)_2$

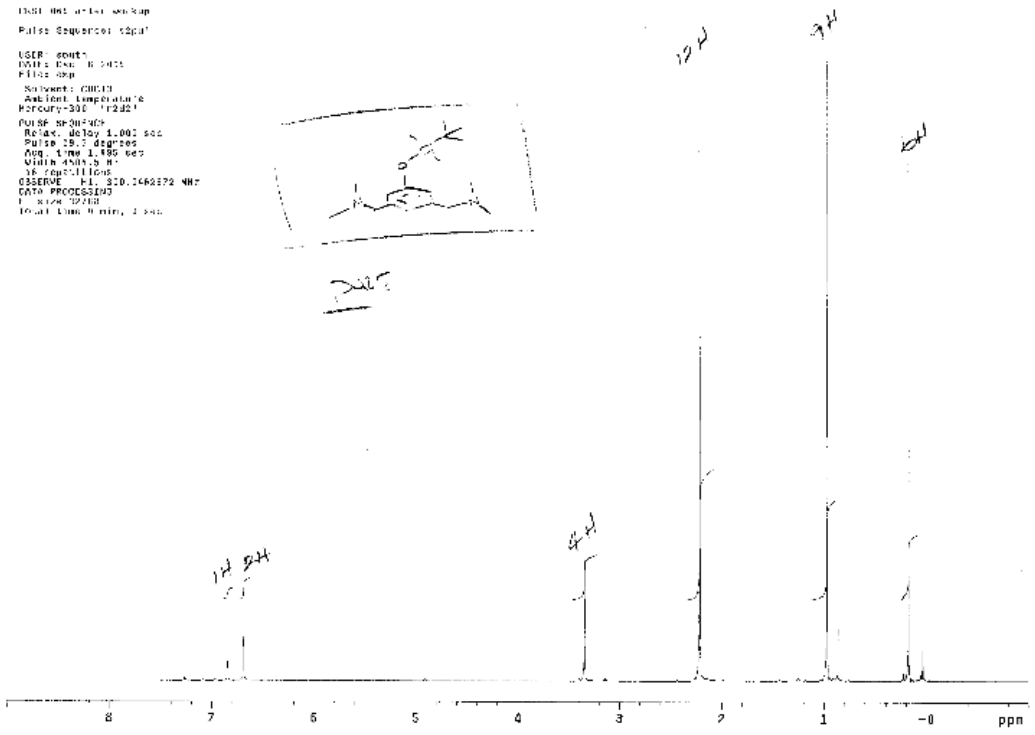

Figure C.2. Diamine used in Pt Pincer complex synthesis.

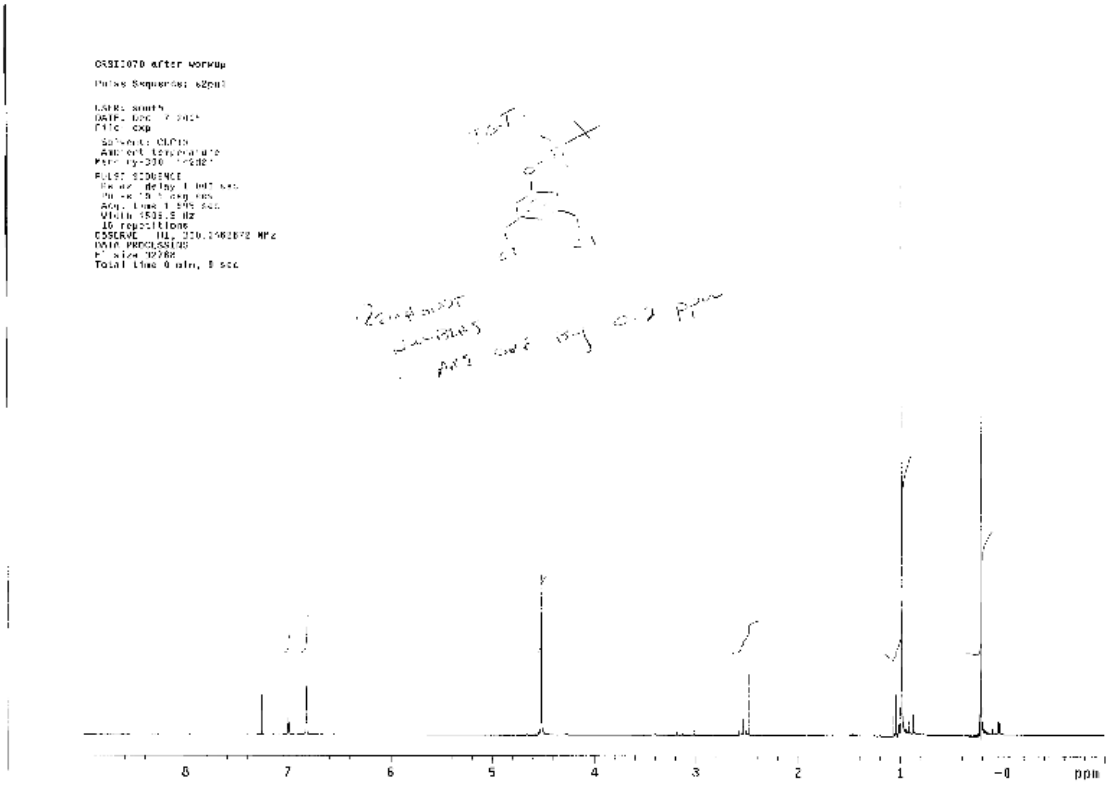

Figure C.3. Dichloride precursor to diamine.

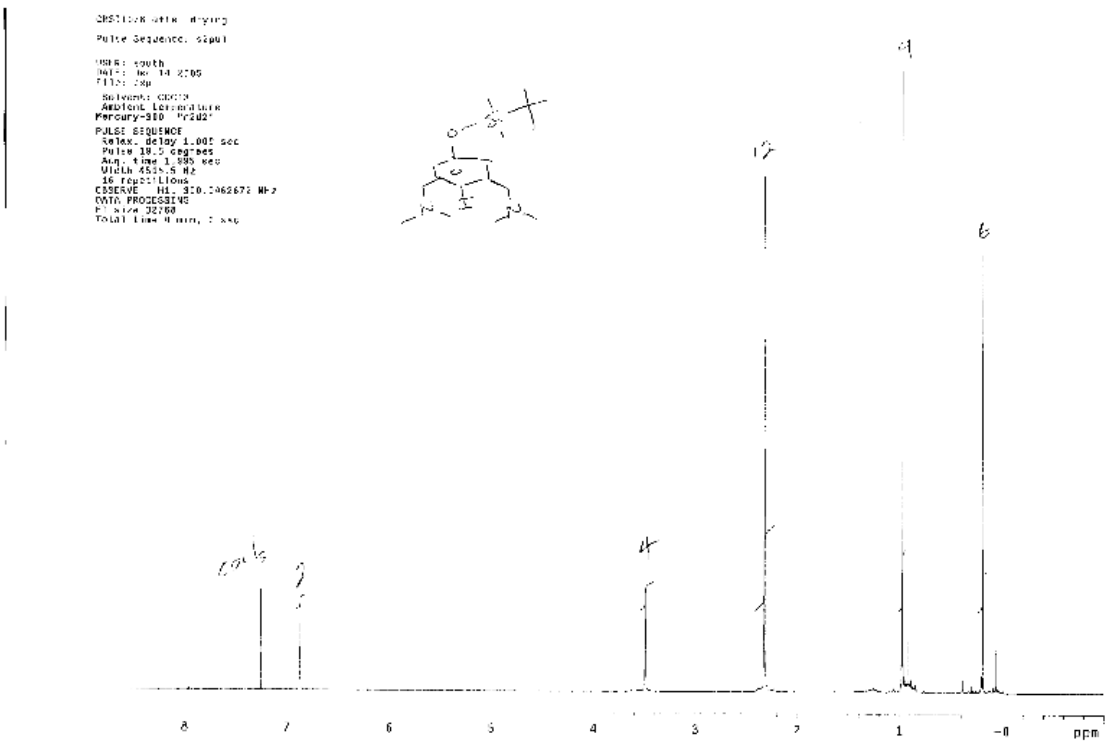

Figure C.4. Iodated diamine precursor to metallated Pincer complex.

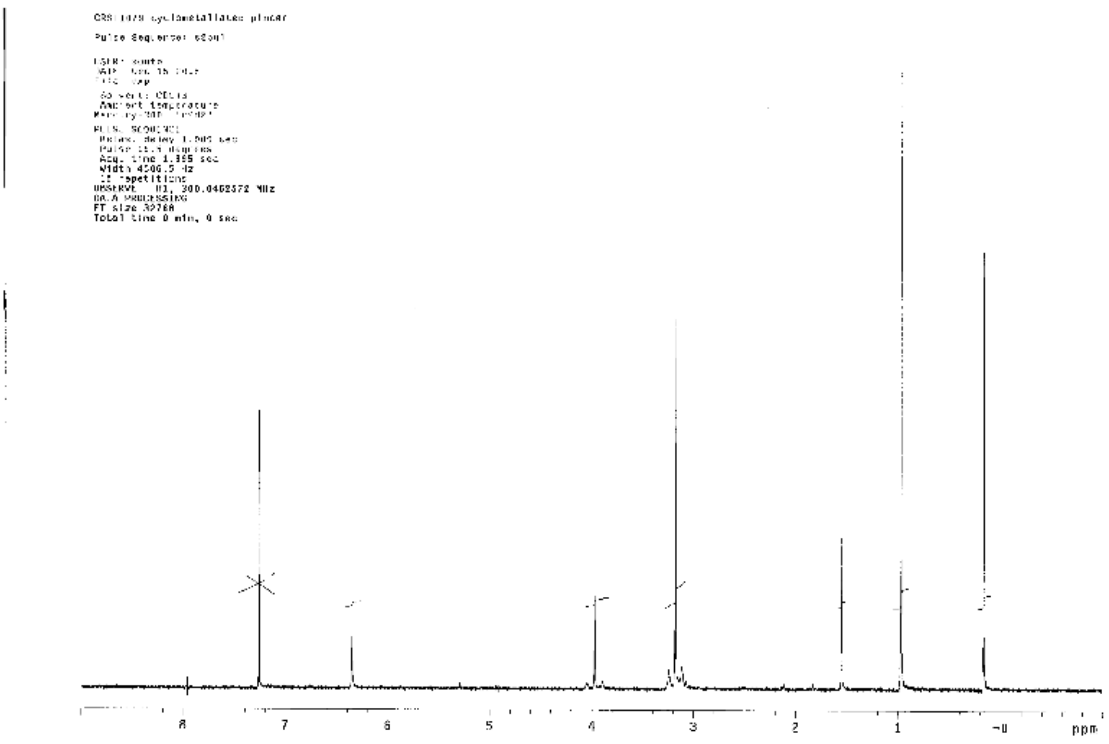

Figure C.5. Protected Pt Pincer complex.

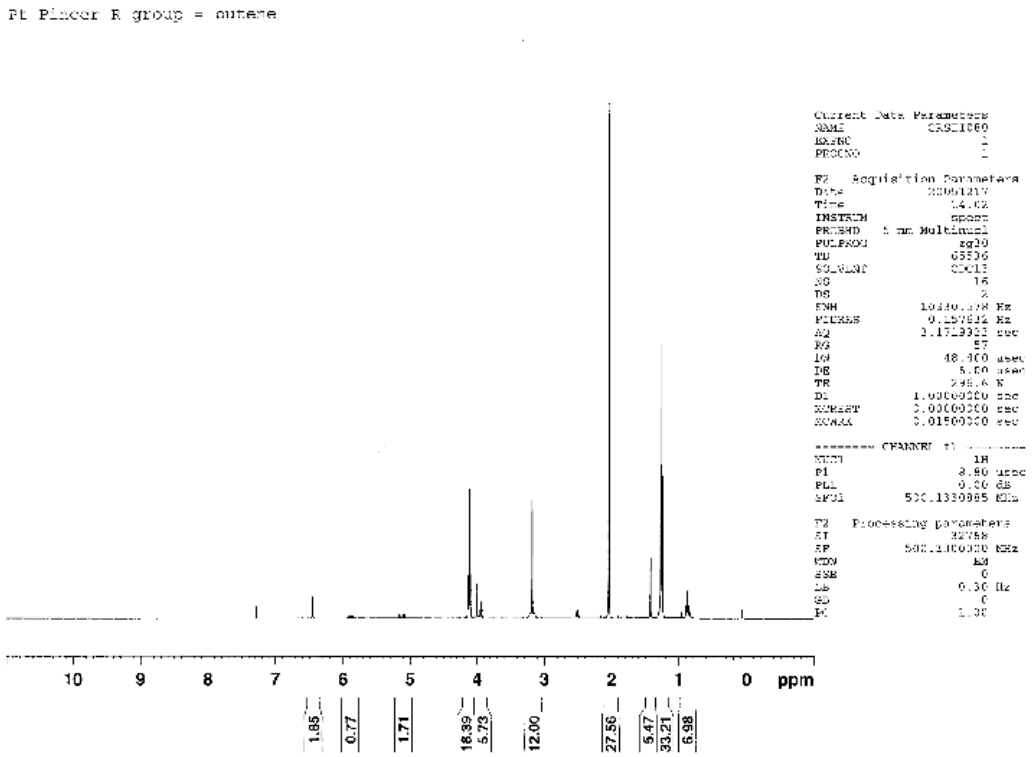

Figure C.6. Pt pincer olefin with four carbon tether.

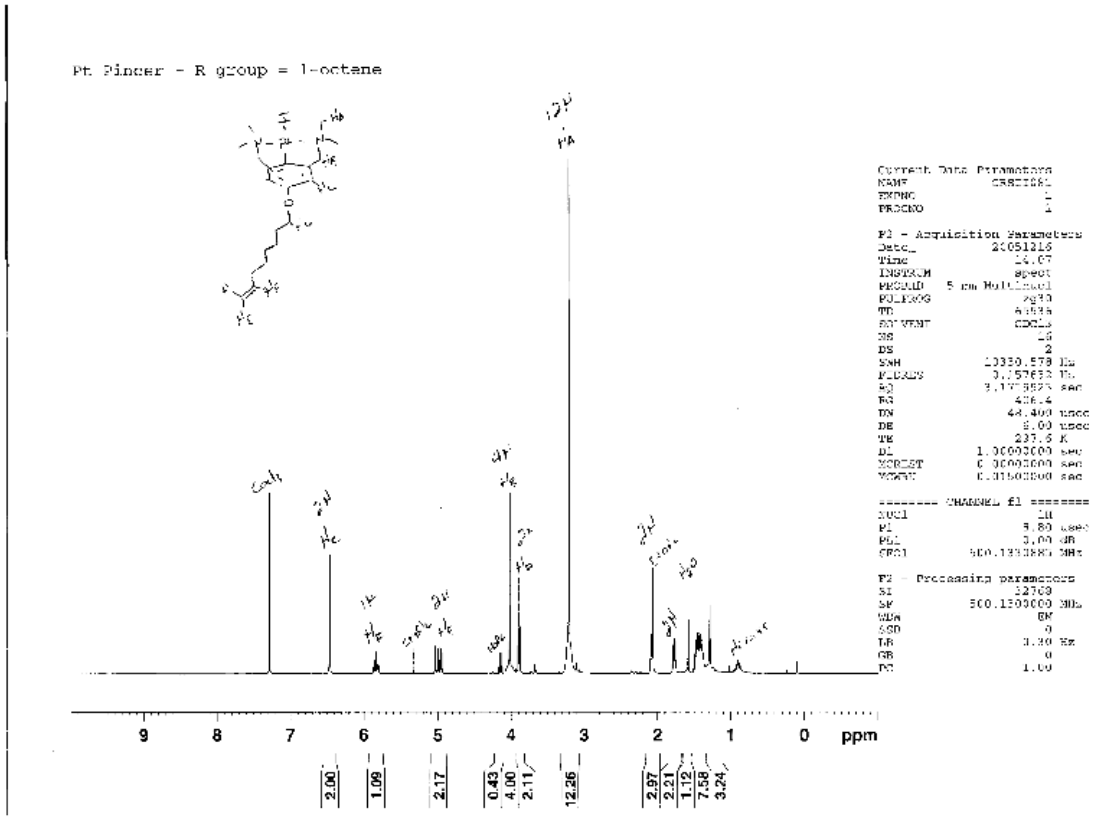

Figure C.7. Octene Pt Pincer complex.

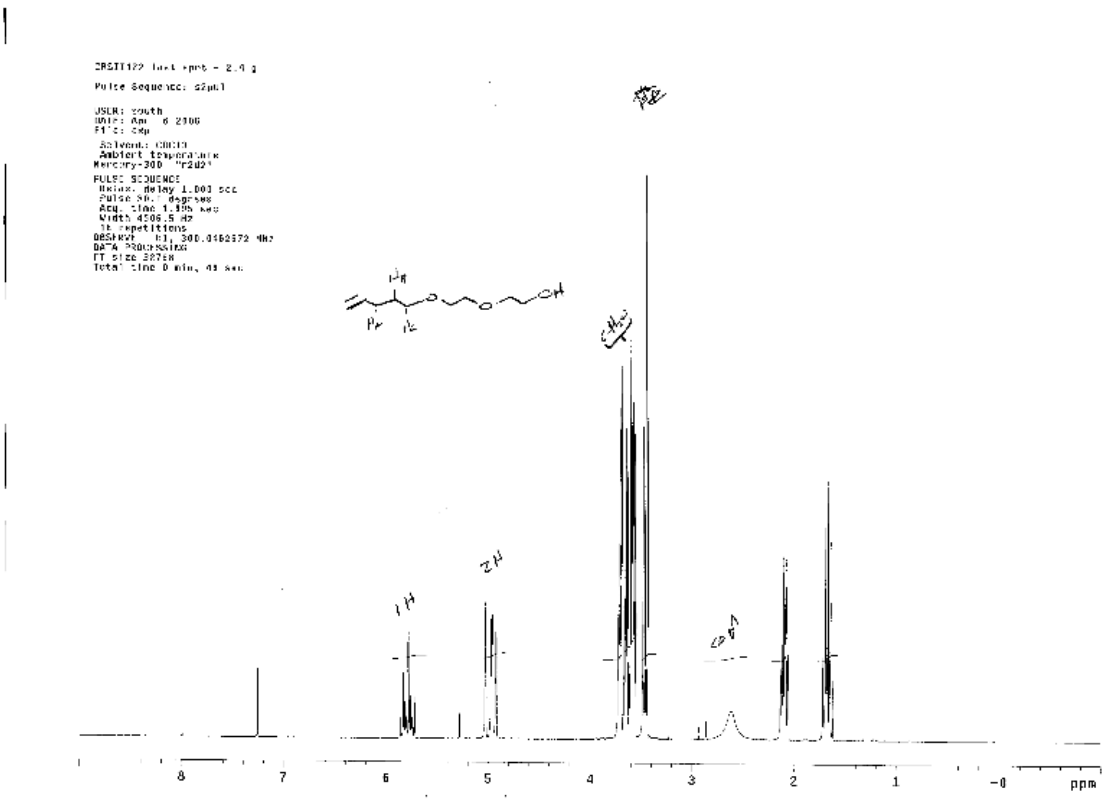

Figure C.8. Heteroatom containing olefinic alcohol.

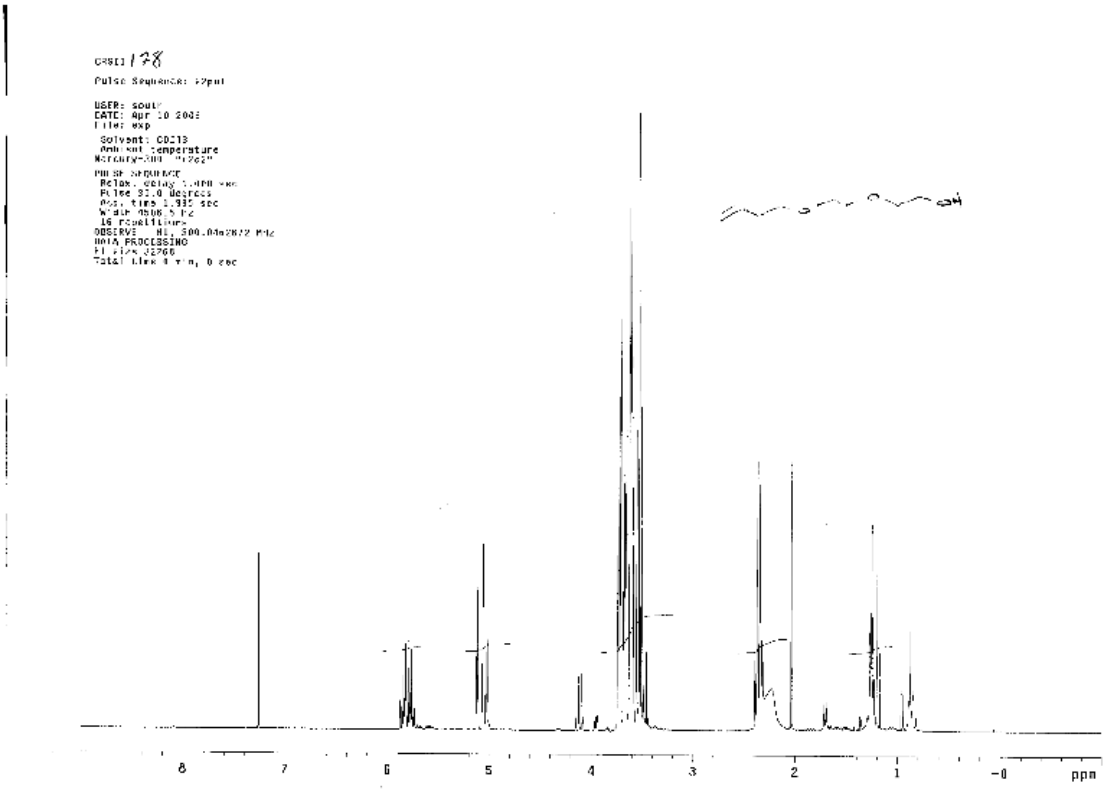

Figure C.9. Homoallylic heteroatom containing olefinic alcohol.

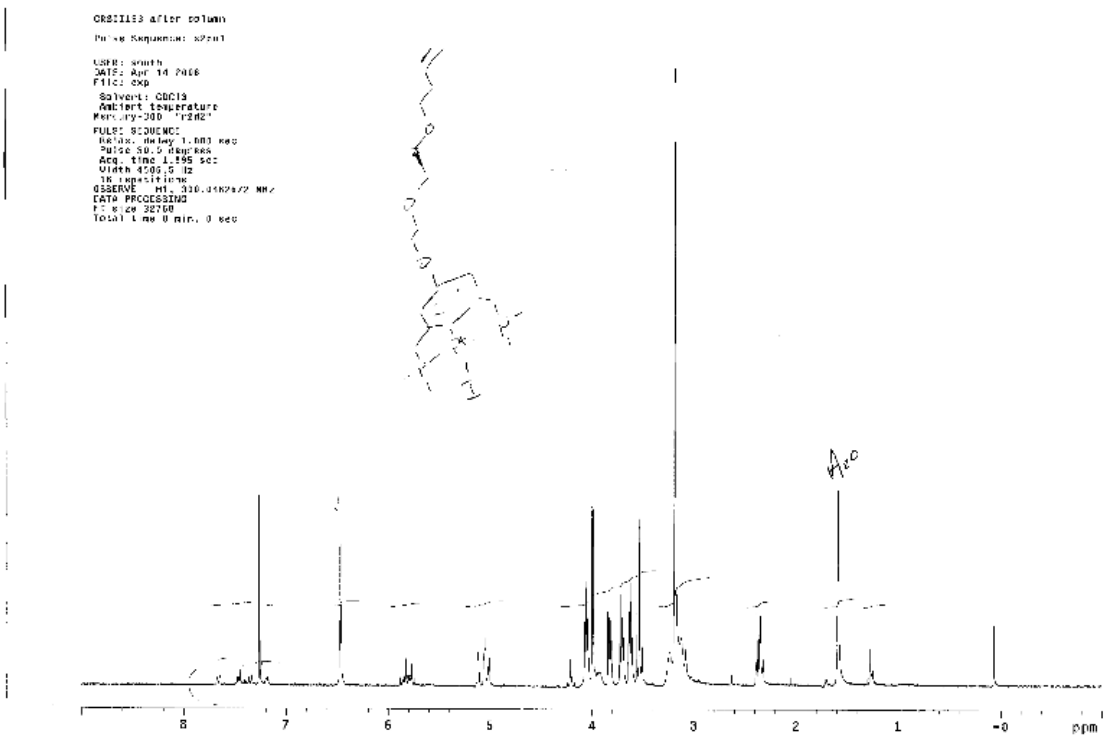

Figure C.10. Homoallylic heteroatom containing pincer complex.

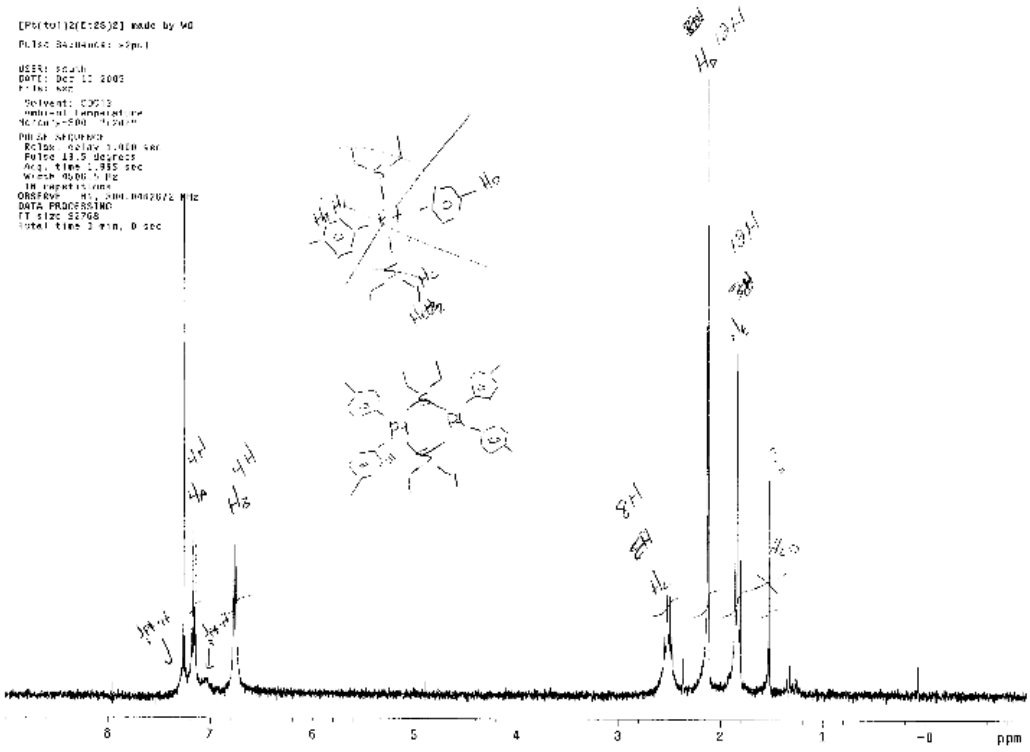

Figure C.11. Pt complex used in pincer olefin synthesis.

APPENDIX D

Supplemental Information for Chapter 6.

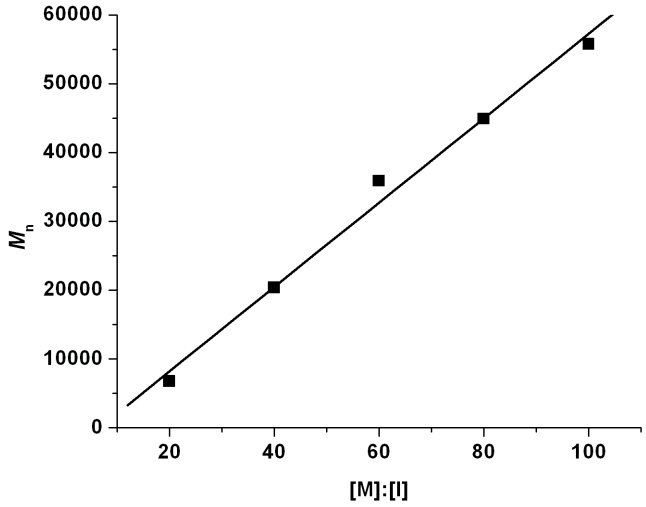

Figure D.1. Plot of M_n vs. [M]:[I] for the polymerization of monomer **5** showing linear dependence of M_n on initiator loading.

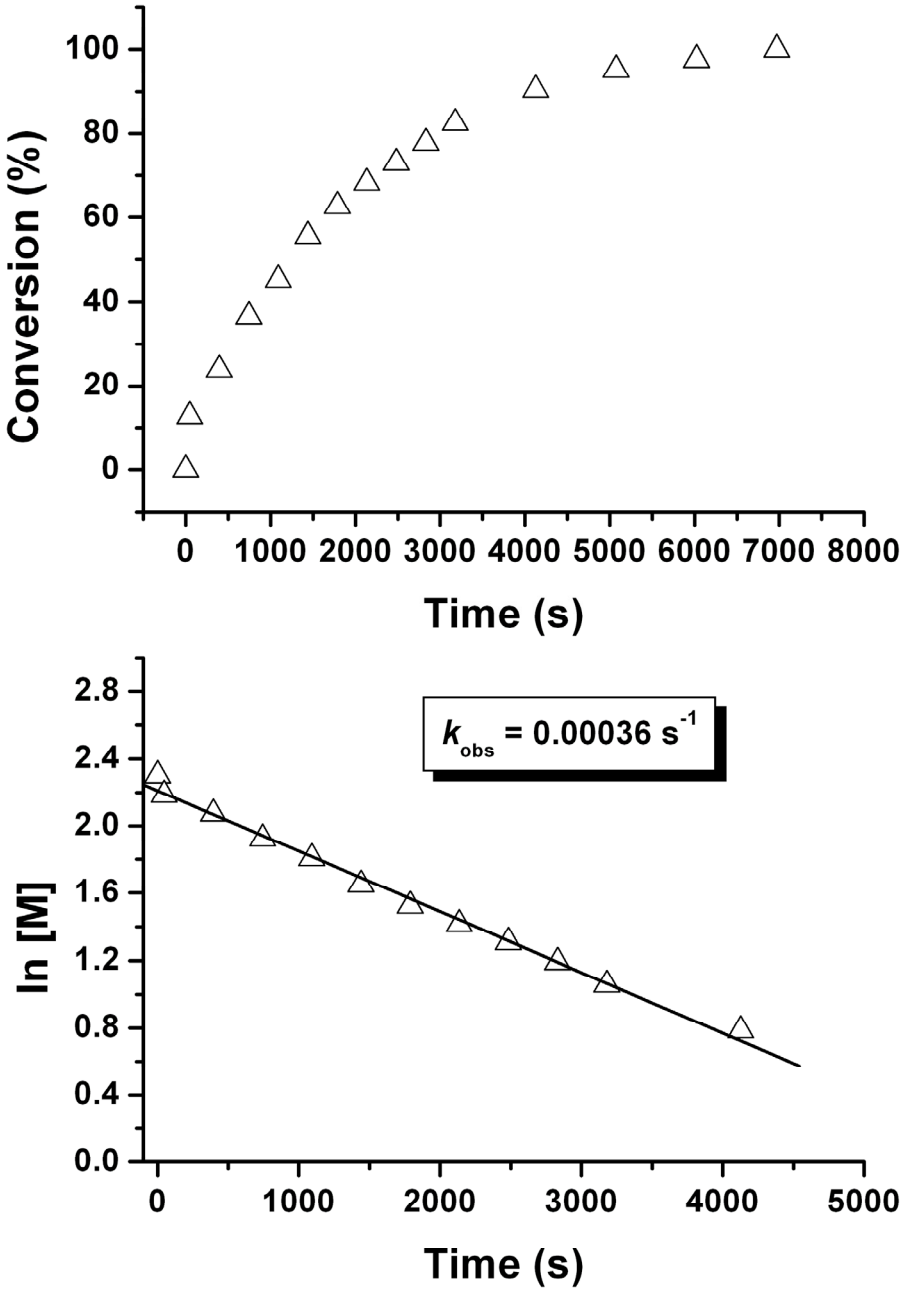

Figure D.2. Polymerization kinetics at 10 mM ($CDCl_3$, 298 K): plot of conversion vs. time (top) and corresponding 1st order kinetics plot (bottom) for the polymerization of **6**.

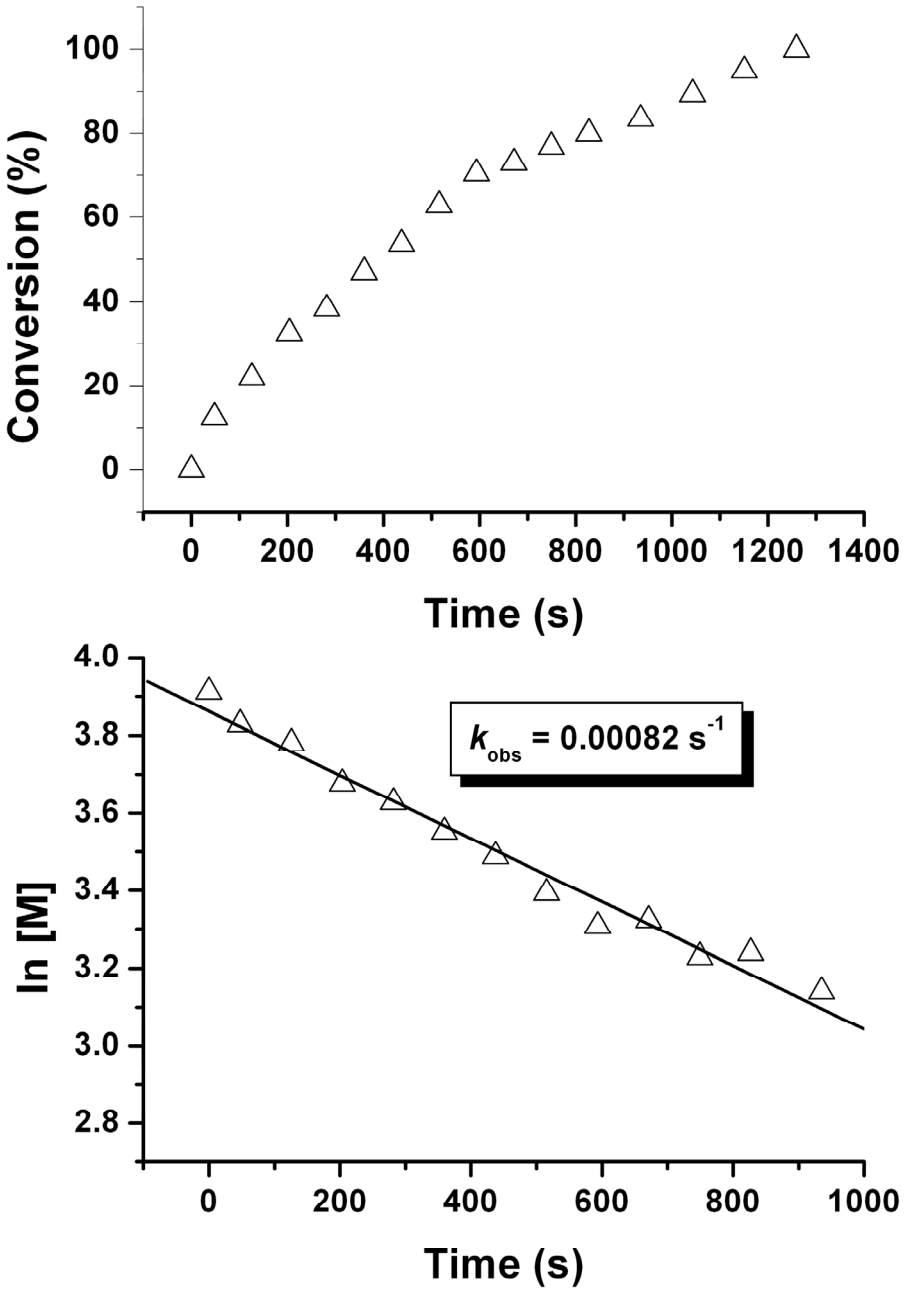

Figure D.3. Polymerization kinetics at 50 mM ($CDCl_3$, 298 K): plot of conversion vs. time (top) and corresponding 1st order kinetics plot (bottom) for the polymerization of **6**.

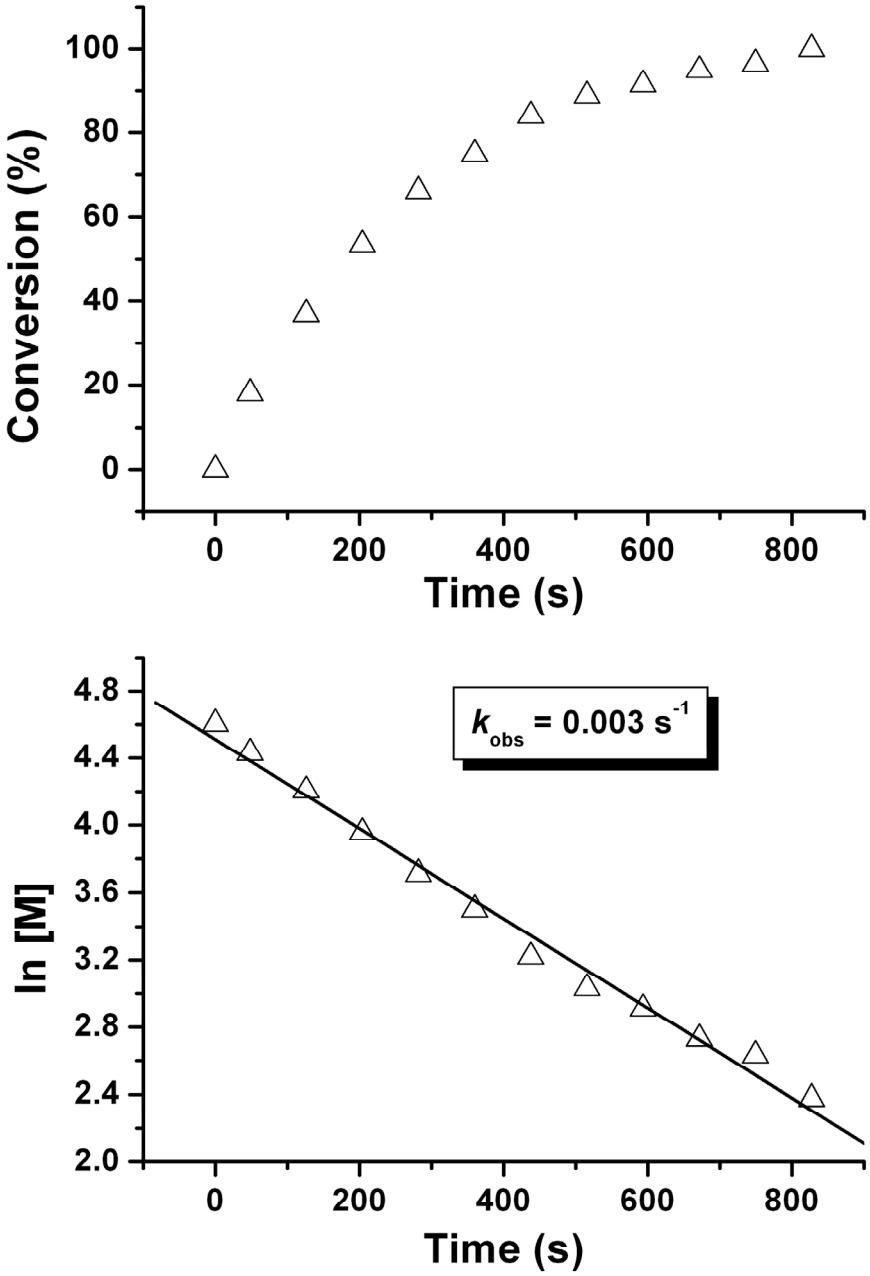

Figure D.4. Polymerization kinetics at 100 mM ($CDCl_3$, 298 K): plot of conversion vs. time (top) and corresponding 1st order kinetics plot (bottom) for the polymerization of **6**.

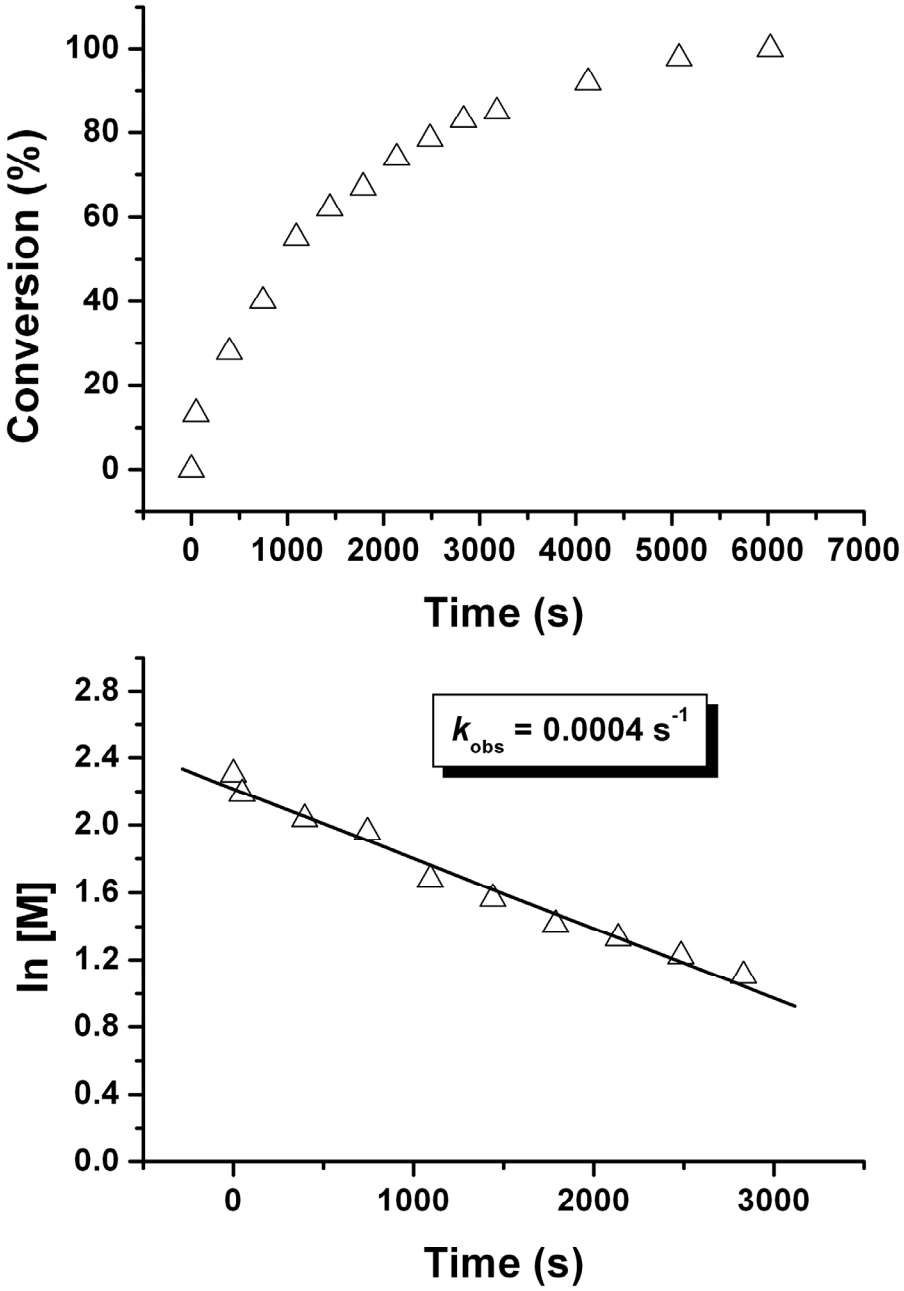

Figure D.5. Polymerization kinetics at 10 mM ($CDCl_3$, 298 K): plot of conversion vs. time (top) and corresponding 1st order kinetics plot (bottom) for the polymerization of **2:6** in the presence of poly(norbornene).

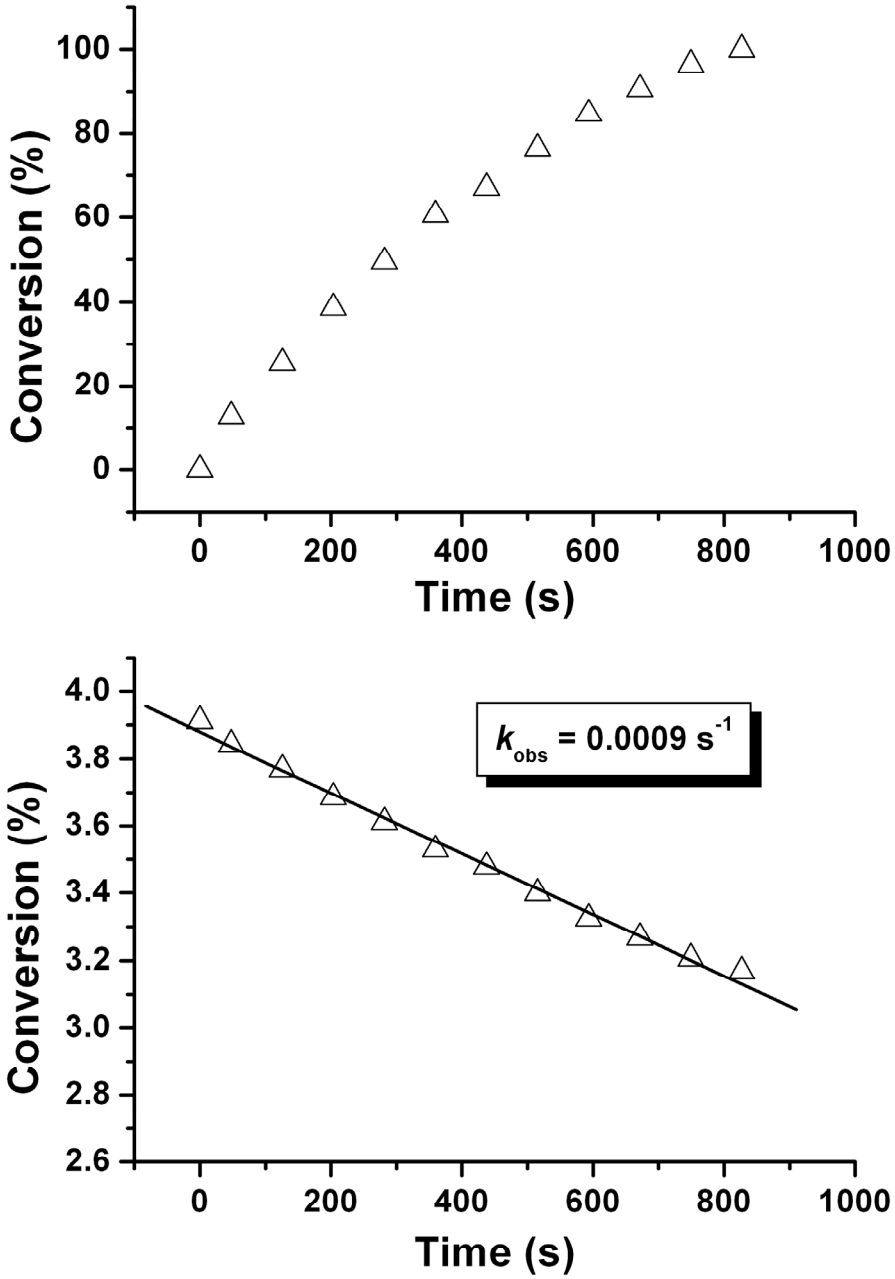

Figure D.6. Polymerization kinetics at 50 mM ($CDCl_3$, 298 K): plot of conversion vs. time (top) and corresponding 1st order kinetics plot (bottom) for the polymerization of **2:6** in the presence of poly(norbornene).

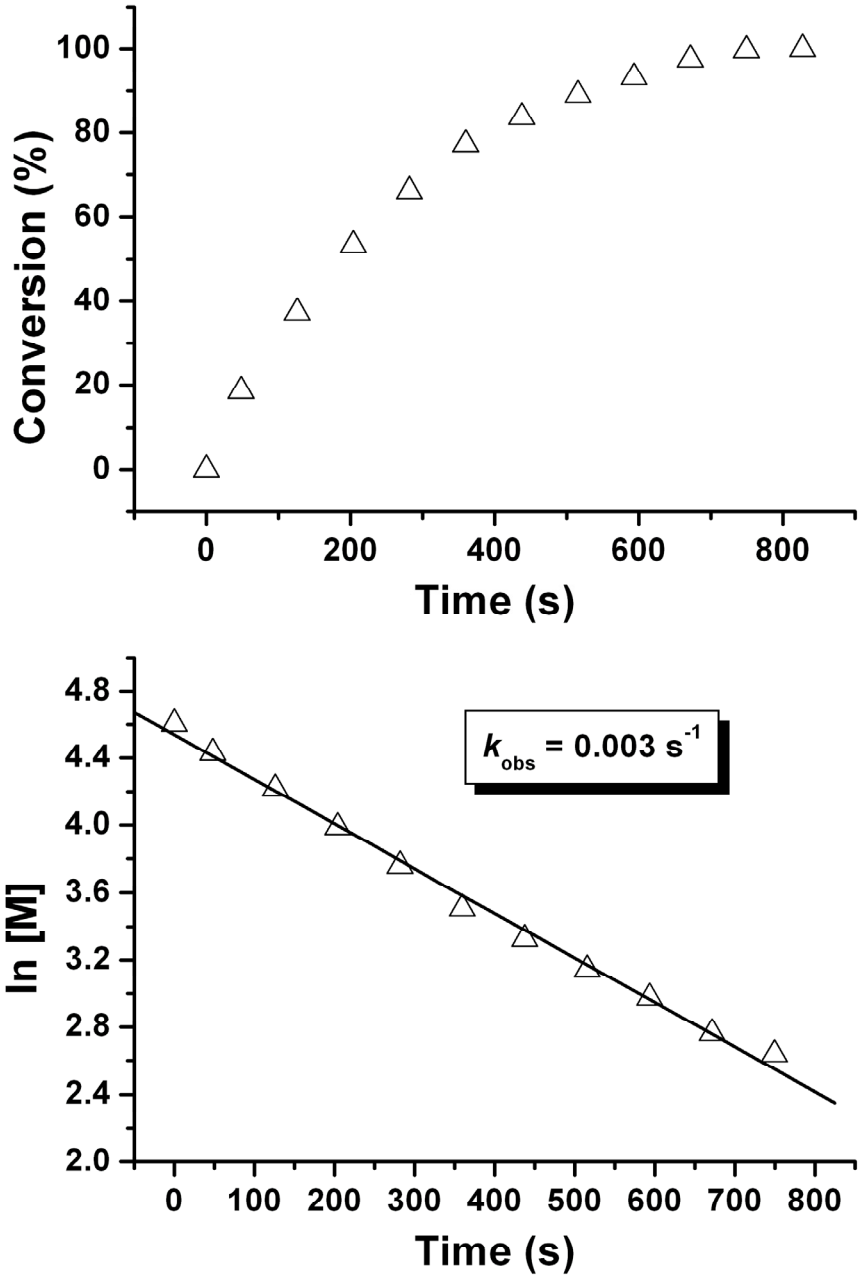

Figure D.7. Polymerization kinetics at 50 mM ($CDCl_3$, 298 K): plot of conversion vs. time (top) and corresponding 1st order kinetics plot (bottom) for the polymerization of **2:6** in the presence of poly(norbornene).

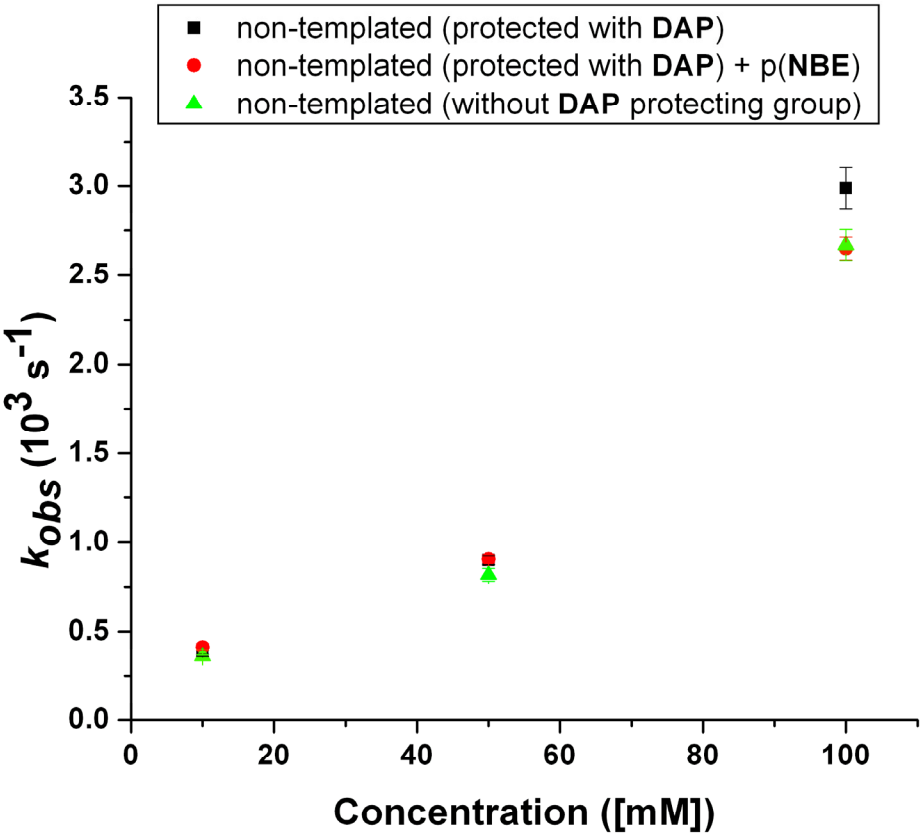

Figure D.8. Rate constant dependence on concentration for control polymerizations (DAP protected non-templated, non-templated DAP protected in the presence of poly(norbornene) and non-templated polymerization of monomer **6** in $CDCl_3$ (298 K).

Table D.1. Raw and processed data acquired from NMR *array* experiments at 10 mM (Varian, 300 MHz)

NON-TEMPLATED (protected with DAP small molecule)

TIME /s	PEAK HEIGHT / mm	[MON]	[POLY]	CONVERSION	LN [MON]	TIME / min
0	153	10	0	0		0
47.93	135	8.823529412	1.176470588	13.44286781	2.17742195	0.798833333
395.9	117	7.647058824	2.352941176	26.88573562	2.034321106	6.598333333
743.8	102	6.666666667	3.333333333	38.08812547	1.897119985	12.39666667
1092	88.7	5.797385621	4.202614379	48.02091113	1.757407061	18.2
1440	77.6	5.071895425	4.928104575	56.31067961	1.623714599	24
1788	68.3	4.464052288	5.535947712	63.25616131	1.496056938	29.8
2135	60.4	3.947712418	6.052287582	69.15608663	1.373136277	35.58333333
2483	53.6	3.503267974	6.496732026	74.23450336	1.25369624	41.38333333
2831	47.9	3.130718954	6.869281046	78.4914115	1.141262676	47.18333333
3179	43.1	2.816993464	7.183006536	82.07617625	1.035670169	52.98333333
4127	33.4	2.183006536	7.816993464	89.32038835		68.78333333
5075	25	1.633986928	8.366013072	95.59372666		84.58333333
6023	23.2	1.516339869	8.483660131	96.93801344		100.3833333
6971	20.7	1.352941176	8.647058824	98.80507842		116.1833333
7919	19.1	1.248366013	8.751633987	100		131.9833333

TEMPLATED

0	168	10	0	0	2.302585093	0
94	123.5	7.351190476	2.648809524	28.70967742	1.99486227	1.566666667
395.9	78.8	4.69047619	5.30952381	57.5483871	1.54553411	6.598333333
743.8	54.7	3.255952381	6.744047619	73.09677419	1.180484823	12.39666667
1092	38.2	2.273809524	7.726190476	83.74193548	0.821456629	18.2
1440	24.7	1.470238095	8.529761905	92.4516129	0.385424357	24
1788	17	1.011904762	8.988095238	97.41935484	0.011834458	29.8
2135	13	0.773809524	9.226190476	100		35.58333333

Table D.2. Raw and processed data acquired from NMR *array* experiments at 50 mM (Varian, 300 MHz)

NON-TEMPLATED (protected with DAP small molecule)

TIME	PEAK HEIGHT	[MON]	[POLY]	CONVERSION	LN [MON]	TIME(Min)
0	162	50	0	0	3.912023005	0
47.93	149	45.98765432	4.012345679	12.46404602	3.828372976	0.798833333
125.9	142	43.82716049	6.172839506	19.17545542	3.780253728	2.098333333
203.8	128	39.50617284	10.49382716	32.59827421	3.676456934	3.396666667
281.7	122	37.65432099	12.34567901	38.35091083	3.628447715	4.695
359.6	113	34.87654321	15.12345679	46.97986577	3.551814489	5.993333333
437.6	106	32.71604938	17.28395062	53.69127517	3.487865764	7.293333333
515.5	96.4	29.75308642	20.24691358	62.89549377	3.392932872	8.591666667
593.4	88.5	27.31481481	22.68518519	70.46979866	3.307429222	9.89
671.3	85	26.2345679	23.7654321	73.82550336	3.267077927	11.18833333
749.3	81.8	25.24691358	24.75308642	76.89357622	3.228703914	12.48833333
827.2	77	23.7654321	26.2345679	81.49568552	3.168232092	13.78666667
935.1	74	22.83950617	27.16049383	84.37200384	3.128491763	15.585
1043	70	21.60493827	28.39506173	88.20709492	3.072921912	17.38333333
1151	66.5	20.52469136	29.47530864	91.56279962	3.021628618	19.18333333
1350	57.7	17.80864198	32.19135802	100	2.879683844	22.5

TEMPLATED

TIME	PEAK HEIGHT	[MON]	[POLY]	CONVERSION	LN [MON]	TIME(Min)
0	164	50	0	0	3.912023005	0
11.98	150	47	3	6.968838527	3.850147602	0.199666667
53.96	146	44.51219512	5.487804878	12.74787535	3.795763199	0.899333333
95.94	133	40.54878049	9.451219512	21.95467422	3.702505706	1.599
137.9	122	37.19512195	12.80487805	29.74504249	3.616177622	2.298333333
179.9	111	33.84146341	16.15853659	37.53541076	3.521686779	2.998333333
221.9	104	31.70731707	18.29268293	42.49291785	3.456547477	3.698333333
263.9	92.3	28.1402439	21.8597561	50.77903683	3.337200719	4.398333333
335.9	82.2	25.06097561	24.93902439	57.93201133	3.22131188	5.598333333
407.8	69.8	22	28	65.04249292	3.091042453	6.796666667
479.8	65.7	20.0304878	29.9695122	69.61756374	2.997255503	7.996666667
551.8	59.5	17	33	76.6572238	2.833213344	9.196666667
623.8	48.4	14.75609756	35.24390244	81.86968839	2.691656391	10.39666667
695.8	48.2	13	37	85.9490085	2.564949357	11.59666667
767.7	40.9	12	38	88.27195467	2.48490665	12.795
839.7	33.8	10.30487805	39.69512195	92.20963173	2.33261738	13.995
911.7	30	9.146341463	40.85365854	94.90084986	2.213353959	15.195
983.7	28.5	8.68902439	41.31097561	95.9631728	2.162060665	16.395
1056	28.7	8	42	97.56373938	2.079441542	17.6
1128	24.4	7.43902439	42.56097561	98.86685552	2.00673971	18.8
1200	22.8	6.951219512	43.04878049	100	1.938917114	20

Table D.3. Raw and processed data acquired from NMR *array* experiments at 100 mM (Varian, 300 MHz)

NON-TEMPLATED (protected with DAP small molecule)

TIME	PEAK HEIGHT	[MON]	[POLY]	CONVERSION	LN [MON]	TIME(MIN)
0	200	100	0	0	4.605170186	0
47.93	151.2	75.6	24.4	26.52173913	4.325456283	0.798833333
125.9	116.824	58.412	41.588	45.20434783	4.067521348	2.098333333
203.9	88.678	44.339	55.661	60.50108696	3.791864651	3.398333333
281.7	67.7333	33.86665	66.13335	71.88407609	3.522430754	4.695
359.6	54.1522	27.0761	72.9239	79.2651087	3.29865142	5.993333333
437.6	43.7958	21.8979	78.1021	84.89358696	3.086390742	7.293333333
515.5	37.4654	18.7327	81.2673	88.33402174	2.93027066	8.591666667
623.4	29.786	14.893	85.107	92.5076087	2.700891304	10.39
731.3	24.8861	12.44305	87.55695	95.17059783	2.521162234	12.18833333
839.3	19	9.5	90.5	98.36956522	2.251291799	13.98833333
947.2	16	8	92	100	2.079441542	15.78666667

TEMPLATED

TIME	PEAK HEIGHT	[MON]	[POLY]	CONVERSION	LN [MON]	TIME(MIN)
0	200	100	0	0	4.605170186	0
47.93	151.2	75.6	24.4	27.308338	4.325456283	0.798833333
125.9	115.935	57.9675	42.0325	47.04252938	4.059882509	2.098333333
203.8	87.48	43.74	56.26	62.96586458	3.778263015	3.396666667
281.7	65.8	32.9	67.1	75.09792949	3.493472658	4.695
359.6	52.2	26.1	73.9	82.70844992	3.261935314	5.993333333
437.6	42.8	21.4	78.6	87.96866256	3.063390922	7.293333333
515.5	35.2	17.6	82.4	92.22160045	2.867898902	8.591666667
593.4	31.3	15.65	84.35	94.4040291	2.750470917	9.89
671.3	27.9	13.95	86.05	96.30665921	2.635479508	11.18833333
749.3	23.4	11.7	88.3	98.82484611	2.459588842	12.48833333
827.2	21.3	10.65	89.35	100	2.365559892	13.78666667

Table D.4. Raw and processed data acquired from NMR *array* experiments (control with p(NBE) added – 100 mM) (Varian, 300 MHz)

TIME	PEAK HEIGHT	[Monomer]	[Polymer]	Conversion	LN
0	180	100	0	0	4.60517019
47.93	151.2	84	16	18.5328185	4.4308168
125.9	122.2	67.8888889	32.1111111	37.1943372	4.21787238
203.9	97	53.8888889	46.1111111	53.4105534	3.98692431
281.7	77.2	42.8888889	57.1111111	66.1518662	3.75861279
359.6	60	33.3333333	66.6666667	77.2200772	3.5065579
437.6	50	27.7777778	72.2222222	83.6550837	3.32423634
515.5	41.7	23.1666667	76.8333333	88.996139	3.14271446
593.4	35.2	19.5555556	80.4444444	93.1788932	2.97325942
671.4	28.5	15.8333333	84.1666667	97.4903475	2.76211742
749.3	25.1	13.9444444	86.0555556	99.6782497	2.63508118
827.2	24.6	13.6666667	86.3333333	100	2.61495978

Table D.5. Raw and processed data acquired from NMR *array* experiments (control with **p(NBE)** added – 50 mM) (Varian, 300 MHz)

TIME	PEAK HEIGHT	[Monomer]	[Polymer]	Conversion	LN
0	162	50	0	0	3.91202301
47.93	151.2	46.6666667	3.33333333	9.67221924	3.84303013
125.9	140.4	43.3333333	6.66666667	19.3444385	3.76892216
203.8	129.2	39.8765432	10.1234568	29.3748881	3.68578826
281.7	120	37.037037	12.962963	37.6141859	3.61191841
359.6	110.5	34.1049383	15.8950617	46.1221565	3.52944219
437.6	105	32.4074074	17.5925926	51.0478238	3.47838702
515.5	97	29.9382716	20.0617284	58.2124306	3.39913765
593.4	90	27.7777778	22.2222222	64.4814616	3.32423634
671.4	85	26.2345679	23.7654321	68.9593409	3.26707793
749.3	80	24.691358	25.308642	73.4372201	3.2064533
827.2	77	23.7654321	26.2345679	76.1239477	3.16823209
905.1	70	21.6049383	28.3950617	82.3929787	3.07292191
1013	60.12	18.5555556	31.4444444	91.2412681	2.92076924
1121	50.34	15.537037	34.462963	100	2.74322666

Table D.6. Raw and processed data acquired from NMR *array* experiments (control with p(NBE) added – 10 mM) (Varian, 300 MHz)

TIME	PEAK HEIGHT	[Monomer]	[Polymer]	Conversion	LN
0	154	10	0	0	2.30258509
47.93	137	8.8961039	1.1038961	13.1274131	2.18561342
395.9	118	7.66233766	2.33766234	27.7992278	2.03631712
743.8	109	7.07792208	2.92207792	34.7490347	1.95698037
1092	82.6	5.36363636	4.63636364	55.1351351	1.67964217
1440	73.6	4.77922078	5.22077922	62.0849421	1.56427752
1788	63.1	4.0974026	5.9025974	70.1930502	1.41035326
2135	58.2	3.77922078	6.22077922	73.976834	1.32951785
2483	52.3	3.3961039	6.6038961	78.5328185	1.22262886
2831	46.5	3.01948052	6.98051948	83.011583	1.1050848
3179	46.7	3.03246753	6.96753247	82.8571429	1.10937666
4127	42.8	2.77922078	7.22077922	85.8687259	1.02217059
5075	27.4	1.77922078	8.22077922	97.7606178	0.5761755
6023	24.5	1.59090909	8.40909091	100	0.46430561

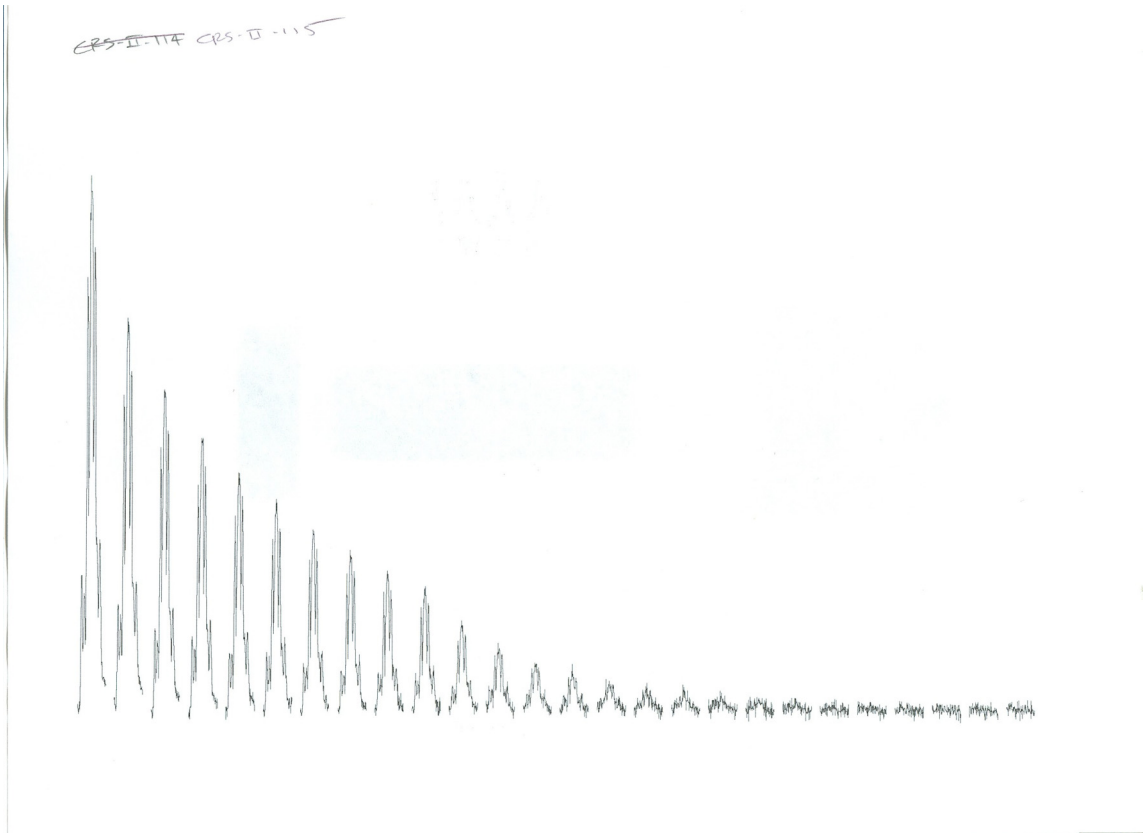

Figure D.9. Example output from a NMR *array* experiment (Varian); peak shown is norbornene monomer peak (~ 6.14 ppm). Each signal corresponds to a spectrum taken at a different time after the polymerization has begun. Note: this is an automated experiment, and the rate constants given by the Varian calculation were *not* used; rate constants were calculated by hand.

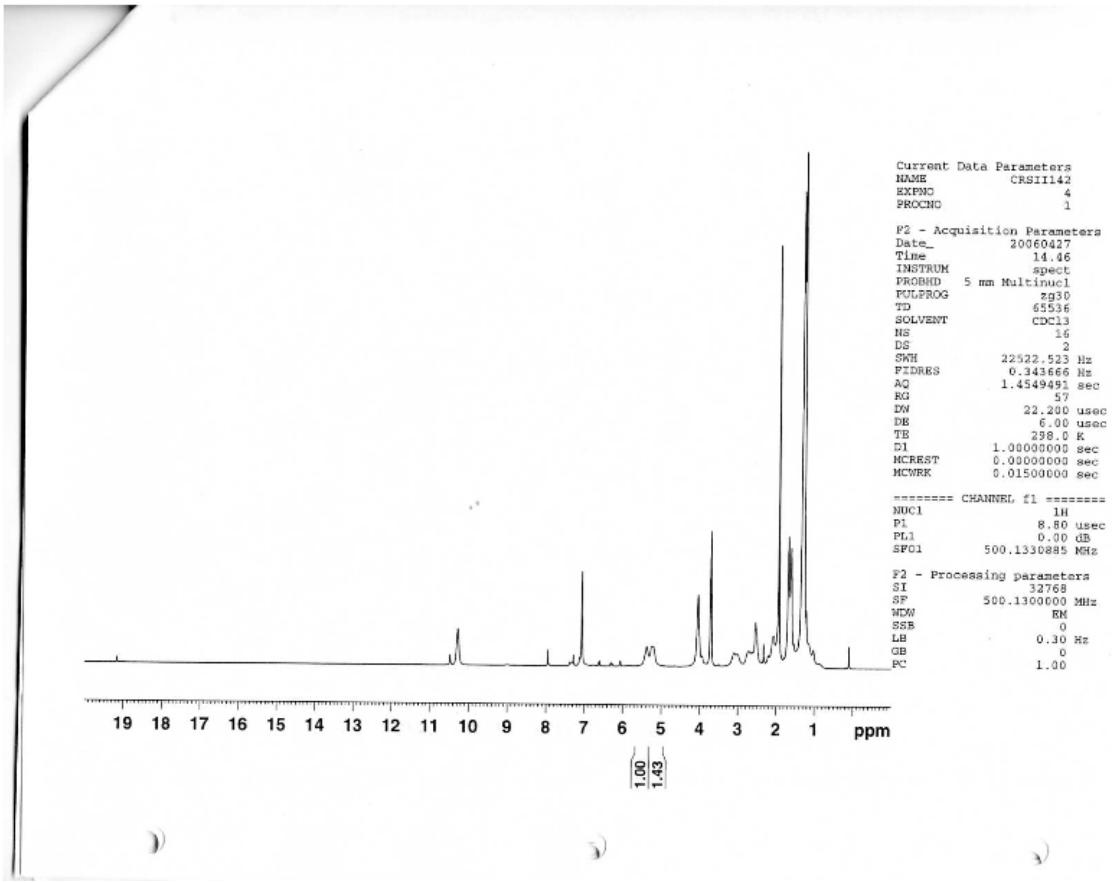

Figure D.10. ^{1}H NMR spectrum of **THY** monomer after polymerization: note the carbene signal present past 19 ppm (Figure D.11)

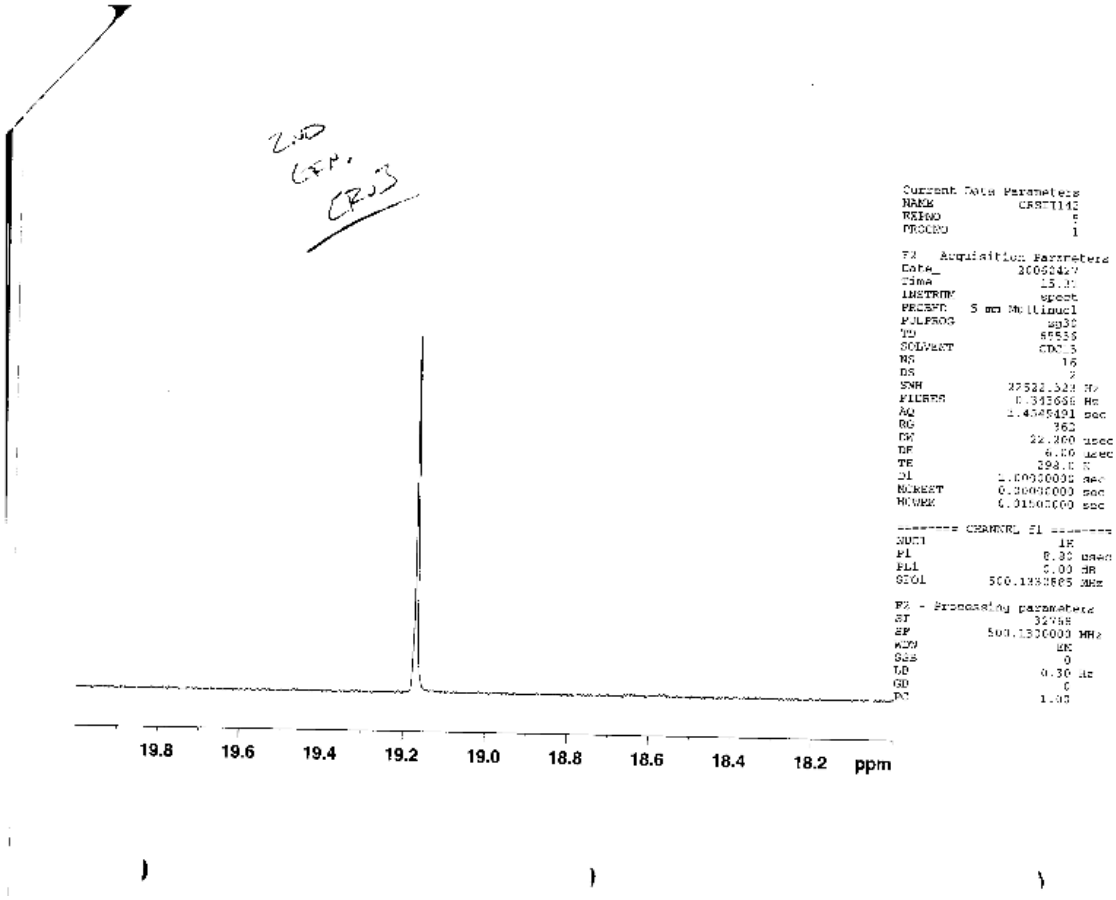

Figure D.11. Partial (carbene region) ^{1}H NMR spectrum of THY monomer after polymerization; the carbene signal suggests an incomplete polymerization consistent with our GPC results.

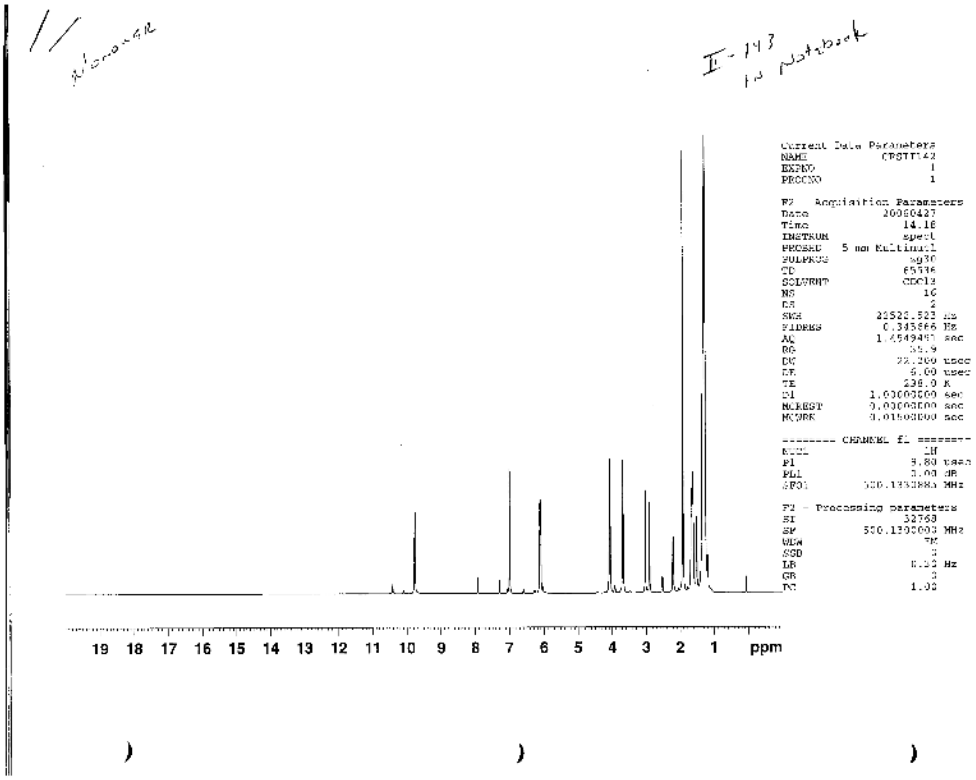

Figure D.12. Reference ^{1}H NMR spectrum of **THY** monomer before polymerization

APPENDIX E

Supplemental Material for Chapter 8

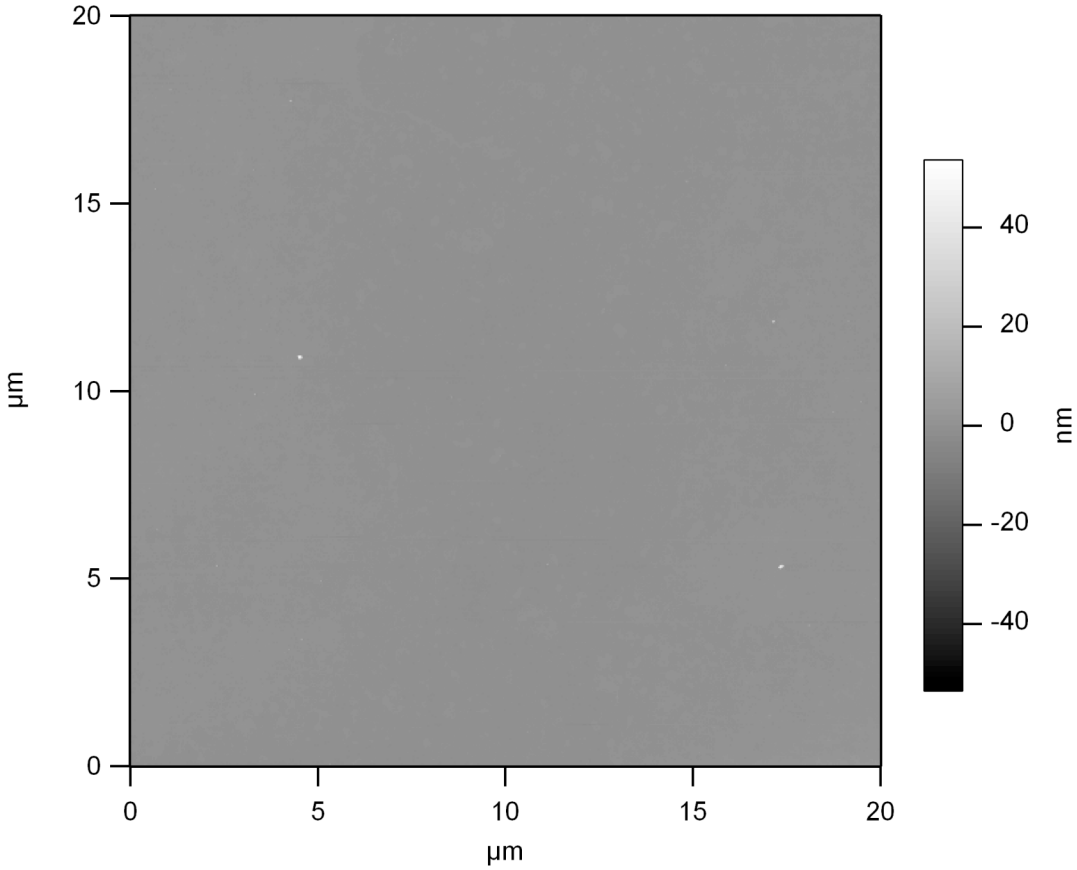

Figure E.1. AFM image of quartz slide functionalized with **2**.

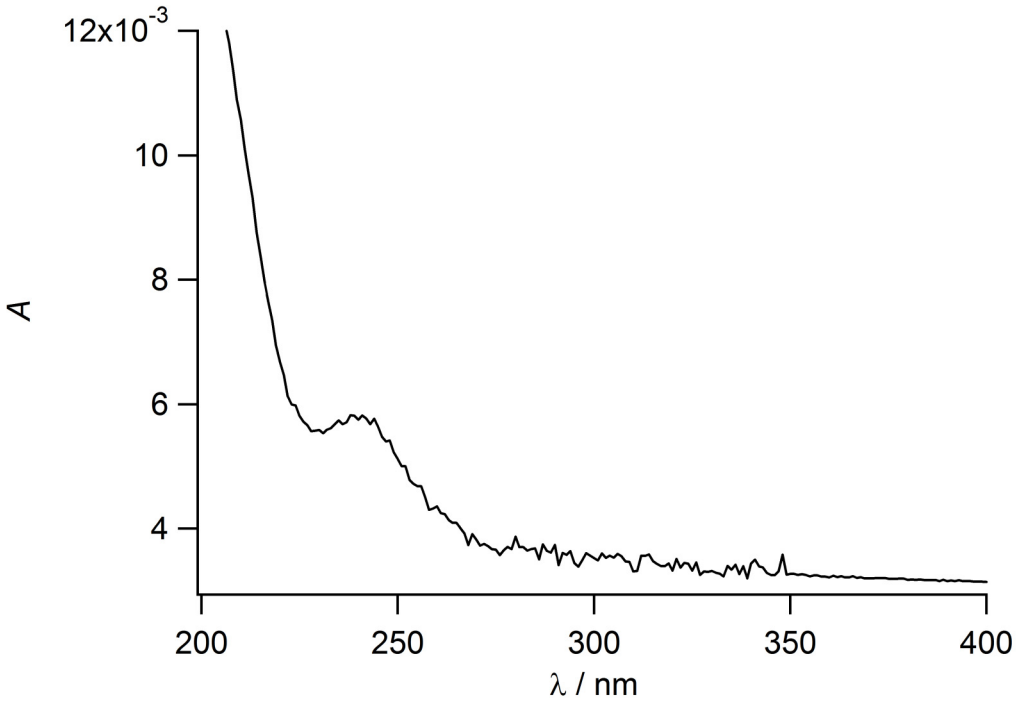

Figure E.2. UV-vis spectra of a quartz slide functionalized with **2**.

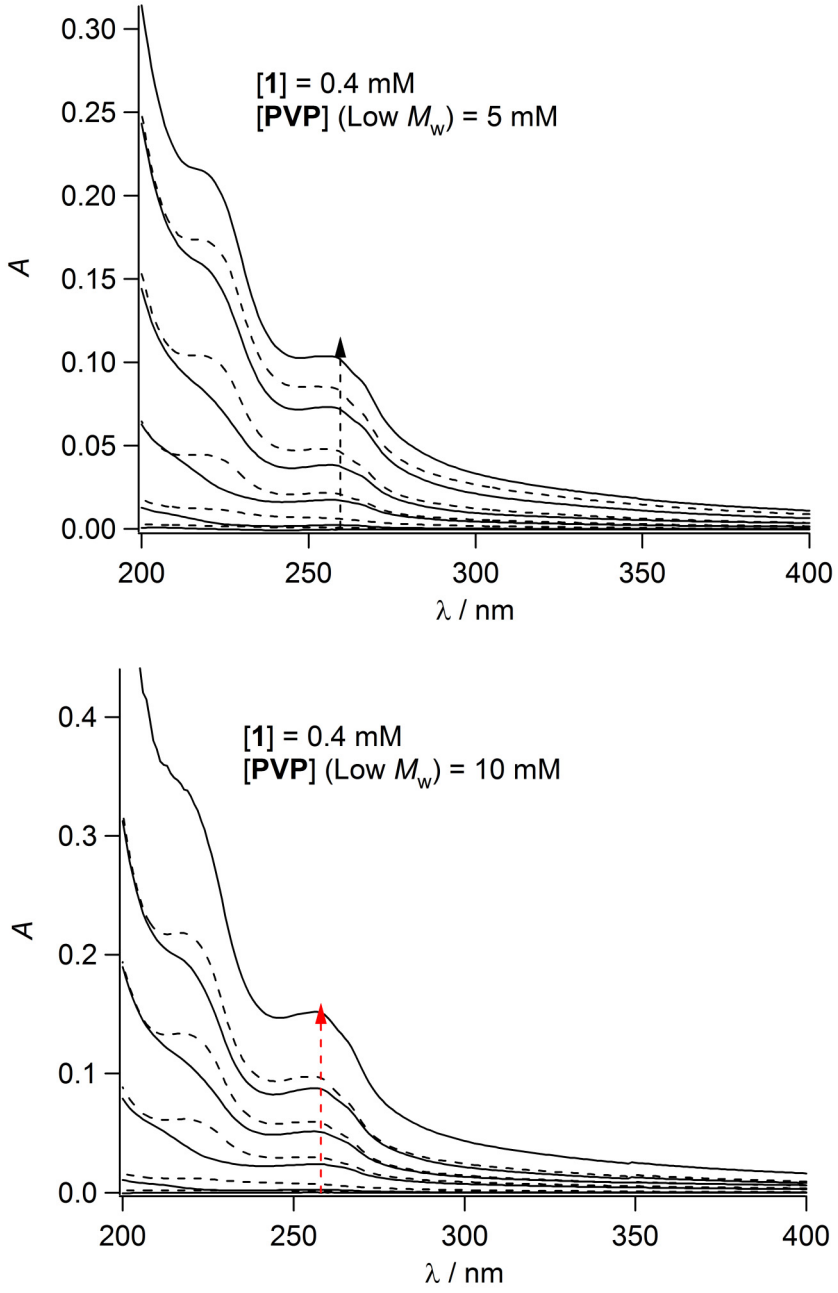

Figure E.3. Remaining UV-vis profiles for the deposition of **PVPa** and **1**; deposition profile taken with [**PVPa**] = 1 mM is shown in Figure 8.1.

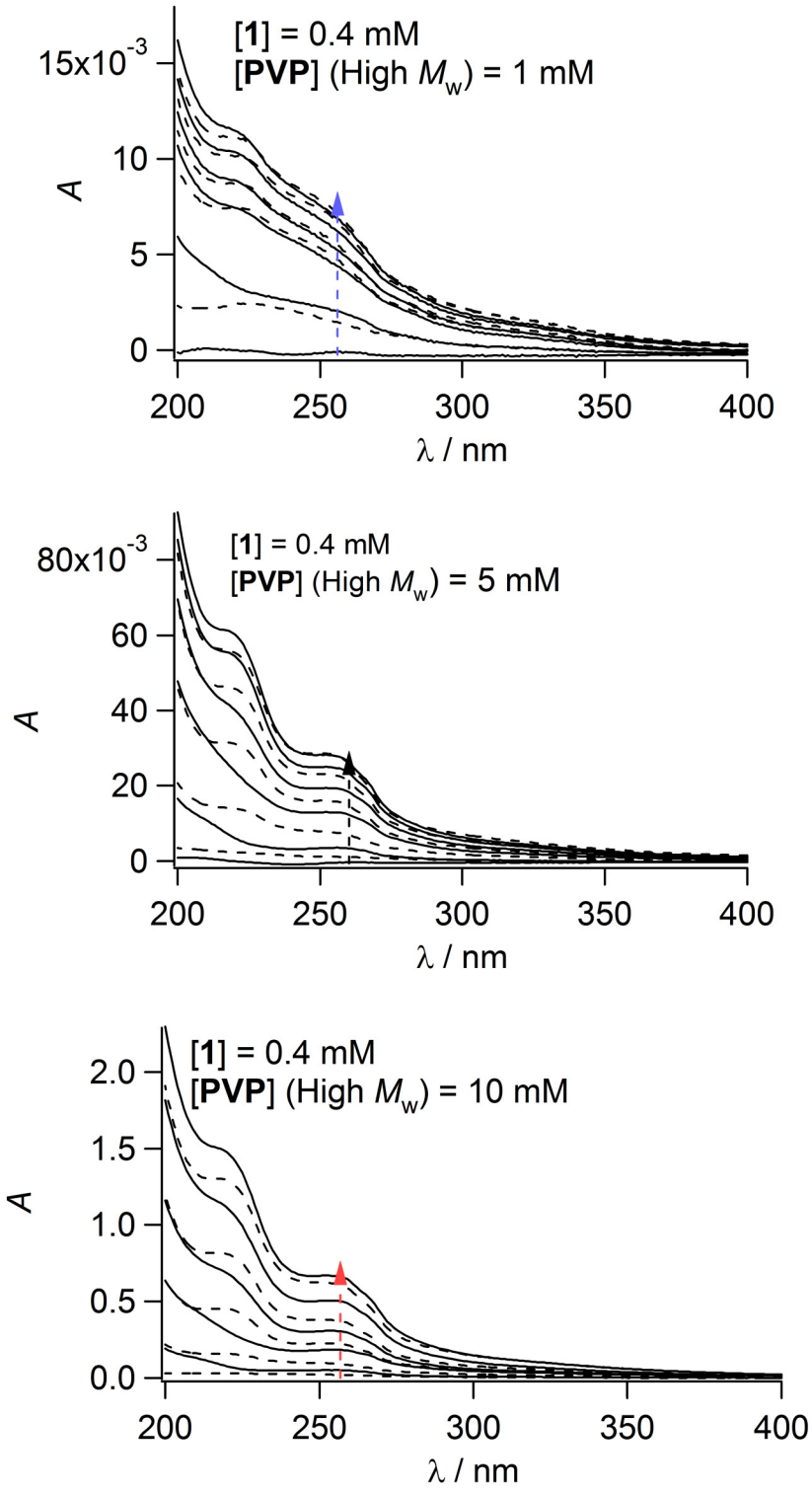

Figure E.4. UV-vis absorption profiles for the deposition of **PVPb** with **1** at different concentrations of **PVPb**.

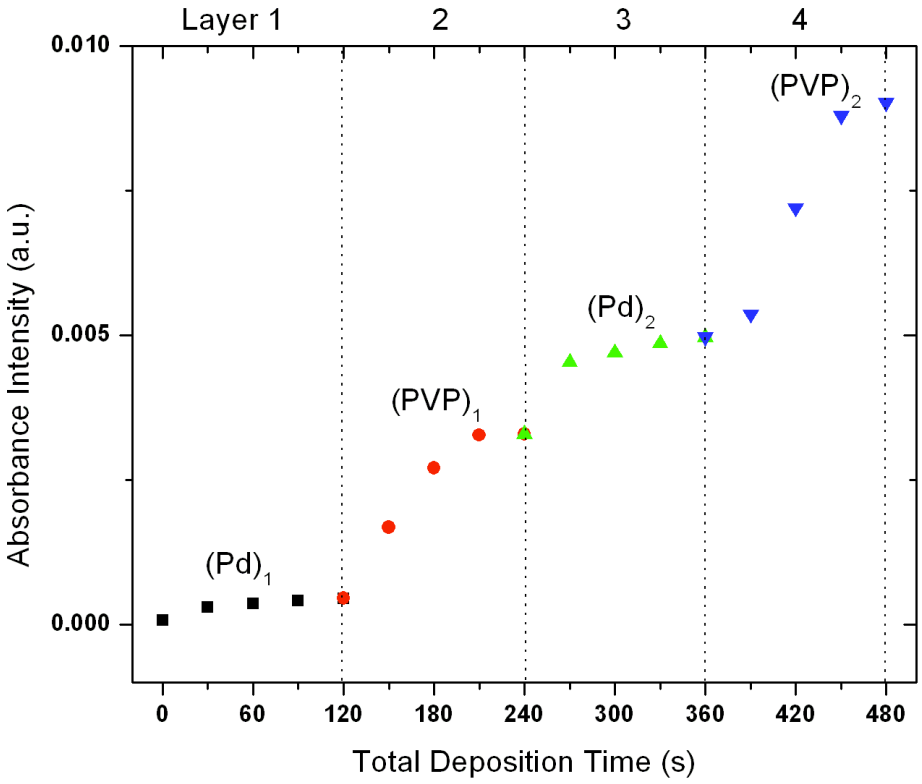

Figure E.5. Kinetic profile taken during the deposition of **PVPa** with **1**.